Investigating stratigraphic evidence for Antarctic glaciation in the greenhouse world of the Paleocene, eastern North Island, New Zealand

A thesis
submitted in partial fulfilment
of the requirements for the degree
of
Master of Science in Earth Sciences
at
The University of Waikato

by
Michael J. S. Tayler

THE UNIVERSITY OF
WAIKATO
Te Whare Wānanga o Waikato

The University of Waikato
2011

ABSTRACT

Early Paleogene (Paleocene-Eocene) climate was significantly warmer than today, with the poles generally considered to have been free of ice. These greenhouse conditions ended in the earliest Oligocene when the formation of the circum-Antarctic seaway between Antarctica and Australia had widened sufficiently to allow thermal isolation of the Antarctic continent and expansion of ice sheets to sea level. The associated invigorated Southern Ocean circulation patterns have been deemed responsible for formation of the Marshall Unconformity (32-29 Ma), a prominent hiatus in many Early Oligocene sedimentary sections in the wider New Zealand region. However, some recent studies have suggested there may have been short periods of significant Antarctic glaciation prior to opening of the circum-Antarctic seaway, including in the Late Paleocene at c. 58-57 Ma, referred to in this study as the "Late Paleocene event" (LPE).

This study investigates the origin(s) of sedimentary sequences from four eastern North Island early Paleogene sections with the aim of determining whether any links can be made between the nature of the sediment facies and their bounding contacts with ice sheet growth on Antarctica. A late Paleogene section that records a possible occurrence of the Early Oligocene Marshall Unconformity has also been studied with the aim of comparing lithologic features from the site with those in the early Paleogene study sections. Methods used include detailed logging and description of sedimentary strata, and petrographic, mineralogical, grain size, elemental, stable carbon and oxygen isotope, organic carbon content, micropaleontologic, and palynofacies analyses.

In the study sections the LPE is represented by dark grey, brown-grey, or black, occasionally glauconitic, non-calcareous mudstone, often with relatively high organic matter contents. Geochemical proxies indicate that during deposition of these lithologies siliceous microbiota were the dominant primary producers in the overlying surface ocean waters, suggesting a period of cooling and enhanced upwelling occurred at the time. Additionally, relative sea-level curves formulated for the studied sections through the Paleocene show three falls in sea level, the

last of which coincides with the LPE. The relative sea-level curves are considered to represent eustatic changes in sea level and thus the fall that coincides with the LPE may record development of continental ice on Antarctica. The two interpreted falls in sea level prior to the LPE are also commonly associated with dominantly siliceous productivity and may record precursor cooling events. The occurrence of possible "dropstones" in Early to Late Paleocene strata at one section may also record fluctuations between glacial and interglacial conditions prior to, and possibly within, the LPE. There is presently inconclusive evidence for the Akitio River section recording the Early Oligocene Marshall Unconformity, but the glaucony bearing unit that has been suggested to mark the event is similar to some LPE lithofacies and is associated with an episode of increased biosiliceous productivity, supportive of climate cooling. Collectively these features suggest that the LPE may be associated with marked cooling and continental ice development on Antarctica, well before the circum-Antarctic seaway had widened sufficiently to allow thermal isolation of the Antarctic continent. This suggests that Antarctic ice sheet growth is less reliant on ocean heat transport than currently believed, and other mechanisms, such as draw down of atmospheric CO_2, may also be involved.

Other results from this study of less relevance to early Paleogene marine climate but of interest to general eastern North Island geology include the possible identification of Awhea Formation and Waipawa Formation at the Pahaoa coastal section in Wairarapa; interpretations of the depositional environments for the lithofacies in the study sections, involving dominantly hemipelagic upper to lower slope mudstone with occasional mass emplaced sandstone and pelagic limestone deposits; a suggested mechanism that led to organic matter enrichment in the Waipawa Formation; a possible explanation for the lateral transition of thick deposits of organic rich mudstone to relatively thin deposits of greensand and glauconitic mudstone; possible explanations for lateral variations in redox conditions; the possible correlation of an Early Eocene olistrostromic unit at Pahaoa with an olistrostomic unit farther south, suggestive of a major tectonic episode; and confirmation of an anomalous trend, noted by previous studies on several Paleocene-Eocene sections, within the Wanstead Formation of increasing terrigenous sediment input during a transgressive period.

ACKNOWLEDGEMENTS

Firstly, I thank my supervisors Cam Nelson (Department of Earth and Ocean Sciences, University of Waikato) and Chris Hollis (GNS, Lower Hutt) for their interest, enthusiasm, guidance, and advice with regard to this project. Thank you also to Cam for your field help, constructive criticism, editing of chapter drafts, and encouragement throughout the production of this thesis. It is greatly appreciated.

I thank GNS (Lower Hutt) staff Joe Prebble for undertaking this studies palynofacies analysis; Denise Kulhanek for calcareous nannofossil biostratigraphic assessment; Hugh Morgans for foraminiferal biostratigraphic and paleoecological assessment, for providing access to unpublished data, and for assistance and advice with field work; and Poul Schiøler for your assistance in the field. Thank you to University of Waikato staff Steve Hood, Renat Radosinsky, Jacinta Parenzee, Annette Rodgers, Roger Briggs, and Indar Singh for assistance and advice with laboratory work. I would also like to thank Deborah Davy for her assistance with field and laboratory work. A big thank you to Carrie Hopkirk and Glen Treweek for devoting their time to help me in the field.

I would like to acknowledge Shaun Morgans, Brian Hales, Bernie Dowrick, Simon Hall, Justin Bell, and Jeanne Diederich for providing access to the study sections. I would also like to thank Pete Shaw and Barry Crene for hosting the research team on the Maungataniwha Forest field trip.

Thank you to my family and friends for your support, encouragement, and occasional distraction from thesis work. Particularly everyone in the office, Sean, Simon, Josh, Anna, Megan, Kirsty, and Karl; Shaun, Richard, and the rest of the Gizzy crew; Carrie for all your help, especially towards the end; and Mum and Dad for your guidance, support, and encouragement.

I wish to acknowledge a University of Waikato Masters Research Scholarship and The Royal Society of New Zealand Marsden Fund for providing funding assistance for this study.

I also acknowledge the assistance of Dr Frank Chanier (Processus et Bilans des Domaines Sédimentaires, Université des Sciences et Technologies de Lille, France) in both directing my attention to the existence of the early Paleogene section at Pahaoa and providing me with general geological information about the section.

TABLE OF CONTENTS

LIST OF FIGURES

Chapter 9 –Akitio River

Chapter 10 -Discussion

LIST OF TABLES

Chapter 1
INTRODUCTION

1.1 Introduction

This thesis study forms part of a larger research project tasked with investigating the rock record for the possible occurrence of a marked cooling in New Zealand climate in the Late Paleocene (early Paleogene, c. 58 Ma). That project, titled "Ice in the Greenhouse: a Paleocene record of Antarctic deep-water flow", is a Marsden funded one led by Dr Chris Hollis at GNS Science (Lower Hutt). Any cooling at this time, traditionally viewed as a time of global warmth in an ice-free world, has implications for the possible build up, extent, and stability of ice sheets on Antarctica during the Paleocene.

This chapter gives a brief description of Paleogene climate and climate drivers, the current state of thought regarding the cause of climate change in the Paleogene, and examples of research that challenges this view. Also addressed are the aims and structure of this thesis. The in text use of official and unofficial epoch and New Zealand stage subdivisions are defined in Appendix A.

1.2 Paleogene climate

Late Cretaceous to early Paleogene climate was significantly warmer by 6-7°C compared to today (Barrett et al., 2009). Ice sheets during this period are considered to be have been absent or of small size, ephemeral, and confined to the interior of Antarctica, while atmospheric CO_2 levels were several times higher than present (Fig. 1.1; Barrett et al., 2009). Earth at this time is considered to have been a 'greenhouse world'. The Tasmanian gateway between Antarctica and Australia was closed to deep sea circulation through this period ensuring a thermal connection between these continents that purportedly limited any significant cooling of the Antarctic continent (Fig. 1.1B; Nelson and Cooke, 2001).

The early Paleogene included two periods of extreme warmth at the Paleocene-Eocene transition (c. 55 Ma) and in the Early Eocene (c. 52-50 Ma), known respectively as the Paleocene-Eocene Thermal Maximum (PETM) and the Early

Eocene Climatic Optimum (EECO) (Fig. 1.1C), the warmest climate intervals in the last 65 million years (Crouch, 2001).

By the late Paleogene (Oligocene) the world is considered to have been in a transitional state ("doubthouse world") between the warm greenhouse conditions described above to the "icehouse world" characterising most of the Neogene through to the present day (Fig. 1.1C; Crouch, 2001; Barrett, 2003).

"Greenhouse" conditions proper are regarded as ending in the latest Eocene/earliest Oligocene when the circum-Antarctic seaway between Antarctica and Australia had widened sufficiently to allow thermal isolation of the Antarctic continent and cool surface currents to develop, and consequently the expansion of developing ice sheets to sea level (Fig. 1.1A, C; Nelson and Cooke, 2001; Barrett, 2003; Smith and Pickering, 2003). As a result, Antarctica cooled and there was a change in ocean circulation patterns that encouraged global climate to cool. Invigorated Southern Ocean circulation patterns have been deemed responsible for formation of the Marshall Unconformity (or Marshall Paraconformity; 32-29 Ma), a prominent hiatus in many Early Oligocene sedimentary sections in the wider New Zealand region, through sediment starvation and/or erosion of the seafloor (Fig. 1.1A, C; Carter and Landis, 1972; Nelson et al., 2004).

What followed was a period of oscillatory, unstable ice sheets in Antarctica, with permanent ice sheets and a true "icehouse world" being established by the middle Miocene (Fig. 1.1C; Barrett, 2003).

1.3 Climate variation, causes and controversies

There are a number of processes that influence Earth's climate (Table 1.1). Different researchers place different weightings to the importance of each of these processes. Zachos et al. (2001) placed emphasis on tectonic processes, which control very long time scale mean global climate, and Earth's orbital parameters (Milankovitch mechanisms) which affect climate at shorter time scales (Table 1.1). Smith and Pickering (2003) placed most emphasis on tectonic processes,

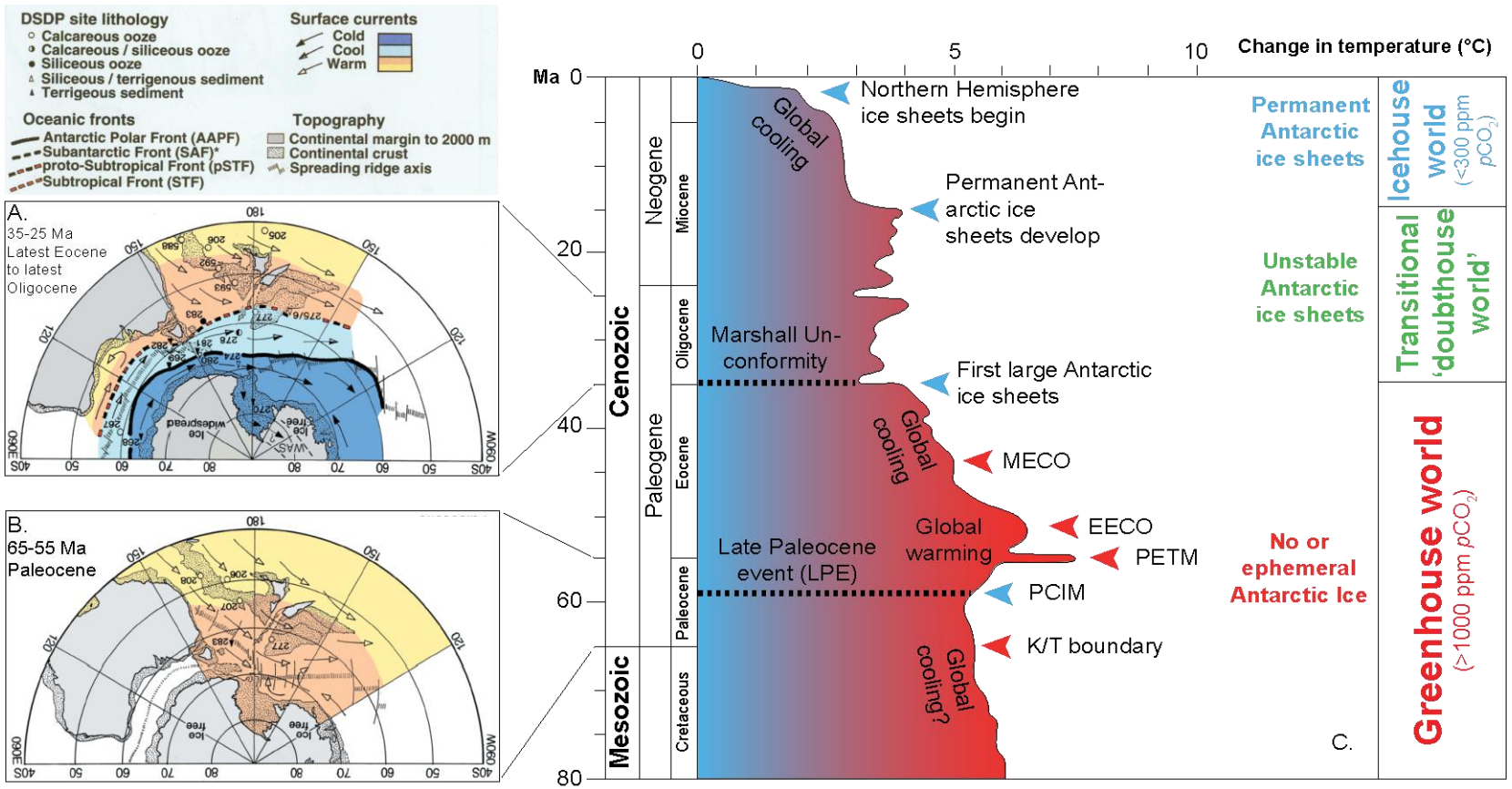

Figure 1.1: Generalised maps of the southwest Pacific circulation patterns and ocean fronts in the Oligocene (A) and the Paleocene (B) (after Nelson and Cooke, 2001) illustrating the role that the opening of the circum-Antarctic seaway had on global climate (C) (after Barrett, 2003). Climate related events are indicated on (C), with the event of interest for this study being the Paleocene Unconformity. K/T boundary = Cretaceous-Tertiary boundary; PCIM = Paleocene carbon isotope maximum; PETM = Paleocene-Eocene thermal maximum; EECO = early Eocene climatic optimum; MECO = middle Eocene climatic optimum.

Table 1.1: Comments on some of the components that influence Earth's climate.

Climate influencing component	Description
Solar output (Salinger, 2001)	Recent models assume that the sun's luminosity varies over several million years. This variation may account for long-term shifts in global climate (Salinger, 2001).
Extraterrestrial impacts (Morrow et al., 1995; Vonhof et al., 2000)	It has been proposed that the impact of extraterrestrial objects (e.g. meteorites) with Earth can cause climate cooling through blocking of sun light by dust, shock formation of NO_x, and the injection of SO_2 into the atmosphere (Vonhof et al., 2000).
Earths orbital parameters (Coe, 2003; Morrow et al., 1995; Salinger, 2001; Zachos et al., 2001)	The latitudinal and seasonal distribution of solar radiation received by the Earth's surface changes due to astronomical variations known as the Milankovitch mechanisms (Salinger, 2001). The variation encourages changes in climate (Coe, 2001). There are three Milankovitch mechanisms, eccentricity, obliquity, and precession (Salinger, 2001). Eccentricity describes the change in the shape of the Earth's orbit around the sun from an ellipse to a circle and back again, with a 95 ka, 123 ka, and 413 ka cyclicity (Coe, 2003). Obliquity is the change in tilt of the Earth's axis relative to its orbital plane around the sun every 41 ka (Coe, 2003). Precession is the wobble of the Earth about its axis of rotation and of the Earth's orbit around the sun (Coe, 2003). The motion is similar to the gyrations of a spinning top, and together these two motions give a mean cycle of 21 ka (Coe, 2003).
Tectonic processes (Smith and Pickering 2003; Morrow et al., 1995; Zachos et al., 2001)	Plate tectonics has been implicated as causing shifts in climate through changes in ocean circulation patterns due to opening and closing of oceanic gateways (Zachos et al., 2001; Smith and Pickering, 2003; Lyle et al., 2008), injection of large amounts of greenhouse gases into the atmosphere as a result of large scale volcanism (Planke et al., 2009), and orogenesis (Morrow et al., 1995). These processes operate on million-year time scales (Zachos et al., 2001).
Massive regional submarine slope failures (Katz et al., 1999)	A massive submarine slope failure has been suggested as the mechanism that caused the possible dissociation of seafloor gas hydrates and a massive injection of methane into the atmosphere, producing the PETM (Katz et al., 1999).
Cryosphere (Salinger, 2001)	Expansion and reduction in the size of continental ice sheets affects the planetary albedo, and consequently influences climate (Salinger, 2001).
Atmospheric composition (Salinger, 2001)	Some outgoing infrared radiation emitted by the Earth is trapped by greenhouse gases in the Earth's atmosphere and then re-emitted in all directions (Salinger, 2001). The process warms the lower atmosphere and the surface of the Earth (Salinger 2001). Consequently, the concentration of greenhouse gases in the atmosphere changes the efficiency with which the Earth cools to space, which in turn causes climate variation. Atmospheric composition is influenced by many of the components listed above.

specifically the opening and closing of oceanic gateways, but also cite Milankovitch-beat processes as being important once continental configurations and gateways are established. Other authors place little emphasis on the opening and closing of oceanic gateways but do recognise that ocean currents are an important mechanism affecting climate variation (Salinger, 2001).

The commonly accepted theory for the late Paleogene transition from a "greenhouse world" to an "icehouse world", as described in the preceding section, is for Antarctic ice sheets to have first developed in the latest Eocene/earliest Oligocene due to sufficient opening of the Tasmanian gateway - a tectonic process (Table 1.1). In this scenario Antarctic ice sheet stability is controlled by ocean heat transport. However, a number of recent studies have challenged this hypothesis.

A climate model developed by DeConto and Pollard (2003) suggests that atmospheric CO_2 is the primary factor controlling Antarctic ice sheet stability. Additionally, near freezing temperatures are suggested to have occurred in the Arctic during the Paleocene (Spielhagen and Tripati, 2009) and other research has suggested that there may have been short periods of significant Antarctic cooling or glaciation as early as the Late Paleocene (c. 58-57 Ma) (Leckie et al., 1995, Schioler et al., 2010, Andrew, 2010). This is within the domain of the "greenhouse world", in the same period as the Paleocene Carbon Isotope Maximum (PCIM) (Fig 1.1C) - a period inferred to record increased burial of carbon - and well prior to opening of the circum-Antarctic seaway. Glaciation at this time is a controversial inference because the period is considered to have been mostly free of polar ice and it suggests that Antarctic ice sheet development would be less reliant on ocean heat transport than is currently believed.

The interval of interest in this study – the aforementioned period of inferred climate cooling in the Late Paleocene at c. 58-57 Ma – is referred to in this thesis as the "Late Paleocene event" (LPE; Fig. 1.1).

1.4 Thesis aims

During the Paleocene the New Zealand region was a passive margin and was

situated closer to Antarctica (Field et al., 1997; Crampton et al., 2003). Consequently it is possible that New Zealand's marine sedimentary deposits hold some record of Antarctic climate at the time. This study aims to utilise these records in an investigation into the possibility of a late Paleocene Antarctic glaciation.

Specific aims of this thesis include:

1) Complete a detailed sedimentological study of four key early Paleogene sections in eastern North Island, New Zealand.

2) Undertake petrographic analysis of the various lithologies represented in the study sections.

3) Based on the sedimentological, petrographic, and geochemical characteristics, establish a lithofacies classification for the sedimentary deposits.

4) Use this information along with micropalaeontological and palynofacies data to:
   (a) Interpret the depositional paleoenvironment of each lithofacies.
   (b) Identify local and regional trends for paleoproxies for ocean productivity, bottom water redox conditions, terrigenous sediment supply, organic rich lithologies, glaucony, and the proximity to the shoreline through the period of interest.
   (c) Determine relative sea level fluctuations through this time.

5) Undertake a detailed sedimentological study of a possible occurrence of the Marshall Unconformity – a late Paleogene hiatus formed in association with known climate cooling (see Section 1.2) – in an eastern North Island section with the aim of comparing data from the unconformity with data from the early Paleogene study sections.

6) Relate findings to the wider southwest Pacific Ocean climate during the Paleocene and the ice budget history of Antarctica at this time.

Andrew (2010) investigated Late Paleocene climate from sedimentary successions in Marlborough in the South Island and on Campbell Island to the south of New Zealand using similar investigative techniques as employed here, and is a companion thesis to this work.

1.5 Thesis structure

Chapter 1 – Introduction

This chapter introduces the thesis topic, gives a brief description of Paleogene climate, climate drivers, and controversies, and describes the relevance of this research in seeking evidence in the rock record for cold climate episodes in an otherwise early Paleogene "greenhouse world".

Chapter 2 – Geological setting of study area

The study area and specific localities are introduced. The geological setting of the area is outlined with specific reference to the tectonic development of New Zealand through the Late Cretaceous-Paleogene, and a brief description of relevant formations in the region is given.

Chapter 3 – Methods

Field and laboratory methods used in this study are described.

Chapter 4 – Lithotypes and lithofacies of the study area

This chapter introduces the lithotypes and lithofacies categories used in this study, gives a broad description of individual lithofacies, and provides explanation for the use of some terms.

Chapters 5 to 8 – Early Paleogene section results

Chapters 5 to 8 present for each of the early Paleogene study sections their stratigraphy, detailed stratigraphic columns and sedimentologic characteristics, the petrography and mineral attributes of the lithofacies present, the geochemical composition (major and trace elements, stable oxygen and carbon values of

carbonate fraction, organic carbon content and stable isotope composition), and selected microfossil and/or palynofacies information. Each chapter is devoted to one section.

Chapter 5 – Pahaoa

Chapter 6 – Angora Road

Chapter 7 – Tawanui

Chapter 8 – Lower Mangahouanga Stream

Chapter 9 – Late Paleogene section results - Akitio River

The same kinds of field and laboratory properties mentioned for Chapters 5 to 8 above are provided for a small portion of the Akitio River section studied. This section is of late Paleogene (Late Eocene/Early Oligocene) age and records a possible occurrence of the aforementioned Marshall Unconformity (see Section 1.2 and thesis aim number 5).

Chapter 10 – Discussion

The results from Chapters 5 to 9 are discussed and interpreted in this chapter. The first part of the chapter discusses results from the study that are significant to general eastern North Island geology, with the second part of the chapter devoted to discussing results directly relevant to the "Ice in the Greenhouse" project. The implications of the results to the "Ice in the Greenhouse" project are considered and some general conclusions drawn.

Chapter 11 – Conclusions

This chapter summarises the main outcomes of this study.

Appendix A – Geological timescale

Appendix B – Stratigraphic column key

Appendix C – Pahaoa detailed stratigraphic columns

Appendix D – Angora Road detailed stratigraphic columns

Appendix E – Tawanui detailed stratigraphic columns

Appendix F – Lower Mangahouanga Stream stratigraphic column

Appendix G – Akitio River stratigraphic column

Appendix H – Udden-Wentworth grain-size scale

Appendix I – XRD intensity-concentration plots

Digital Appendix J – Scanned sample images

Digital Appendix K – Micropaleontologic data

Digital Appendix L – Palynofacies counts data

Digital Appendix M – Geochemical data

Digital Appendix N – Laser diffraction particle size data

Digital Appendix 0 – Petrographic data

Digital Appendix P – XRD data

Chapter 2
GEOLOGICAL SETTING OF STUDY AREA

2.1 Study area

The study area is in eastern North Island, New Zealand, extending from northern Hawke's Bay south into Wairarapa (Fig. 2.1 and 2.2). The research focuses on five sections involving mainly Paleocene-Eocene strata, but one with Oligocene deposits: one of these are located in northern Hawke's Bay (Lower Mangahouanga Stream), three in southern Hawke's Bay (Tawanui, Akitio River, Angora Road), and one in Wairarapa (Pahaoa) (Fig. 2.2). All sections are within the wider East Coast Basin, a Late Cretaceous-Cenozoic sedimentary basin encompassing eastern North Island and northeastern South Island (Fig. 2.1).

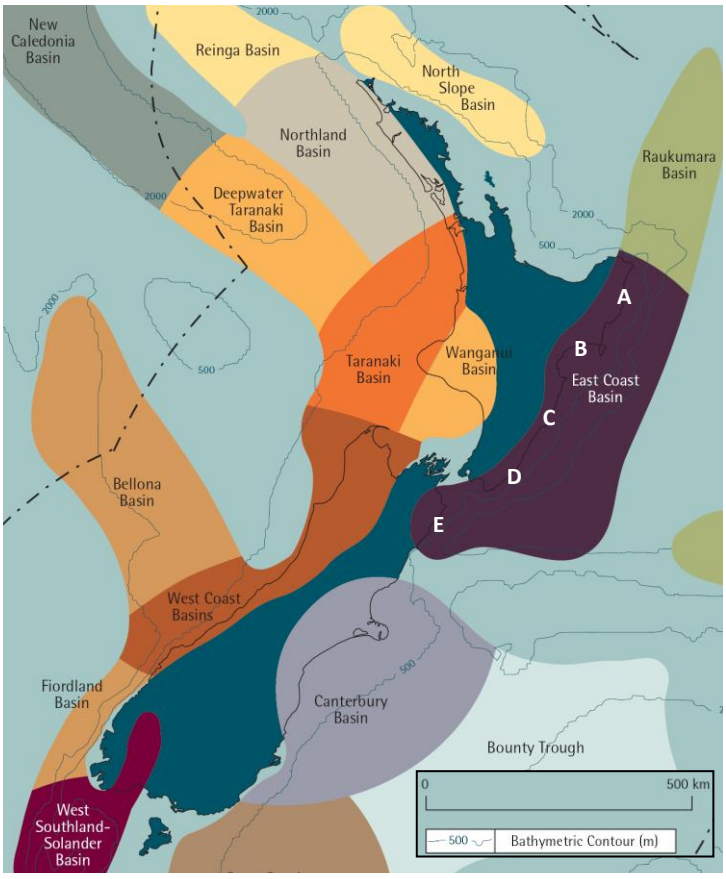

Figure 2.1: Location of the East Coast Basin and sub-regions of the eastern North Island (modified from MED, 2003). The study area extends from northern Hawke's Bay (B) in the north to Wairarapa (D) in the south. A = Raukumara Peninsula; B = northern Hawke's Bay; C = southern Hawke's Bay; D = Wairarapa; E = Marlborough.

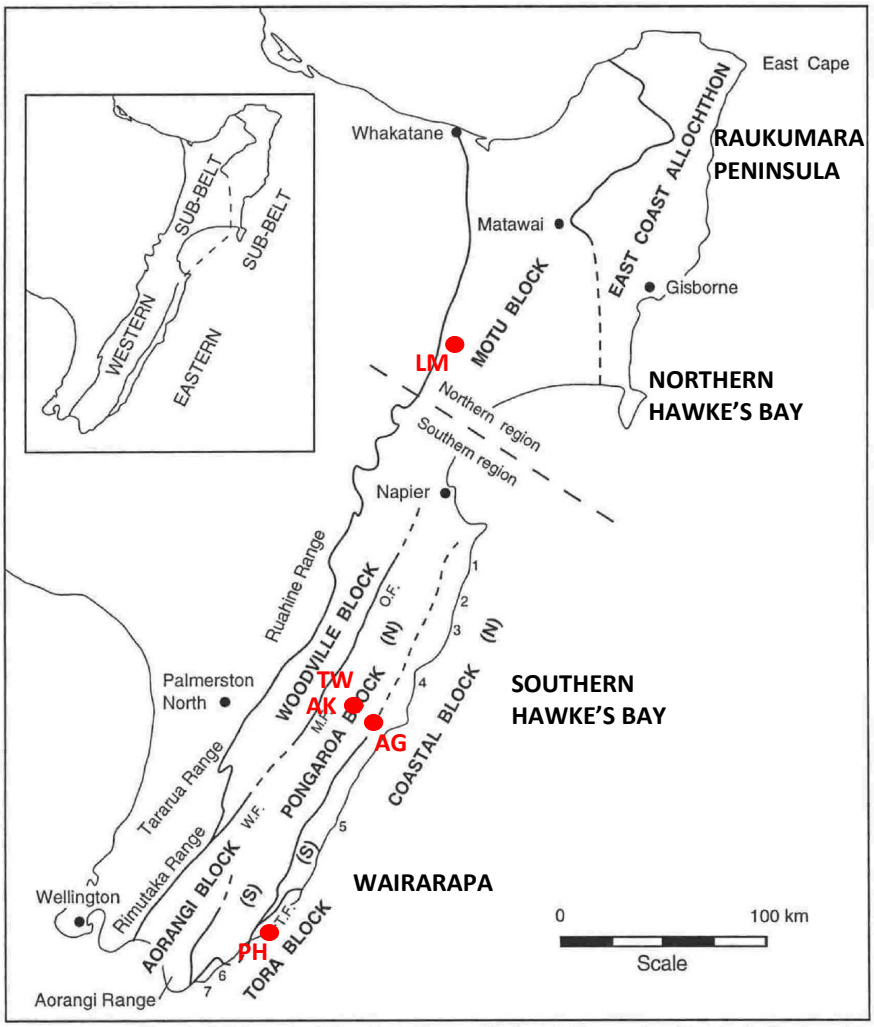

1. Waimarama Beach; 2. Mangakuri Beach; 3. Paoanui Point; 4. Porangahau Beach; 5. Castlepoint; 6. Tora; 7. Te Kaukau Point/White Rock; W.F.=Wairarapa Fault; M.F.=Makuri Fault; O.F.=Oruawharo Fault; T.F.=Tutu Fault.

Figure 2.2: Structural subdivisions and location of studied sections (large red dots) (modified from Moore, 1988). Abreviations: LM = Lower Mangahouanga Stream; TW = Tawanui; AK = Akitio River; AG = Angora Road; PH = Pahaoa.

2.2 Geological setting

Late Cretaceous-Cenozoic sedimentary successions in eastern North Island, and indeed throughout New Zealand, were deposited during a 1st order transgressive-regressive 'megasequence' that began about 100 million years ago and continues today (Fig. 2.3; King, 2000). Transgression began in the Late Cretaceous, following on from a period of uplift, exhumation and erosion of relief generated during Early Cretaceous convergent tectonics (Rangitata Orogeny) along the eastern margin of Gondwanaland (King, 2000). The transgression was initiated by intracontinental rifting during the separation of the New Zealand subcontinent (Zealandia) from Gondwanaland to initiate formation of the Tasman Sea, and

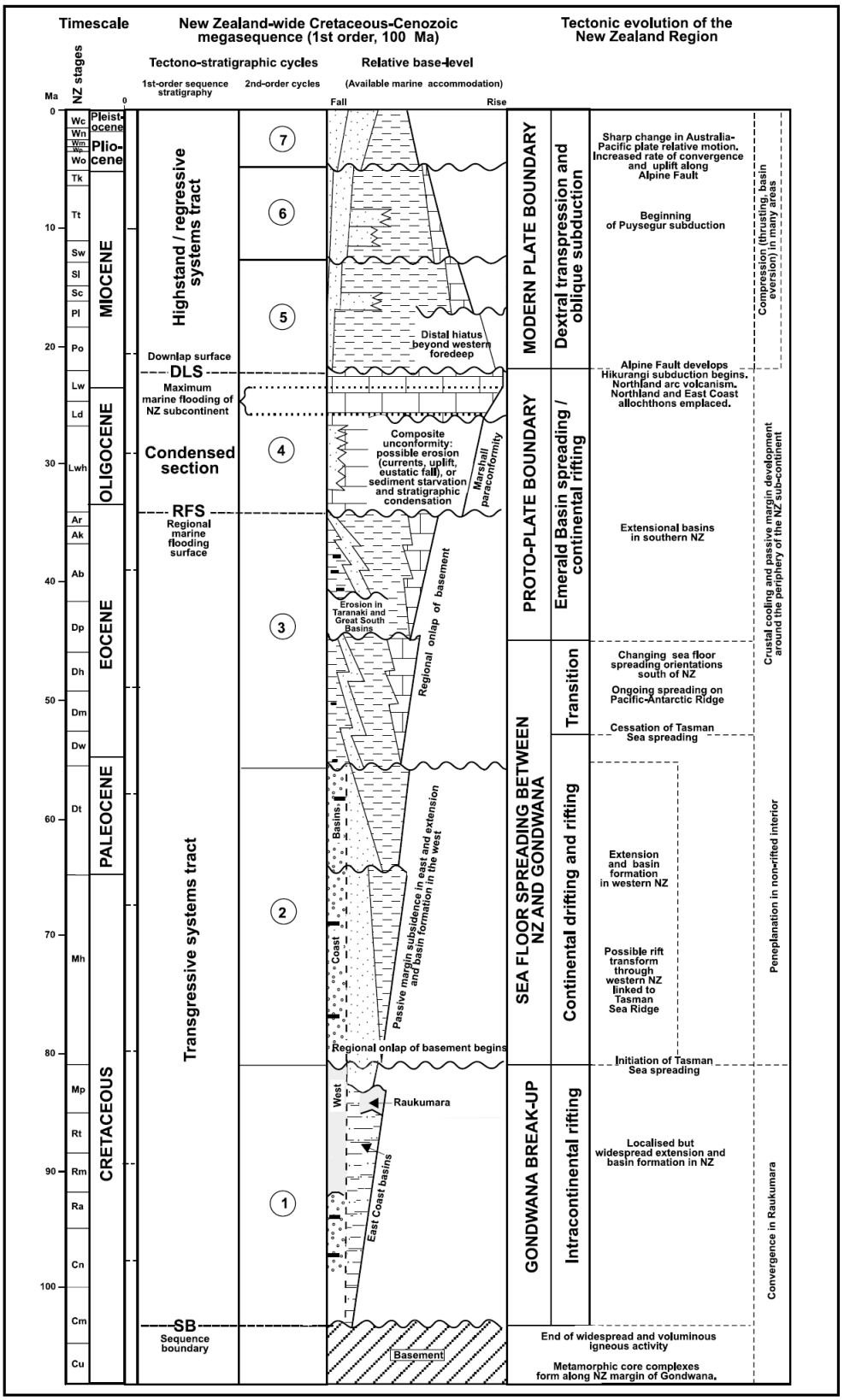

Figure 2.3: Diagram illustrating depositional trends through the New Zealand region (Zealandia) in response to 1st and 2nd order sequences (modified from King, 2000). Formations encountered in this study were deposited during the 1st order transgression and cycles 2, 3, and 4 of the 2nd order depositional cycles. New Zealand stages defined in Appendix A.

maintained by gradual submergence of Zealandia as it drifted away from Gondwanaland out into the paleo-Pacific Ocean (King, 2000). Transgression continued until the Oligocene, with regression taking over through the Neogene as a consequence of the inception and propagation of the modern plate boundary through Zealandia with its associated convergent margin orogenesis (King, 2000).

A number of tectonically controlled 2nd order depositional cycles of shorter duration (c. 10-25 m.y.) overprint the general depositional trends of the 'megasequence' (Fig. 2.3; King, 2000). The Late Cretaceous-Paleogene aged sedimentary successions encountered in this study were deposited within the 1st order 'megasequence' transgressive phase and during cycles 2, 3 and 4 of the 2nd order depositional cycles. The resulting depositional sequence is represented by six formations encountered in the field area, namely the Whangai Formation, Awhea Formation, Waipawa Formation, Kaiwhata Limestone, Wanstead Formation, and Weber Formation.

Cycles 2, 3 and 4 of the 2nd order depositional cycles are described below along with general basin wide descriptions of the formations encountered in this study that were deposited within each of the cycles. New Zealand stage abbreviations used in the text are defined in Appendix A.

2.2.1 Cycle 2 deposition

Cycle 2 deposition began with the initiation of Tasman Sea spreading and significant marine flooding in the east of the New Zealand region at c. 80 Ma (Fig. 2.3; King, 2000). Passive margin deposition developed, and by Early to "middle" Paleocene times, was prevalent throughout most of the New Zealand region (King, 2000). It was during this period that the fine siliciclastic Whangai Formation and coarser siliciclastic Awhea Formation were deposited (Field et al., 1997). By the end of the Paleocene full passive margin conditions had developed throughout the region under tectonically quiescent conditions (King, 2000). The organic matter enriched Waipawa Formation and fine grained Kaiwhata Limestone were deposited at this time (Field et al., 1997).

Whangai Formation (Mh to Dt)

The Whangai Formation is a thick, poorly bedded, bioturbated, non-calcareous to calcareous, siliceous, mudstone-dominated unit widely recognised throughout eastern New Zealand (Fig. 2.4; Killops et al., 1996; Stewart et al., 1999; Mazengarb et al., 2000). It is typically 300-500 m thick but can be up to 600 m thick (Field et al., 1997). It consists of three main members, the Rakauroa, Upper Calcareous, and Porangahau Members, and two local members, the Kirks Breccia and Te Uri Members (Moore, 1988). All of these members excepting the Kirks Breccia Member were encountered during section descriptions in the field area.

Rakauroa Member (almost entirely Mh)

The Rakauroa Member is a widespread dark grey, hard, generally poorly bedded, bioturbated, non-calcareous, micaceous mudstone, which typically forms the basal portion of the Whangai Formation (Fig. 2.4; Moore, 1988; Field et al., 1997; Stewart et al., 1999). Thin glauconitic sandstone beds, dikes, calcareous concretions, pyrite nodules, and rare chert and calcareous beds also occur within the member (Moore, 1988). Basal Rakauroa Member is often thin-bedded in eastern areas, resembling the 'zebra beds' of the Porangahau Member (Stewart et al., 1999).

Upper Calcareous Member (upper Mh to Dt in west, Dt in east)

The Upper Calcareous Member commonly overlies the Rakauroa Member (Fig. 2.4; Field et al., 1997). It is a medium grey, hard, generally poorly bedded, bioturbated, laminated, slightly to moderately calcareous, micaceous mudstone with occasional beds of glauconitic sandstone, calcareous concretions, pyrite nodules, and rare breccia (Moore, 1988; Field et al., 1997; Stewart et al., 1999).

Porangahau Member (Dt)

The Porangahau Member is present in eastern areas and is the lateral equivalent of the Upper Calcareous Member (Fig. 2.4; Field et al., 1997). It is a light grey to white, hard, well-bedded (cm-bedded), slightly to highly calcareous mudstone, with common glauconitic sandstone beds (Moore, 1988; Field et al., 1997; Stewart et al., 1999). The mudstones are often bioturbated (Moore, 1988). Thin

alternating light and darker grey mudstone layers within the member are referred to as the ‘zebra beds’ (Moore, 1988).

Te Uri Member (Dt)

The Te Uri Member disconformably overlies the Upper Calcareous Member, is more restricted in its distribution than the other Whangai Formation members, and its upper part appears to be a lateral equivalent of the Waipawa Formation (Fig. 2.4; Moore, 1988; Field et al., 1997; Stewart et al., 1999). It is a light grey, hard, bioturbated, non-calcareous to moderately calcareous, interbedded glauconitic sandstone and laminated glauconitic siltstone (Field et al., 1997, Stewart et al., 1999).

Awhea Formation (Dt)

The Awhea Formation is present in southeastern North Island in the Tora block (Fig. 2.2) where it has either a gradational, erosional, or highly burrowed basal contact with the underlying Manurewa Formation (Fig. 2.4; Laird et al., 2003). Manurewa Formation was not confidently identified during field work whereas Awhea Formation may be present at one locality; consequently only the Awhea Formation is described. Laird et al. (2003) described the base of the formation as a regularly bedded, highly bioturbated, parallel laminated, fine sandstone in some locations, and as an interbedded calcareous and glauconitic very fine sandstone and thin mudstone elsewhere. The sandstone beds are sometimes cross laminated (Laird et al., 2003). Waterhouse and Bradley (1957) described the formation as alternating blue-grey, uniform, ungraded, sandstones and black mudstones. Field et al. (1997) describe the Awhea Formation as ‘alternating cm-bedded glauconitic, fine-grained sandstone and calcareous, micaceous siltstone’.

Waipawa Formation (Middle to latest Dt)

The Waipawa Formation is widely distributed in several New Zealand sedimentary basins and conformably overlies Whangai Formation in the East Coast Basin (Fig. 2.4; Moore, 1989). Its upper contact is typically sharp (Moore, 1988). It is a dark grey-brown to brownish black, hard to moderately soft, generally poorly bedded but with some local laminations, bioturbated with common *Terebellina* tubes, non-calcareous, micaceous mudstone with occasional

calcareous concretions (Moore, 1989; Killops et al., 1996). Typically the formation has total organic carbon contents between 1.8 and 12.3%, averaging c. 6% (Moore, 1989), is enriched in ^{12}C, and has an unusually high abundance of 24-n-propylcholestanes (Hollis et al., 2005). Intervals of Whangai-like calcareous mudstone are included in the formation at some localities (Moore, 1989; Killops et al., 1996). At Mead Stream in Marlborough the Waipawa Formation consists of cm bedded, weakly laminated, grey, siliceous mudstone interbedded with fissile, laminated, dark grey to dark brown, argillaceous mudstone (Andrew, 2010).

Kaiwhata Limestone (Dt)

Kaiwhata Limestone is present in the northern Tora block (Fig. 2.2) and is considered to be a northern equivalent of the Mungaroa Formation (Fig. 2.4; Field et al., 1997). It is a cm-bedded, interbedded quartzose sandstone, glauconitic sandstone, calcareous siltstone and micritic limestone (Nelson, 1968; Field et al., 1997). The base of the formation consists of grey-green, calcareous mudstone with minor limestone (Morgans and Wilson, 1989).

2.2.2 Cycle 3 deposition

Cycle 3 began with the termination of Tasman Sea spreading in the latest Paleocene and continued to the latest Oligocene (Fig. 2.3; King, 2000). Tectonic quiescence continued on from cycle 2 and post-rift crustal cooling and passive continental margin subsidence allowed continued marine transgression (King, 2000). Extension south of New Zealand, within the Emerald Basin, began in the Middle Eocene and in the far north a subduction zone is inferred to have been extending southwards towards Zealandia (King, 2000). The fine-grained smectitic Wanstead Formation was deposited during this period of dominantly passive margin sedimentation (Field et al., 1997). The mudstones of the Weber Formation also began to be deposited in some areas towards the end of this cycle, although it was predominantly deposited during cycle 4 (Field et al., 1997).

Wanstead Formation (Dt to lower Lwh)

The Wanstead Formation is widely distributed throughout eastern North Island

and includes all fine-grained smectite-rich sediments of Paleocene-Eocene age (Fig. 2.4; Field et al., 1997). It is mostly a poorly bedded, highly bioturbated, green-grey, calcareous mudstone, but greensands, breccia and conglomeratic units, intraformational slump folding, glauconitic sandstones and mudstones, flysch facies, red, white and green-grey coloured units, and siliceous units also occur within the formation (Field et al., 1997; Mazengarb et al., 2000; Lee et al., 2002).

2.2.3 Cycle 4 deposition

Maximum submergence of the New Zealand subcontinent (Zealandia) and extensive deposition of carbonates over shallow marine platforms and in deep water occurred during cycle 4 (latest Eocene to earliest Miocene) (King, 2000). A number of unconformities formed within these deposits, possibly due to: (a) erosion by deep-sea currents that developed with the formation of the circum-Antarctic current; and/or (b) sediment starvation as sources of terrigenous material were flooded or when clastic sediments were diverted away from the depositional area; and/or (c) local tectonism associated with early stages in the development of the Australian-Pacific convergent plate boundary (King, 2000). It was during this period of maximum regional flooding, sediment erosion, and sediment starvation that the mudstones of the Weber Formation were deposited (Field et al., 1997). The Wanstead Formation continued to be deposited in some areas through the beginning of this cycle but it was predominantly deposited during cycle 3 (Field et al., 1997).

Weber Formation (Ab/Ak to Lw)

The Weber Formation occurs throughout eastern North Island except in the Tora block and is typically a moderately hard, light grey, bioturbated, calcareous, massive mudstone (Field et al., 1997). Well bedded sandstones are locally present. Four informal lithofacies are recognised within the formation, namely the glauconitic lithofacies, limestone lithofacies, flysch lithofacies, and siltstone lithofacies (Stewart et al., 1999). Only the limestone lithofacies was possibly encountered during the course of field work, and appears as a massive, hard, light grey, calcareous siltstone and muddy limestone with indistinct bedding.

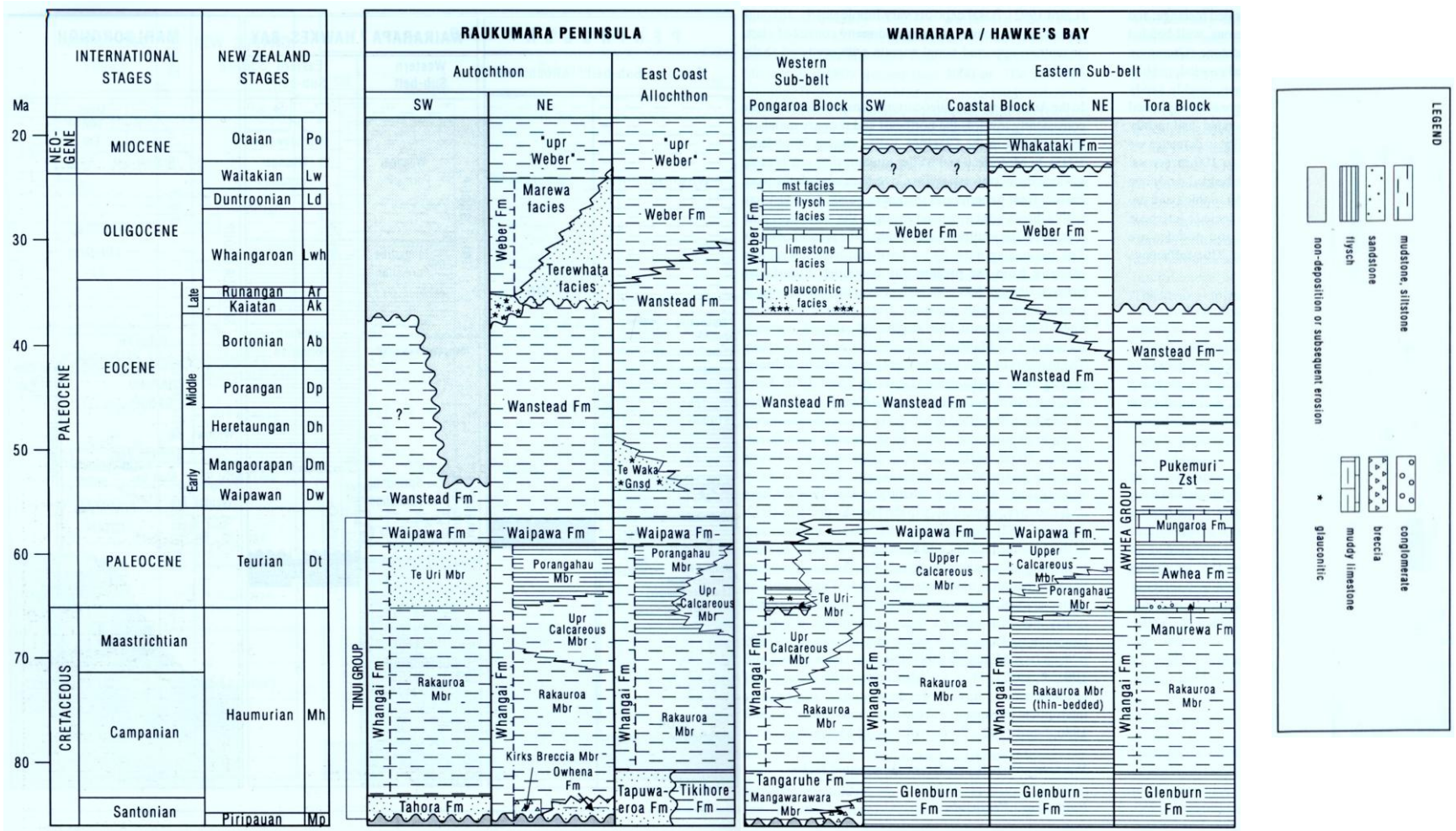

Figure 2.4: Lithostratigraphy of the study area (after Field et al., 1997). Formations shown relevant to this study are the Whangai, Awhea, Waipawa, Wanstead, and Weber Formations.

Chapter 3
METHODS

3.1 Introduction

The techniques used in this study are detailed field descriptions and sample collections of study sites, and petrographic, mineralogical, grain size, elemental, stable isotope, average percent organic carbon, micropaleontologic, and palynofacies analyses of samples (Fig. 3.1). Such a multiple technique approach was used to aid with interpretations, where comparing and contrasting results from the various techniques can help reduce the number of ways the data could be interpreted. The methods employed within these techniques and the petrographic rock classification used in this study are described briefly here.

3.2 Field work

Field work involved the detailed description and systematic sampling of several sedimentary sections. Aspects described in the field included the lithologies present, the nature of the contacts between lithologies, and bed/unit thickness. Detailed stratigraphic columns of measured sections were constructed using this information and are provided in Appendices C – G.

3.2.1 Lithology description

Specific lithologic characteristics described were rock colour when fresh and weathered, degree of induration (hardness), nature of stratification (bedding) and any other sedimentary structures (e.g. concretions, sedimentary dikes, trace fossils etc.), sediment texture and textural name (e.g. coarse sandstone), and compositional aspects such as the carbonate (using acid test) and glaucony content (after Andrews, 1982).

Strata at all the studied sections were dipping. Consequently, thickness was measured by running a tape measure along the base of the outcrop about perpendicular to strike, recording the horizontal distance, then calculating the true thickness using the dip angle and trigonometry. Where possible, the true thickness was measured directly by running a tape measure perpendicular to

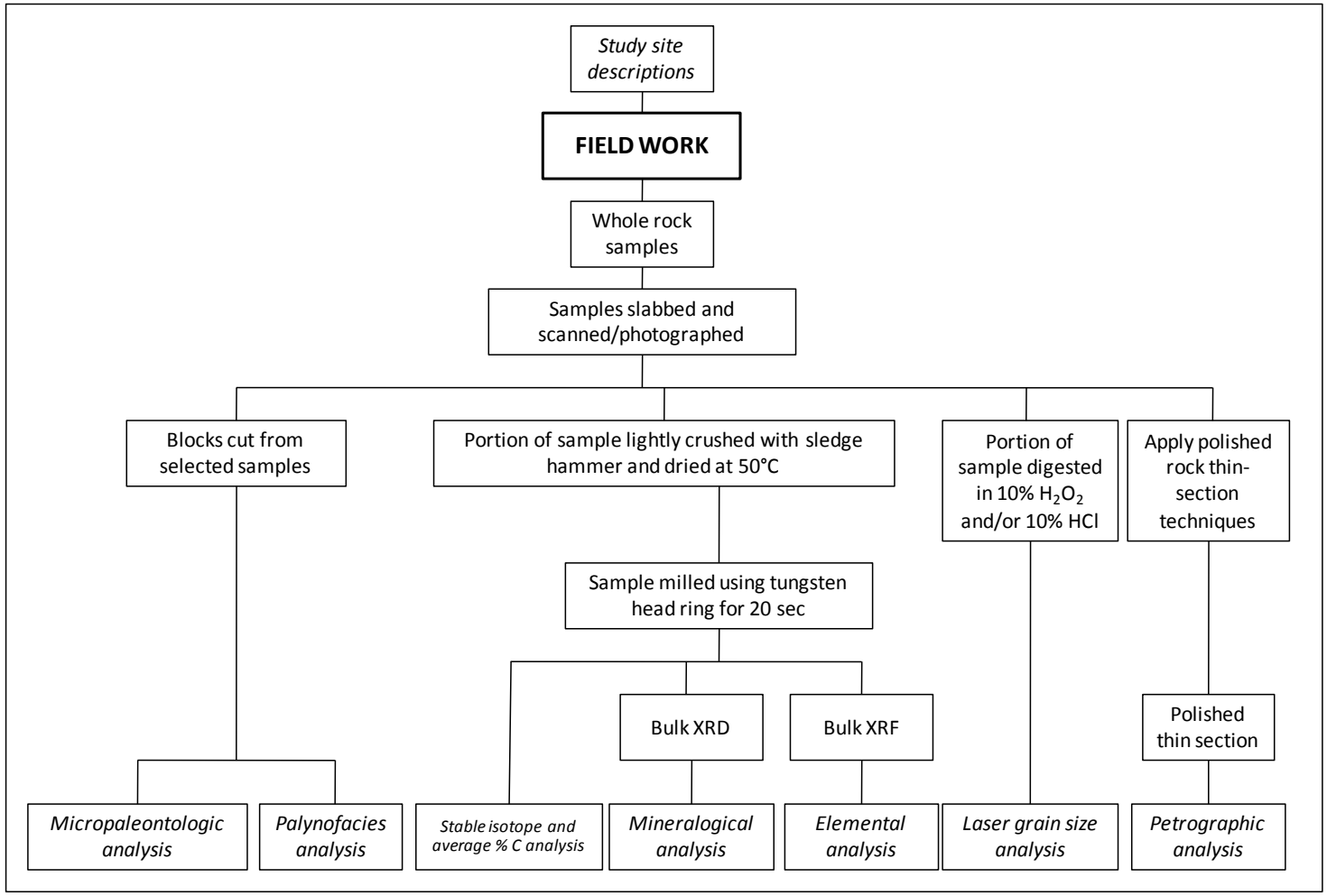

Figure 3.1: Flow chart illustrating the analyses used (italicised) and the processes involved within each analysis.

bedding or by measuring individual bed thicknesses.

A different method was used to measure the thickness of strata exposed in the quarry at the lower Angora Road because the section showed little or no bedding. A strike was obtained by lining up a similar dark horizon that was visible on both the lower and upper quarry terraces and sighting a Silva compass along this line to obtain an approximate strike (Fig. 3.2). The compass was then fixed to a Jacob staff and set up so that the point of the staff would be pointing in the direction of dip (90° to strike) when the compass bearing was with strike. The butt of the staff was placed on the face of the outcrop and positioned so that it pointed in the direction of dip, as just described (Fig. 3.3). 0.5 m or 1 m spaced points on the outcrop were found by visually sighting off the ruler on the Jacob staff along the line of strike (perpendicular to staff orientation) (Fig. 3.3). These points were marked with spray paint. The butt of the Jacob staff was then placed on the face of the outcrop at the 0.5 or 1 m mark and the process repeated to measure the next 0.5-1 m of strata. The true thickness of the strata was calculated using these measurements, the dip angle (taken from strata below the quarry and estimated from vague bedding within the quarry), and trigonometry.

Figure 3.2: Position of the dark horizon on the lower and upper terraces at the lower Angora Road quarry (5 m long Jacob staff for scale). An approximate strike for the outcrop was obtained by lining up the dark horizons and sighting a Silva compass along this line.

3.2.2 Sampling

Samples collected ranged from between one to three fists in size and, where possible, the orientation was marked on the sample with an arrow pointing in the

up-section direction. Sampling frequency depended on the nature of the strata being logged and access. In seemingly similar sections of sedimentary rock the sample spacing was in the order of two or more metres. In areas of interest or near contacts between lithologies the sample spacing was in the order of centimetres/decimetres and up to one metre. Some areas could not be sampled due to poor access. All sample positions are located on the stratigraphic columns in Appendices C – G.

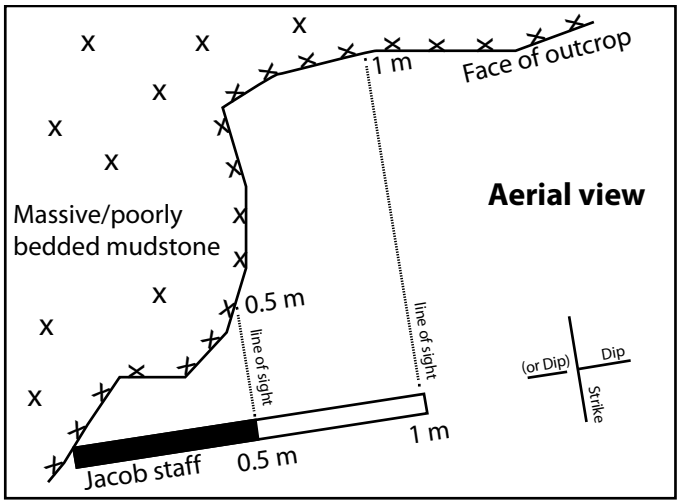

Figure 3.3: Generalised diagram illustrating how thickness measurements were made on the massive to poorly bedded strata in the Angora Road Quarry. This diagram is not specific to the Angora Road outcrop – the relation of the dip/strike direction to the orientation of the outcrop face is generalised.

3.3 Laboratory analyses

305 samples were cut into slabs and scanned to record bedding structures. A Benq S2W 4300U/3300U desktop scanner was used with a transparent sheet of plastic, similar to an overhead projector transparency, placed between the sample and the glass of the scanner to prevent scratching. Most slabs were scanned with the cut face dry but occasionally the face was dampened to better show sedimentary structures. All scanned sample images are in Digital Appendix J.

A fresh portion of rock was cut from selected slabs for micropaleontologic and palynofacies analysis. The remainder of the slab and the whole rock sample was used for petrographic, grain size, mineralogical, and elemental analysis.

The freshest representative portions of samples were used for mineralogical, elemental, average percent carbon, and stable isotope analysis and an attempt was made to remove weathered surfaces from these samples. The selected portion of sample was crushed using a sledge hammer and dried in an oven or over a hot plate at 50°C. The drying time depended on the rock type and its initial dampness and varied between a few hours to a few days. The dried sample was crushed to a fine powder in a tungsten head ring mill for 20 seconds.

Representative portions of the whole sample were selected to be made into polished thin sections and for grain size analysis.

3.3.1 Micropaleontologic analysis

Biostratigraphic age data for this study comes from micropaleontologic analysis carried out by GNS Science. A total of 37 samples were analysed and data are presented in Digital Appendix K. The following methodology was provided by D. Kulhanek.

Calcareous nannofossil samples were prepared following standard smear-slide techniques. A small amount of sediment was scraped onto a coverslip from a fresh surface of each sample using a razor blade. The sediment was mixed with a drop of distilled water and spread evenly over the coverslip, dried on a hotplate, affixed to a glass microscope slide using Norland Optical Adhesive 61, and cured under ultraviolet light.

Slides were examined at 1000x and 630x using a Leitz Ortholux II POL-BK microscope under cross-polarized and plane-transmitted light. A minimum of four coverslip traverses (approximately 800 fields of view) were observed for each slide and presence/absence data collected to document the calcareous nannofossil assemblage.

Results are correlated to the biostratigraphic zonation scheme of Martini (1971) (Appendix A). Taxonomic concepts for species are those given in Perch-Nielsen (1985) and Bown (1998).

3.3.2 Palynofacies analysis

Palynofacies analysis investigates changes in depositional environments based on the total assemblage of particulate organic matter (Tyson, 1995). Some components of terrestrially derived organic matter have a limited offshore depositional range so up section variations in the relative abundance of woody plant derived material, pollen, marine dinoflagellates, and amorphous organic matter can indicate changes in shoreline proximity relative to the site of deposition (J. Prebble, pers. comm. 2001). In this study the terms proximal and distal are used in an oceanic sense and are in relation to the shoreline of a landmass moving closer to (more proximal), or further away from (more distal) the site of deposition. In addition, preservation of the different particulate organic matter components can indicate oxidation of the water column during deposition (J. Prebble, pers. comm. 2011). The significance of the palynofacies proxies used in this study are presented in Table 3.1.

Table 3.1: Paleoenvironmental significance of palynofacies proxies used in this study (modified from Schiøler, 2010)

Proxy	Significance
Palynomorphs	Kerogen assemblages with high percentages of palynomorphs indicate an open marine, mud-dominated oxic setting.
Percent amorphous organic matter (AOM)	A high percentage of granular AOM is indicative of bottom water anoxia and is typical of a distal oceanic setting or stratified sea.
Percent phytoclasts	Assemblages heavily dominated by phytoclasts (higher land plant tissue debris) are characteristic of proximal depositional settings under strong terrestrial/freshwater influx.
Log black:brown phytoclasts	A high ratio of black to brown phytoclasts generally indicates distal depositional settings. However, the ratio may also be high in turbulent proximal settings (e.g. shoreface sands).
Log marine algae/sporomorphs	A high ratio of marine algae to sporomorphs indicates a distal oceanic setting.
Percent marine dinoflagellate cysts	Higher percentages of marine dinoflagellate cysts indicate a more distal oceanic setting.

Palynofacies analysis was carried out by GNS Science. A total of 62 samples were analysed and count data are presented in Digital Appendix L. The following methodology was provided by J. Prebble.

Samples were oven dried at 40˚C, crushed to sand size, carbonates removed by treatment in hot 30% hydrochloric acid, and silicate removed in 40% hydrofluoric acid followed by a second 30% HCl wash. Samples were then oxidised for exactly two minutes in 40% nitric acid, sieved over a 6 µm mesh, and mounted under glass cover slips in glycerine jelly. At least 300 palymorph specimens were counted per slide.

Processing and counting followed the techniques and classification system described in Schiøler et al. (2010) and included recounting seven of the samples presented in that article to achieve 'operator calibration'. Maximum offset of duplicate counts is 8%, and all duplicates fell within the same classification fields as the primary counts of the ternary "AOM-phytoclast-palynomorph" plot.

3.3.3 Stable isotope analysis and average percent organic carbon

$\delta^{18}O$, $\delta^{13}C$(carb), $\delta^{13}C$(org), and average percent organic carbon analyses were performed by GNS Science at the National Isotope Centre. 78 samples underwent $\delta^{18}O$ and $\delta^{13}C$(carb) analysis and 75 samples underwent $\delta^{13}C$(org) and average percent organic carbon analyses. These data are available in Appendix M. The following methodology was provided by A. Phillips.

Carbonate samples were analysed on the GVI IsoPrime Carbonate Preparation System at a reaction temperature of 60^{o}C and run via dual inlet on the IsoPrime mass spectrometer. All results are reported with respect to VPDB and normalized to the laboratory's internal standards (GNS marble) with reported values of 2.04‰ for $\delta^{13}C$(carb) and -6.40‰ for $\delta^{18}O$. The external precision for these measurements is 0.05‰ for $\delta^{13}C$(carb) and 0.12‰ for $\delta^{18}O$. A few samples were run in duplicate giving standard deviations from 0 – 0.15‰ for $\delta^{13}C$(carb) and 0 – 0.31‰ for $\delta^{18}O$.

Organic carbon samples were acid treated to remove carbonate and analysed on

the Europa Geo 20-20 continuous flow coupled with an elemental analyser (EA). All results for $\delta^{13}C$(org) are reported with respect to VPDB and N-Air, normalized to the laboratory's internal standards: Leucine (-22.7‰ for $\delta^{13}C$), Buffalo sediment (-19.8‰ for $\delta^{13}C$), Caffeine (-37.9‰ for $\delta^{13}C$), GNS Moa Bone (-21.0‰ for $\delta^{13}C$), and Montana soil (-17.1‰ for $\delta^{13}C$). The analytical precision for these measurements is 0.2‰ for $\delta^{13}C$(org). A few samples had analytical errors higher than usual due to their very low carbon contents (<0.05%).

The $\delta^{18}O$ signal from carbonates can be affected by burial diagenesis and interaction with pore waters (Hollis et al. 2003). Of particular relevance in this study is the finding by Nelson and Smith (1996) that the $\delta^{18}O$ values of Late Cretaceous to "early" Tertiary micritic limestones in New Zealand yield more depleted results than many other New Zealand Cenozoic limestones. This could be a function of their increased burial pressures and tectonic stresses, to their wide age range, and/or to the warmer and more $\delta^{18}O$-depleted ocean water during the Late Cretaceous-"early" Paleogene. In this study oxygen isotope data are considered on a case by case basis, where significant covariance between $\delta^{18}O$ and $\delta^{13}C$ is suggestive of diagenetic alteration of the $\delta^{18}O$ signal (Andrew, 2010). Even when there is no covariance between the carbon and oxygen signals the approach is taken of only interpreting the oxygen isotope signal in terms of its trends. Assigning temperatures to data points is avoided due to the possible depression of $\delta^{18}O$ values in rocks of Late Cretaceous-"early" Paleogene age.

Carbon isotopes are less prone to diagenetic alteration than oxygen isotopes and seem to be reliable when there is sufficient carbon within the sample to counter any diagenetic effects (Hollis et al. 2003). Following Hollis et al. (2003), carbon isotope data are considered reliable when $CaCO_3$ is greater than 5% or when organic carbon is greater than 0.05%.

3.3.4 Elemental analysis

234 samples were analysed as pressed briquettes using a Spectro X-Lab 2000 fully automated X-ray Fluorescence (XRF) spectrometer at the University of Waikato. Briquettes consisted of c. 5 g of the homogenous milled powders of samples, bound with c. 15 drops of PVA and pressed in aluminium cups.

Moderate errors (c. 5%) are associated in major element determinations using pressed briquettes and trace element determinations have variable precision, with errors of 1-5% depending on the type of element and its abundance. Major and trace element values are presented in Appendix M.

The elemental data have been used to generate paleoproxies for productivity, nutrient availability, terrigenous input, eolian sediment flux, and redox. The normative equations and background values used to estimate the components used for these paleoproxies are presented below along with a note on the use of TiO_2 as a terrigenous proxy. Excess (exc) and terrigenous sediment (TRG) equations are from Hollis et al. (2003). Enrichment factor (ef) equations are after Turgeon and Brumsack (2006). An enrichment factor of one indicates that the concentration of an element is similar to its concentration in an average shale (Andrews, 1982). Turgeon and Brumsack (2006) consider values ≥ 5 and ≤ 0.5 to indicate enrichment and depletion, respectively. The proxy values are presented in Appendix M.

Productivity proxies

Barium is often used as an indicator for surface productivity due to its association in modern oceans (in the form of barite) with sediments underlying water masses with high surface productivity (Hollis et al., 2003, Weedon and Hall, 2004). Calcium carbonate and silica can be associated with the calcareous and siliceous remains of organisms such as foraminifera and radiolarians, and consequently can be associated with productivity when other influences (terrigenous input) are taken into account. Excess barium (Ba[exc]), calcium carbonate (Ca[exc]), and silica (Si[exc]) values represent elemental levels above 'normal' detrital background and are used here as proxies for productivity (Andrew, 2010, Hollis et al., 2003). The relevant equations are:

$$Ba[exc] = Ba_{[sample]} - (TiO_{2[sample]} \times (Ba_{[background]}/TiO_{2[background]}))$$

$$Ca[exc] = CaO_{[sample]} \times 100/56 - (TiO_{2[sample]} \times (CaCO_{3[background]}/TiO_{2[background]}))$$

$$Si[exc] = SiO_{2[sample]} - (TiO_{2[sample]} \times (SiO_{2[background]}/TiO_{2[background]}))$$

Hollis et al. (2003) used TRG and the Ba/Al ratio as a test for Ba[exc] biogenic association, where a biogenic association is likely when Ba[exc] co-varies with Ba/Al and when Ba[exc] has poor correlation with TRG trends. This approach is also used in this study, however, for reasons discussed below, Ba/Ti is used instead of Ba/Al (see "The use of TiO_2 as the terrigenous proxy for normative equations"). Additionally, Ba[exc] has been used as a productivity indicator when Mo and U values indicate that the sediments were deposited under oxic conditions. When redox proxies indicate low oxygen levels during deposition other productivity proxies are used in preference to Ba[exc] (see "Uranium (U)" below).

Nutrient availability proxy

Covariance of P with productivity proxies under oxic paleoredox conditions indicates nutrient availability (Weedon and Hall, 2004). Increasing P with increasing productivity suggests increasing nutrient availability, and vice versa (Weedon and Hall, 2004). In this study the relative enrichment of P is calculated using the enrichment factor equation:

$$P[ef] = (P/Ti)_{sample} \div (P/Ti)_{average\ shale}$$

Terrigenous and aeolian sediment supply proxies

The TiO_2 background levels used in the normative equations are average shale values (see below). Terrigenous sediment (TRG) thus represents terrigenous supply relative to the average background terrigenous supply for an average shale, where a TRG value of 100% indicates a terrigenous supply similar to that of an average shale. Values above and below 100% indicate a terrigenous supply greater than and less than that of an average shale, respectively. Terrigenous supply is calculated using the following equation:

$$TRG = TiO_{2[sample]}/TiO_{2[background]} \times 100$$

Iron and potassium are important constituents within glaucony minerals (Amorosi, 2003) and are used here as proxies for the abundance of glaucony in a sample. High concentrations of glaucony can indicate low rates of sediment deposition (McRae, 1972). The relevant equations are:

$$Fe[ef] = (Fe/Ti)_{sample} \div (Fe/Ti)_{average\ shale}$$

$$K[ef] = (K/Ti)_{sample} \div (K/Ti)_{average\ shale}$$

Ti tends to become enriched in sediments when they receive increased aeolian sediment input (Sageman et al., 2003). Ti concentrations can also be elevated due to a reduction in terrigenous input coupled with a steady influx of aeolian sediment (Sageman et al., 2003). Consequently the TiO_2/Al_2O_3 (Ti/Al) ratio is used as an indicator of wind strength, or terrigenous input if the proxy does not covary with TRG. The 0.04 threshold used by Hollis et al. (2003), above which increased offshore wind or current strength may be inferred, is used as a reference point in this study.

Redox

Molybdenum becomes enriched in sediments under low oxygen and euxinic conditions (Fig. 3.4). It has been used in its raw form (Mo ppm) as an indicator of redox and euxinic conditions at the sediment-water interface at the time of sediment deposition.

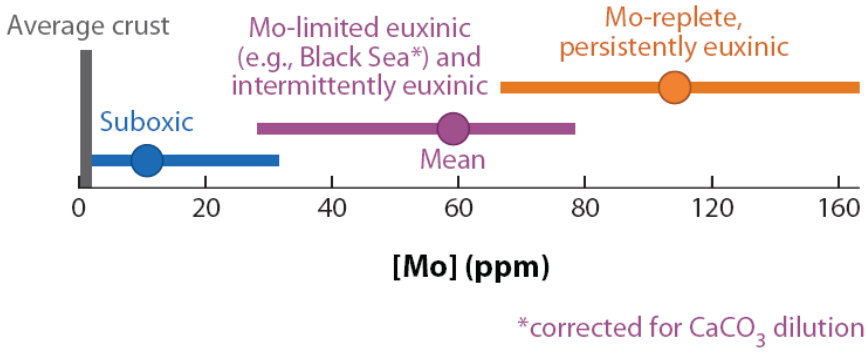

Fig. 3.4: The mean and range of molybdenum concentrations from modern oxic, suboxic, and euxinic environments (Lyons et al., 2009).

Uranium (U)

Ba preservation in marine sediments can be reduced under suboxic diagenetic conditions which are characterised by low bottom water oxygen and high organic carbon respiration rates (McManus et al., 1998). Sediments subjected to these conditions are recognisable by high U concentrations, because U becomes

insoluble in seawater under reducing conditions (McManus et al., 1998, Henderson, 2002).

Reducing conditions can be caused by high fluxes of organic material to the seafloor due to enhanced primary productivity, or low oxygen in the overlying water due to other processes, such as a stratified stagnant water column (Henderson, 2002; Werne et al., 2002). Henderson (2002) recommended that additional proxies should be used to determine which process is responsible for U enrichment. The relative enrichment of U can be calculated using the enrichment factor equation:

$$U[ef] = (U/Ti)_{sample} \div (U/Ti)_{average\ shale}$$

In this study U[ef] has been used:

1. In conjunction with Mo to determine whether Ba[exc] reflects productivity, where U and Mo enrichment indicate that it is likely that Ba is an unreliable productivity proxy (McManus et al., 1998).
2. As a productivity indicator when it co-varies with Ca[exc] and/or Si[exc].
3. As a redox indicator when it has poor correlation with Ca[exc] and Si[exc] and co-varies with Mo.

Background values

Background values used in the normative equations represent detrital background levels for the study area (Table 3.2; Andrew, 2010). TiO_2 and Ba values are average shale values (AS) from Wedepohl (1971). The SiO_2 value is from Moore (1988) and is used in preference to the average shale value of 58.9 wt% (Wedepohl, 1971) to better reflect the high silica content of the dominant Whangai Lithofacies in the study area. The $CaCO_3$ value is from Hollis et al. (2003).

Table 3.2: Estimated background values for TiO_2, SiO_2, Ba, and $CaCO_3$ for the study area (‡Hollis et al. 2003; †Moore, 1988; *Wedepohl, 1971).

TiO_2 (wt%)	Minimum $CaCO_3$-free SiO_2 (wt%)	Ba (ppm)	Minimum $CaCO_3$ (wt%)
0.78*	73†	580*	0.2‡

The use of TiO_2 as the terrigenous proxy for normative equations

TiO_2 has been used as the terrigenous proxy in all normative equations because samples of limestone and calcareous mudstone from the Pahaoa section have excess Al values. This implies that there is a scavenged component of Al in these lithologies and consequently Al is an unsuitable terrigenous proxy for this locality. Although there were few excess Al values from any of the other sections, TiO_2 has been used as the terrigenous proxy throughout the study area for ease of comparison between localities and to maintain consistency. Correlation between Al and Ti is very good (r^2 values of 0.94 – 0.98) in the sections studied therefore TiO_2 is considered to be an appropriate terrigenous proxy for the study area.

3.3.5 Laser diffraction particle size analysis

Disaggregation of samples prior to grain size analysis followed the basic theory of ultrasonic disaggregation of shale used by Gipson (1963). Sonicator equipment and chemicals used for digestion and disaggregation differ in this study but perform the same task. Detailed grain size data were acquired for 26 samples and are recorded in Digital Appendix N. The Udden-Wentworth grain-size scale was used to classify sediment size (see Appendix H).

Samples were crushed into chips c. 5 mm to > 2 mm in size with a sledge hammer. For calcareous samples about one level teaspoon of chips was immersed in 10% HCl in a small beaker and allowed to digest. Occasionally the chips were gently crushed with a stirring rod to aid disaggregation. Once the reaction in HCl had ceased fresh HCl was added and the sample placed in a sonicator (Astrason Ultrasonic Cleaner) for 15 min to further aid disaggregation. If the sample continued to react with acid following sonification, then the reaction was allowed to finish and the process repeated until there was no further reaction after sonification. Occasionally the sediment was allowed to settle overnight allowing the old acid to be siphoned out of the beaker and replaced with fresh acid.

For non-calcareous samples the process was the same except 10% H_2O_2 was used instead of HCl and old H_2O_2 was evaporated off by heating the solution to 60 – 70°C on a hotplate. Heating also sped up the reaction.

A few calcareous samples that were suspected to also have organic matter cementing grains together underwent both treatments.

Once sufficiently disaggregated, any undigested chips were removed from the beaker and the grain size distribution of the remaining sediment was determined using a Malvern Mastersizer 'S' laser diffraction particle size analyser. The data were scrutinised and obvious outlier (large) grain sizes that did not fit in with the typical modal or bimodal grain size distribution were discounted as it was likely that they were chips that had not fully disaggregated. Comparisons with grain size data obtained from petrography mainly showed good agreement. Where disagreement occurred it related to maximum grain size. The assumption was made that partially disaggregated chips were the cause of this disagreement and the conflicting grain sizes were discounted from the laser results.

3.3.6 Petrographic analysis

76 polished thin sections were analysed using an Olympus AX70 petrographic microscope. Digital images were taken using a Nikon Digital Camera DXM1200. The maximum and modal grain sizes, sorting, and shape were recorded separately for the clastic, glauconite, and skeletal components in each thin section. The percent gravel, sand, mud, and the mineralogy of the clastic portion of the thin section was recorded, as well as the percent glauconite and skeletal material and the type of skeletal material. The abundance of the clastic components was recorded through the textural name given to the sample and percent abundances of the chemical components were recorded using semi-quantitative abundance limits (see Section 3.4, 'Rock classification'). Petrographic data are provided in Digital Appendix O.

3.3.7 Mineralogical analysis

Mineralogy was determined with unorientated milled samples analysed by a Philips (XPERT) X-ray diffraction (XRD) system with nickel-filtered copper radiation. X-ray diffraction peaks were identified using the mineral powder diffraction data book (JCPDS, 1980). 63 samples were analysed by XRD and the data are available in Digital Appendix P.

Nelson and Cochrane (1970) used XRD data to produce intensity-concentration plots for some common minerals in their sedimentary rock samples. The intensity-concentration plots were used to determine mineral weight percents from certain peak heights. XRD data in this study are used in a similar fashion. The samples used by Nelson and Cochrane (1970) were used on an earlier XRD machine at the University of Waikato to produce intensity-concentration plots for quartz, plagioclase, potash feldspar, calcite, and clay minerals. However, it was found that the plots made for the earlier XRD machine are specific only to that machine. Consequently the plots could not be used directly in this study to semi-quantitatively determine mineral abundance, but were instead used in an indirect way. The 4.26Å quartz peak, 3.20Å plagioclase peak, 3.25Å potash feldspar peak, 4.46Å total clay minerals peak, and 3.04Å calcite peak were used for this analysis (Fig. 3.5). Peak heights are given in counts (cts).

1. The intensity-concentration plots for the earlier University of Waikato XRD machine (Appendix I) were used to find the height of each mineral's XRD peak at a set weight percent. From these values the peak height ratios between each mineral was calculated by dividing the peak heights by one another. The ratios describe how high a minerals peak height must be, relative to another minerals peak height, in order for both minerals to have the same weight percent. For example, the quartz : plagioclase peak height ratio was found to be 0.48. This means that the quartz peak height must be about 48% of the plagioclase peak height for them to have equal weight percents.

2. With relation to peak heights from samples analysed in this study, the quartz, potash feldspar, plagioclase, and clay mineral peaks were divided by one another to find the ratios between the minerals. The ratios describe how large peaks are relative to one another. For example, the quartz : plagioclase peak height ratio for sample MT1.14 was found to be 0.96 (499 cts (quartz) ÷ 522 cts (plagioclase) = 0.96; Fig. 3.5). This means that the quartz peak height is 96% the height of the plagioclase peak height.

3. The ratio from step 2 was divided by its corresponding ratio from step 1 (quartz : plagioclase from step 2 ÷ quatz : plagioclase from step 1). The resulting value describes the relative weight percents of the two minerals involved in the ratio. For example, for sample MT1.14 the resulting value for a quartz : plagioclase ratio was found to be 2 (0.96 ÷ 0.48 = 2). This means that there is double the weight percent of quartz in the sample compared to plagioclase.

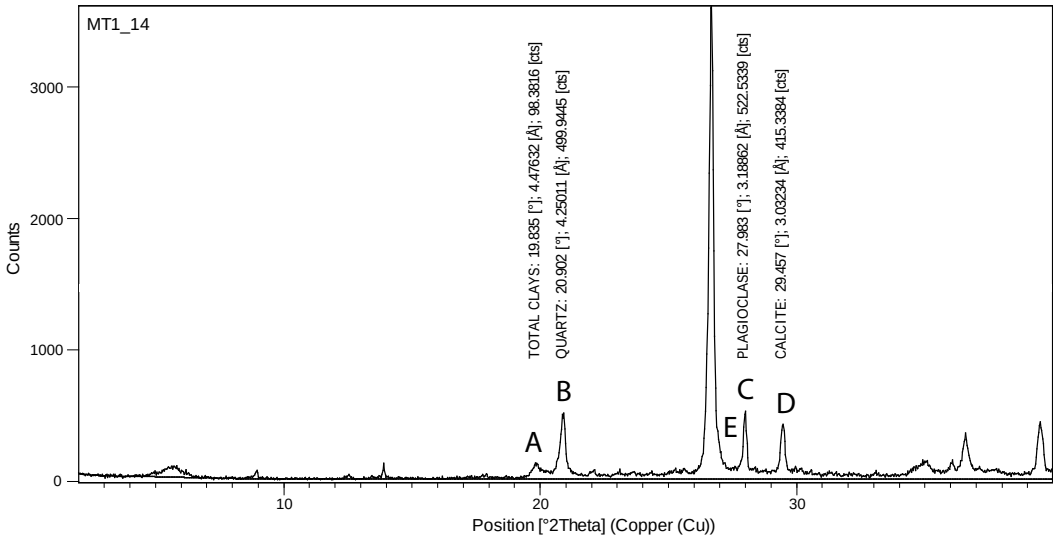

Fig. 3.5: Mineral peaks for sample MT1.14 showing the location of the total clays (A), quartz (B), plagioclase (C), and calcite peaks (D) used for semi-quantitative analysis. A potash feldspar peak is not evident in this sample but would be located at 3.25Å, or approximately 27.5°2θ (E).

4. In order to convert the relative weight percents from step 3 into semi-quantitative weight percents, the assumption was made that the height of the quartz peak from the pure quartz standard is equal to a quartz weight percent of 100. This assumption meant that the quartz standard peak could be used like a ruler, with quartz peak heights from samples being measured against it, since its height was of a known weight percent (Fig. 3.6). In practice the quartz heights from samples were divided by the quartz standard peak height and multiplied by 100. The resulting value is the total weight percent of quartz in the sample. Continuing with the MT1.14 example, the sample's quartz peak height (499 cts) divided by the standards peak height (1643 cts) and multiplied by 100 gives a value of 30, or 30 weight percent quartz in the sample (Fig. 3.6).

5. The weight percent quartz values were then used in conjunction with the relative weight percent ratios, from step 3, to determine the total weight percents of the other minerals. For example, in step 3 it was found that MT1.14 has double the weight percent quartz compared to plagioclase, or conversely, the weight percent of plagioclase is half that of quartz. Half of 30 (from step 4) is 15, therefore the weight percent of plagioclase in the sample is 15.

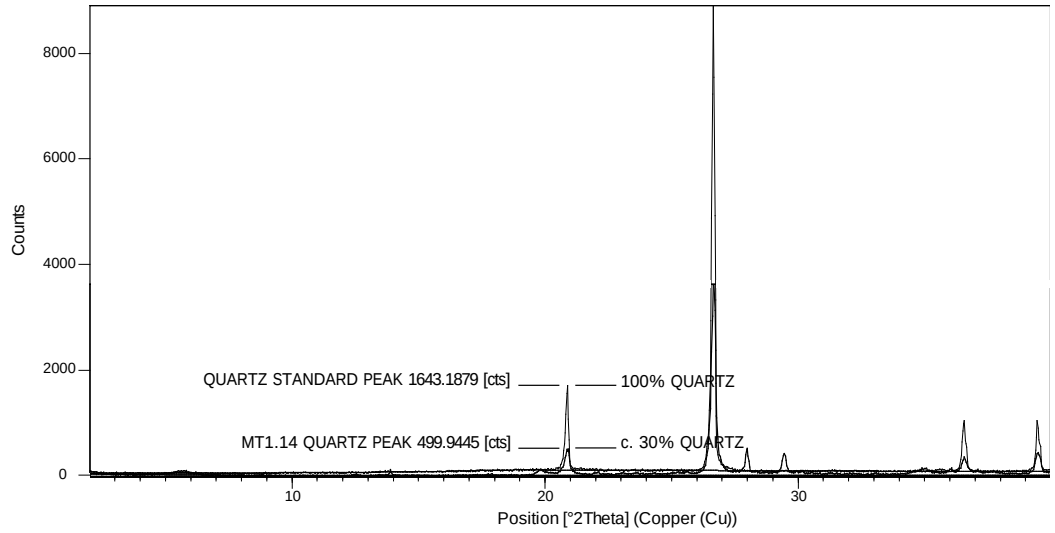

Fig. 3.6: Mineral peaks from sample MT1.14 superimposed on the quartz peaks from the pure quartz standard. The MT1.14 quartz peak is about 30% the height of the quartz standards peak height. Because the quartz peak height of the quartz standard corresponds to 100% quartz, the MT1.14 quartz peak height is taken to represent 30% quartz in that sample.

For rock classification purposes the weight percent values for plagioclase and potash feldspar were combined to give the relative abundance of feldspar (see Section 3.4). In addition, when used in the classification systems described in the following section the semi-quantitative values for the relevant minerals were normalised using SigmaPlot 2004 version 9.0.

There are well recognised inaccuracies associated with estimating mineral abundances from XRD data. Consequently the weight percent values calculated here are regarded as only general indicators of the mineral composition of samples.

3.4 Rock classification

The fine grained nature of many of the rocks dealt with in this study meant that

rock classification (and lithofacies classification) was partly made based on textures observed during petrography and on the composition determined using XRD and petrography. These data are provided in Digital Appendices P and O respectively. The classification schemes used, some additional details specific to this study, and sources of error are outlined in this section.

3.4.1 Textural classification

Use of the terms glaucony and glauconitic

Following Andrew (2010), the term "glaucony" is used for the facies of green grains which include glauconitic smectite and glauconitic mica minerals. Similarly to that work the term glaucony is used here because differentiation between the glauconitic minerals cannot be made with the available geochemical data. The term 'glauconitic' is used in an equivalent sense to 'glaucony' when incorporated into a rock name as a descriptive term (see below).

Clastic lithologies

Classification of clastic lithologies is based on the Folk (1954) classification scheme (Fig. 3.7A) and the maturity index (Prothero and Schwab, 1996; see Table 3.3). The Udden-Wentworth grain-size scale was used to classify sediment size (see Appendix H). The lithologies encountered in this study are in most cases dominated by mud with various proportions of sand, so further subdivisions of the mud-sand portion of the Folk (1954) classification system have been made to enable better recognition of mud-sand variations (Fig. 3.7B). No modifications have been made to the mud-gravel and sand-gravel component of the Folk (1954) classification scheme.

Textural data for classification were obtained from petrography. Interpretation of the depositional areas proximity to a paleoshoreline is an important factor for interpretations made in this study. Thus, in this study it is seen as important that rock names reflect the environmental energy (proximity to the shoreline and/or water depth) of the sedimentary environment in which the lithology was deposited. For this reason the rock name is based on the clastic portion of the rock (i.e. the transported/introduced siliciclastic grains), with the chemical portion (i.e. the authigenic components such as glaucony, skeletal material, and cement) being

included in the name mainly as a descriptive term. For glauconitic lithologies this is the case even when the clastic portion of the rock is less abundant than the glaucony portion (for lithologies dominated (> 50%) by carbonate material the limestone classification (see below) applies).

The reason for this approach with respect to glaucony is because sand-sized glaucony grains can form *in situ* (be authigenic) in a low energy environment. Consequently their coarser texture can be a poor reflection of the environmental energy of that depositional environment. Glaucony grains can also be perigenic (Lewis and McConchie, 1994), whereby they have been transported locally from their area of formation to their area of deposition. In these cases the size of the glaucony grains begins to reflect environmental energy, however, the source area of perigenic glaucony is not at the shoreline, but offshore of the shoreline in deeper water. Consequently the grain size of the glaucony still does not reflect the proximity of the depositional site to the shoreline, but rather its proximity to the glaucony source area. Because it is shoreline proximity that is of particular interest in this study, the grain-size of the glaucony fraction of lithologies is excluded from the rock textural name. The abundance of the chemical portion (including glaucony) of the rock is rather reflected in the rocks name with the comparative terms outlined in Table 3.4.

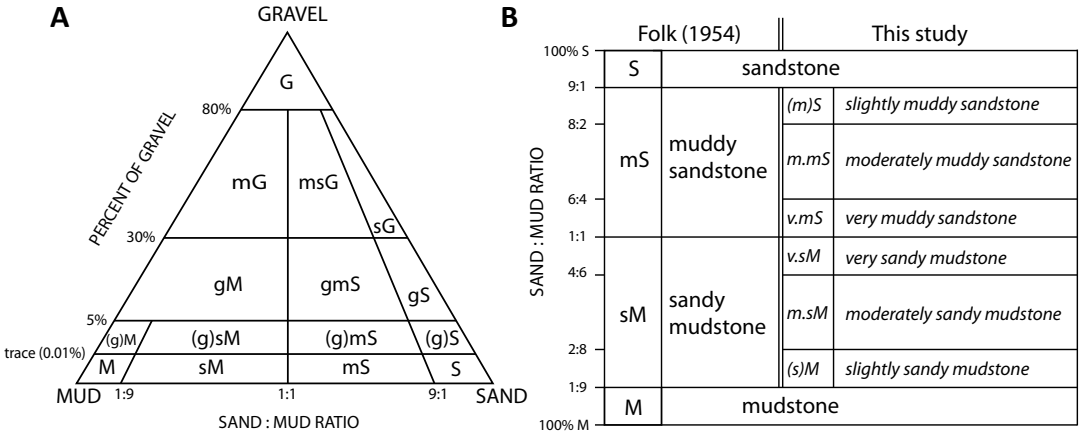

Fig. 3.7: Classification schemes for clastic lithologies that were used in this study. (A) The Folk (1954) classification scheme was used to classify mudstones and sandstones that have a gravel component. (B) Mudstones and sandstones with little or no gravel component were classified using a scheme modified from the Folk (1954) scheme. For the Folk (1954) scheme, G = gravel; g = gravelly; (g) = slightly gravelly; S = sand; s = sandy; M = mud; m = muddy.

Table 3.3: Maturity index used in this study for the classification of the clastic component of rocks (adapted from Prothero and Schwab, 1996).

	% Mud (= matrix)	Sorting of sand grains	Abrasion of sand grains
Immature	>5	Very poor	Angular
Submature	tr - 5	Poor	Subangular
Mature	0 - tr	Moderate	Subrounded
Supermature	0	Well	Rounded

Table 3.4: Semi-quantitative abundance limits used during petrographic analysis and the corresponding in text use of abundance terms in their comparative sense.

% Abundance	Term	Abbreviation	Term in its comparitive sense
> 75	Very abundant	VA	Extremely
50 - 75	Abundant	A	Very highly
25 - 50	Very common	VC	Highly
15 - 25	Common	C	Moderately
5 - 15	Many	M	Slightly
1 - 5	Some	S	Very slightly
< 1	Rare	R	
0	Absent	-	

A hypothetical example of the combined use of Fig. 3.7 and Tables 3.3 and 3.4, is classification of a lithology that is composed of poorly sorted, subangular detrital grains – 7% mud and 3% sand – and 90% sand-sized glaucony. Such a lithology would normally be termed a submature "greensand" or highly glauconitic sandstone, but using the classification scheme adopted in this study the rock would be an extremely glauconitic, submature, moderately sandy mudstone.

In summary, the petrographic classification scheme in this study uses textural data as a rough proxy for shoreline proximity. A problem encountered with this approach is that the classification scheme poorly describes the in-field character of lithologies dominated by glaucony. The hypothetical example above provides a good example of this issue, whereby the lithology described would look in outcrop and in hand specimen to be sandstone, would be classified as a sandy

mudstone following petrographic analysis. This becomes an issue at the Tawanui (Chapter 7), lower Mangahouanga Stream (Chapter 8) and Akitio River (Chapter 9) sections where glaucony dominated lithologies often occur. To aid the reader, where a glaucony dominated lithology is referred to in the text using this "new" classification scheme, the approximate percent glaucony and its conventional name are also given in square brackets (e.g. for the above hypothetical example, "extremely glauconitic, submature, moderately sandy mudstone [c. 80% glc – muddy greensand]").

The lithologies shown on stratigraphic columns produced in this thesis are also based on the above classification scheme. Consequently the same "problem" applies to the stratigraphic columns. Fig. 3.8A shows an example of a stratigraphic column from the Tawanui section (Chapter 7) that uses the "new" classification system. Fig. 3.8B shows the same column using a conventional textural classification that includes the grain size of glaucony. The difference between the two schemes is apparent through the glaucony rich bed. Ideally

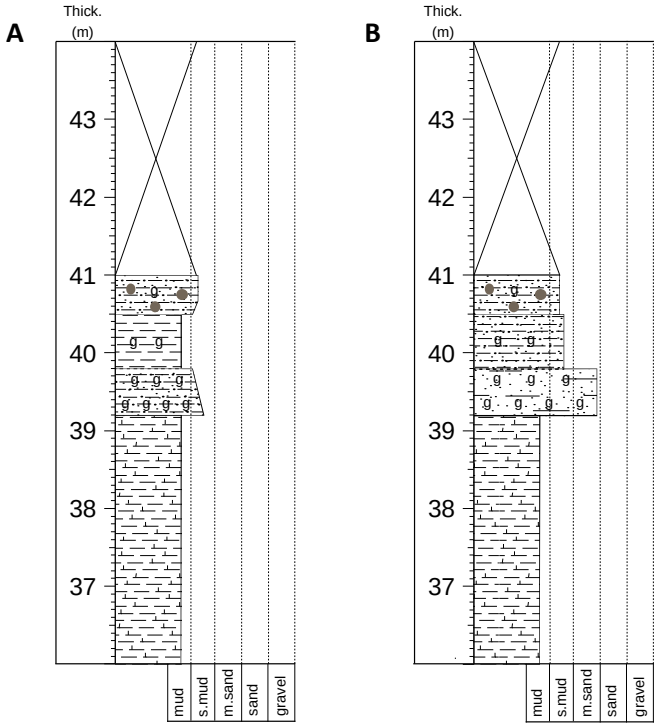

Fig. 3.8: Stratigraphic columns for a portion of the Tawanui section (Chapter 7) that has a glaucony dominated unit within it. A = Profile of the stratigraphic column using this studies textural classification scheme, where only the grain size of the clastic portion of the lithology is considered; B = profile of the stratigraphic column using a conventional textural classification system that includes the size of glaucony grians in grain size determination.

stratigraphic column pairs such as in Fig. 3.8 could be produced for all the studied sections, where type A columns are used for interpretive purposes and type B columns as field columns. However time constraints do not permit such a task, so instead the reader is made aware of the issue here.

Limestone

The textural classification of limestones follows the Folk (1962) classification scheme (Fig. 3.9). With limestones the clastic portion of the rock was included in the name as a descriptive term when in high enough abundance. The abundance of the clastic portion of the limestone is reflected in the classification with the comparative terms listed in Table 3.4. For example, a very fine grained limestone with 10% sand would be classified as a slightly sandy micrite (Table 3.4, Fig 3.9).

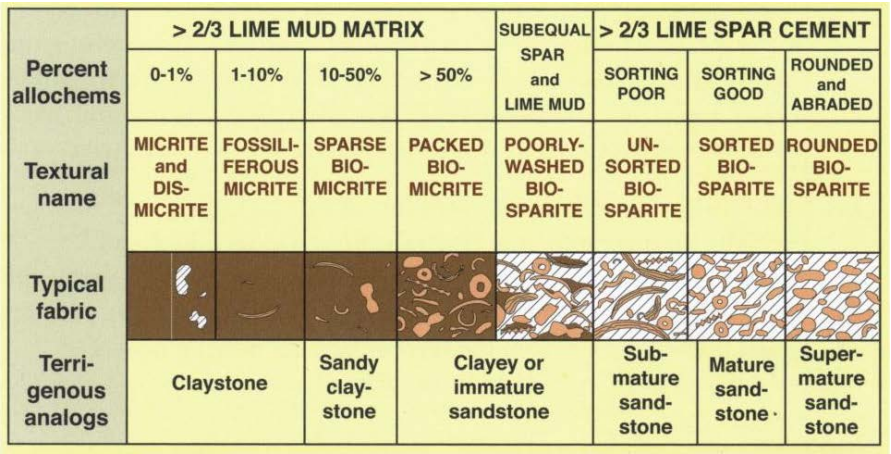

Fig. 3.9: The classification scheme for limestones used in this study (Scholle and Ulmer-Scholle, 2003; after Folk, 1962)

3.4.2 Compositional classification

Sandstones

Compositional classification of sandstones is based on the Folk et al. (1970) classification scheme (Fig. 3.10). The generally fine grained nature of the majority of lithologies encountered in this study (including sandstones) often made it difficult to positively identify minerals and their abundances using petrographic techniques. XRD has been used to give a broad estimate of the relative abundances of quartz and feldspar in sandstone samples. However, XRD cannot differentiate rock fragments, made up of these minerals, from the discrete

quartz and feldspar minerals making up the host rock. Consequently, the abundance of rock fragments is assessed petrographically.

In thin section most of the rocks studied are composed of fine to very fine sand grains and silt grains set in a dominant muddy matrix. Rock fragments that themselves are made up of fine grained muddy material can be difficult to differentiate from the muddy matrix. Consequently, more fine grained and muddy rock fragments may exist in the rocks described than has been recorded.

Errors associated with using XRD to determine mineral abundance and the possible underestimation of rock fragments using petrography mean that the compositional classification of many of the rock samples in this study should be regarded as approximate at best, providing only a general indication of their compositional makeup.

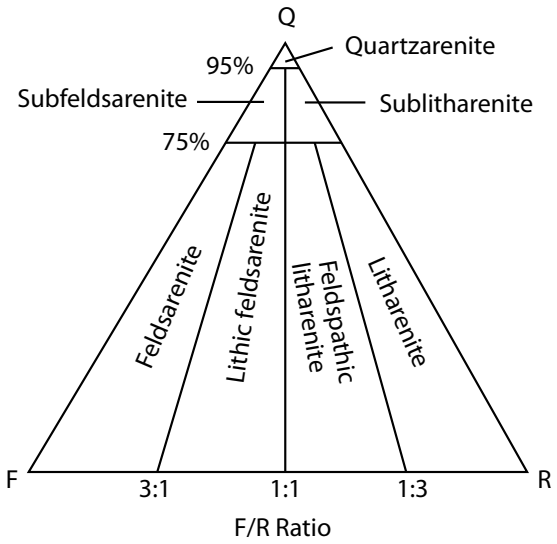

Fig. 3.10: The compositional classification system of Folk et al. (1970). This system was used in conjunction with XRD and petrograhic data to classify lithologies based on their composition. Q = quartz; F = feldspar; R = rock fragments.

Mudstones

Normally compositional classification of mudstones is not attempted because of the difficulty in identifying very fine grained minerals and determining their abundances using standard petrographic techniques. However, the XRD data produced in this study, coupled with the semi-quantitative processing technique discussed in Section 3.3.7, has allowed general classification of mudstone composition based on their three main clastic components of quartz, feldspar, and

clay (Fig. 3.11). The classification system is loosely based on the Folk et al. (1970) sandstone classification scheme, and similar terminology is used. However, “arenite” is replaced by “lutite”, and “lith” or “lithic” is replaced by “argil” or “argillaceous” (Fig. 3.11). In addition, it was found that the quartz and clay components show the most variation in the samples analysed in this study. Consequently, the clay-quartz section of the ternary diagram has been further subdivided so the quartz and clay variations are better reflected in the mudstone compositional name (Fig. 3.11).

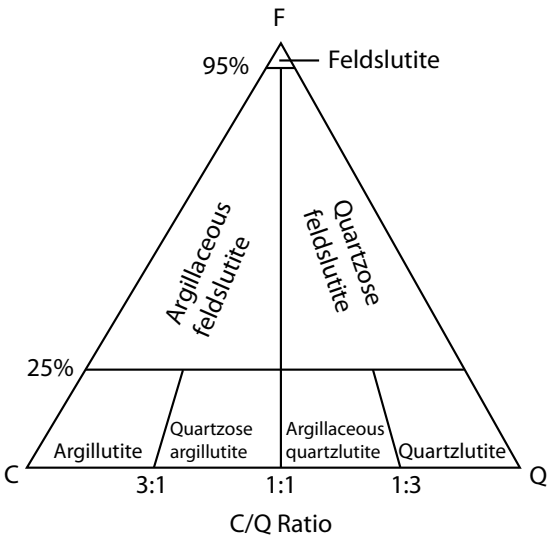

Fig. 3.11: The compositional classification for mudstones used in this study. This system was used in conjunction with XRD to classify lithologies based on their composition. F = feldspar; C = clay; Q = quartz.

Limestones

Compositional classification of limestone is based on the abundance of calcite, combined quartz and feldspar, and clay, (Fig. 3.12) as determined using XRD data and the semi-quantitative XRD data processing technique outlined in Section 3.3.7. The classification is used as a visual aid to demonstrate shifts in limestone lithofacies compositions. No compositional names have been assigned to the classification scheme, with brief in text descriptions used instead.

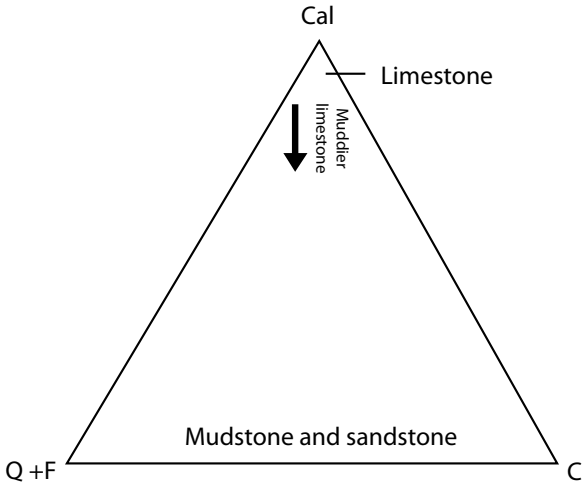

Fig. 3.12: The compositional classification for limestones used in this study. This system was used in conjunction with XRD to classify lithologies based on their composition. Cal = calcite; Q+F = quartz and feldspar; C = clay.

3.5 Maps

Locality maps used in Chapters 5 to 9 are sourced from MapToaster Topo (New Zealand topographical maps and aerial photography [V5.0.246]) and Google Earth (6.0.0.1735 (beta)).

Chapter 4
FIELD LITHOTYPES AND LITHOFACIES

4.1 Introduction

To aid interpretation and presentation of data, lithologies encountered in this study have been grouped under three lithotypes and eleven lithofacies (Table 4.1). Lithotypes and lithofacies have been classified based on the field characteristics of rock types, with bedding character, grain size, and glaucony and carbonate content the discriminating factors. For the interbedded lithofacies the first named lithology is subordinate and the second named is dominant (i.e. interbedded subordinate-dominant). This chapter introduces the lithotypes and lithofacies categories used in this study, gives a broad description of individual lithofacies, and provides explanation for the use of some terms.

Table 4.1: Lithotype and lithofacies categories employed in this study, and their occurrence in the study area. PH = Pahaoa; AG = Angora Road; TW = Tawanui; LM = Lower Mangahouanga Stream; AK = Akitio River.

Lithotypes	Lithofacies	Code	Occurrence
Limestone (L)	Interbedded sandstone-limestone	L1	PH
	Muddy limestone	L2	PH, AK
Mudstone (M)	Calcareous mudstone	M1	PH, AG, TW, LM
	Siliceous mudstone	M2	PH, AG, TW, LM
	"Waipawa Black Shale"	M3	AG
	Sandy mudstone	M4	TW
	Glauconitic mudstone	M5	TW, LM, AK
	Muddy greensand	M6	TW, LM
	Interbedded sandstone-mudstone	M7	PH
Sandstone (S)	Muddy sandstone	S1	AG
	Interbedded mudstone-sandstone	S2	AG

4.2 Lithofacies description

Lithofacies descriptions reported in this section are generalised and variations

often occur. Detailed, locality specific descriptions that include these variations are presented in Chapters 5-9. A suffix (a, b, c, etc.) has been added to the end of names of lithofacies when there are multiple varieties of that lithofacies.

4.2.1 Limestone lithotype

Interbedded sandstone-limestone (L1)

This lithofacies consists of flaggy micritic limestone with occasional calcareous sandstone and mudstone interbeds (Fig. 4.1A). The limestone succession is generally creamy-white in colour, well indurated, flaggy, massive, occasionally burrowed, calcareous, and very fine grained. The sandstone beds are blue-green-grey, well to very well indurated, massive, calcareous, and glauconitic. The lithofacies was encountered at Pahaoa (Table 4.1).

Muddy limestone (L2)

The lithofacies consists of light coloured, moderately to well indurated, occasionally burrowed, calcareous, very fine grained limestone with variable amounts of mud (Fig. 4.1B). It was encountered at Pahaoa and Akitio River (Table 4.1).

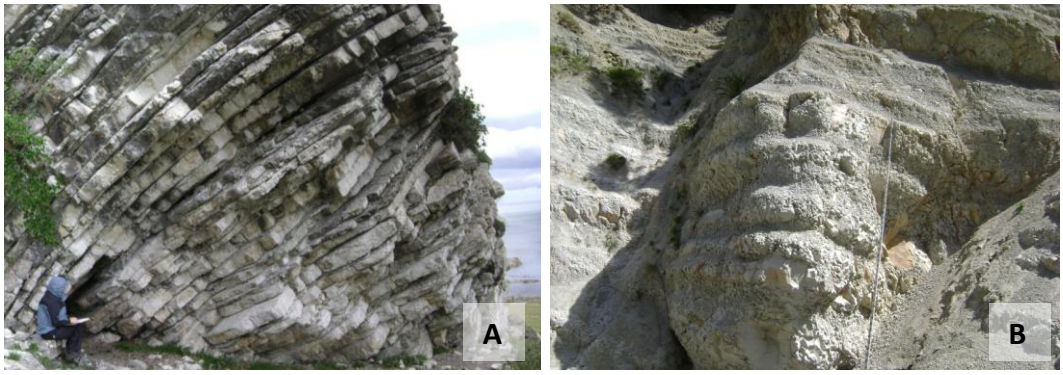

Figure 4.1: Outcrop examples of the limestone lithotype. A = interbedded sandstone-limestone lithofacies (L1) at Pahaoa (Kaiwhata Limestone); B = muddy limestone lithofacies (L2b) at Akitio River (Weber Formation).

4.2.2 Mudstone lithotype

Calcareous mudstone (M1)

The calcareous mudstone lithofacies occurs at most of the studied sections (Table 4.1). It consists of red-grey, green-grey, or grey, moderately to well indurated, massive, sometimes glauconitic, calcareous mudstone (Fig. 4.2A). Occasional

sandstone, siltstone, or conglomeratic beds occur within the calcareous mudstone at some localities.

Siliceous mudstone (M2)

This mudstone lithofacies is characteristically non-calcareous. The siliceous mudstone is moderately to well indurated, mostly massive but sometimes laminated, and is occasionally glauconitic (Fig 4.2B). The lithofacies occurs at most of the studied sections (Table 4.1).

"Waipawa Black Shale" (M3)

The "Waipawa Black Shale" lithofacies is a dark grey to black, well to poorly indurated, massive, mostly non-calcareous mudstone with common *Terebellina* tubes (Fig. 4.2C). It occurs only at the Angora Road section (Table 4.1). Explanation for the use of the historical term "Waipawa Black Shale" is given in Section 4.3.

Sandy mudstone (M4)

The sandy mudstone lithofacies occurs at Tawanui (Table 4.1). It consists of light grey, moderately well to well indurated, mainly massive, sometimes burrowed, slightly glauconitic, non-calcareous sandy mudstone (Fig. 4.2D).

Glauconitic mudstone (M5)

M5 consists of very poorly to well indurated, massive, sometimes burrowed, slightly to moderately glauconitic, calcareous or non-calcareous mudstone (Fig. 4.2E). It occurs at Tawanui, Lower Mangahouanga Stream, and Akitio River (Table 4.1).

Muddy greensand (M6)

The muddy greensand lithofacies was encountered at Tawanui and Lower Mangahouanga Stream (Table 4.1). It is a green, poorly to well indurated, massive, mostly non-calcareous, highly to extremely glauconitic mudstone or sandy mudstone (Fig. 4.2F). Explanation for the use of "greensand" is given in Section 4.3.

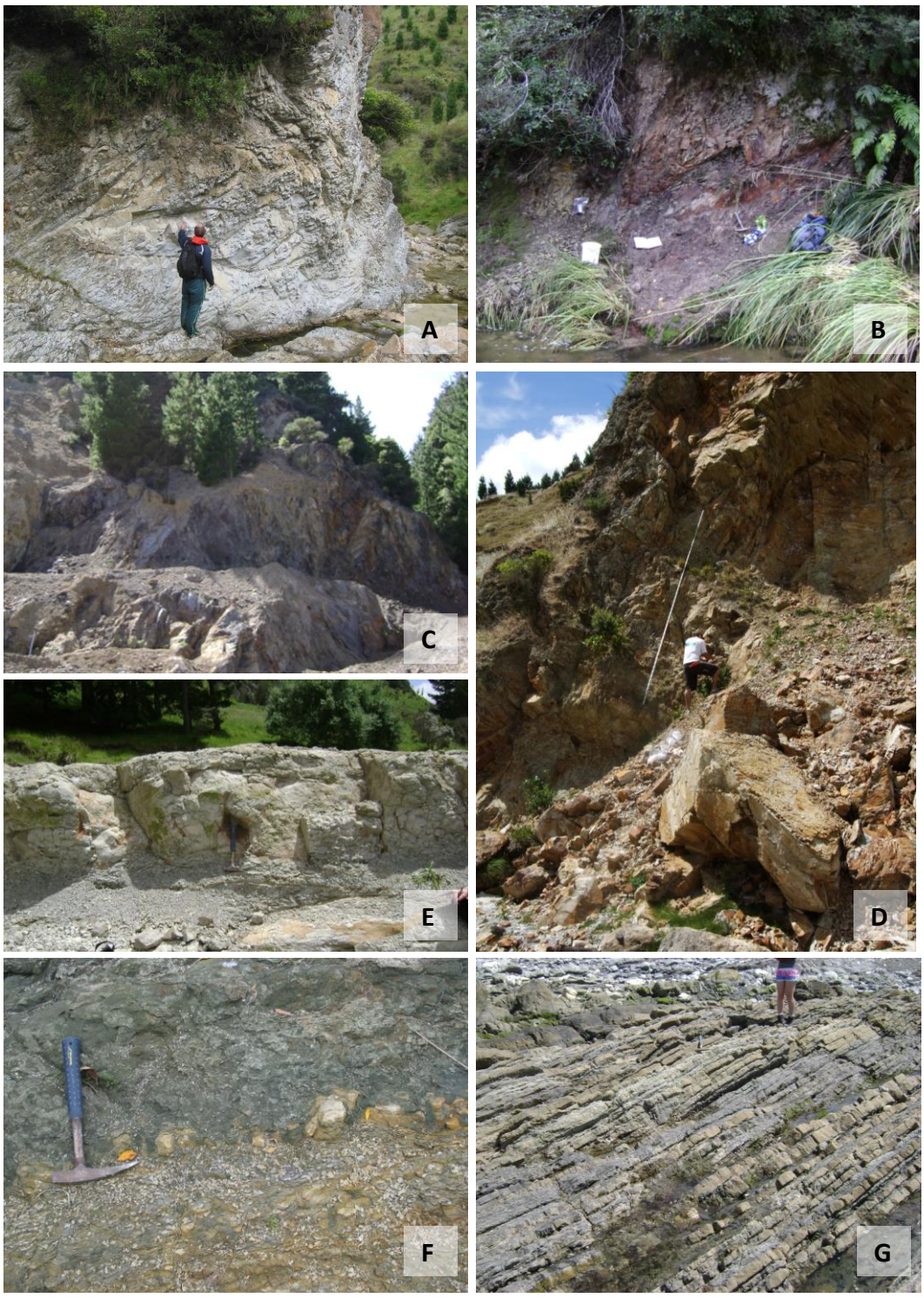

Figure 4.2: Outcrop examples of the mudstone lithotype. A = calcareous mudstone lithofacies at Tawanui (M1b; Upper Calcareous Member, Whangai Formation); B = siliceous mudstone lithofacies at Lower Mangahouanga Stream (M2d; Rakauroa Member, Whangai Formation); C = Waipawa black shale lithofacies at Angora Road (M3; Waipawa Formation); D = sandy mudstone lithofacies at Tawanui (M4; Te Uri Member, Whangai Formation); E = glauconitic mudstone lithofacies at Akitio River (M5b; Weber Formation); F = muddy 'greensand' lithofacies at Tawanui (M6a; Te Uri Member, Whangai Formation); G = interbedded sandstone-mudstone lithofacies at Pahaoa (M7a; ?Awhea Formation)

Interbedded sandstone-mudstone (M7)

This lithofacies consists of dominant dark grey mudstone interbedded with light grey, slightly glauconitic, medium sandstone (Fig. 4.2G). Both lithologies are well indurated, often calcareous, and occasionally burrowed or laminated. The lithofacies was encountered at Pahaoa (Table 4.1).

4.2.3 Sandstone lithotype

Muddy sandstone (S1)

S1 consists of green-grey, massive or laminated, occasionally slightly glauconitic, non-calcareous sandstone or slightly muddy sandstone (Fig. 4.3A). It occurs at Angora Road.

Interbedded mudstone-sandstone (S2)

The interbedded mudstone-sandstone lithofacies consists of decimetre beds of green-grey, massive, non-calcareous, glauconitic sandstone interbedded with centimetre beds of dark grey, non-calcareous mudstone (Fig. 4.3B). The lithofacies occurs at Angora Road.

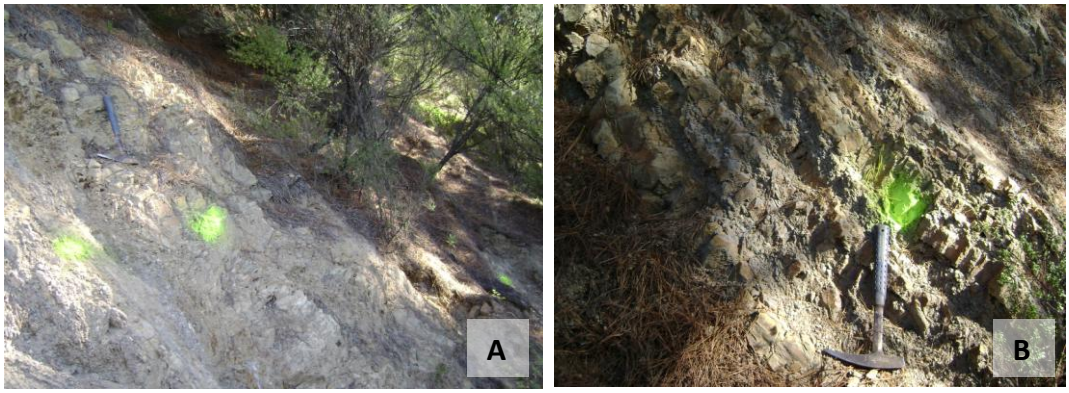

Figure 4.3: Outcrop examples of the sandstone lithotype. A = muddy sandstone lithofacies (S1) at Angora Road (Wanstead Formation); B = interbedded mudstone-sandstone lithofacies (S2) at Angora Road (Wanstead Formation).

4.3 Use of "Waipawa Black Shale" and muddy greensand

Lithologies with a similar appearance to the Waipawa Black Shale of Moore (1989) have been grouped under the lithofacies name "Waipawa Black Shale" even though the name Waipawa Formation is now used in preference for rocks of this specific lithology. The reason for naming the lithofacies the "Waipawa Black

Shale" is that lithologies identified as Waipawa Formation in Marlborough (Hollis et al., 2005), and tentatively in Wairarapa and southern Hawke's Bay (this study, see Chapters 5 and 6), are slightly different in character to the traditional Waipawa Black Shale description of Moore (1989). Consequently, "Waipawa Black Shale" has been used as the name for the lithofacies because the lithologic characteristics associated with this term best describe the rock type, and exclude the other slightly different lithologies identified within the Waipawa Formation. Giving the lithofacies this name was seen as a way of quickly communicating where lithologies having the traditional Waipawa Black Shale character were present, and where they were absent, within the Waipawa Formation.

In section 3.4.1, 'Rock classification', it was stated that in this study the classification of lithologies is primarily based on the clastic portion of the rock (i.e. the transported/introduced siliciclastic grains), with the chemical portion (i.e. the authigenic components such as glaucony, skeletal material, and cement) being included in the name as a descriptive term. On this basis the muddy greensand lithofacies should really be named the highly to extremely glauconitic mudstone lithofacies. An exception to the study's classification scheme was made in this case because muddy greensand better describes the character of the lithology as seen in the field, and also more concisely than the alternative name of highly to extremely glauconitic mudstone.

Chapter 5
PAHAOA

5.1 Location

The Pahaoa section is located in southeast Wairarapa on the coast immediately north of the Pahaoa River mouth (Fig. 2.2 and 5.1). Three areas, chosen for their ease of access and quality of exposure, were logged to form a continuous stratigraphic column (Fig. 5.1 and 5.2). The lowermost strata described are at the "beach" section, middle strata crop out at the "high bluff" section, and the uppermost units are best exposed at the "cove" section (Fig. 5.1). Overall the Pahaoa section is well exposed. The "cove" and "beach" sections are tide dependent.

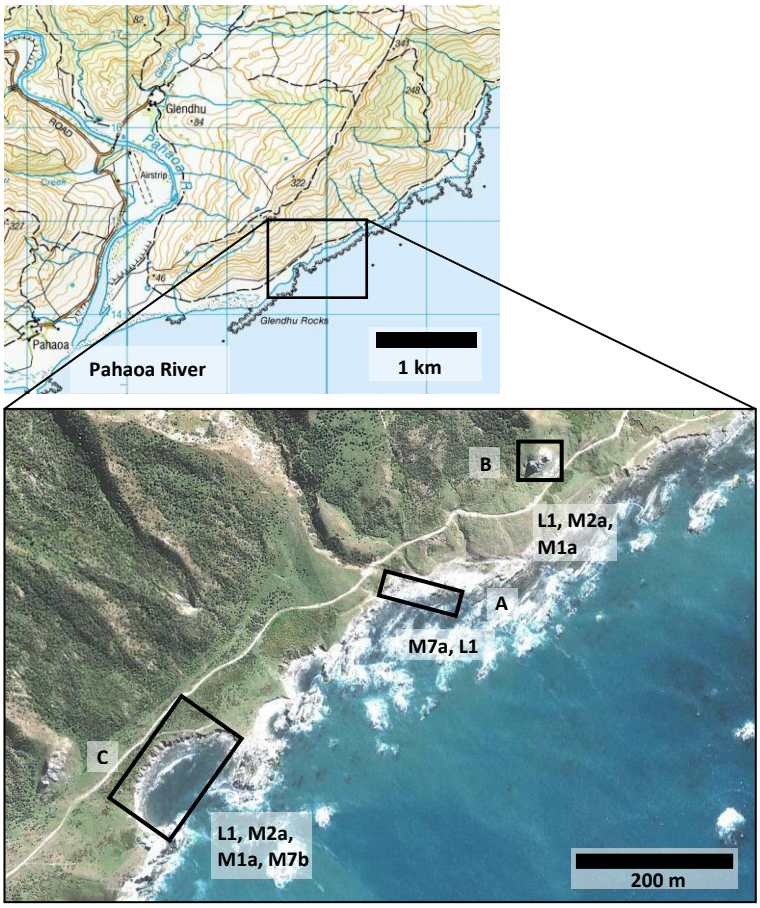

Figure 5.1: Location of the coastal Pahaoa section showing the three areas logged and the lithofacies observed within them (see Table 4.1). A = "beach" section; B = "high bluff" section; C = "cove" section. Strata exposed along the coast have been offset by faulting and as a consequence the lowermost strata described are at A, middle strata crop out at B, and the uppermost units are best exposed at C.

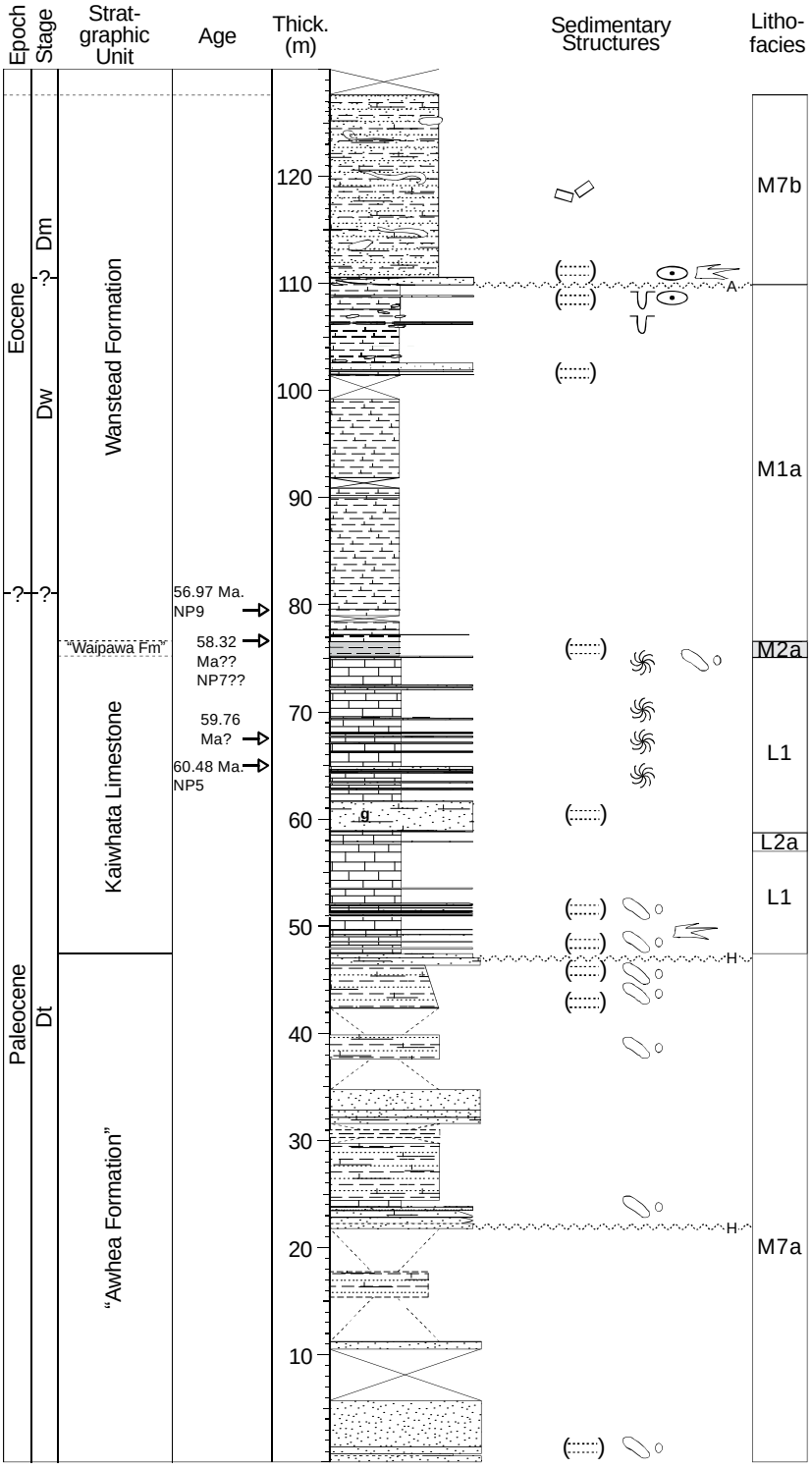

Figure 5.2: Stratigraphic column and lithofacies for the Pahaoa section. Lithostratigraphic units: Kaiwhata Limestone is after Nelson (1968) and Wanstead Formation is after Lee and Begg (2002). Other units are tentatively proposed in this study (see Chapter 10 for discussion on this topic). The New Zealand stages shown are derived from reconnaissance biostratigraphic assessment of foraminiferal samples by Hugh Morgans (GNS Science) (pers. comm. 2010). Specific ages are based on calcareous nannofossil biostratigraphy (this study). Calcareous nannoplankton zones for the Paleogene (NP) are defined in Appendix K. Graphic log lithology and sedimentary structures symbols are defined in Appendix B.

5.2 Facies characteristics

The sedimentary succession logged at Pahaoa is presented in Fig. 5.2. The formation name Kaiwhata Limestone is after Nelson (1968) and the Wanstead Formation is after Lee and Begg (2002). The "Awhea Formation" and "Waipawa Formation" names are tentatively proposed in this study based on geochemical characteristics and/or field lithology and stratigraphic correlation with previously studied Tora block (Fig. 2.2) sections north and south of the Pahaoa section. Discussion on this topic is presented in Chapter 10.

The logged section at Pahaoa consists of an c. 47 m thick succession of interbedded sandstone and mudstone ("Awhea Formation") conformably overlain by c. 28 m of dominantly micritic limestone (Kaiwhata Limestone). This is capped by a thin (c. 2 m) dark mudstone ("Waipawa Formation") which is in conformable contact with an overlying c. 33 m thick succession of grey, and red and green striped mudstone (Wanstead Formation). This latter unit has an erosional upper contact with a clast rich interbedded sandstone and mudstone (Wanstead Formation). Six lithofacies have been identified in the succession (Fig. 5.2) and their field lithology, contacts, and petrography are described below.

5.2.1 Interbedded sandstone-mudstone lithofacies (M7a, b)

M7 (Table 4.1) has two variants at the Pahaoa section (M7a and b), M7a occupying the lowermost and M7b the uppermost portions of the logged area (Fig. 5.2).

M7a

Field lithology

The succession consists of centimetre to decimetre interbedded light grey, slightly glauconitic medium sandstone (minor) and dark grey mudstone (dominant) (Fig. 5.3A, B). Both lithologies are well indurated and often calcareous. Some beds are highly burrowed and occasional semi-parallel, swaley and cross laminations are evident (Fig. 5.3C, D, E). Some beds with exposed contacts appear to have sharp lower and gradational upper contacts while other beds have both sharp lower and upper contacts. An c. 2 m thick interval of burrowed sandstones

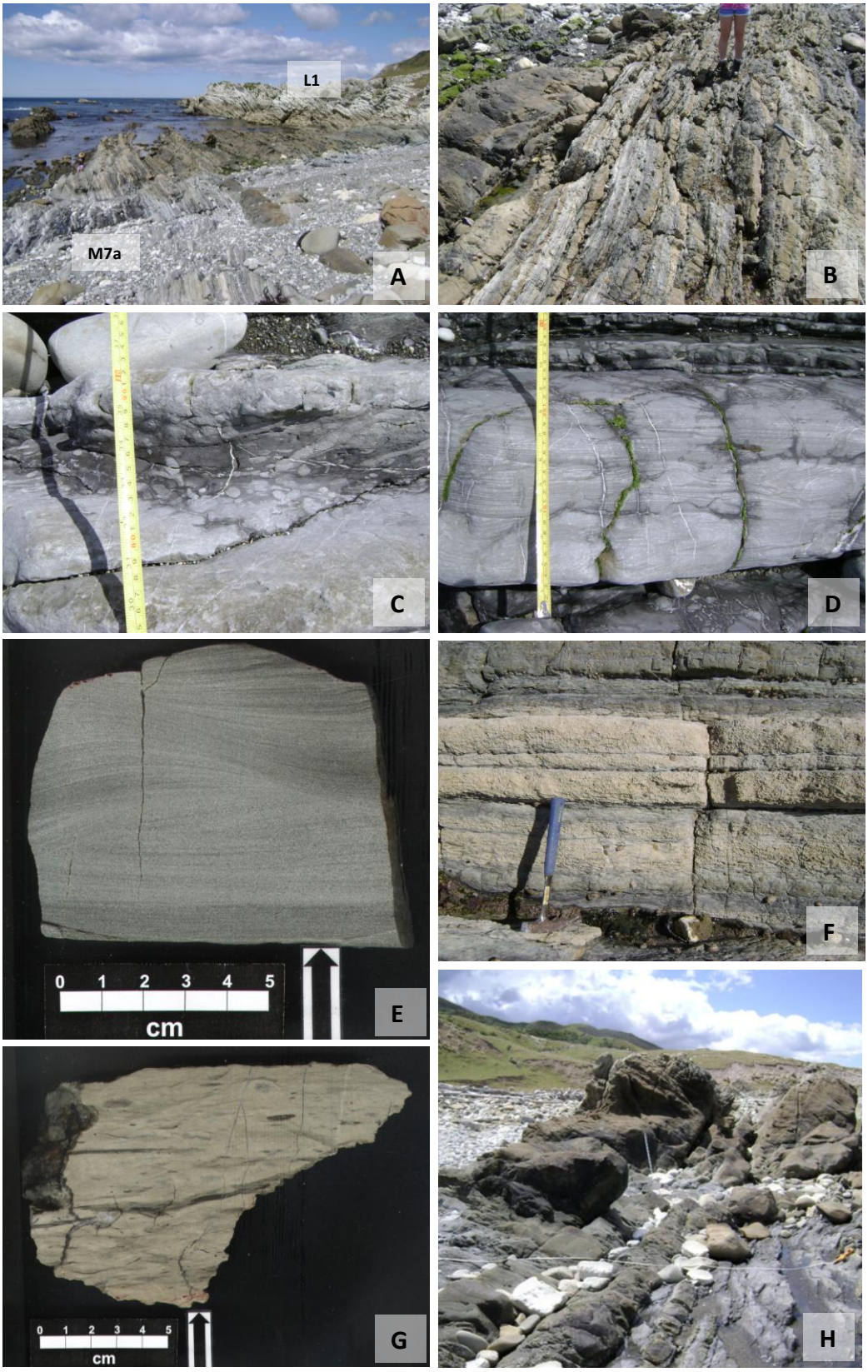

Figure 5.3: Features of the M7a lithofacies. A = M7a at the "beach" section; B = centimetre interbedded sandstone and mudstone; C = burrowing in a mudstone; D and E = semi-parallel laminations and swaley cross laminations in sandstone; F and G = burrowed micritic limestone (G) with web-like veins on weathered surfaces (F); H = examples of the thick sandstone beds that occur sporadically through M7a. 1 m long Jacob staff for scale.

capped with an c. 0.5 m thick burrowed micritic limestone occurs near the middle of the lithofacies (Fig. 5.3F, G). The weathered surface of the limestone has web-like veining and resembles sandstone in outcrop (Fig. 5.3F). However, percent CaCO3 values exceed 80% (Appendix M) for the lithology suggesting it is a limestone. A number of thick (up to c. 4 m), non-calcareous sandstone beds occur throughout the succession (Fig. 5.3H). When wet, these medium sandstones have a brown weathered surface and the mudstones a dark grey weathered surface; when dry, both lithologies have a light grey weathered surface (Fig. 5.3B, C, D).

Towards the top of M7a the succession becomes centimetre bedded and consists of alternating beds of dark grey to black, burrowed, calcareous mudstone and beds of dark grey, sometimes laminated, calcareous sandstone (Fig. 5.4A). This bedding style grades upwards into a lighter coloured, thicker bedded version of the underlying centimetre interbedded sandstone-mudstone (Fig. 5.4B). The colour change may be due to the area of the outcrop described spending gradually less time in the ocean, as it is near the high tide mark. However, slabbed samples do show a colour shift from dark grey-black in the thinly bedded part of the unit to light green-grey in the upper thicker bedded portion. The thicker bedded portion of the unit is decimetre bedded and consists of alternating beds of medium to dark grey, intensely burrowed, calcareous mudstone, and blue-grey, calcareous sandstone. The sandstones appear to have sharp lower contacts and gradational upper contacts with the mudstones.

Contacts

The lower contact of M7a is not within the logged area. The gradual shift from centimetre to decimetre interbedded sandstone-mudstone and increased burrowing towards the top of the M7a unit, described above, is interrupted by an c. 0.6 m thick laminated fine sand-sized sandstone (Fig. 5.4C). The sandstone grades upwards into an intensely burrowed sandstone (Fig. 5.4D) which in turn grades upwards into burrowed micritic limestone of the basal interbedded sandstone-limestone lithofacies (L1) (Fig. 5.4C).

Petrography

The mudstone and sandstone components of M7a are described separately. The

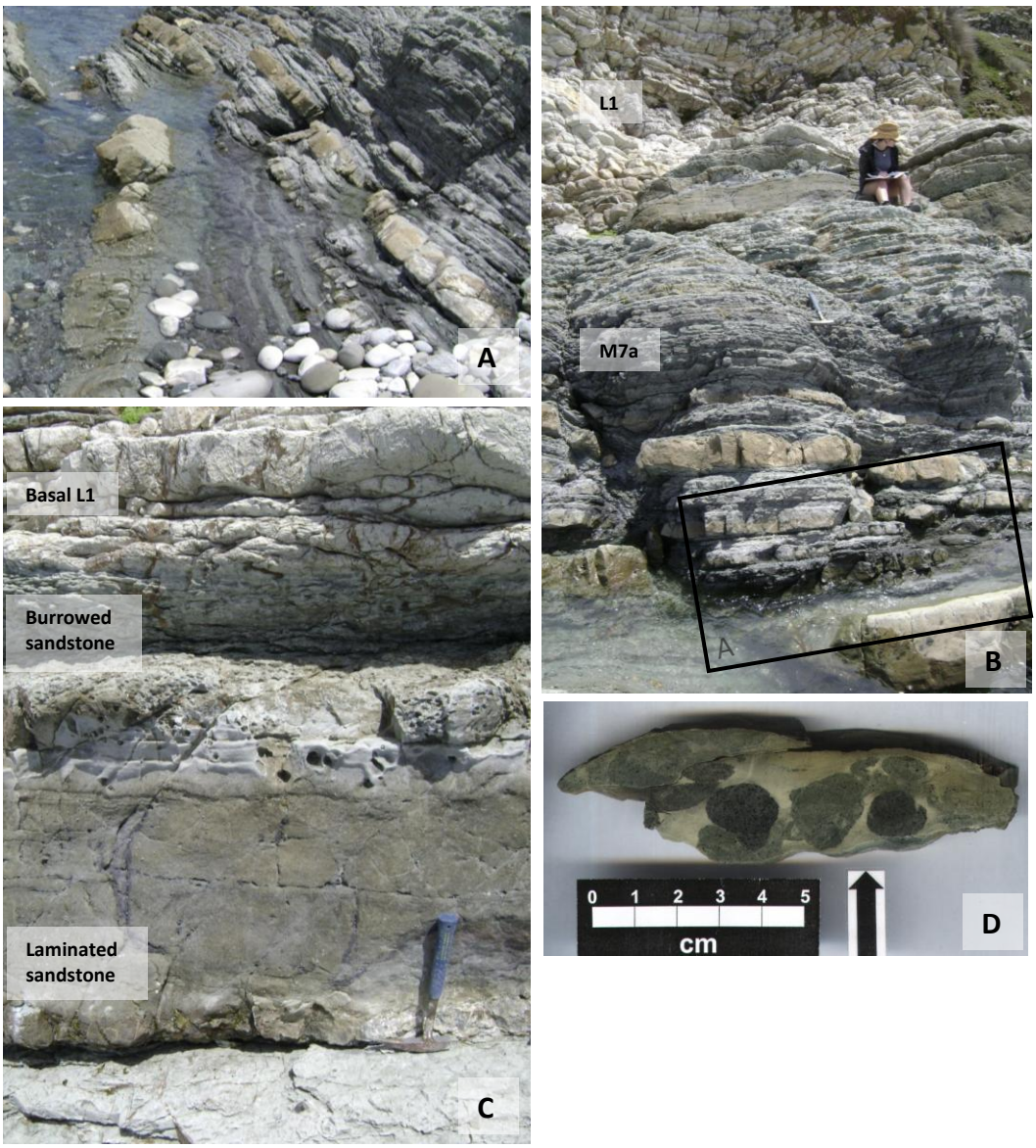

Figure 5.4: The upper portion of M7a leading into its upper contact with L1. A = centimetre interbedded sandstone-mudstone (M7a) with occasional thicker sandstone beds; B = centimetre interbedded sandstone-mudstone transitioning into decimetre interbedded sandstone-mudstone (M7a); C = Upper contact of M7a consists of a laminated sandstone bed grading into a highly burrowed sandstone in turn grading into burrowed micritic limestone; D = prominently burrowed sandstone at the contact between M7a and L1.

description is based on one representative sample from each lithology

Mudstone description (MT4.37): The mudstones of M7a are composed of silt and rarer very fine sand sized clastic grains set in a dark muddy (argillaceous) matrix (Fig. 5.5A), with small shreds of muscovite widely dispersed throughout the rock. Sorting is poor and most visible grains are subangular to angular. The sample examined displayed normal grading, with coarser silt sized grains concentrated at

its base. Coarse silt sized clastic grains are also concentrated in burrows and crude mineralogical laminations are evident. Quartz and clay are the dominant minerals present with feldspars and calcite secondary in abundance (Fig. 5.6). Microfossil tests and glaucony grains are rare. Calcite spar is present in veins and as an infilling of some microfossil tests.

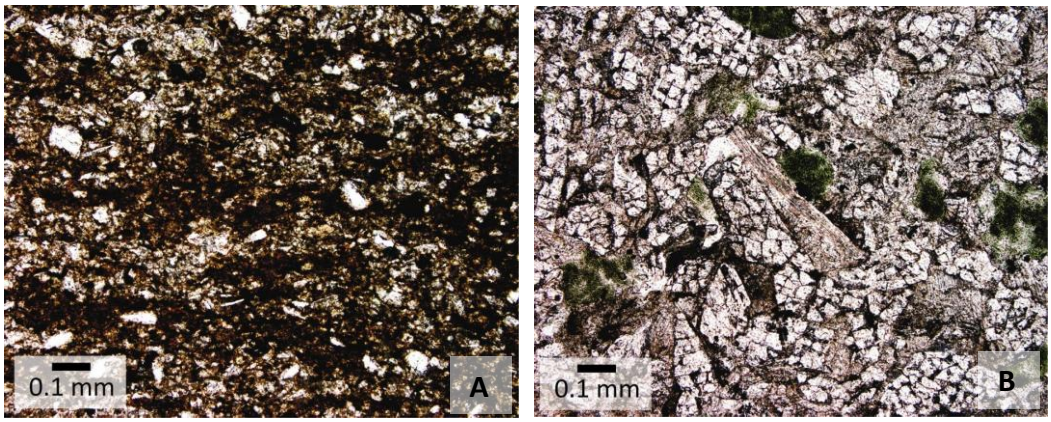

Figure 5.5: Photomicrographs of representative samples from the M7a lithofacies. A = typical mudstone with coarser silt-sized clastics set in a dark argillaceous matrix (MT4.37); B = typical sandstone comprising very fine to fine quartz (and ?feldspar) grains (fractured), glaucony grains, and a large muscovite flake in the centre of the image (MT3.36).

Mudstone classification: Immature quartzose argillutite with common calcite veins and burrows infilled with coarse siltstone (Fig. 3.11 and 5.6).

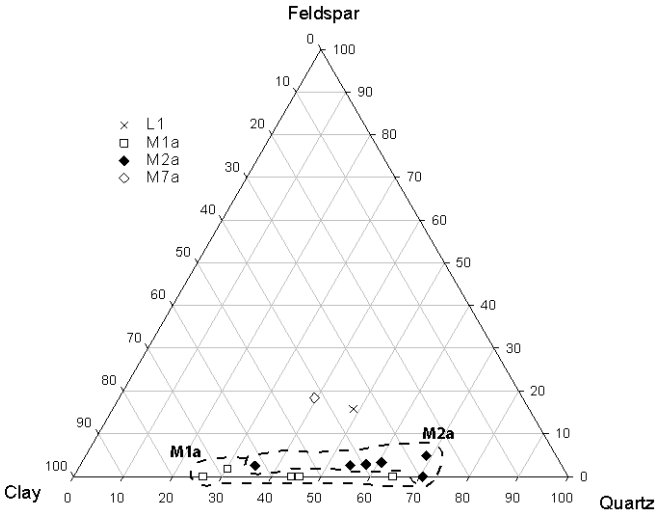

Figure 5.6: Ternary diagram of relative proportions of feldspar, clay minerals, and quartz in the mudstone lithotype variants (M1a, M2a, M7a), and of mudstone in the L1 lithofacies, at the Pahaoa section. See Fig. 3.11 for lutite classification names and fields.

Sandstone description (MT4.36): The representative sandstone sample from M7a is composed of very fine to medium sand sized clastic grains, including rare muscovite flakes up to 0.85 mm long, set in calcite cement (Fig. 5.5B). The grains are moderately sorted and mostly subangular to subrounded. Most quartz/feldspar grains have a "shattered" internal appearance, probably a consequence of the resin impregnation process used during thin section preparation (Andrew, 2010). Quartz, calcite, and feldspar (seen in thin section as plagioclase) are the dominant minerals present (Fig. 5.7). Rounded rock fragments, some with high interference colours, and clay are also significant components. Calcite infills pore spaces and forms veins. Many glaucony grains are present, occasionally appearing to be glauconitised benthic foraminiferal tests.

Sandstone classification: Calcite cemented, slightly glauconitic, mature to submature fine to medium feldsarenite (Fig. 3.10 and 5.7).

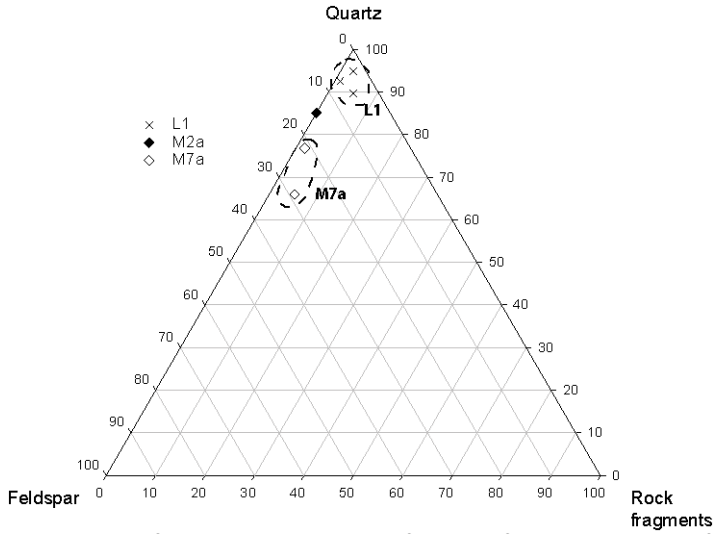

Figure 5.7: Ternary diagram of relative proportions of quartz, feldspar, and rock fragments in the sandstone lithologies within the mudstone (M) and limestone (L) lithotypes at the Pahaoa section. See Fig. 3.10 for arenite classification names and fields.

M7b

Field lithology

M7b consists of dark grey, well indurated, locally glauconitic, calcareous, cm to mm interbedded sandstone-mudstone (Fig. 5.8A-C). The bedding appears folded or slumped in places and there can be included foreign clasts of various lithologies (Fig. 5.8D-F). Some clasts appear to be muddy micritic limestones that have been compressed into lenses and smeared, twisted, and folded back on

Figure 5.8: Features of the interbedded sandstone-mudstone of the M7b lithofacies. A = M7b at the "cove" section; B and C = centimetre to millimetre interbeds of sandstone and mudstone making up the M7b matrix; D = twisted and contorted limestone clasts; E = a clast of M7b matrix within M7b; F = large subrounded mudstone clast.

themselves (Fig. 5.8D). Other clasts appear to be of the same lithology as the matrix (Fig. 5.8E), while still others are rounded sandstone or mudstone clasts (Fig. 5.8F). Clasts can be very large (4.4 × 0.55 m). It appears that sections of distorted matrix and clasts may form horizons between non-distorted intervals, but this needs closer study.

Contacts

The lower contact of the M7b lithofacies is described when discussing the upper

contact of the M1a lithofacies in Section 5.2.5. The upper contact of M7b is not exposed.

Petrography

The petrography of this lithofacies is beyond the scope of this thesis.

5.2.2 Interbedded sandstone-limestone lithofacies (L1)

L1 was observed at Pahaoa and has no variants within this (Fig. 5.2) or the other studied sections (Table 4.1).

Field lithology

L1 is dominated by limestone with occasional interbeds of sandstone (Fig. 4.1A and 5.9A). The limestone is generally cream or white, well indurated, flaggy, massive with often common trace fossils, calcareous, and micritic (very fine grained). Rare thin (c. 3 cm) marly beds reside within the succession. Tubular and ovoidal/lensoidal shaped trace fossils (?*Planolites*) occur at the base and top of the succession and *Zoophycos* dominates the trace fossil assemblage through its upper half (Fig. 5.9B, C). Some of the flags near the base of the succession appear slightly folded and distorted (Fig. 5.9D). The weathered surface of the limestone is white with common brown staining, massive, and has a light cover of black lichen upon outcrops set back from the beach.

The sandstone beds are blue-green-grey, well to very well indurated, massive or occasionally faintly laminated, glauconitic, calcareous fine sandstone (Fig. 5.9E). The sandstones have sharp lower contacts, and gradational to rapidly gradational upper contacts with mudstone or limestone (Fig. 5.9F). A thin (c. 5 cm) sandstone

Figure 5.9: Features of the interbedded sandstone-limestone lithofacies (L1). A = upper half of L1 logged at the "high bluff" section including the prominent thick sandstone bed and underlying L2a; B = ovoidal/lensoidal burrows (?*Planolites*) in basal L1; C = *Zoophycos* and lensoidal (?*Planolites*) burrows in uppermost L1; D = buckled limestone flags in lower L1; E = cut slab of one of the thicker sandstone interbeds from L1; F = an interbedded sandstone showing a sharp lower and gradational upper contact with limestone in L1; G = thin sandstone dikes (marked by arrows) penetrating into overlying limestone from a thin interbedded sandstone in lower L1; H = laminations in the upper portion of the prominent thick sandstone bed in the middle of the L1 (see Fig. 5.2).

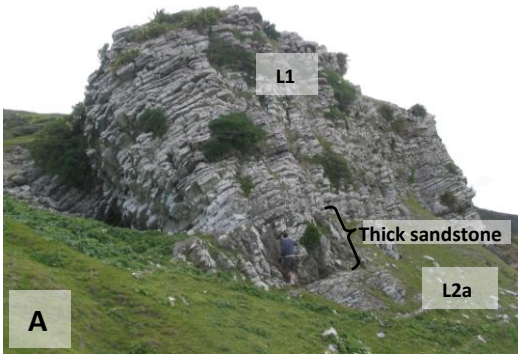
L1
Thick sandstone
L2a
A


0 1 2 3 4 5
cm
B


0 1 2 3 4 5
cm
C


D


F


0 1 2 3 4 5
cm
E


H

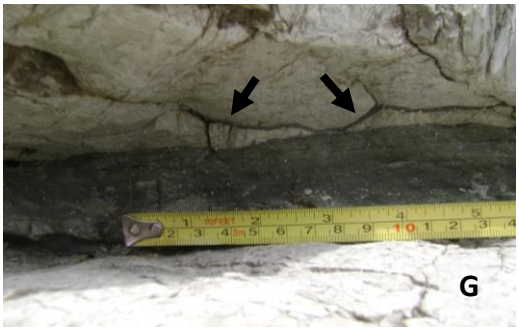
G

bed near the base of the succession has tiny sedimentary dikes veining up into the overlying micritic limestone (Fig. 5.9G). The dikes extend < 2 cm into the overlying limestone and are approximately 6-7 cm long. They penetrate the overburden at an angle of approximately 20°. The interbedded sandstones of the L1 lithofacies have a brown-green, massive weathered surface and the upper contact is preferentially eroded and frittery when the sandstone grades into a mudstone.

A prominent, almost 3 m thick, green-grey, well indurated, massive in its lower two thirds and laminated in its upper third, slightly glauconitic, calcareous fine sandstone occurs approximately midway through the L1 succession (Fig. 5.9A, H). A thin (c. 10 cm) mudstone caps the sandstone and the muddy limestone lithofacies (L2a) underlies it (Fig. 5.9A).

Contacts

The lower contact of L1 was discussed previously when describing the upper contact of M7a (see Section 5.2.1). The upper contact between L1 and the siliceous mudstone lithofacies (M2a) is sharp (Fig. 5.10A). The limestone flag immediately below the contact is burrowed to about the same degree as other underlying burrowed limestone flags. Ovoidal/lensoidal burrows (?*Planolites*) occur in this flag along with *Zoophycos* trace fossils (Fig. 5.9C and 5.10B). Immediately above the contact the lowermost bed of M2a has large, c. 7 cm wide, voids (possibly burrows) infilled with unconsolidated white powdery fine sand.

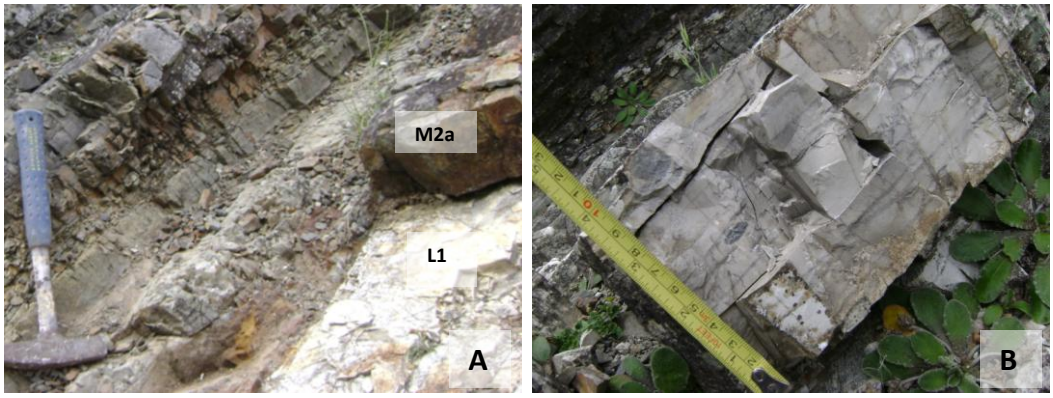

Figure 5.10: The upper contact of L1 is sharp (A) and burrowed (B) to about the same extent as most other underlying flags. Ovoidal/lensoidal shaped burrows (?*Planolites*) and *Zoophycos* are present through the uppermost limestone flag of L1 (B).

Petrography

The limestone and sandstone portions of L1 are described separately. The description is based on three representative samples from the limestone and one from the thick bed of sandstone that occurs about midway through the L1 succession. Description of the common thin sandstone beds is based on Nelson (1968).

Limestone description (MT4.17, 54, 60): The petrographic description and mineralogy of the limestone in L1 varies with the degree of burrowing and the amount of clastic material. Limestone with no burrowing is composed of many planktic foraminiferal tests, many to common radiolarian tests, some benthic foraminiferal tests, rare glaucony and phosphate grains, and very rare quartz/feldspar grains, all set in a micrite matrix (Fig. 5.11A). Of the rare clastic grains, almost all are from agglutinated tests and almost all are quartz. Many of the tests are intact and infilled with calcite. Calcite is also present as veins.

Burrowed limestone of L1 is much the same as unburrowed limestone but has the added feature of common burrows infilled with either coarse silt to fine sand sized quartz grains, or shell fragments (Fig. 5.11B, C). The rare marly limestone beds are dominated by micrite matrix and have a higher proportion of coarse silt and very fine sand sized clastic grains than the majority of the L1 limestone (Fig. 5.11D). Very little glaucony is present within these marly beds.

Limestone classification: Unburrowed flags are sparse biomicrite with an argillaceous quartzlutite clastic component. Burrowed flags are sparse biomicrite with common burrows infilled with either very slightly glauconitic very fine quartzarenite, or packed biomicrite. Rare marly beds are slightly muddy to very fine sandy sparse biomicrite with a feldsarenite and quartzose argillutite clastic component. Fig. 5.12 illustrates the varying degrees of L1 limestone purity at Pahaoa with the uppermost, middle, and lowermost L1 data points corresponding to unburrowed limestone, marly limestone, and burrowed limestone respectively

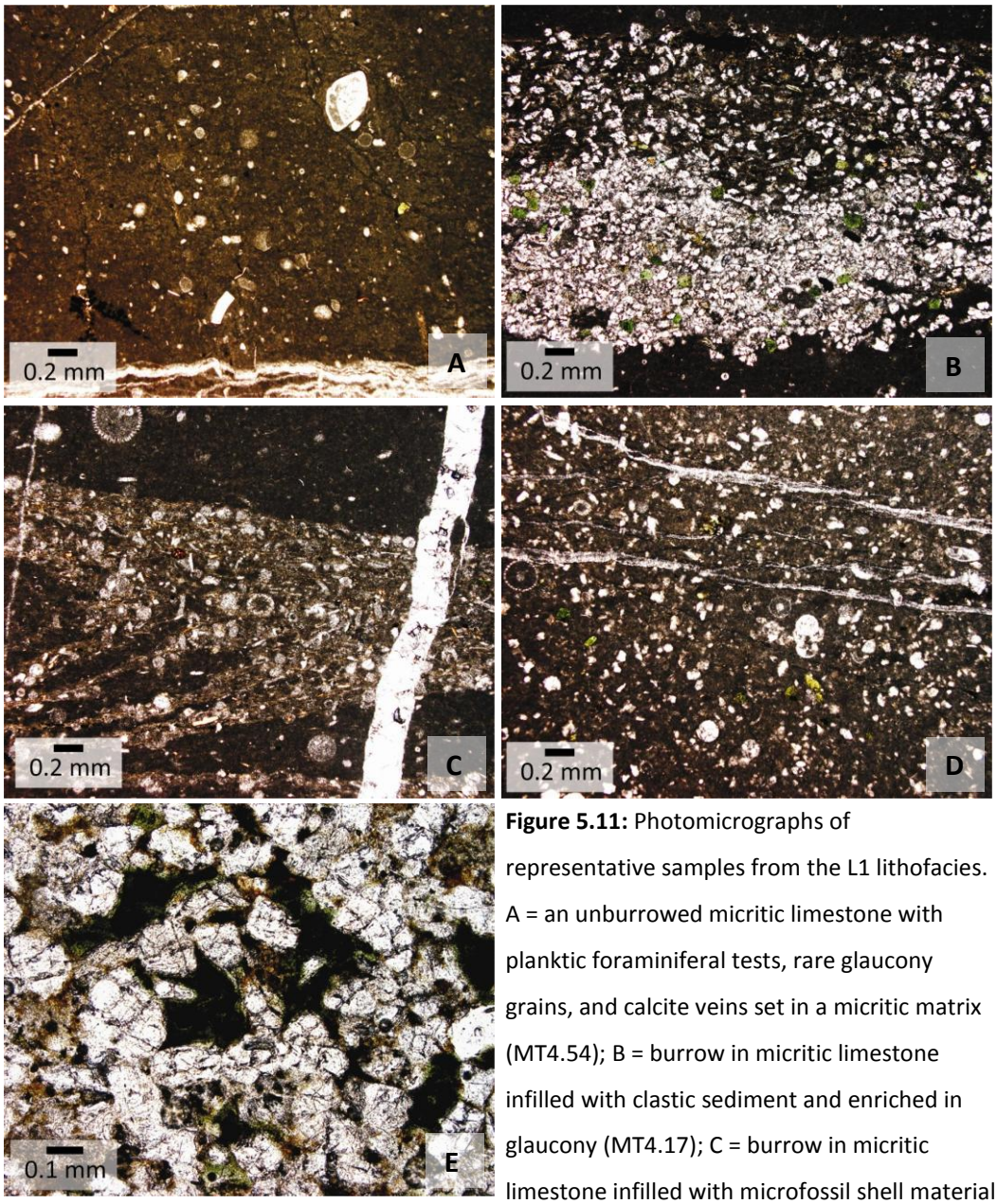

Figure 5.11: Photomicrographs of representative samples from the L1 lithofacies. A = an unburrowed micritic limestone with planktic foraminiferal tests, rare glaucony grains, and calcite veins set in a micritic matrix (MT4.54); B = burrow in micritic limestone infilled with clastic sediment and enriched in glaucony (MT4.17); C = burrow in micritic limestone infilled with microfossil shell material (MT4.17); D = a clastic sediment enriched marl (MT4.60); E = glaucony infilling pore spaces between quartz grains in the prominent sandstone bed within L1 (MT4.15).

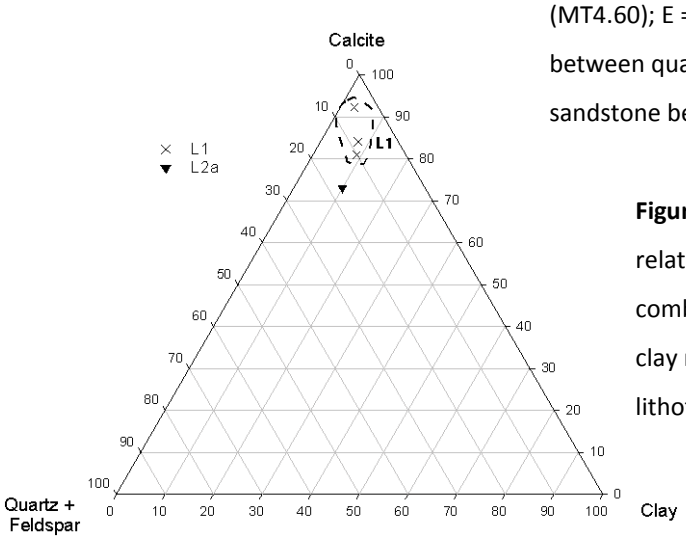

Figure 5.12: Ternary diagram of relative proportions of calcite, combined quartz and feldspar, and clay minerals in the limestone (L) lithotypes at the Pahaoa section.

Sandstone description (MT4.15, Nelson, 1968): The sandstone component of L1 consists of the thinly interbedded sandstones and the single thick sandstone bed mentioned above. Description of the interbedded sandstones is after Nelson (1968), where they are described as coarse silt to coarse sand sized clastic grains set in either a calcite cement or muddy matrix. The grains are moderately sorted and subangular to angular. The sandstones are usually normally graded with concentrations of clastics increasing towards the base of sandstones. Clastic quartz dominates the rock, with rock fragments, feldspar, and muscovite secondary in abundance (Fig. 5.7). Calcite infills void spaces and forms veins throughout the rock.

The thick sandstone bed is composed of grain supported coarse silt to medium sand sized clastic grains (Fig. 5.11E). Very little mud is present, and where it is it infills pore spaces between sand grains. The clastic grains are moderately to well sorted and subrounded to subangular. Fine grained rock fragments with speckly high interference colours occur in the sample. Quartz dominates the mineral assemblage with clay minerals, calcite, and feldspar minor components (Fig. 5.7). No microfossil tests were observed. Glaucony infills void spaces between quartz grains making it most likely authigenic (Fig. 5.11E).

Sandstone classification: The common thin sandstone beds are calcite cemented, very slightly to moderately glauconitic, submature subfeldsarenites (Fig. 5.7; based on Nelson, 1968). The thick sandstone bed that occurs midway through the L1 succession is a slightly glauconitic, submature to mature fine subfeldsarenite (Fig. 5.7).

5.2.3 Muddy limestone lithofacies (L2a)

L2 was encountered at Pahaoa (L2a; Fig. 5.2) and Akitio River (L2b) (Table 4.1). The description of the Pahaoa lithofacies is given here.

L2a

Field lithology

L2a occurs beneath a prominent, almost 3 m thick, sandstone about midway through the L1 succession (Fig. 5.13A, B). L2a is poorly exposed in the logged

area and its thickness is estimated as c. 2 m based on observations from this research and from previous work at Pahaoa (Fig. 5.13A, B; Nelson, 1968). The lithofacies consists of light green, well indurated, massive, flaggy, glauconitic, calcareous muddy micritic limestone, interbedded with micritic limestone and glauconitic sandstone lithologies similar to L1 (Fig. 5.13A, C). Its upper contact with the overlying thick sandstone bed is sharp. The flags in L2A are not as prominent as in L1, and L2a is more easily erodible (Fig. 5.13B).

Contacts

The upper contact with the prominent thick sandstone bed is sharp. The lower contact is poorly exposed but appears to be gradational (Fig. 5.13A, B).

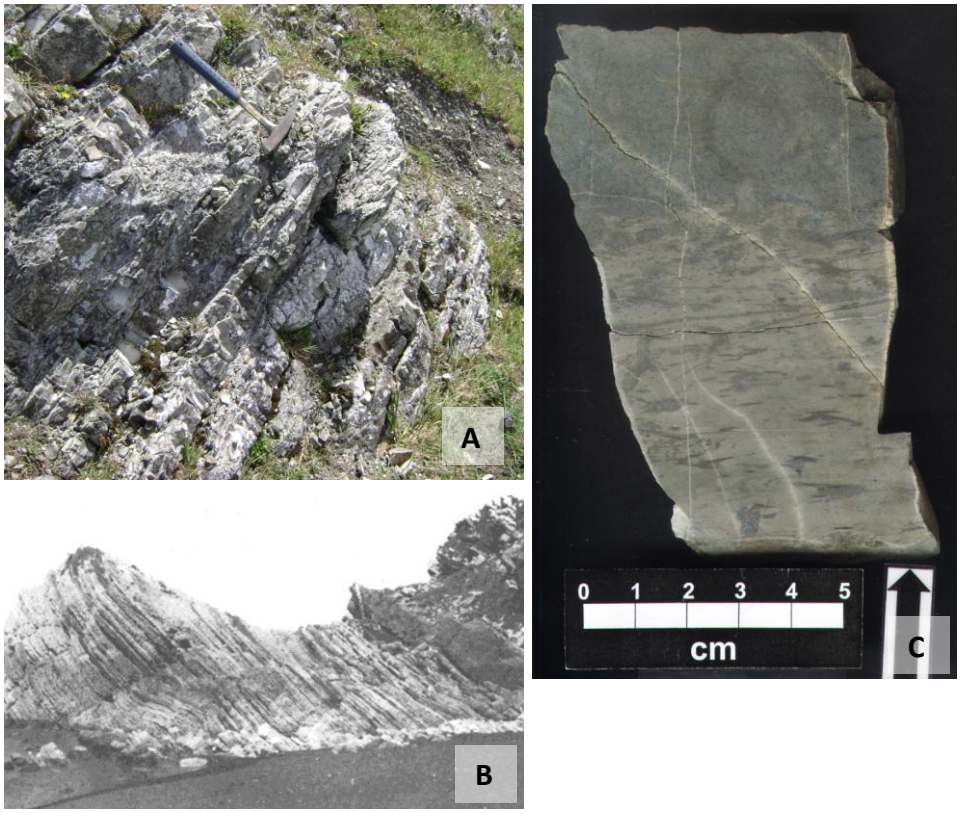

Figure 5.13: The muddy limestone lithofacies at Pahaoa (L2a). A = exposure of L2a as seen at the "high bluff" section; B = a better exposure of L2a beneath the thick prominent sandstone bed that is identifiable by its preferential weathering susceptability compared to L1 (photo from Nelson, 1968); C = green colouration and more clastic nature of L2a.

Petrography

Description (MT4.12): Description of L2a is based on one representative sample from the succession. The lithofacies comprises areas of relatively muddy and

relatively less muddy limestone. Less muddy areas are composed of coarse silt and very fine sand sized clastic grains infilling burrows within a dominant micrite matrix (Fig. 5.14A). The muddier areas are composed of very common coarse silt sized clastics with some muscovite and glaucony (an increase from the limestone of L1) set in a micrite matrix (Fig. 5.14B). Taken as a separate entity, the muddier portion of L2a could qualify as a siltstone due to the high abundance of silt sized clastics. However, each flag taken as a whole (including the less muddy portions) is here considered to be muddy limestone. Quartz and clay minerals dominate the clastic fraction, with minor feldspar. Some planktic and benthic microfossil tests float in the micritic matrix of the less muddy L2a and are rare in the muddier portions. There are fewer radiolarians compared with the L1 limestone.

Classification: Less muddy areas are fossiliferous micrite with abundant very slightly glauconitic, very muddy, micritic burrows. Muddy areas are very slightly glauconitic very muddy micrite with common fossiliferous micrite burrows or laminations. Taken as a whole the muddy limestones have an argillaceous quartzlutite clastic component. Fig. 5.12 compares the composition of L2 with L1 limestones, and illustrates the more clastic rich character of the L2 lithofacies.

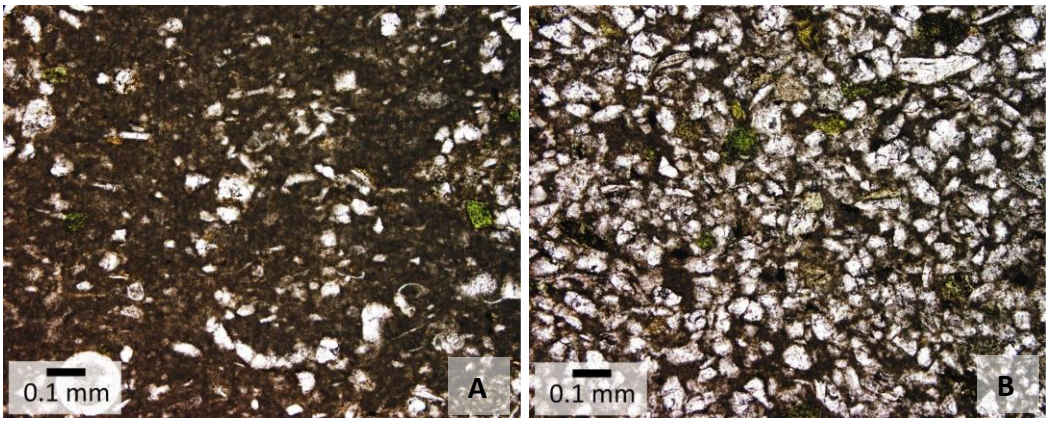

Figure 5.14: Photomicrographs of representative samples from the L2a lithofacies. In general the lithofacies is a muddy or silty micrite (A; MT4.60), but much higher abundances of silt-sized clastic grains occur in some flags (B; MT4.60).

5.2.4 Siliceous mudstone lithofacies (M2a)

Variations of M2 occur at four sections, including Pahaoa (M2a; Fig. 5.2)) (Table 4.1). Description of the Pahaoa variety follows.

M2a

Field lithology

The basal bed of M2a, briefly described above, consists of two lithologies. The lower lithology is fine grained (mudstone) and has very fine to fine sand-sized grains scattered through it. The upper lithology is a vaguely laminated, glauconitic muddy sandstone with a sharp undulating contact between it and the lower lithology. The basal bed as a whole is 10 cm thick, light blue-green-grey, well indurated, burrowed, and non-calcareous (Fig. 5.15A, B). As was mentioned above, the bed contains large, c. 7 cm wide, voids infilled with unconsolidated white powdery fine sand. The voids may be large burrows and are similar to, but larger than, burrows that occur at the Angora Road section (Fig. 6.3D). Phosphate/pyrite concretions occur at its base and it weathers to a rusty colour. The bed has sharp lower and upper contacts (Fig. 5.15A).

The rest of the M2a succession generally consists of fissile, poorly to moderately well bedded, often laminated, non-calcareous mudstone with occasional *Zoophycos* trace fossils in its lower portion (Fig. 5.15A, C-F). There is a shift in colour within the unit from dark grey in the basal c. 0.5 m (Fig. 5.15A), to dark green through the upper c. 0.5 m (Fig. 5.15C). The vague bedding of the unit is apparent through slight variations in grain size and/or cementation of sediments, with some horizons displaying more frittery weathering than others (Fig. 5.15A). Contacts between beds are mostly gradational, but several beds have sharp contacts, some of which undulate.

Contacts

The lower contact of M2a was discussed previously when describing the upper contact of the L1 lithofacies (see Section 5.2.2). The upper contact of M2a consists of the dark green upper part of the lithofacies grading upwards into light grey calcareous mudstone of basal M1a (Fig. 5.15C). The contact undulates and the bedding within and immediately above the contact interval mimics the undulating relief, so that the lateral thickness of M2a pinches and swells (Fig. 5.16A, B).

Figure 5.15: Features of the siliceous mudstone lithofacies at Pahaoa (M2a). A = exposure of the basal bed and dark grey lower half of M2a as seen at the "high bluff" section; B = the basal bed of M2a comprises a coarser grained upper half and common limonite staining; C = the upper dark green beds of M2a as seen at the "high bluff" section grading into basal M1a; D and E = examples of the dark grey mudstone of M2a with *Zoophycos* trace fossils; F = example of the dark green upper lithologies of M2a.

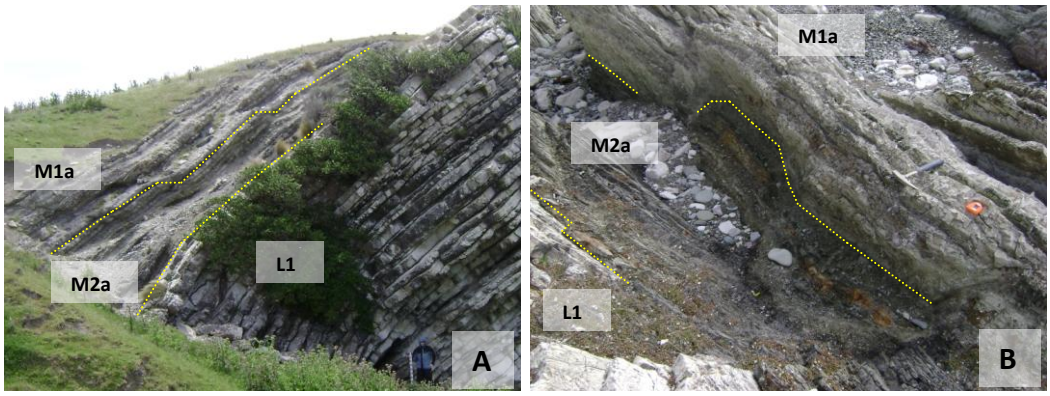

Figure 5.16: A = Undulating upper contact and pinch and swell nature of M2a at the "high bluff" section; B = M2a at the "cove" section where it is thinner than at the "high bluff" section.

Petrography

The basal bed, middle dark grey beds, and upper dark green beds of M2a are described separately. The basal bed description is based on one representative sample, description of the middle dark grey beds is based on three samples, and the upper dark green beds description is also based on three samples.

Basal bed description (MT4.18): The base of the basal bed is composed of very common radiolarian tests set in a very fine grained matrix (Fig. 5.17A). The radiolarians are mostly intact and appear flattened (Fig. 5.17B). Overlying this bed is a horizon of alternating millimetre scale laminations of more and less radiolarian rich sandy mudstone. The two basal horizons have very little glaucony (c. 1%) and some of the radiolarian rich beds have a fabric in which the matrix appears to be flowing around the radiolarians. Overlying the radiolarian rich horizons is a more glauconitic (c. 7%) moderately muddy sandstone with rare radiolarians (Fig. 5.17C). The visible clastic grains are well sorted and angular to subangular. An orange mineral, possibly limonite, infills pore spaces between

Figure 5.17: Photomicrographs of some of the microscopic features of M2a. A = basal fossiliferous horizon in the basal bed of M2a (MT4.18); B = a flattened planktic test (?radiolarian) within a muddy matrix with abundant coarse silt and sand sized clastics near the base of M2a (MT4.18); C = coarse upper portion of the basal bed in M2a with possible limonite infilling pore spaces between clastics (MT4.18); D = very fine mudstone rich in radiolarians (MT4.19); E = example of stretched or "flowing banded" fabric observed in M2a (MT4.19); F = veins infilled with an opaque mineral (MT4.21); G = radiolarian test (?*Amphisphaera kina* Hollis) showing pyrite replacement (MT4.22); H = calcite and pyrite occurring side by side within veins (MT4.22); I = glauconitised planktic microfossil tests and web-like pyrite veins within a fine matrix (MT4.22).

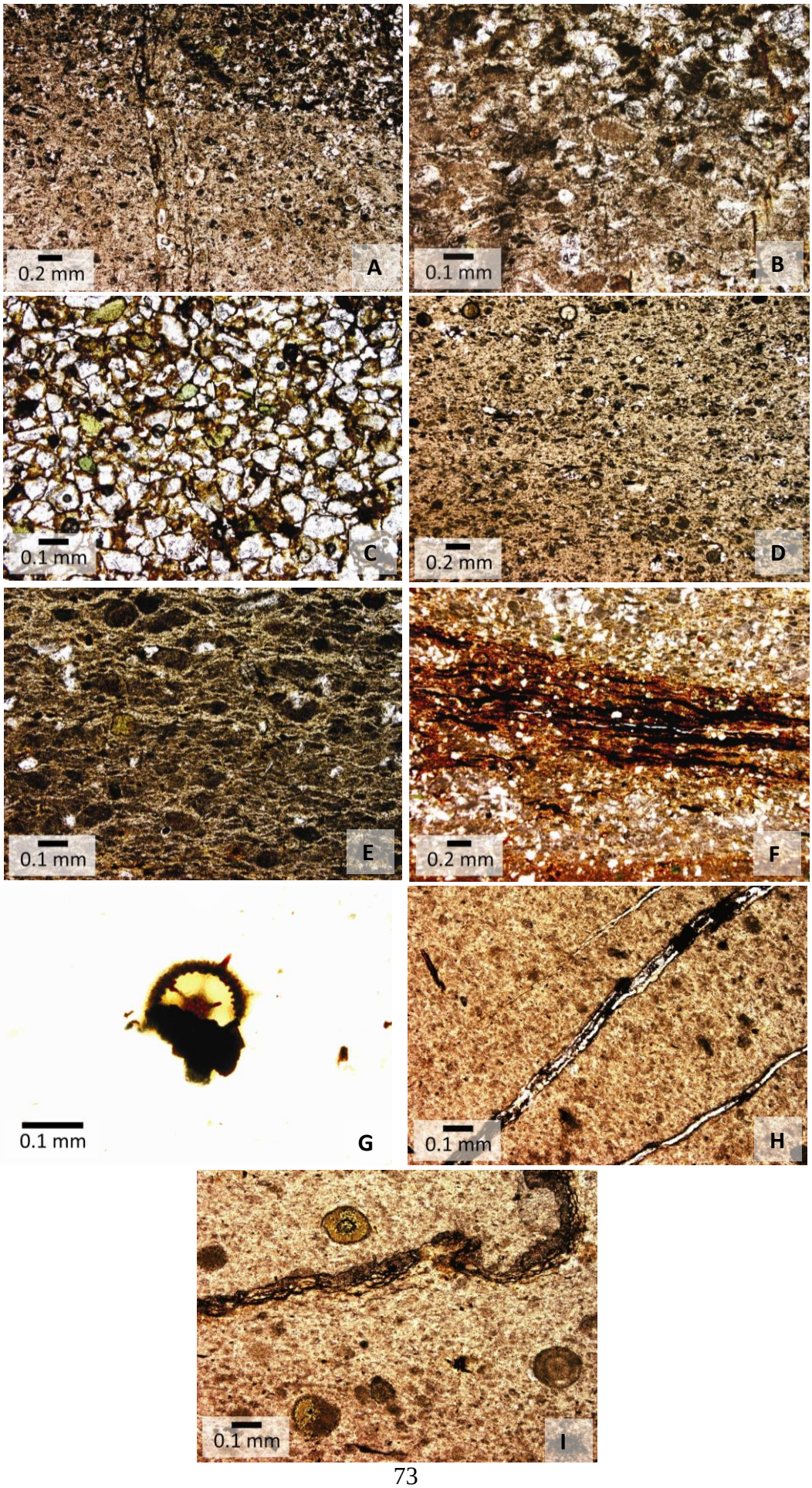
0.2 mm
A
0.1 mm
B
0.1 mm
C
0.2 mm
D
0.1 mm
E
0.2 mm
F
0.1 mm
G
0.1 mm
H
0.1 mm
I

grains in the uppermost horizon. Throughout the sample limonite and an opaque mineral, that does not appear to be pyrite, infill veins. The black veining tends to be more prevalent along bedding planes at the edges of burrows.

Basal bed classification: Very highly to non-fossiliferous (radiolarian dominated), burrowed, very slightly to non-glauconitic mudstone and submature very fine subfeldsarenite with veins possibly infilled with limonite and an opaque mineral.

Middle beds description (MT4.19, 20, 21): This unit corresponds to the dark grey beds described above. The base of the interval consists of some (c. 3%) very fine sand sized clastic grains set in a very fine muddy matrix (Fig. 5.17D). The rock is poorly sorted and the visible grains are angular to subrounded. Very fine sand sized muscovite grains occur. The grains that make up the muddy matrix are too small to be distinguished but appear to be aligned and anisotropic, as much of the matrix shows "straight extinction". Glaucony grains are rare. Radiolarian tests are very common, most are intact and some appear slightly flattened as they have a more lensoidal shape. The fabric of the matrix has a stretched or "flow banded" appearance in some horizons (Fig. 5.17E) and a black mineral (seemingly not pyrite) is present in the form of grains, veins that run parallel to bedding, and as an infill of trace fossil stractures (Fig. 5.17F).

Middle beds classification: Highly fossiliferous (radiolarian dominated) argillaceous quartzlutite with occasional black laminations and slightly sandy mudstone burrows.

Upper beds description (MT4.22, 23, 24): This unit corresponds with the dark green beds described above. There is a decrease in the abundance of sand and silt sized clastics and an overall fining of this unit compared to the lower units. The fining continues through the unit. There is also a reduction in the abundance of radiolarians and an increase upwards in the abundance of planktic and benthic foraminifera. The interval is composed of rare to absent sand sized clastics set in a very fine mud matrix. The coarser clastics are angular to subangular and poorly sorted. Possible faint burrows may be present through the top of the unit. Similarly to the underlying beds, the matrix is anisotropic and displays "straight

extinction". The lithology is dominated by quartz with subordinate clay minerals and minor feldspar, although, through the middle of the unit clay minerals dominate (Fig. 5.6). Occasional brown tinted calcite veins are apparent at the base of the interval and pyrite can be seen replacing tests, infilling veins alongside calcite, and forming web-like veins (Fig. 5.17H, I). Glaucony is rare and appears to be replacing and infilling tests (Fig. 5.17I). The abundance of radiolarians ranges from many to absent, with some or no planktic foraminifera present, and rare or no benthic foraminifera observed.

Upper beds classification: Slightly to very slightly fossiliferous (radiolarian or planktic foraminifera dominated) argillaceous quartzlutite and quartzose argillutite (through the middle of unit), with possible vague burrows in the upper most portion of the unit.

5.2.5 Calcareous mudstone lithofacies (M1a)

M1 is a widespread and variable lithofacies (Table 4.1). Its character at Pahaoa (M1a; Fig. 5.2) is described below.

M1a

Field lithology

The base of M1a consists of c. 1.5 m of grey to white, moderately indurated, bedded, calcareous mudstone with rare dark green, laminated, calcareous mudstone and blue-grey, faintly laminated, calcareous sandstone beds punctuating the sequence (Fig. 5.15C and 5.18A). Within beds the rock is either massive or laminated.

The basal lithologies of M1a grade upwards into the dominant M1a rock type of striped mudstone. However, at the "cove" section the gradual transition is interrupted by an c. 0.7 m thick interval of highly distorted red and light green striped mudstones (Fig. 5.18B). The colours of the mudstone are folded and intertwined with one another. The distorted mudstone appears to scour into the underlying bed and consequently the lower contact undulates (Fig. 5.18B). A single sandstone bed in the immediately underlying succession is faulted (Fig. 5.18A). Basal M1a is also exposed at the "high bluff" section where it forms a

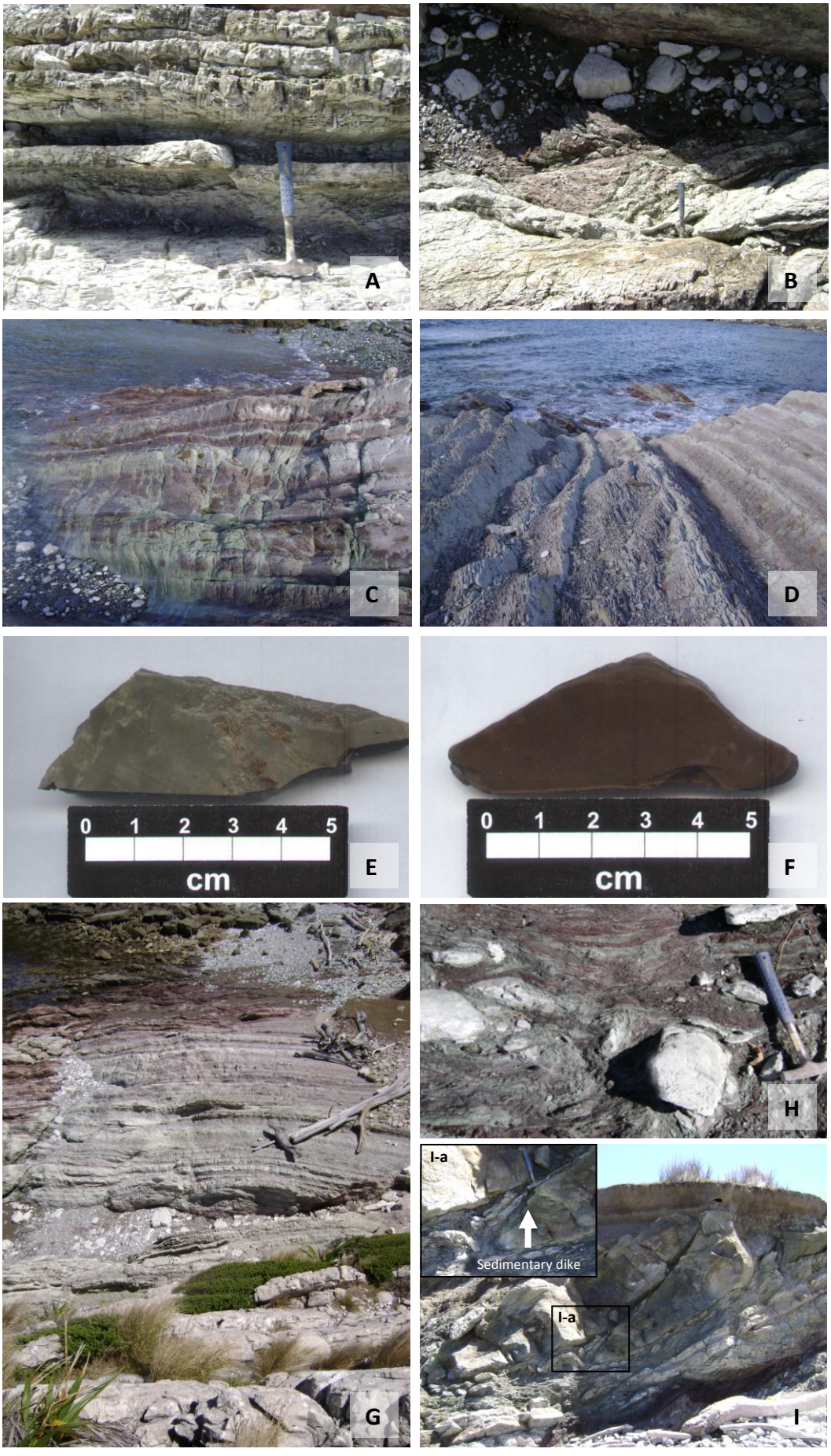
A
B
C
D
0 1 2 3 4 5
cm
E
0 1 2 3 4 5
cm
F
G
H
I-a
Sedimentary dike
I-a
I

thicker succession. Here the interval of distorted mudstone is missing and the dominant M1a rock type is unexposed (Fig. 5.15C).

The dominant rock type in M1a consists of mudstones with red and green (and minor grey) stripes (Fig. 5.18C, E, F). The mudstones are moderately indurated, poorly to moderately well bedded in outcrop (Fig. 5.18D), massive in hand pecimen, and calcareous. The coloured stripes form continuous and semi-continuous alternating bands that run parallel to semi-parallel with bedding (Fig. 5.18C). The contacts between some of the stripes undulate and within a single stripe thin streaks of another colour are occasionally observed. The stripes are more distinct and patchy when they are wet (Fig. 5.18C). The bedding of M1a appears to have formed as a result of different weathering susceptibility between the coloured stripes. The colour and intensity of the stripes changes through the succession, with a greater proportion of green mudstone at the base, more red to light red mudstone through the middle, and dark red mudstone dominates through the upper portion of the succession (MT5.18G). The redder upper portion of the sequence is more susceptible to erosion and it has a number of horizons where the coloured stripes have been folded and become intertwined with one another. These horizons often include foreign clasts (Fig. 5.18H). Broken up and intact sandstone beds occur in the upper portion of the sequence.

Contacts

The lower contact of M1a was discussed previously when describing the upper contact of the M2a lithofacies (see Section 5.2.4). The contact between M1a and M7b is sharp and erosional. It occurs above a thick broken up sandstone bed and a few phosphate/pyrite nodules are at the contact. Sedimentary dikes and broken

Figure 5.18: The calcareous mudstone lithofacies at Pahaoa (M1a). A = basal M1a with a thin sandstone bed that has been faulted; B = distorted striped mudstone with an undulating lower contact within basal M1a; C = the red and green stripes of the lower half of M1a; D = example of M1a bedding which appears to result from differing weathering susceptibility of the red, green, and grey mudstones; E and F = examples of the green and red mudstone of M1a respectively; G = exposed lower half of M1a with the dominant mudstone colour transitioning from green to red upwards; H = distorted upper M1a with foreign clasts; I = M1a upper contact marked by broken up sandstone beds and sedimentary dikes (inset I-a).

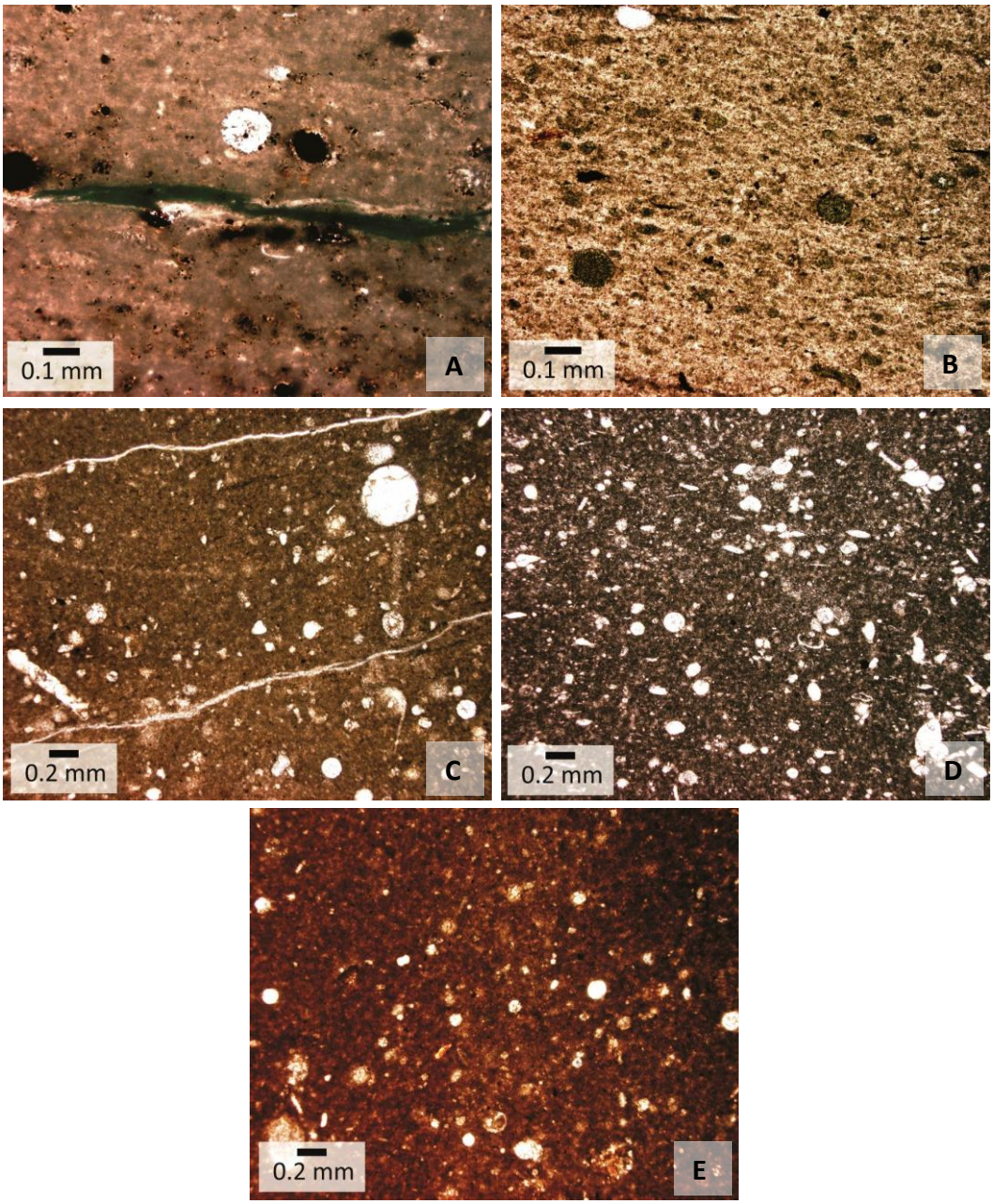

Figure 5.19: Photomicrographs of some of the microscopic features of the M1a lithofacies. A (MT4.25) and B (MT4.26) = basal M1a with pyritised tests, green veins (possibly fluorite; A) and glauconitised tests (B) set within a very fine grained matrix; C – E = examples of the green mudstone (C; MT4.71), mixed red and green mudstones (D; MT4.75) and red mudstone (E; MT4.76) of M1a. These mudstones are much the same except the red mudstone matrix has a red colour, and the mixed red and green mudstones have more planktic foraminifera.

up and distorted sandstone and mudstone beds are present in the strata immediately below the contact (Fig. 5.18I).

Petrography

The basal unit and striped mudstone of M1a are described separately. The basal

unit description is based on two samples. Description of the striped mudstone is based on three samples.

Basal unit description (MT4.25, 26): The basal unit of M1a consists of very rare to absent sand sized clastics (two grains total observed) set within a very fine muddy matrix (Fig. 5.19A, B). Parts of the matrix showed simultaneous extinction. The rare clastics are angular to subangular and the maximum size is fine sand sized. Quartz and clay minerals dominate the clastic fraction of the mineral assemblage (Fig. 5.6) with calcite a significant component of the whole rock mineral assemblage. Laminations of a light green mineral, possibly fluorite, occur in the lower portion of the unit (Fig. 5.19A) with glaucony rich horizons occurring in the units upper part (Fig. 5.19B). Some planktic foraminifera float in the muddy matrix throughout the unit with many radiolarian tests occurring through the upper part. Benthic foraminifera are rare. Calcite and pyrite form veins and infill tests through the unit.

Basal unit classification: Very slightly fossiliferous (planktic foraminifera dominated) quartzose argillutite with calcite veining, pyritised tests, and possibly pyritised glaucony. Shifts upwards to a slightly fossiliferous (radiolarian dominated), very slightly pyritic argillaceous quartzlutite.

Striped mudstone description (MT4.71, 75, 76): The succession contains virtually no visible clastic grains, and those that are present are of very fine to fine sand size. Glaucony is rare to absent and set in a very fine muddy matrix. Calcite is present in the form of veins and infilling tests. The green coloured mudstones contain many planktic foraminifera, possibly some rare radiolarians, and rare benthic foraminifera (Fig. 5.19C). The red mudstone has a similar fossil assemblage, but radiolarians are absent (Fig. 5.19E). Mixed red and green mudstones have common planktic foraminifera and rare benthic tests (Fig. 5.16D).

Striped mudstone classification: Slightly to moderately fossiliferous (planktic foraminifera dominated) quartzose argillutite.

5.3 Mineralogical trends

M7a is relatively high in feldspar, and this generally decreases upwards through the section. Quartz is high in M7a, through the middle of L1 – in the vicinity of L2a and the thick sandstone bed – and through M2a. Clay minerals are high through M7a, M2a, and M1a, but also increase in L2a and in the thick sandstone bed in L1. Radiolarians are apparent in L1 but are most abundant in M2a.

5.4 Geochemistry and palynofacies results

Geochemical and palynofacies proxies used in this study were introduced in Chapter 3 (Sections 3.3.2 to 3.3.4) and are presented here for the Pahaoa section. Fig. 5.20 and 5.21 present the up section trends for carbonate carbon and organic carbon stable isotopes (a) and elemental proxies for ocean surface water biological productivity (b, c), seawater nutrient availability (d), bottom water oxygen levels (e), aeolian sediment supply (f), glaucony (g), and terrigenous sediment supply (h). Up section variations in ocean surface water biological productivity and bottom water oxygen levels are also indicated by the average percent organic carbon plot (i). Included in the figures are palynofacies proxies for the depositional areas proximity to the paleoshoreline (j-o).

Fig. 5.20 displays up section trends of the above mentioned proxies for the entire portion of the Pahaoa section that was sampled, whereas Fig. 5.21 presents the same data, but for only a small portion of the section centred on M2a. M2a is focused on in this figure because of its potential correlation to lithologic units elsewhere in the East Coast Basin that span the Late Paleocene event (LPE) – a period of inferred short-term climate cooling. Preliminary interpretations of geochemical and palynofacies trends are offered in this section, even though this is a results chapter, to aid later interpretations (see Chapter 10).

5.4.1 Elemental geochemistry and organic carbon proxies

In this section the results for elemental geochemistry and organic carbon proxies (Fig. 20b-i and 21b-i) are described. However, first the ocean surface water biological productivity proxies are tested for biogenic association using the methods outlined in Chapter 3. This is done in order to assess their reliability as paleoproductivity indicators for the logged area of the Pahaoa section. If a

productivity proxy is found to have no biogenic association its trends will not be described in detail.

Testing for productivity proxy biogenic association

Ba[exc] appears to have a biogenic association through M7a but poor correlation between Ba[exc] and Ba/Ti in L1 suggests that the proxy is not a reliable productivity proxy through this lithofacies (Fig. 5.20b). Additionally, the two biggest Ba/Ti spikes in L1 are associated with relatively "normal" Ba values for the section and very low TiO_2 values, suggesting the elevated values may be a function of sediment starvation rather than increased productivity.

Ba[exc] co-varies with Ba/Ti and is poorly correlated with TRG through M2a and the base of M1a indicating that the Ba[exc] proxy has a biogenic association through this portion of the section (Fig. 5.20b). Ba[exc] through the majority of M1a co-varies with TRG and slightly with Ba/Ti, which may suggest a mixed terrigenous and biogenic association with Ba[exc] through M1a (Fig. 5.20b).

Si[exc] appears to record siliceous productivity through the section and is not influenced by detrital fluxes. There is no dramatic change in Si[exc] between the siliciclastic rich M7a and the siliciclastic poor L1, and the thin quartz rich sandstone beds within L1 often show a decrease in Si[exc] relative to the bounding limestone (Fig. 5.20b). These trends support the inference that Si[exc] is recording a biogenic silica signal.

Proxy results

Entire sampled section

Based on Ba[exc], M7a is a low productivity lithofacies. Siliceous productivity increases slightly near the limestone bed within M7a and then remains relatively steady through the section except for two spikes, the lower in L2 and the thick sandstone bed, and the upper in M2a. Based on Ba[exc], M2a also shows increased productivity. Calcareous productivity is negatively correlated with the Si[exc] spikes and is at its maximum in the limestone bed in M7a, through L1, and within M1a. A spike in Ba[exc] at the base of M1a seems to coincide with an

increase in Ca[exc] and so probably records an increase in calcareous productivity at the transition from M2a to M1a.

The seawater nutrient availability proxy (P[ef]) does not co-vary with Ba[exc] and only to a limited extent with calcareous and siliceous productivity proxies, bringing into question its effectiveness as a nutrient availability proxy at Pahaoa (Fig. 5.20d). Similarly to Ba/Ti, P[ef] spikes in L1 are associated with "normal" P_2O_5 values and low TiO_2 values and so may be a function of sediment starvation rather than increased nutrient availability.

Generally the Pahaoa strata record an oxic environment of deposition, but two intervals of suboxic conditions are also evident, the lower near the top of M7a and the upper at the base of M2a (Fig. 5.20e).

M7a has Ti/Al values slightly above 0.04, and it is especially high near the lithofacies upper contact, while M2a and M1a have values close to the threshold (Fig. 5.20f). The sandstone beds in L1 and the muddy limestones of L2a usually slightly exceed the threshold value, while the limestone bed in M7a and the limestones in L1 have Ti/Al values well below 0.04. The low values in the limestone are probably due to Al scavenging depressing the Ti/Al ratio. Overall the proxy may indicate an increase in offshore wind or current strength, or terrigenous sediment starvation in M7a and L1 (based on the clastic components), however the subtlety in enrichment means that it is not a strong inference.

Trends in Fe[ef] and K[ef] mostly mimic Ba/Ti and P[ef] trends and are likely to be influenced by terrigenous input.

TRG is relatively high through M7a but drops at the limestone bed (Fig. 5.20h). It is low through L1, with spikes at the interbedded sandstone and the prominent sandstone beds, and an increase in L2a. Towards the top of the section, in M2a and M1a, TRG increases and remains relatively high.

M2a

As has been mentioned in this sections introductory comments, M2a is looked at

in more detail (Fig. 5.21) because it was possibly deposited during the time period of particular interest to this study. From Fig 5.21e it is apparent that suboxic conditions within the lithofacies occur not *at* the base, but *near* the base of the succession, and then become oxic upwards. Fe[ef] trends do not correlate with K[ef] trends so the proxy is not considered to reflect glaucony content. Maximum organic carbon content and maximum TRG within the lithofacies coincides with suboxic conditions (Fig. 5.21h, i). TRG remains relatively high through the interval and the trend in organic carbon generally follows the TRG trend. Organic carbon is absent or very low through the analysed portion of M1a.

5.4.2 Palynofacies proxies

The palynofacies proxies used in this study and their significance to paleodepositional environments are outlined in Chapter 3 (Section 3.3.2). At Pahaoa, palynofacies analysis was performed on M2a and the basal half of M1a. Palynomorphs are rare throughout the analysed succession (Fig. 5.21j). The percent of amorphous organic matter (AOM), percent phytoclasts, and LOG black:brown phytoclast analyses all show the general trend suggesting that the shoreline became more proximal from the basal sandstone of M2a to the immediately overlying mudstone (Fig. 5.21k-m). This is followed by the shoreline becoming more distal through the remainder of M2a. This trend is briefly reversed over the boundary between M2a and M1a before continuing to become more distal through the base of M1a (Fig. 5.21k-m). In the middle of the logged area of M1a there appears to be a gradual slowing of the trend, with a reversal to more proximal conditions occurring in the uppermost portion of the logged area.

5.4.3 Stable isotopes

Carbonate and organic carbon stable isotopes show some distinct trends through the Pahaoa section (Fig. 5.20a). Carbonate carbon isotopes are lowest within M7a, but a positive trend begins in the upper portions of the lithofacies synchronous with relatively low Ca[exc] and high Si[exc] values for that lithofacies. The positive trend continues through into basal L1 and remains high through L1 and M2a. Two negative excursions occur within this interval, one associated with the mudstone overlying the prominent thick sandstone bed within

L1, and the other in uppermost L1. There is a sharp positive organic carbon isotope excursion near the base of M2a followed by a more gradual negative trend through the remainder of the lithofacies. Organic carbon isotope values remain relatively steady and carbonate carbon isotopes show a gradual decrease through M1a.

Up section trends for stable oxygen isotopes are presented in Fig. 5.22. Oxygen isotope values do not appear to be affected by diagenetic alteration as they do not co-vary with the carbon isotope values (cf. Fig. 5.21a and 5.22). M7a and the lower two thirds of L1 generally show decreasing oxygen isotope values, with a slight positive trend occurring through upper L1 leading into the M2a contact. These gradual tends are punctuated by three intervals of sharply fluctuating oxygen isotope values. The two lowermost intervals each consist of a sharp positive excursion followed immediately by a negative excursion. The lower of these two intervals occurs near the upper contact of M7a, and the higher of the two begins in the L2a lithofacies and ends in the upper half of the L1 lithofacies. The third, and uppermost, interval of sharply fluctuating oxygen isotope values occurs through M2a and basal M1a and consists of a negative excursion followed by a positive excursion.

Figure 5.20: Variations for the entire Pahaoa section in carbon isotopes (a), ocean surface water productivity proxies (b, c, i), proxies for seawater nutrient availability (d), bottom water oxygen levels (e, i), aeolian sediment input (f), glaucony (g), and terrigenous sediment input (h), and various palynofacies proxies for shoreline proximity to the site of deposition (j – o).

Figure 5.21: Variations for M2a lithofacies at Pahaoa in carbon isotopes (a), ocean surface water productivity proxies (b, c, i), proxies for seawater nutrient availability (d), bottom water oxygen levels (e, i), aeolian sediment input (f), glaucony (g), and terrigenous sediment input (h), and various palynofacies proxies for shoreline proximity to the site of deposition (j – o).

Fig. 5.20

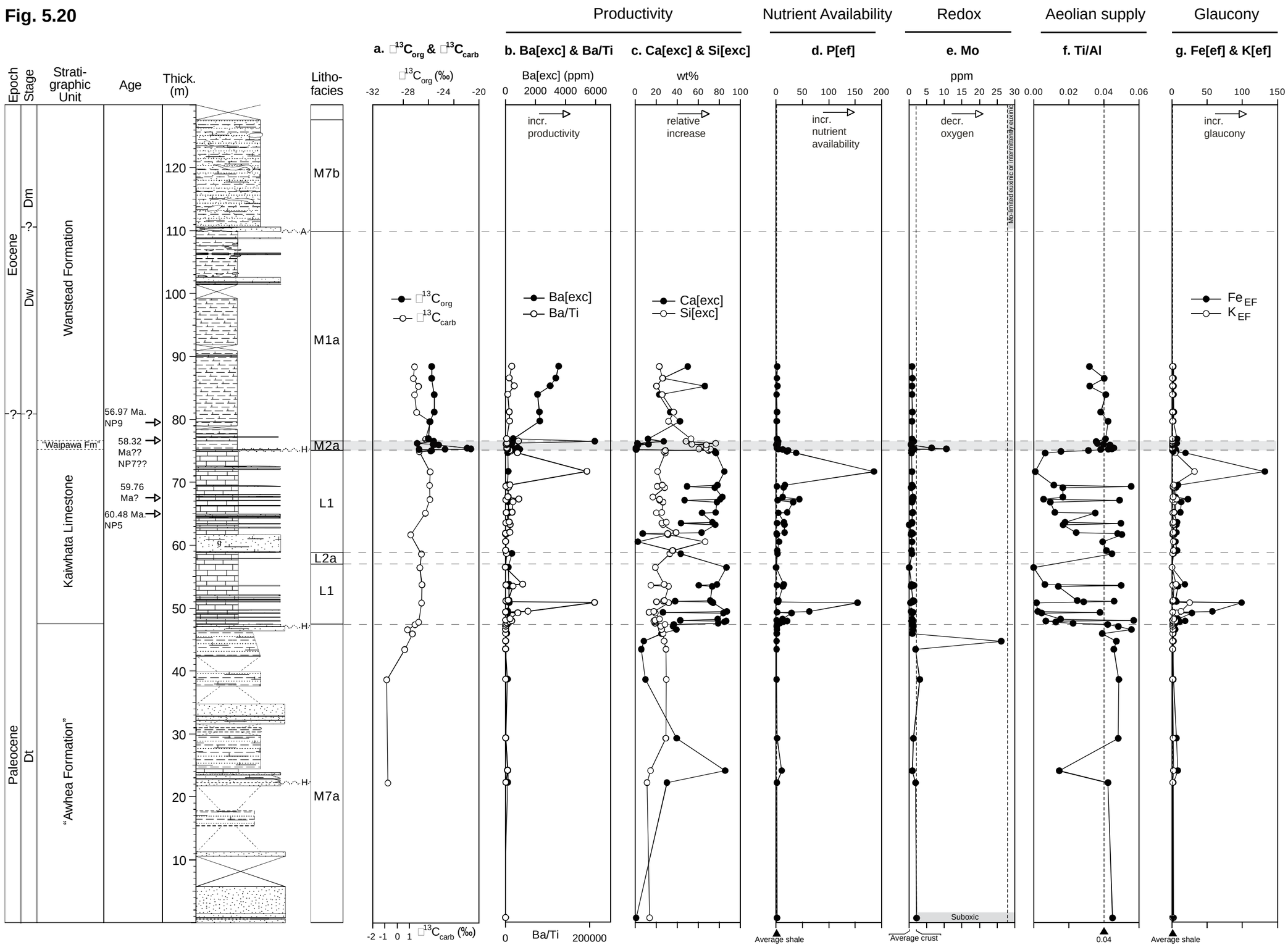
Productivity
Nutrient Availability
Redox
Aeolian supply
Glaucony
a. δ13Corg & δ13Ccarb
b. Ba[exc] & Ba/Ti
c. Ca[exc] & Si[exc]
d. P[ef]
e. Mo
f. Ti/Al
g. Fe[ef] & K[ef]
Epoch
Stage
Strati-graphic Unit
Age
Thick. (m)
Litho-facies
Eocene
Paleocene
Dm
Dw
Dt
Wanstead Formation
Kaiwhata Limestone
"Awhea Formation"
56.97 Ma. NP9
58.32 Ma?? NP7??
59.76 Ma?
60.48 Ma. NP5
"Waipawa Fm"
M7b
M1a
M2a
L1
L2a
L1
M7a
δ13Corg (‰)
Ba[exc] (ppm)
wt%
ppm
incr. productivity
relative increase
incr. nutrient availability
decr. oxygen
Mo-limited euxinic or intermittently euxinic
incr. glaucony
δ13Corg
δ13Ccarb
Ba[exc]
Ba/Ti
Ca[exc]
Si[exc]
Fe EF
K EF
Suboxic
Average shale
Average crust
0.04
Average shale

Fig. 5.20 cont.

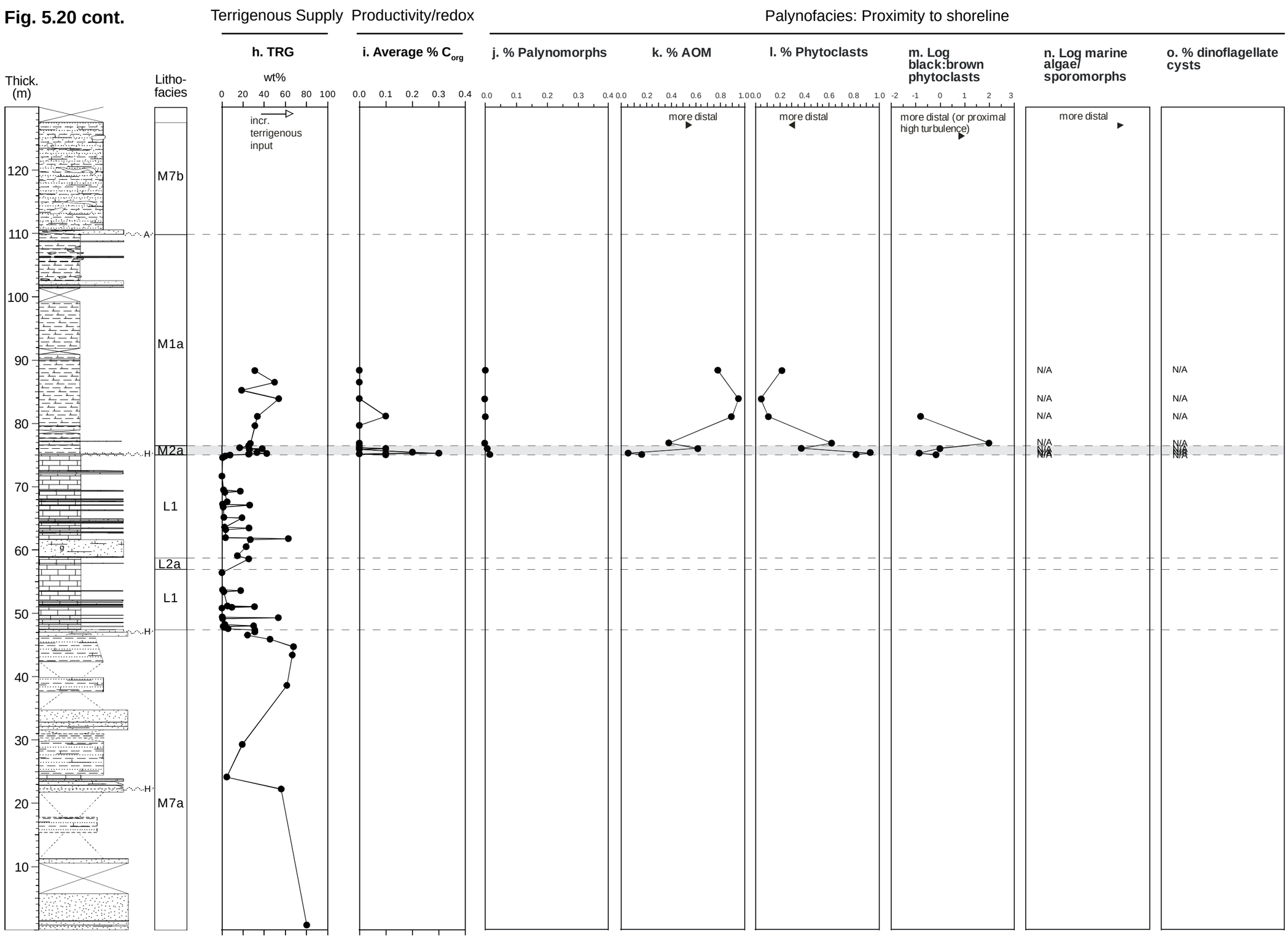
Terrigenous Supply
Productivity/redox
Palynofacies: Proximity to shoreline
Thick. (m)
Litho-facies
h. TRG
wt%
0 20 40 60 80 100
incr. terrigenous input
i. Average % C org
0.0 0.1 0.2 0.3 0.4
j. % Palynomorphs
0.0 0.1 0.2 0.3 0.4
k. % AOM
0.0 0.2 0.4 0.6 0.8 1.0
more distal
l. % Phytoclasts
0.0 0.2 0.4 0.6 0.8 1.0
more distal
m. Log black:brown phytoclasts
-2 -1 0 1 2 3
more distal (or proximal high turbulence)
n. Log marine algae/ sporomorphs
more distal
o. % dinoflagellate cysts
N/A
120
110
100
90
80
70
60
50
40
30
20
10
M7b
M1a
M2a
L1
L2a
L1
M7a
A
H
g
H
H

Fig. 5.21

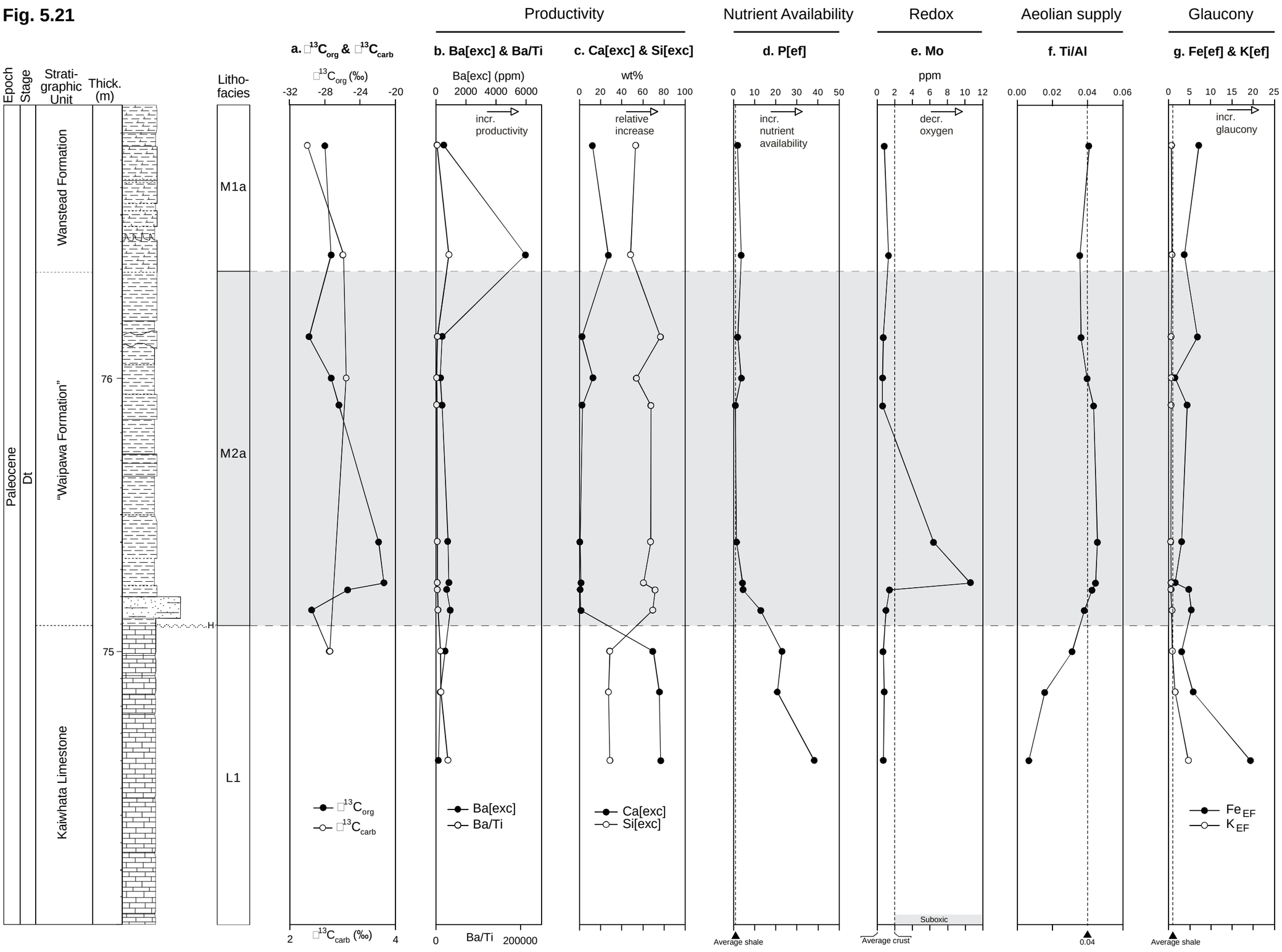
Productivity
Nutrient Availability
Redox
Aeolian supply
Glaucony
Epoch
Stage
Strati-graphic Unit
Thick. (m)
Litho-facies
Paleocene
Dt
Wanstead Formation
"Waipawa Formation"
Kaiwhata Limestone
76
75
H
M1a
M2a
L1
a. δ13Corg & δ13Ccarb
δ13Corg (‰)
-32 -28 -24 -20
b. Ba[exc] & Ba/Ti
Ba[exc] (ppm)
0 2000 4000 6000
incr. productivity
c. Ca[exc] & Si[exc]
wt%
0 20 40 60 80 100
relative increase
d. P[ef]
0 10 20 30 40 50
incr. nutrient availability
e. Mo
ppm
0 2 4 6 8 10 12
decr. oxygen
f. Ti/Al
0.00 0.02 0.04 0.06
g. Fe[ef] & K[ef]
0 5 10 15 20 25
incr. glaucony
δ13Corg
δ13Ccarb
Ba[exc]
Ba/Ti
Ca[exc]
Si[exc]
FeEF
KEF
2 δ13Ccarb (‰) 4
0 Ba/Ti 200000
Average shale
Suboxic
Average crust
0.04
Average shale

Fig. 5.21 cont.

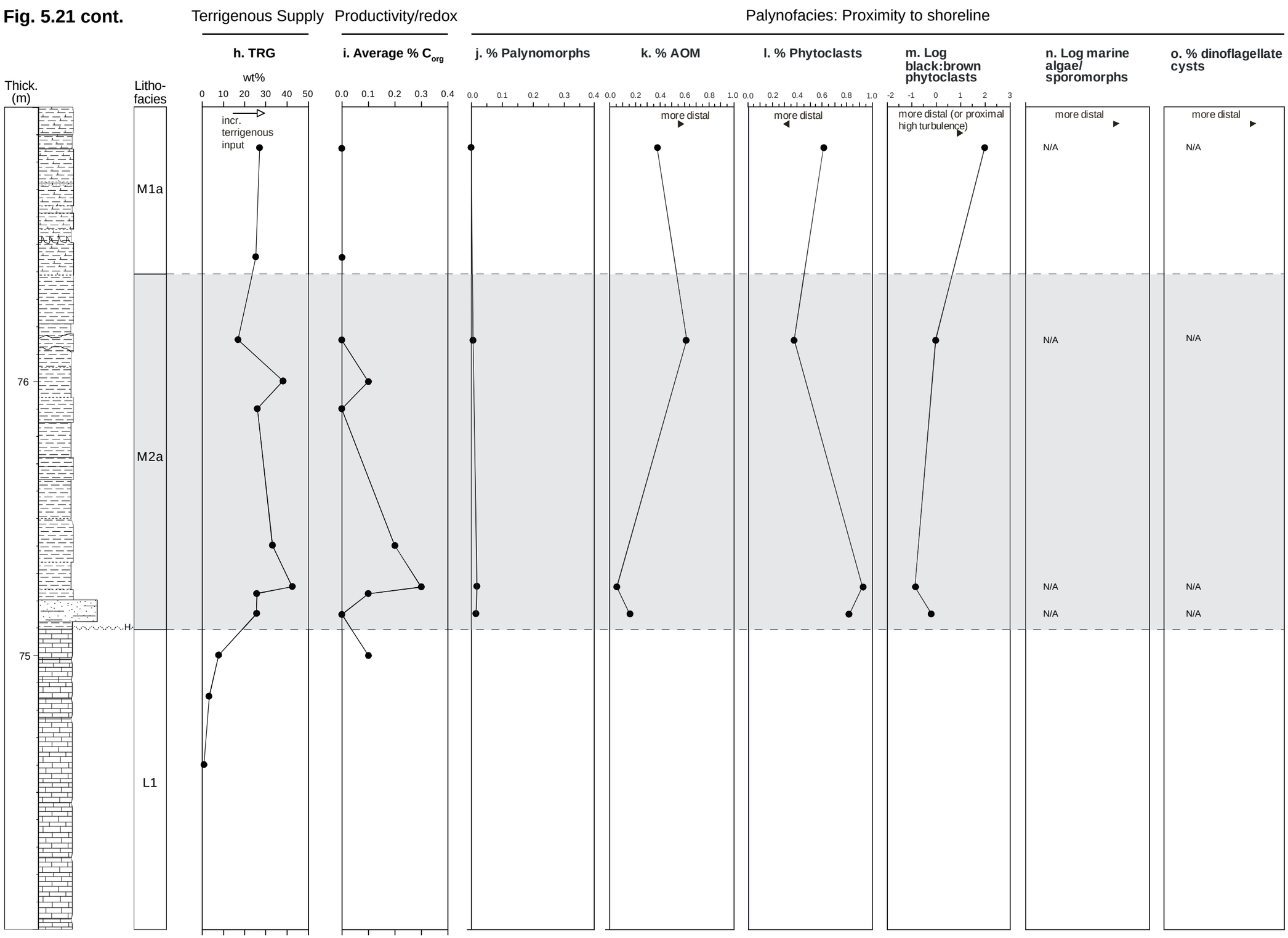
Terrigenous Supply
Productivity/redox
Palynofacies: Proximity to shoreline
Thick. (m)
Litho-facies
h. TRG
wt%
0 10 20 30 40 50
incr. terrigenous input
i. Average % C org
0.0 0.1 0.2 0.3 0.4
j. % Palynomorphs
0.0 0.1 0.2 0.3 0.4
k. % AOM
0.0 0.2 0.4 0.6 0.8 1.0
more distal
l. % Phytoclasts
0.0 0.2 0.4 0.6 0.8 1.0
more distal
m. Log black:brown phytoclasts
-2 -1 0 1 2 3
more distal (or proximal high turbulence)
n. Log marine algae/ sporomorphs
more distal
N/A
o. % dinoflagellate cysts
more distal
N/A
M1a
M2a
L1
76
75
H
N/A
N/A
N/A
N/A
N/A
N/A

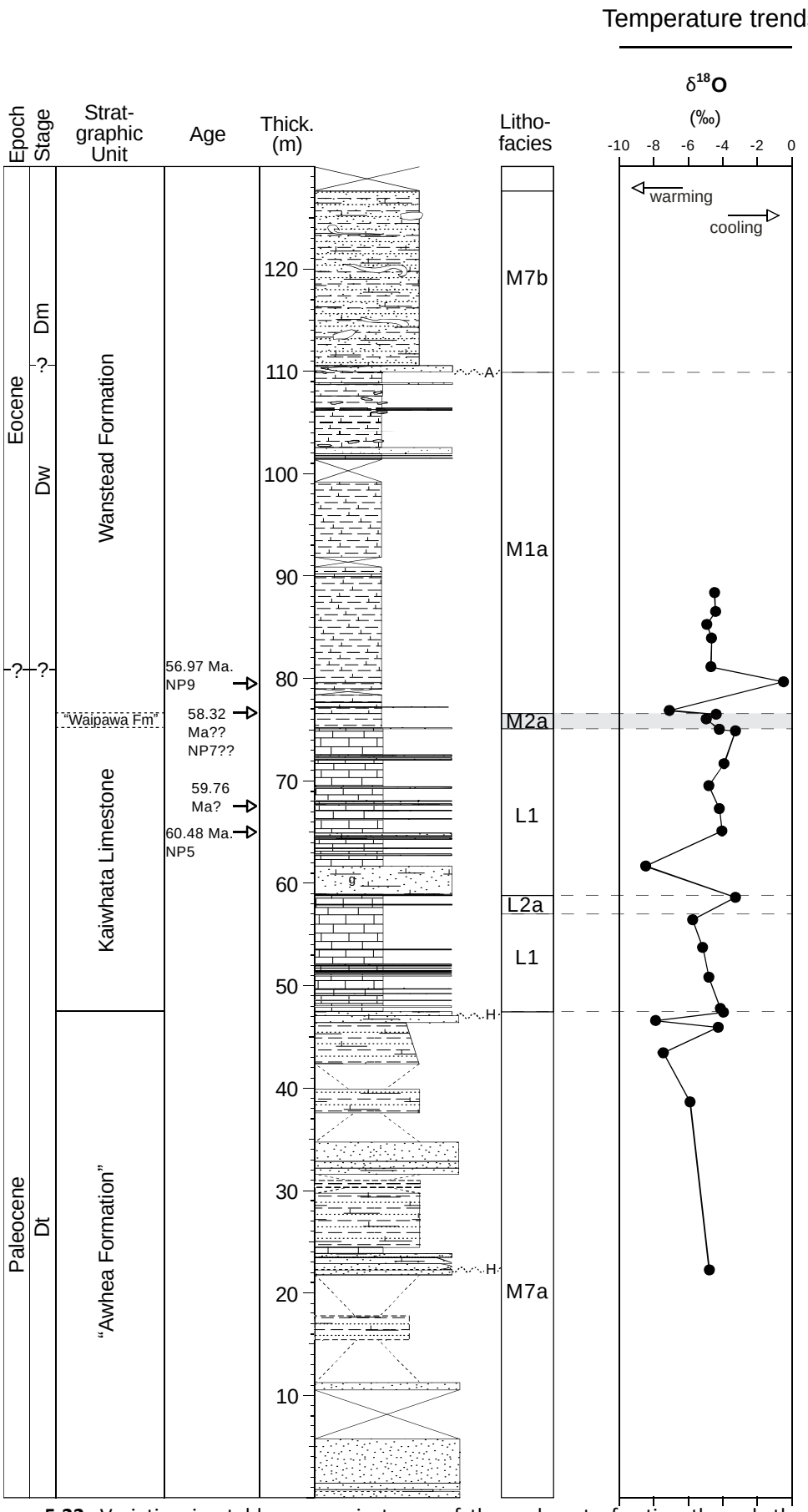

Figure 5.22: Variation in stable oxygen isotopes of the carbonate fraction through the entire logged section at Pahaoa.

6.1 Location

The Angora Road section is located in southern Hawke's Bay between the small settlements of Weber and Wimbledon, on Angora Road (off Route 52) (Fig. 2.2 and 6.1). Two sections were logged to form a semi-continuous stratigraphic column (Fig. 6.1 and 6.2). The majority of strata described crop out in Angora Stream and a nearby quarry, both located c. 1 km from the main road, on Angora Road, and collectively named here the "lower" Angora Road section (Fig. 6.1). The uppermost lithologies logged were exposed a further c. 1.7 km up Angora Road at what is referred to as the "upper" Angora Road section in this study (Fig. 6.1). Exposure through the two sections is variable.

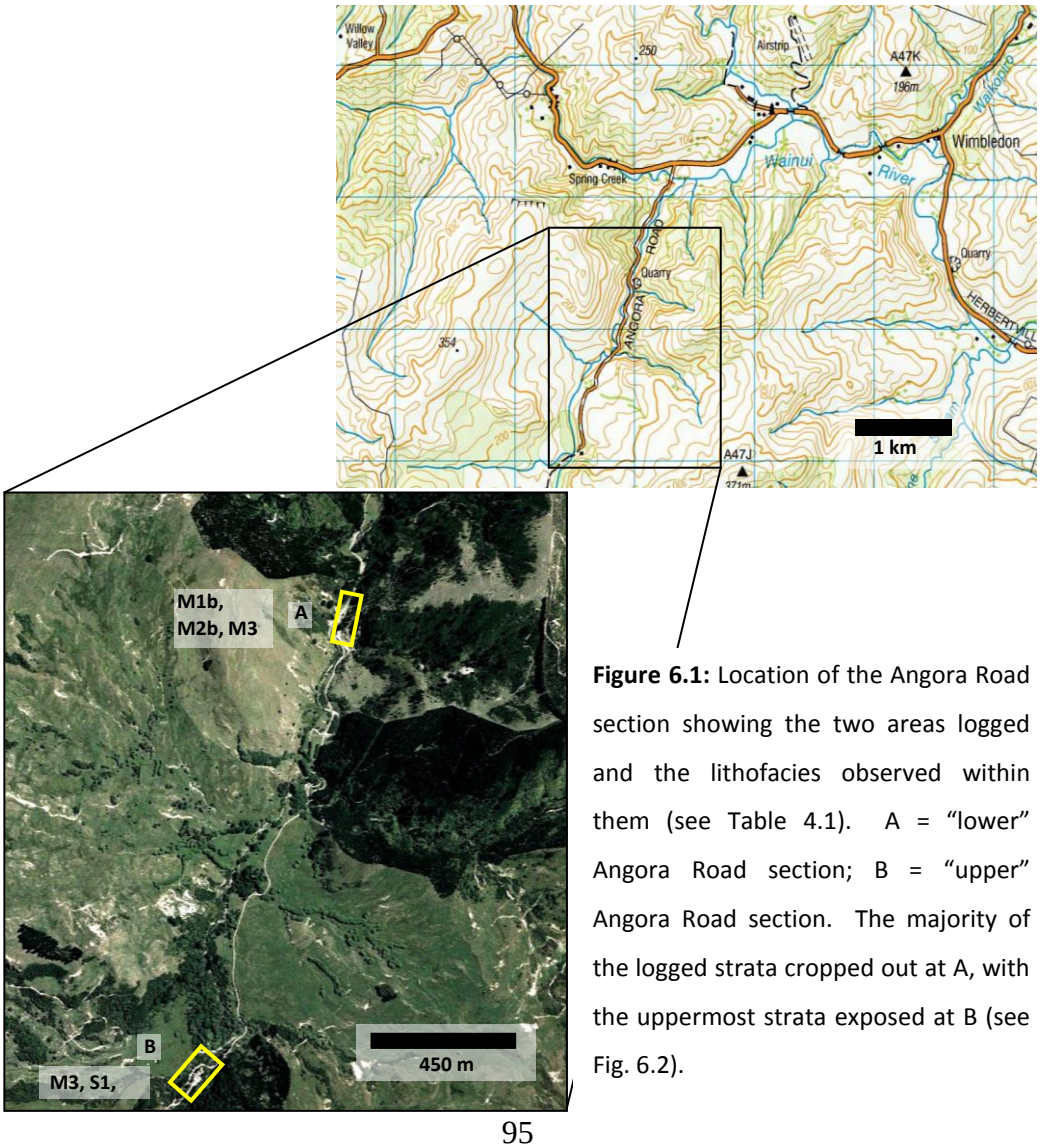

Figure 6.1: Location of the Angora Road section showing the two areas logged and the lithofacies observed within them (see Table 4.1). A = "lower" Angora Road section; B = "upper" Angora Road section. The majority of the logged strata cropped out at A, with the uppermost strata exposed at B (see Fig. 6.2).

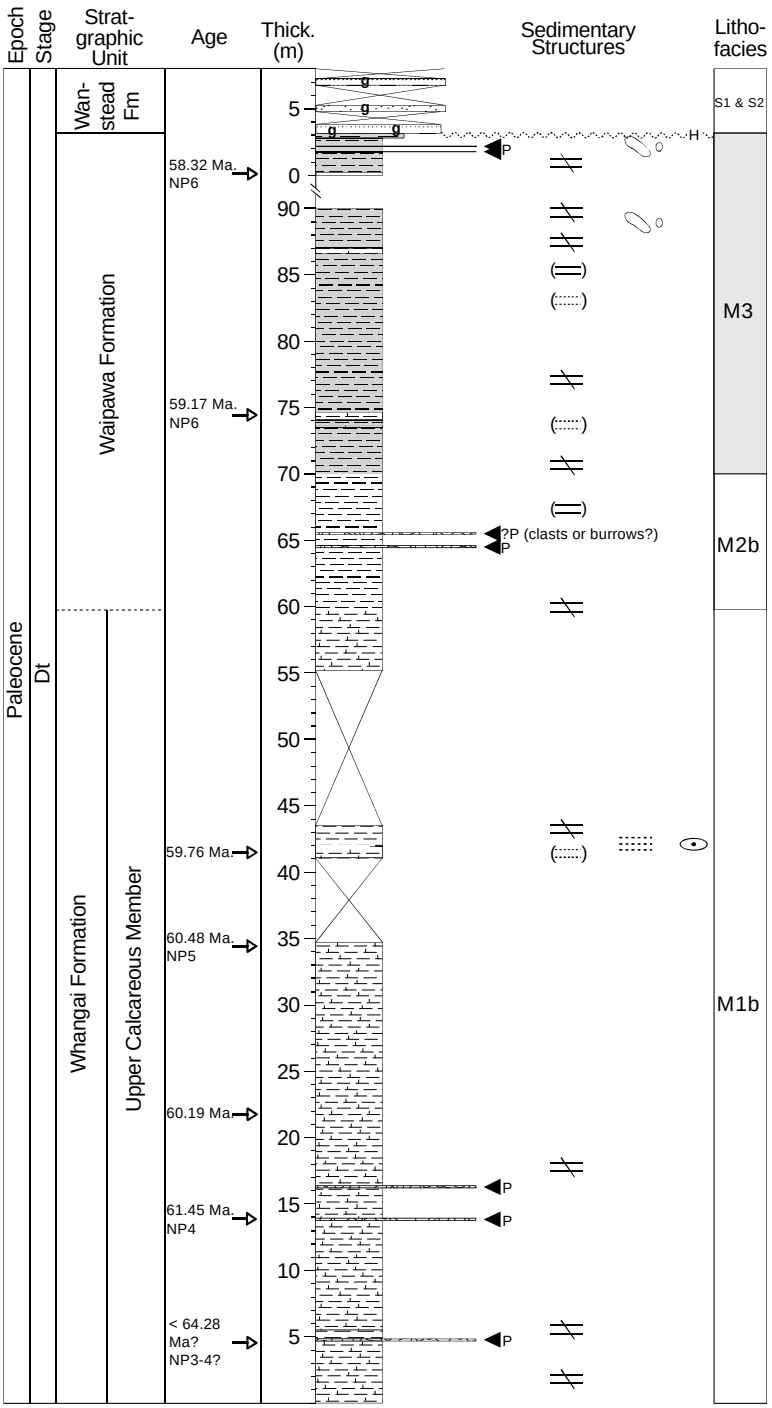

Figure 6.2: Stratigraphic column and lithofacies for the Angora Road section. Strata from 0 to 90 m occur at the "lower" Angora Road section and the uppermost strata from 0 to 8 m occur at the "upper" Angora Road section (see Fig. 6.1). Stratigraphic nomenclature and New Zealand stages are after Stewart et al. (1999). The lower boundary of the Waipawa Formation is tentatively placed at the calcareous to non-calcareous mudstone transition point. Placement is discussed in Chapter 10. Specific ages are based on calcareous nannofossil biostratigraphy (this study). Calcareous nannoplankton zones for the Paleogene (NP) are defined in Appendix A. Pebbly zones are labelled with an arrow and "P" symbol. Graphic log lithology and sedimentary structures symbols are defined in Appendix B.

6.2 Facies characteristics

The sedimentary succession logged at Angora Road is presented in Fig. 6.2. The "lower" and "upper" Angora Road sections are a significant distance apart (Fig. 6.1) and an appropriate marker bed to correlate stata between the two sections is not evident within the logged area. This is reflected in the stratigraphic column in Fig 6.2 by the "upper" Angora Road section (uppermost strata of the column, 0-8 m) sitting disconnected from the "lower" Angora Road section (majority of the column, 0-90 m). The thickness of strata missing from, or repeated in, the column between the two sections is unknown.

The lithostratigraphic nomenclature shown in Fig. 6.2 is after Stewart et al. (1999). In this study the lower boundary of the Waipawa Formation at the Angora Road section has tentatively been placed at the point where lithologies change from dominantly calcareous to dominantly non-calcareous mudstone. Placement of this boundary is discussed in Chapter 10.

The logged strata at the Angora Road section consist of c. 60 m of calcareous mudstone (Upper Calcareous Member of the Whangai Formation) conformably overlain by at least 33 m of non-calcareous mudstone with, in general, a higher organic carbon content (Waipawa Formation) (Fig. 6.2). This succession is conformably overlain by lithologies dominated by sandstone (Wanstead Formation). Five lithofacies have been identified in the succession (Fig. 6.2) and their field lithology, contacts, and petrography are described below.

6.2.1 Calcareous mudstone lithofacies (M1b)

M1 was logged at most of the East Coast Basin study sections (Table 4.1). The features of the Angora Road variety of this lithofacies (M1b) are given below.

M1b

Field lithology

The M1b succession consists of dark grey, well indurated, massive, calcareous mudstone that usually weathers to a light blue-grey slightly frittery surface (Fig. 6.3A). Near the base of the logged section the succession is interrupted by a bed of dark grey to black, poorly to well indurated, massive, variably calcareous

mudstone (Fig. 6.3C). The bed is slightly calcareous at its base and non-calcareous through its upper two thirds, has a sharp undulating lower contact, and a sharp to abruptly gradational upper contact. Ovoidal cavities c. 4 cm across

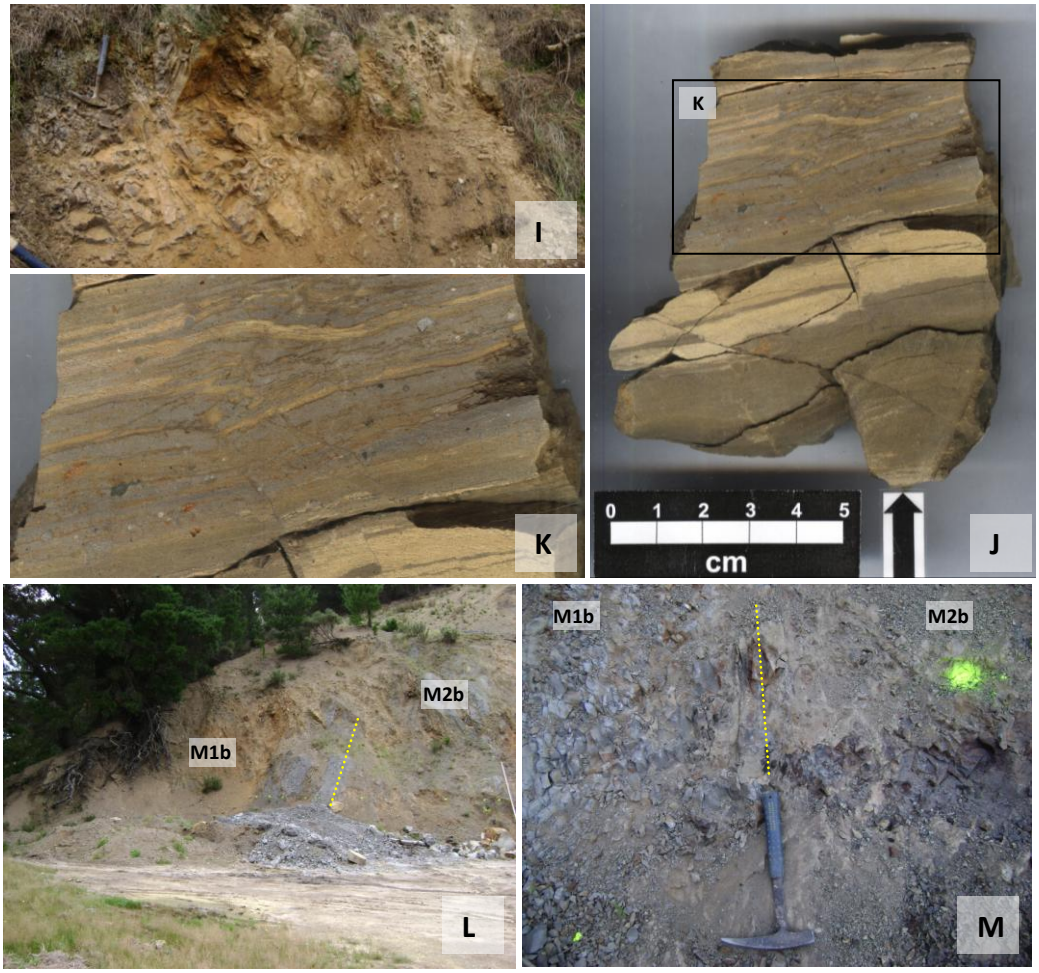

Figure 6.3: Some features of the calcareous mudstone forming M1b at the Angora Road section. A = Typical M1b at the "lower" Angora Road section; B = foreign (very sandy) mudstone clast at the base of the dark non-calcareous bed (C); C = dark non-calcareous bed near the base of the logged section (hammer head sits on bed); D = ovoidal cavity (possible burrow) infilled with unconsolidated sandy sediment; E and F = foreign mudstone clast with sandy and shelly material on its surface; G = cluster of foreign clasts that occur at about the same stratigraphic level as the mudstone clast (E and F); H = the "dropstone" of Leckie et al. (1995); I = deeply weathered out crop where a shift from calcareous to non-calcareous mudstone occurs; J and K = laminations and coarse foreign clasts in highly weathered outcrop of M1b (I); L and M = contact between the calcareous mudstone of M1b and the siliceous mudstone of M2b (L) is evident by an abrupt change from calcareous to non-calcareous mudstone and an increase in the number of red-brown coloured joints (M).

(possibly burrows) infilled with a poorly consolidated very light orange sandstone reside at the lower contact of the bed (Fig. 6.3D). The bed weathers to a red-metallic-grey colour with a light dusting of yellow powder and has a slightly frittery surface. Approximately 4 m of the mudstone overlying this bed has developed an orange tint on its weathered surfaces. Coarse sand and pebble sized subangular foreign mudstone clasts sit at the lower contact of the bed (Fig. 6.3B),

and are one of 6 to 7 “pebbly” zones identified at the “lower” and “upper” Angora Road sections. The foreign clasts are generally inconspicuous in outcrop and mainly became evident only when slabs were cut from whole rock samples during laboratory work. Consequently the known extent of the “pebbly” zones is limited to locations where sampling verifies their existence, so that they may be more extensive than shown in Fig. 6.2.

M1b contains two more “pebbly” zones above the dark non-calcareous bed described above (Fig. 6.2 and 6.3 E-H). Both consist of foreign mudstone clasts encased in calcareous mudstone and the higher of the two also includes foreign sandstone clasts (Leckie et al., 1995). A foreign mudstone clast from the lower of the two “pebbly” zones is c. 6 cm long, c. 3 cm wide and appears very similar to the surrounding mudstone, although it appears to have coarser sediment and possibly shelly material on parts of its surface (Fig. 6.3E, F). The higher pebbly zone was previously noted by Leckie et al. (1995) and consists of a 3.3 cm long, 2 cm wide, dark grey, subangular pebble (Fig. 6.3H). A faint lamination below the pebble is bowed downwards and hugs the clast. About 10 cm above the pebble there is a cavity within the calcareous mudstone – the inside of which looks and feels coarser than the surrounding mudstone – that is possibly the cast of a second pebble that has since fallen out of the outcrop.

In the upper half of the logged M1b succession there is an c. 5 m thick interval of dark grey, well to moderately indurated, sometimes laminated, variably calcareous mudstone with occasional coarse grains and nodules (Fig. 6.3J, K). The interval is generally deeply weathered and has a light grey or light brown colour (Fig. 6.3I-K). There appears to be a transition from calcareous to non-calcareous mudstone within the unit but this may be a weathering affect. There is some question as to whether this outcrop is *in situ*.

Contacts

The lower contact of M2b is not within the logged area. The contact between M1b and the overlying siliceous mudstone lithofacies (M2b) is marked by an abrupt change from calcareous to non-calcareous rock. There is very little visual expression of the contact but it seems to coincide with an increase in the number

of red-brown coloured joints, possibly a very slight darkening in the unweathered colour of the mudstone, and a slight change in its weathered colour from light blue-grey to metallic grey (Fig. 6.3L, M). All the visual changes are gradational.

Petrography

The calcareous mudstone succession and the dark non-calcareous mudstone bed within M1b are described separately. Description of the calcareous mudstone and dark non-calcareous mudstone is based on three and two samples respectively.

Calcareous mudstone description (MT3.01, 08, 13): The calcareous mudstone of M1b is composed of some very fine sand sized clastic grains set within a muddy (argillaceous) matrix with some small shreds of muscovite dispersed throughout the rock (Fig. 6.4A). Sorting is poor and most visible grains are subangular. Generally clay and quartz dominate the mineral assemblage, with calcite, feldspar and rock fragments relatively minor components (Fig. 6.5). In pebbly areas rock fragments are more abundant and can consist of angular to subrounded clasts of variably glauconitic muddy sandstone and sandy mudstone. An unusual clast is opaque and has an amorphous and smooth appearance (Fig. 6.4D). The foreign mudstone clast with coarser sediment and possibly shelly material on parts of its surface (see M1b "Field lithology") contains tabular (Fig. 6.4C) and honeycomb structures (Fig. 6.4B). These structures may be the shelly remains of an organism. Very small grains of an opaque mineral, possibly pyrite, occur throughout the muddy matrix and planktic microfossil tests and glaucony grains are rare throughout the calcareous mudstone succession of M1b.

Calcareous mudstone classification: Immature to submature, occasionally slightly conglomeratic quartzose argillutite, and less commonly, argillaceous quartzlutite (Fig. 3.11 and 6.5). Foreign clasts, when present, are angular to subrounded and generally composed of immature to submature, variably glauconitic muddy sandstone or sandy mudstone.

Dark non-calcareous mudstone bed description (MT3.04, 07): The bed is composed of some very fine sand sized clastics and small shreds of muscovite set in a muddy (agillaceous) matrix. Possible rare small *Terebellina* tubes float in the

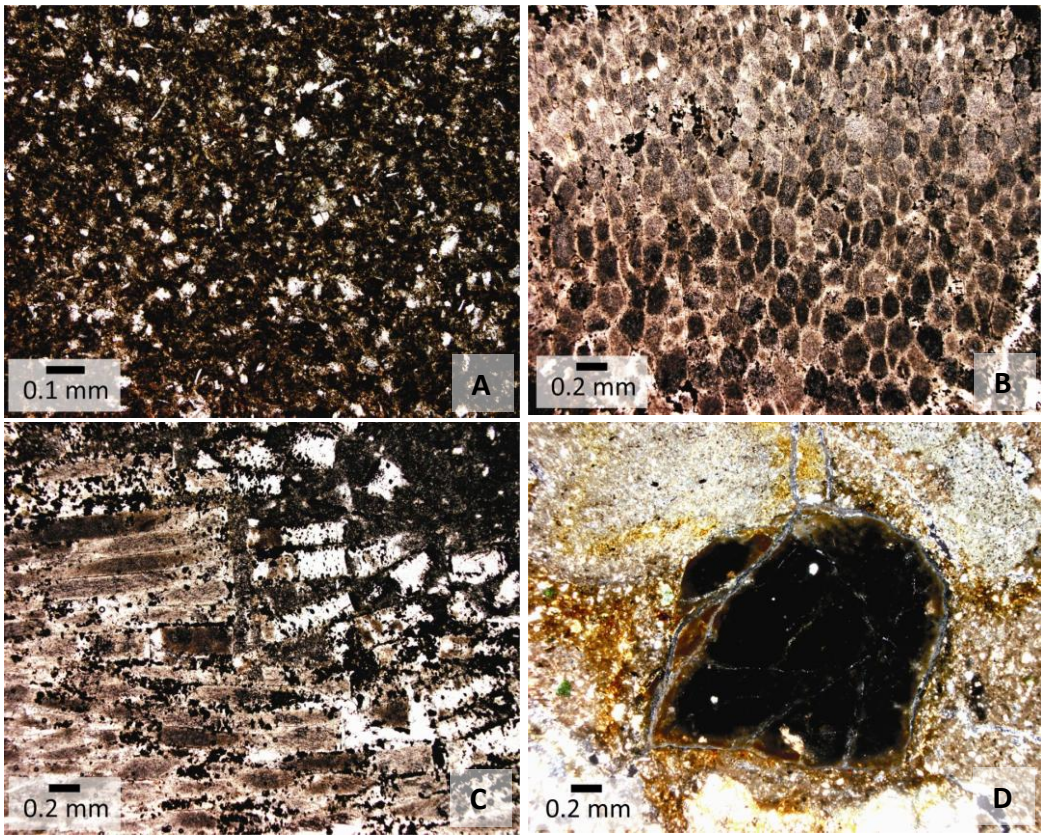

Figure 6.4: Photomicrographs of some features of the M1b lithofacies. A = Typical mudstone of M1b with silt and very fine sand-sized clastics set in a dark argillaceous matrix (MT3.01); B and C = honeycomb (B) and tabular (C) structures within typical M1b mudstone (MT3.13); D = opaque foreign clast with an amorphous and smooth appearance under bright plane polarised light.

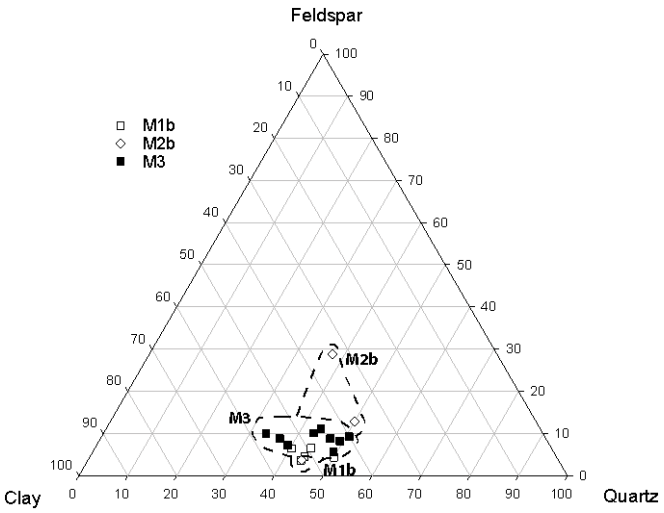

Figure 6.5: Ternary diagram of relative proportions of feldspar, clay minerals and quartz in the mudstone (M) lithotype at the Angora Road section. See Fig. 3.11 for lutite classification names and fields.

matrix. Clay and quartz are the dominant minerals but feldspars and rock fragments can also be relatively significant components. Very small grains and short laminations of an opaque mineral, possibly pyrite, occur within the muddy matrix, and planktic microfossil tests and glaucony grains are rare through the bed. Many sedimentary rock fragments occur at the base of the bed and become rare upwards. The rock fragments are up to pebble sized, angular to rounded in shape, and composed mostly of mudstone and sandy mudstone. An ovoidal cavity c. 4 cm across at the base of the bed (see M1b "Field lithology") is infilled with moderately muddy sandstone and with many rock fragments.

Dark non-calcareous mudstone bed classification: Immature to submature, possibly slightly conglomeratic quartzose argillutite with ?burrows infilled with immature to submature, moderately muddy very fine sandstone. Foreign clasts, when present, are angular to rounded, and generally composed of submature very sandy mudstone and immature mudstone.

6.2.2 Siliceous mudstone lithofacies (M2b)

M2 occurs at four of the studied East Coast Basin sections (Table 4.1). The lithofacies characteristics differ between sections and description for the Angora Road variety (M2b) follows.

M2b

Field lithology

M2b is a dark grey, well indurated, massive, non-calcareous mudstone that usually weathers to a metallic grey frittery surface, but there is some variation in places. An c. 1 m thick horizon of mudstone with a brown weathered surface occurs near the middle of M2b (Fig. 6.6A). The outcrop exposure of mudstone in this horizon appears massive, but within the mudstone a subangular pebble sized rock fragment was observed with underlying laminations bowed downwards (Fig. 6.6B, C). Approximately 1 m above the pebble, poorly indurated fragments occur within the mudstone. The fragments may be foreign clasts or, less likely, angular burrows. At the Angora Road section M2b appears to be a transitional phase between the calcareous mudstone lithofacies (M1b) and the "Waipawa Black Shale" lithofacies (M3).

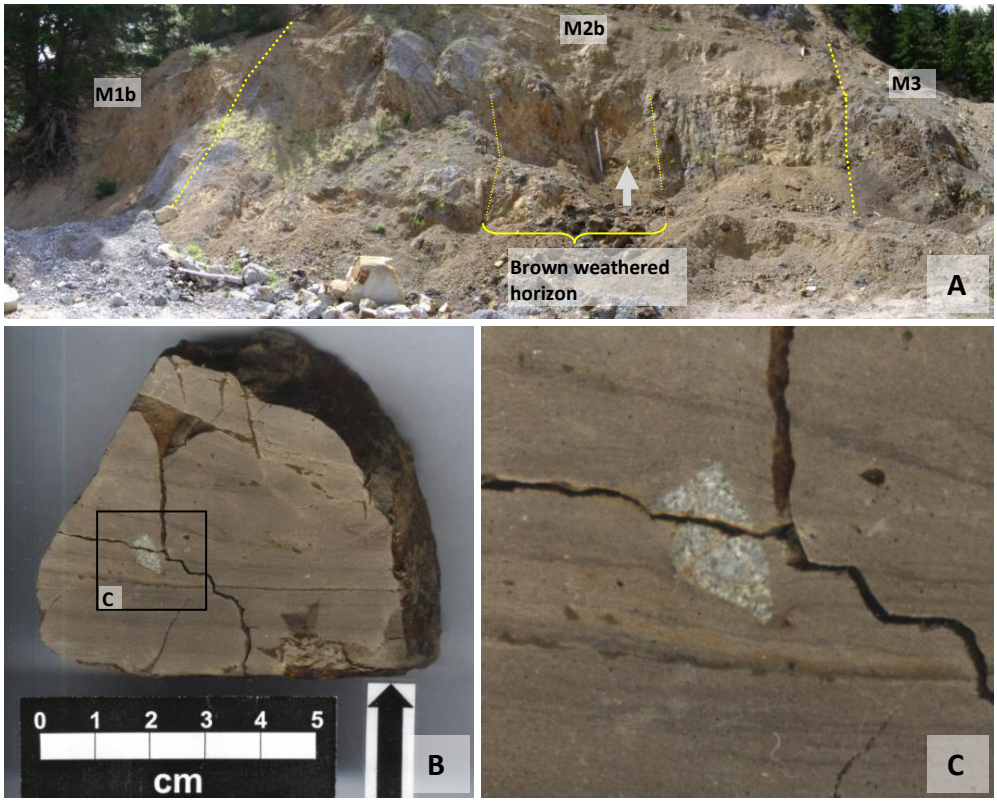

Figure 6.6: Some features of the siliceous mudstone of M2b at Angora Road. A = M2b at the "lower" Angora Road section with the upper contact with M3 and lower contact with M1b shown (2 m long Jacob staff for scale), as well as the extent of the brown weathered horizon and the location of the foreign clast (B and C) within that horizon (marked by arrow); B = foreign moderately sandy mudstone clast from the brown weathered horizon with underlying laminations depressed downwards.

Contacts

The lower contact of M2b was discussed previously when describing the upper contact of the M1b lithofacies in Section 6.2.1. The upper contact of M2b with the M3 lithofacies appears to be gradational or rapidly gradational.

Petrography

Description (MT3.38, 40, 47): Description of M2b is based on three representative samples from the lithofacies. The lithofacies is composed of some very fine and fine sand sized clastic grains set within a muddy matrix with some shreds of muscovite, of variable size, dispersed throughout the rock. Sorting is poor and most visible grains are angular to subrounded. The horizon of brown weathered rock, described above (see M2b "Field lithology"), has a coarser (siltier) mud fraction than the underlying M1b lithologies (Fig. 6.7A). There appears also to be a general coarsening upwards through M2b. Planktic and benthic microfossil tests

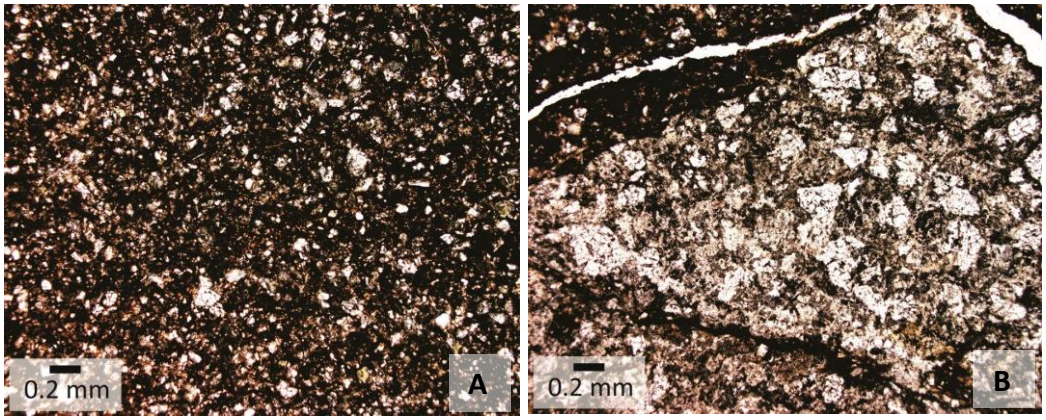

Figure 6.7: Photomicrographs of some features of the M2b lithofacies. A = Relatively coarse (silty) mudstone of the brown weathered horizon in M2b, with silt and very fine sand-sized clastics set in a dark argillaceous matrix (MT3.40); B = foreign moderately sandy mudstone clast from the brown weathered horizon (MT3.38; see Fig. 6.6).

and glaucony are absent or rare through the brown weathered horizon but their abundance increases slightly up through the lithofacies. Generally quartz and clay dominate the mineral assemblage with rock fragments minor or absent (Fig. 6.5). The feldspar component is at least as high, or higher than, M1b, and in at least one part of the brown weathered horizon it is a significant component and nears the abundance of quartz and clay (Fig. 6.5). A number of rock fragments are present in the brown weathered horizon, with the largest the pebble sized clast noted in the field lithology description above. The pebble is composed of moderately sandy mudstone with some rock fragments and plagioclase (Fig. 6.7B).

Classification: Immature to submature possibly slightly conglomeratic quartzose argillutite (Fig. 3.11 and 6.5) with subangular rock fragments composed of submature to immature mudstone, and moderately sandy mudstone with some rock fragments and plagioclase. M2b is an argillaceous quartzlutite in its upper portion.

6.2.3 "Waipawa black shale" lithofacies (M3)

M3 was observed at Angora Road and has no variants within this or other studied sections (Table 4.1).

Field lithology

M3 consists of dark grey to black, well to poorly indurated, massive, mainly non-

calcareous mudstone with common *Terebellina* tubes (Fig. 6.8B, C). At the "lower" Angora Road section there are two calcareous beds from 0.3 to 0.5 m in thickness in M3 (Fig. 6.8A), with two thinner calcareous beds leading into the lower of the thicker calcareous beds. Laminations are common in the vicinity of the lower thicker calcareous bed and underlying thin calcareous beds (Fig. 6.8D). Contacts between the calcareous and non-calcareous lithologies usually appear sharp or abruptly gradational. The upper relatively thick calcareous bed occurs in isolation and its thickness appears to vary.

The calcareous beds are mostly grey, occasionally dark grey, well indurated, massive calcareous mudstone (Fig. 6.8G) with erratic thin black lines observed through a single bed. They usually weather to a blue-grey frittery surface (Fig. 6.8E). The difference between the calcareous and non-calcareous lithologies in M3 is usually subtle and consequently contacts between the lithologies are often vague. The visible change at the lower contact of the calcareous bed is usually sharp but occasionally there is no change in visual appearance, with a change in calcareousness the only apparent difference between rock types. The upper contact can be sharp or gradational and both upper and lower contacts appear to sometimes undulate (Fig. 6.8E).

Underlying the lower, relatively thick, calcareous bed, the dark non-calcareous mudstone of M3 weathers to a black frittery surface with a dusting of yellow powder. Above the lower, relatively thick, calcareous bed the dark non-calcareous mudstone weathers to a black frittery or blocky surface with a subtle metallic grey tint to its weathered colour. Burrowing and sandy laminations become more common towards the top of the sequence at the "lower" Angora Road section (Fig. 6.8F).

At the "upper" Angora Road section a calcareous bed sits at the very base of the logged area. It is not known if this bed is the lateral equivalent of the higher, relatively thick, calcareous bed at the "lower" Angora Road section. At the "upper" Angora Road section foreign clasts (Fig. 6.8H) and wisps of grey mud occur in the upper portion of M3 and burrowing becomes evident near the top of this lithofacies (Fig. 6.8J). M3 is capped by an c. 0.3 m thick dark grey, poorly

indurated, very slightly glauconitic, non-calcareous slightly sandy mudstone that weathers to a grey frittery surface with a dusting of yellow powder (Fig. 6.8I). Burrowing is particularly evident in slabbed samples from this bed (Fig. 6.8K).

Contacts

The lower contact of M3 was discussed previously when describing the upper contact of the M2b lithofacies in Section 6.2.2. The upper contact of M3 consists of M3 mudstone grading upwards into the poorly indurated, burrowed, very slightly glauconitic, slightly sandy mudstone bed that caps the M3 lithofacies (described above) (Fig. 6.8I, K). This bed appears to be conformably overlain by the sandstones of S2 and S1.

Petrography

The dominantly non-calcareous mudstone of M3 is described separately to the uppermost sandy mudstone bed of the lithofacies. Description of the dominantly non-calcareous mudstone is based on eight representative samples and description of the uppermost sandy mudstone bed is based on one representative sample.

Dominantly non-calcareous mudstone description (MT3.54, 82, 92, 123, 127, 132, 136, 138): The majority of M3 is generally composed of some very fine sand sized clastic grains set within a dark argillaceous matrix with some small shreds of muscovite dispersed throughout the rock (Fig. 6.9A). Sorting is poor and most visible grains are angular to subrounded. The calcareous mudstone beds appear to be slightly finer than the non-calcareous mudstone. Towards the top of the lithofacies sand sized clastics become more abundant (Fig. 6.9C), but then become rare closer to the lithofacies upper contact. Rare benthic microfossil tests occur in some calcareous beds and in some areas in the upper part of the succession. Planktic foraminiferal tests are absent through the non-calcareous areas of the lithofacies and rare in the calcareous beds. Calcite occasionally infills the planktic foraminiferal tests in the calcareous beds (Fig. 6.9B). *Terebellina* tubes occur throughout most of M3 but appear to be absent from the upper portion of the lithofacies. Glaucony is absent or rare throughout the succession. Quartz and clay are the dominant minerals present, with feldspars a less significant component (Fig. 6.5). The abundance of feldspars seems to gradually increase up

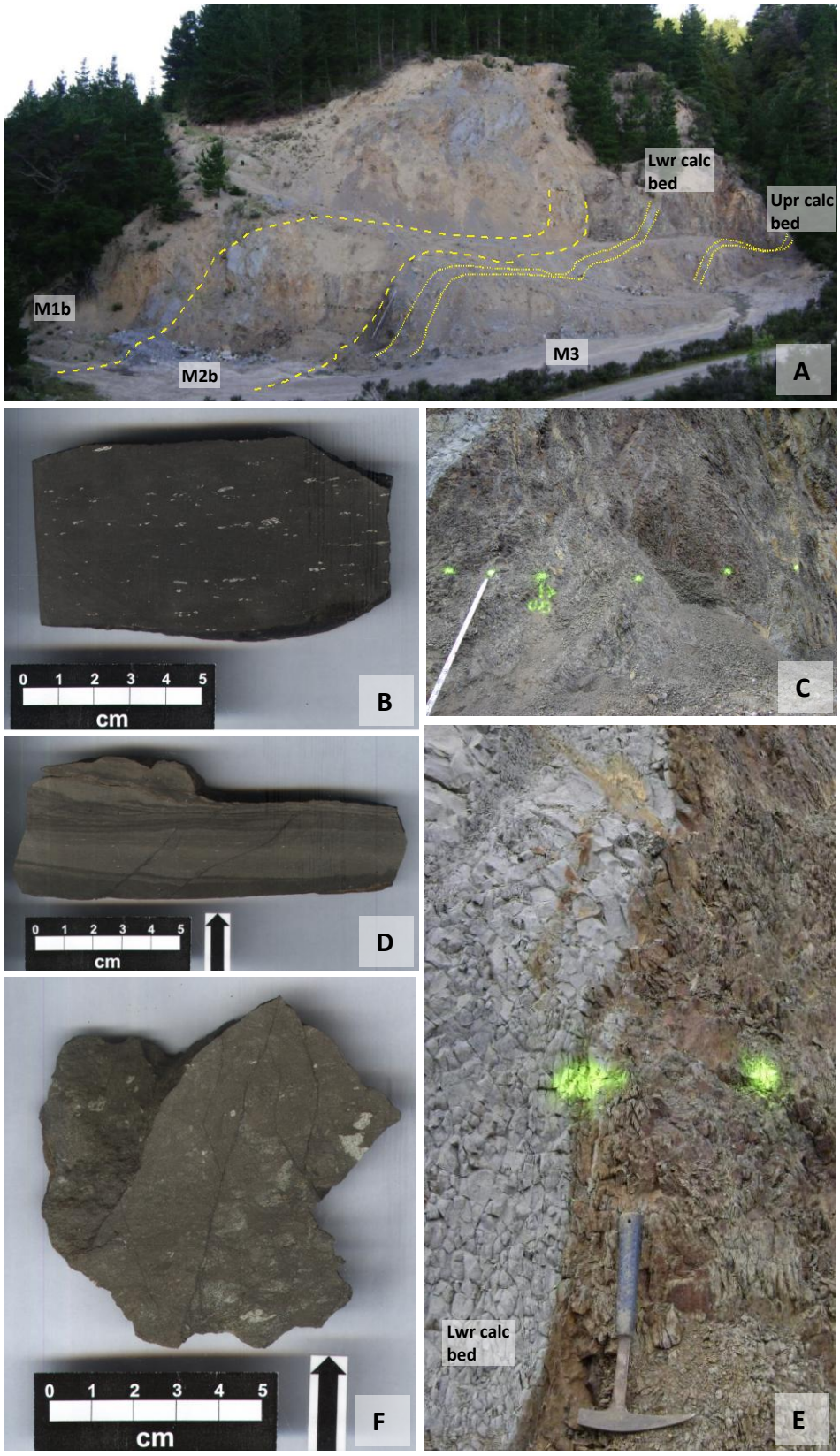
Lwr calc bed
Upr calc bed
M1b
M2b
M3
A
0 1 2 3 4 5
cm
B
C
D
F
Lwr calc bed
E

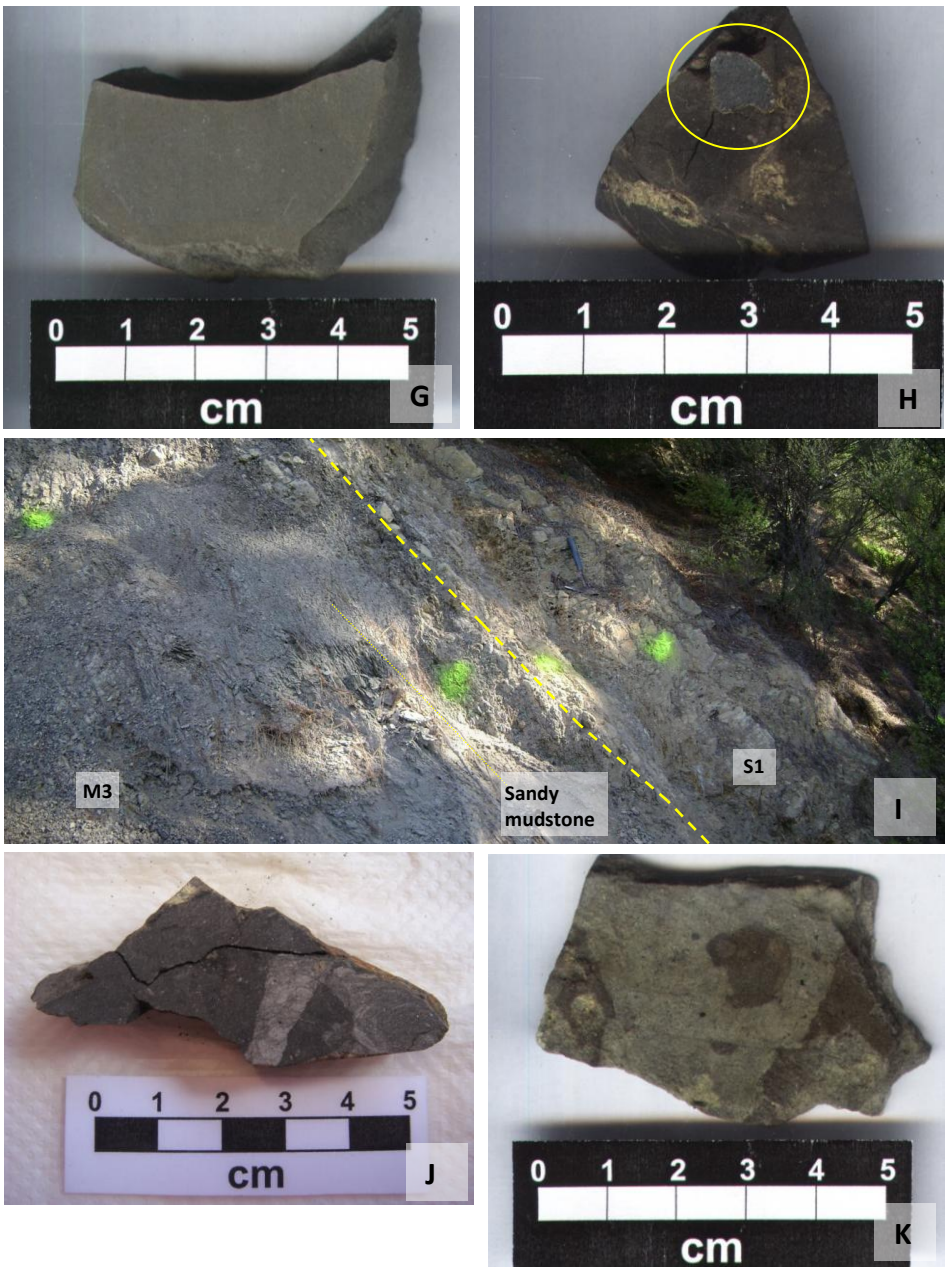

Figure 6.8: Some features of the M3 lithofacies at the Angora Road section. A = Inferred position of M3 relative to M1b and M2b at the "lower" Angora Road section; B = black massive mudstone with *Terebellina* tubes, typical of M3; C = outcrop example of M3 displaying a dark grey slightly frittery surface; D = example of laminations that occur in the strata leading up to the lower of the relatively thick calcareous beds in M3; E = sharp undulating upper contact of the lower relatively thick calcareous bed in M3; F = example of the burrowed, sandier mudstone that occurs in the upper portion of the "lower" Angora road section; G = example from the calcareous bed at the base of the logged section at the "upper" Angora Road section of the lighter grey calcareous mudstone in M3; H = example of a foreign mudstone clast (circled) in upper M3 at the "upper" Angora Road section; I = the upper contact of M3 with S1 is marked by a gradational shift to a sandy mudstone in uppermost M3, with this sandy mudstone conformably overlain by muddy sandstone of lowermost S1 ; J = example of burrowing in upper M3 at the "upper" Angora Road section; K = burrows in sandy mudstone in uppermost M3.

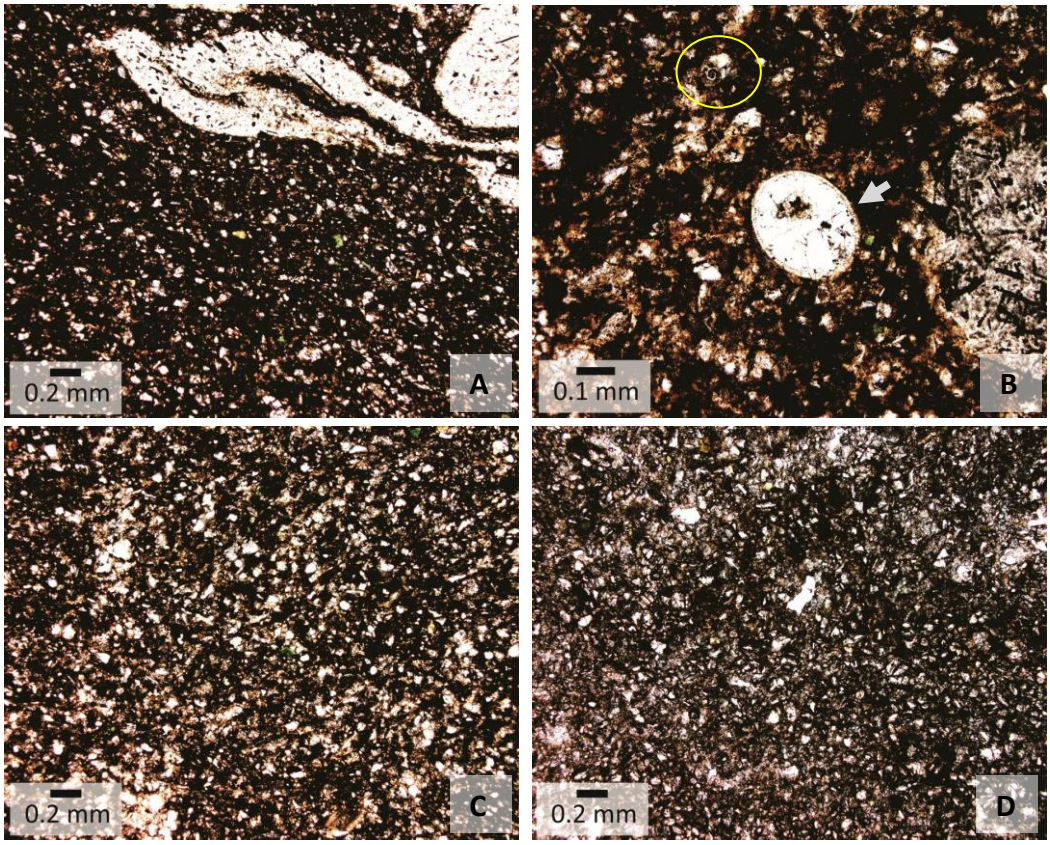

Figure 6.9: Photomicrographs of some features of the M3 lithofacies. A = Typical mudstone of M3 with silt and very fine sand-sized clastics set in a dark argillaceous matrix with some *Terebellina* tubes (MT3.92); B = benthic microfossil (circled), and planktic microfossil infilled with calcite (arrowed), in the lower calcareous bed at the "lower" Angora Road section (MT3.82); C = silty mudstone in burrowed strata in the upper portion of M3 at the "lower" Angora Road section (MT3.127); D = sandy mudstone immediately beneath the M3-S1 contact (MT3.140).

through M3. Rock fragments are generally either a minor component or absent in M3 as a whole, although near the upper contact of the lithofacies rock fragments become more abundant. A subangular foreign clast composed of submature, slightly sandy mudstone occurs in this interval.

Dominantly non-calcareous mudstone classification: The succession is composed of immature to submature mudstone with some *Terebellina* tubes, rare slightly sandy mudstone laminations, and rare rock fragments. At the base and top of the succession the mudstone is a quartzose argillutite (Fig. 6.5). The middle portion of the succession is an argillaceous quartzlutite (Fig. 6.5).

Sandy mudstone bed description (MT3.140): The sandy mudstone that forms the uppermost unit in M3 consists of many sand sized clastic grains set in a muddy

matrix (Fig. 6.9D). The visible grains are poorly sorted and range from angular to subrounded in shape. There is a slight increase in glaucony in the unit compared to the underlying mainly non-calcareous mudstone. Rare planktic and benthic microfossil tests float in the matrix.

Sandy mudstone bed classification: Immature to submature, very slightly glauconitic slightly sandy quartzose argillutite (Fig. 3.11 and 6.5).

6.2.4 Sandstone lithotype (S1 and S2)

The sandstone lithotype was observed at the Angora Road section and has no variants at any of the other studied sections (Table 4.1). It consists of the muddy sandstone lithofacies (S1) and the interbedded mudstone-sandstone lithofacies (S2). S1 and S2 are exposed at the "upper" Angora Road section, but the exposure is poor and as a consequence description of the lithotype is limited. A combined description of S1 and S2 follows.

Figure 6.10: Some features of the S1 and S2 lithofacies at Angora Road. A = Poorly exposed outcrop example of decimetre bedded sandstone interbedded with centimetre beds of mudstone in S2; B and C = burrowed basal S1 (B) and glauconitic sandstone with possible graded bedding (C) in S1; D = example of the sandstone lithology of S2.

Field lithology

S1 consists of green-grey, massive or possibly normally graded, slightly glauconitic, non-calcareous slightly muddy sandstone with burrows at its base (Fig. 6.10B, C). S2 consists of decimetre beds of green-grey, massive, glauconitic, non-calcareous sandstone interbedded with centimetre beds of dark grey, non-calcareous mudstone (Fig. 6.10A, D).

Contacts

The lower contact of the sandstone lithotype was discussed previously when describing the upper contact of the M3 lithofacies in Section 6.2.3. The upper contact of the sandstone lithotype is not exposed at the Angora Road section.

Petrography

S1 description (MT3.142): Petrographic description was performed on one sample from S1. Based on this sample the lithofacies consists of grain supported, abundant fine sand-sized clastics with muddy matrix infilling pore spaces (Fig. 6.11). The clastic grains are mostly well sorted and rounded to subangular. Common glaucony grains occur in S1 and planktic and benthic microfossil tests are absent. Quartz is the dominant mineral with clay minerals and feldspar minor constituents. Rock fragments are rare (Fig. 6.12).

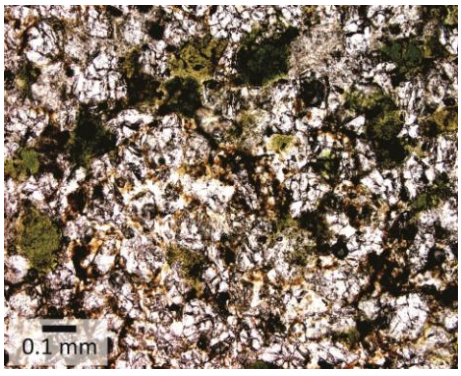

Figure 6.11: Photomicrograph of a glauconitic sandstone in S1 (see Fig. 6.10C) composed of grain supported fine sand-sized quartz (and minor feldspar) and common glaucony, with muddy matrix infilling pore space (MT3.142).

S1 classification: Submature, slightly glauconitic, slightly muddy subfeldsarenite (Fig. 3.10 and 6.12).

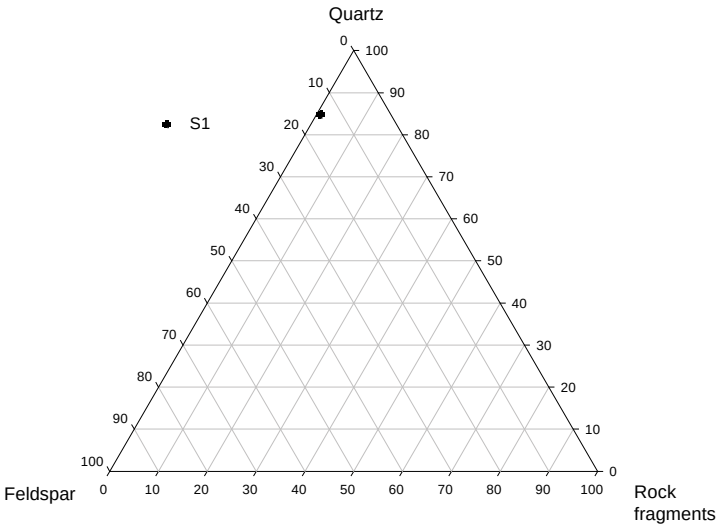

Figure 6.12: Ternary diagram of relative proportions of quartz, feldspar, and rock fragments in the muddy sandstone lithofacies (S1) at the Angora Road section. See Fig. 3.10 for arenite classification names and fields.

6.3 Mineralogical trends

Feldspar abundance remains fairly static through M1b and basal M2b, but gradually and steadily increases through the rest of the section following a spike in the brown weathered horizon in M2b. Quartz abundance gradually increases through the entire succession, with a rapid increase at S1. Clay minerals gradually increase through M1b and basal M2b, peaking in the brown weathered horizon, and then declining leading into M3. They increase once more in M3 and then remain relatively steady for the majority of the lithofacies, but increase quickly leading into the M3 upper contact, peaking in the uppermost non-calcareous mudstone and the sandy mudstone bed before decreasing rapidly into S1.

Terebellina tubes occur throughout most of M3 but appear to be rare or absent from the upper area of the lithofacies. Rare small tubes may be present in the dark mudstone bed in M1b. They are absent from the rest of the section. Planktic microfossil tests are rare or absent in M1b and M2b, absent in M3 apart from in calcareous beds and at the upper contact, and absent in S1. The general trend appears to be a decrease in planktic microfossil tests upwards. Benthic microfossil tests are rare and their occurrence sporadic.

Glaucony is most abundant at the M3-S1 contact, and burrowing is most abundant near the top of M3.

6.4 Geochemistry and palynofacies results

Geochemical and palynofacies proxies used in this study were introduced in Chapter 3 (Sections 3.3.2 to 3.3.4) and are presented here for the Angora Road section. Fig. 6.13 presents the up section trends for carbonate carbon and organic carbon stable isotopes (a) and elemental proxies for ocean surface water biological productivity (b, c, d, j), seawater nutrient availability (e), bottom water oxygen levels (f), aeolian sediment supply (g), glaucony (h), and terrigenous sediment supply (i). Up section variations in ocean surface water biological productivity and bottom water oxygen levels are also indicated by the average percent organic carbon plot (j). Included in Figure 6.13 are palynofacies proxies for the depositional areas proximity to the paleoshoreline (k-q). Preliminary interpretations of geochemical and palynofacies trends are offered in this section, even though this is a results chapter, to aid later interpretations (see Chapter 10).

6.4.1 Elemental geochemistry and organic carbon proxies

In this section the results for elemental geochemistry and organic carbon proxies (Fig. 6.13b-j) are described. However, first the ocean surface water biological productivity proxies are tested for biogenic association using the methods outlined in Chapter 3. This is done in order to assess their reliability as paleoproductivity indicators for the logged area of the Angora Road section. If a productivity proxy is found to have no biogenic association its trends will not be described in detail.

Testing for productivity proxy biogenic association

Ba[exc] co-varies with Ba/Ti and has poor correlation with TRG throughout the Angora Road succession and therefore appears to have biogenic association (Fig. 6.13b). However, Mo indicates that parts of the succession at Angora Road were deposited under suboxic conditions, especially in M3 but also in parts of M2b (Fig. 6.13f). M1b appears to have been deposited in oxic to slightly suboxic conditions and S1 and S2 in oxic conditions (Fig. 6.13f). Consequently, Ba[exc] is used as the primary productivity indicator for M1b, S1, and S2, and is used in conjunction with U[ef] in M2b.

U[ef] co-varies with Si[exc] through M2b and the majority of M3, but has poorer correlation with Si[exc] and Ca[exc] through M1b (Fig. 6.13c, d). U[ef] is used as the primary productivity indicator for M3 and is used in conjunction with Si[exc] and Ba[exc] in M2b. U[ef] co-varies with Si[exc] in S1 and S2 (Fig. 6.13c, d), but given the low Mo values Ba[exc] is used in preference as the primary productivity indicator through these two lithofacies.

Proxy results

The productivity proxies indicate fairly steady productivity levels through M1b, with two relatively small spikes, one at the base of the dark non-calcareous bed introduced in the M1b "Field lithology" description, and a second near the top of the lithofacies (Fig. 6.13b-d). The former appears to be associated with increased siliceous productivity while it is unclear what type of productivity the second spike is associated with. The mudstone with the "drop stones" of Leckie et al. (1995) is associated with a small increase in siliceous productivity.

Ba[exc], U[ef], and Si[exc] indicate an increase in siliceous productivity in M2b, peaking in the weathered brown horizon (that contains the foreign clast with downward bowed underlying laminations – see M2b "Field lithology"; Fig. 6.13b-d). It is difficult to compare relative levels of productivity between M1b, M2b, and M3 because different proxies are used for each. Based on U[ef] productivity is relatively high through M3, but based on Si[exc] (siliceous) productivity is relatively low through M3 (Fig. 6.13c, b). This could be because U[ef] may be recording a combination of calcareous productivity and siliceous productivity, giving it high values. The calcareous productivity records may have been lost from the Ca[exc] data due to poor preservation of calcium carbonate, due to organic carbon degradation of organic matter in the organic rich M3 (Archer and Maier-Reimer, 1994; Martin and Sayles, 2005). Or the proxy is detecting greater influx of algae material and greater terrestrial organic matter inputs through the interval (Killops et al., 2000). An alternative explanation may be that U[ef] is elevated due to U enrichment in response to low oxygen conditions at the sea-floor, caused by degradation of organic matter in the organic rich M3 (Rogers, 2000).

P[ef] generally appears to co-vary with Ca[exc] and average $\%C_{org}$, with maximum P[ef] values occurring in the calcareous beds in M3 and at the maximum average $\%C_{org}$ value (Fig. 6.13d, e, j). For this reason P[ef] is interpreted as reflecting seawater nutrient levels. Seawater nutrient values (P[ef]) are generally higher in M3 (Fig. 6.13e). This observation can be related back to the question of whether the U[ef] record of higher productivity through M3 is justified, or if the Si[exc] record of lower productivity through the interval is correct. Based on the relatively high P[ef] values through M3 the U[ef] record is favoured over the Si[exc] record. Based on geochemical results from Killops (2000) which show an abundance of algal material and a terrestrial organic material contribution to the organic matter of the Waipawa Formation, M3 is thus interpreted as having moderate siliceous productivity and an increased input of algal and terrestrial organic matter, with overall relatively high productivity and seawater nutrient levels. Low seawater nutrient levels correspond with the dark non-calcareous bed in M1b, the weathered brown bed in M2b, and areas of M3 that are burrowed or have faint laminations (Fig. 6.13e).

Much of the Angora Road section records a slightly suboxic, or bordering between oxic and suboxic, environment of deposition (Fig. 6.13f). This is particularly the case through M1b and the upper half of M2b. However, through the lower half of M2b and through much of M3 suboxia is more intense. A spike of Mo-limited euxinic or intermittently euxinic deposition occurs near the upper contact of M3. Oxic conditions developed during deposition of S1 and S2 (Fig. 6.13f).

Increased oxygen depletion seems to generally increase with increased productivity through much of the Angora Road section but there are some exceptions, with negative correlation between Mo and Ca[exc] and Si[exc] near the top of the M3 succession at the "lower" Angora Road section and near the base of M3 at the "upper" Angora Road section (Fig. 6.13b-d, f). The degree of oxygen depletion has variable correlation with seawater nutrient levels (Fig. 6.13e, f). Through M3 at the "lower" Angora Road section oxygen depletion broadly increases with increasing nutrient levels, however some of the lowest nutrient levels also correspond with enhanced oxygen depletion (e.g. the period of the

greatest oxygen depletion in the Angora Road section corresponds with the period of lowest seawater nutrient levels for the section ("upper" Angora Road euxinic spike)).

In summary it appears that productivity is higher when seawater nutrient levels are higher, and occasionally enhanced organic matter degradation due to increased productivity seems to lead to greater oxygen deficiency. However, increased nutrient supply and productivity often does not seem to be the cause for oxygen depletion and other processes may be involved.

Ti/Al values are slightly above the 0.04 threshold through all lithofacies, except S1 and S2, at the Angora Road section (Fig. 6.13g). The highest Ti/Al values occur within the 3 m of strata overlying the dark non-calcareous bed in M1b. Through the rest of the section Ti/Al slowly decreases, with a rapid decrease near the upper contact of M3 with S1. These trends could signify an initial increase in offshore wind or current strength or terrigenous sediment starvation near the base of the logged section, followed by a decline in these processes through the remainder of the section. However, the subtlety in enrichment means that it is not a strong inference.

Fe[ef] is slightly above average shale values through the section, however it does not co-vary with K[ef] through the majority of the section so a glaucony source is unlikely (Fig. 6.13h). It is more likely that Fe[ef] variations through the majority of the Angora Road section are the result of other processes, such as detrital clay input and the *in situ* formation of iron sulphides (Werne et al., 2002). Fe[ef] and K[ef] do co-vary through S1 and S2 so a glaucony source is likely in these lithofacies (Fig. 6.13h). The highest concentration of glaucony in the section occurs immediately above the M3 upper contact in basal S1. This inference agrees with petrographic observations of glaucony variations through the section.

TRG gradually increases up through the logged area but three decreases are also observed, the first in the immediate vicinity of the non-calcareous dark bed in M1b (see M1b "Field lithology"), the second centred on the brown weathered horizon in M2b (see M2b "Field lithology"), and the third immediately below and

above the M3-S1 contact (Fig. 6.13i). The decrease through the M3-S1 contact area is abrupt and the largest decrease in TRG for the section. It corresponds with increased burrowing, more glaucony, enhanced siliceous productivity, and is initiated at the euxinic spike near the top of M3 (Fig. 6.2 and 6.13d, f). The first two decreases in TRG are associated with increases in siliceous productivity.

Organic carbon increases up section, peaking at the top of M3 at the "lower" Angora Road section and generally decreasing leading into the M3-S1 contact (Fig. 6.13j). M3 generally has the highest organic matter content and enrichment approximately parallels TRG through the section (Fig. 6.13i, j). This may reflect better preservation of the organic matter, through burial, during slightly higher sedimentation rates (Lyons et al., 2009).

6.4.2 Palynofacies proxies

The palynofacies proxies used in this study and their significance to paleodepositional environments is outlined in Chapter 3 (Section 3.3.2). The percent palynomorphs is low throughout the Angora Road section (Fig. 6.13k). The highest values occur at the base of M1b with a general decline up into M2b and the lowest values occurring in M3. A relatively rapid decrease in the percent palynomorphs occurs at the dark non-calcareous bed in M1b and a relatively rapid increase occurs at the burrowed slightly sandy mudstone that caps the M3 succession.

Percent amorphous organic matter (AOM) and percent phytoclasts proxies both show a general trend of the shoreline becoming more distal through the middle of M1b followed by more proximal conditions at the top of the lithofacies (Fig. 6.13l, m). The most distal conditions of the logged area occur in M2b, centred on the brown weathered horizon, and is associated with increased siliceous productivity, and reduced seawater nutrient levels, oxygen, and TRG (Fig. 6.13b-f, i). Relatively consistent proximal conditions occur in M3. The dark non-calcareous bed in M1b is associated with a shift to more proximal conditions; the "dropstones" of Leckie et al. (1995) and the calcareous beds in M3 at the "lower Angora Road section occur during overall increasingly distal trends; and the burrowed non-calcareous mudstone in upper M3 and the burrowed sandy

mudstone in the uppermost M3 are associated with shifts to more distal conditions.

The log black:brown phytoclasts proxy has a poor to negative correlation with the percent AOM and phytoclasts proxies through M1b and lower to mid M3 and may indicate proximal high turbulence in these areas (Fig. 6.13n).

6.4.3 Stable isotopes

Carbonate carbon stable isotope values show little variation through M1b, but a shallow and broad positive trend appears to take place in the upper half of the lithofacies (Fig. 6.13a). Values are more negative near the base of M3 then recover to near M1b values in the upper portion of M3.

Organic carbon isotope values are relatively low near the base of M1b (Fig. 6.13a). A generally positive trend is evident through M2b and M3, with negative excursions punctuating the overall trend in the lower half of M2b, and in the middle and in the upper half of M3. The positive excursion is broadly associated with increased productivity and relatively proximal conditions, however it does not always co-vary with productivity and shoreline proximity proxies at a finer resolution. A sharp decrease in organic carbon isotope values occurs at the upper contact of M3.

Oxygen isotope values do not appear to co-vary with carbon isotope values at a fine scale through M1b, although the shallow and broad positive trends of carbonate carbon values through M1b are also apparent in the oxygen isotope record (Fig. 6.14). Consequently the oxygen isotope values may have been slightly diagenetically altered, although the poor correlation at a finer resolution suggests that some temperature changes could be preserved. The negative shift in oxygen isotope values at c. 10 m from the base of the start of the log supports warming at the time of deposition of these sediments. Oxygen isotope trends through M3 co-vary with carbonate carbon trends and so are regarded as mainly diagenetically altered and not discussed further here.

Figure 6.13: Variations for the Angora Road section in carbon isotopes (a), ocean surface water productivity proxies (b, c, d, j), proxies for seawater nutrient availability (e), bottom water oxygen levels (f, j), aeolian sediment input (g), glaucony (h), terrigenous sediment input (i), and various palynofacies proxies for shoreline proximity to the site of deposition (k - q).

Fig. 6.13

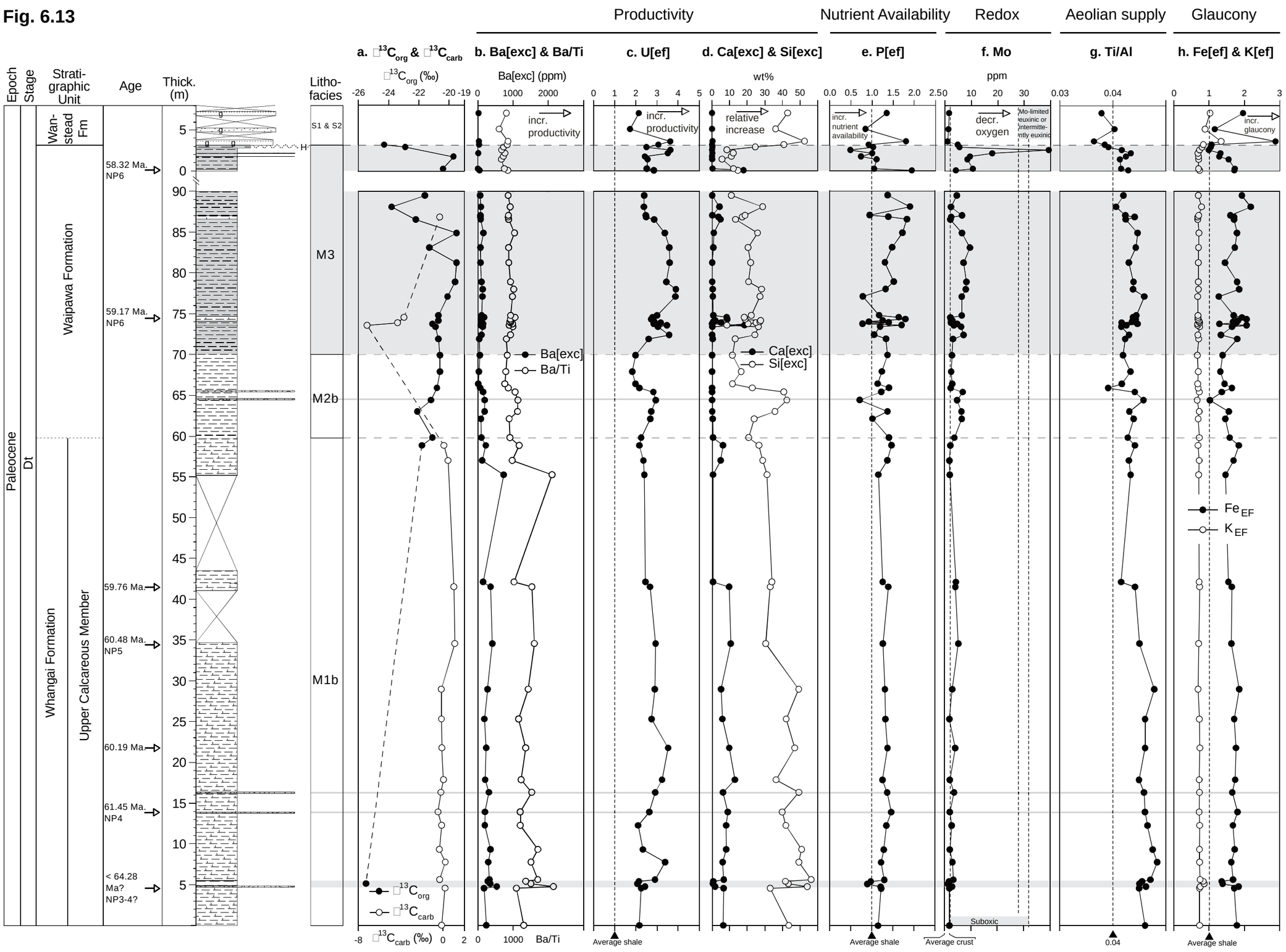
Productivity
Nutrient Availability
Redox
Aeolian supply
Glaucony
Epoch
Stage
Strati-graphic Unit
Age
Thick. (m)
Litho-facies
a. δ13Corg & δ13Ccarb
b. Ba[exc] & Ba/Ti
c. U[ef]
d. Ca[exc] & Si[exc]
e. P[ef]
f. Mo
g. Ti/Al
h. Fe[ef] & K[ef]
δ13Corg (‰)
Ba[exc] (ppm)
wt%
ppm
Paleocene
Dt
Wan-stead Fm
Waipawa Formation
Whangai Formation
Upper Calcareous Member
58.32 Ma. NP6
59.17 Ma. NP6
59.76 Ma.
60.48 Ma. NP5
60.19 Ma.
61.45 Ma. NP4
< 64.28 Ma? NP3-4?
S1 & S2
M3
M2b
M1b
incr. productivity
relative increase
incr. nutrient availability
decr. oxygen
Mo-limited euxinic or intermitte-ntly euxinic
incr. glaucony
Ba[exc]
Ba/Ti
Ca[exc]
Si[exc]
FeEF
KEF
δ13Corg
δ13Ccarb
δ13Ccarb (‰)
Ba/Ti
Average shale
Average crust
Suboxic
0.04

Fig. 6.13 cont.

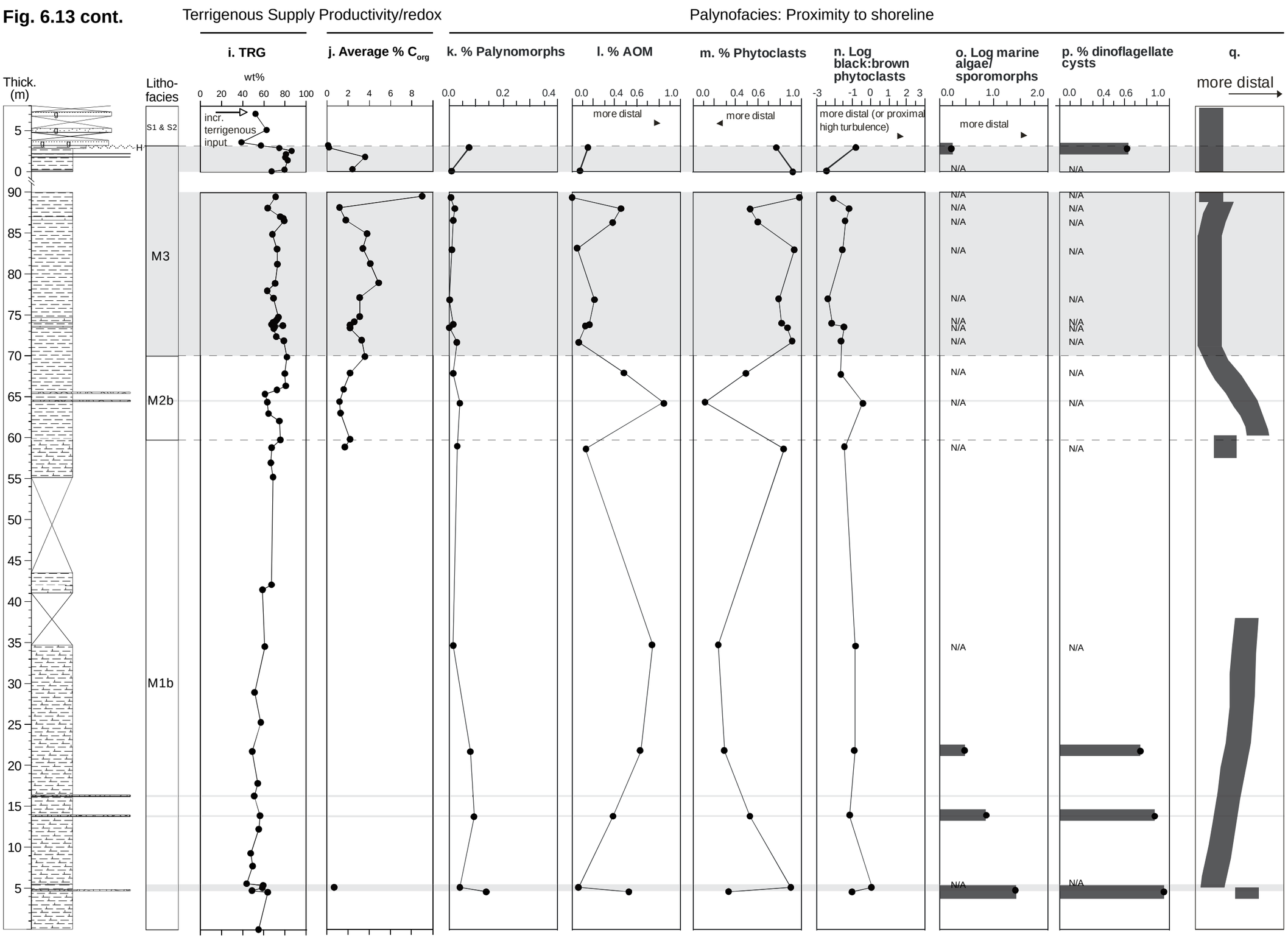
Terrigenous Supply Productivity/redox
Palynofacies: Proximity to shoreline
Thick. (m)
Litho-facies
i. TRG
wt%
0 20 40 60 80 100
incr. terrigenous input
j. Average % C_{org}
0 2 4 6 8
k. % Palynomorphs
0.0 0.2 0.4
l. % AOM
0.0 0.4 0.6 1.0
more distal
m. % Phytoclasts
0.0 0.4 0.6 1.0
more distal
n. Log black:brown phytoclasts
-3 -1 0 1 2 3
more distal (or proximal high turbulence)
o. Log marine algae/ sporomorphs
0.0 1.0 2.0
more distal
p. % dinoflagellate cysts
0.0 0.4 0.6 1.0
q.
more distal
S1 & S2
M3
M2b
M1b
N/A
0
5
10
15
20
25
30
35
40
45
50
55
60
65
70
75
80
85
90

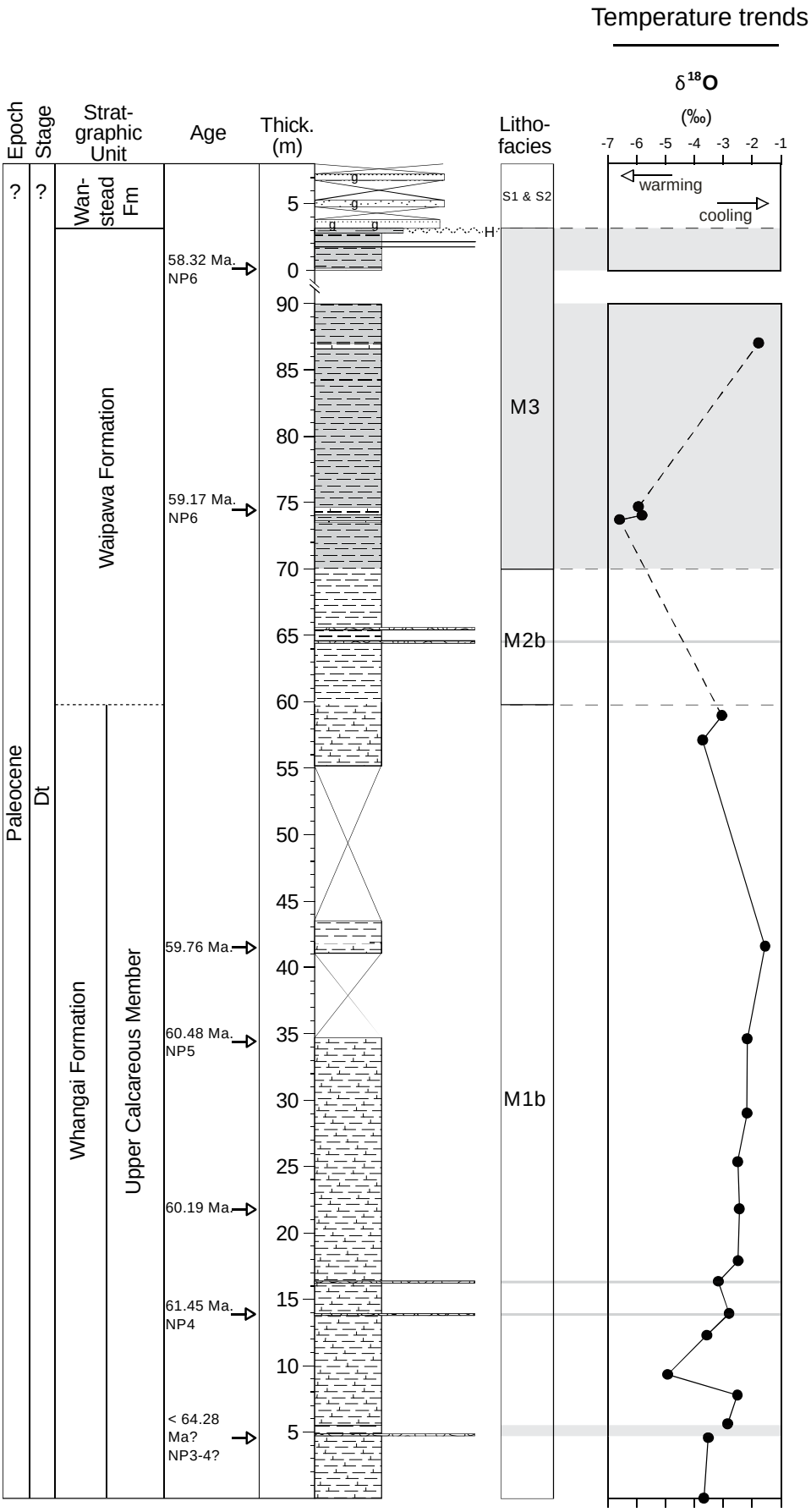

Figure 6.14: Variation in stable oxygen isotopes of the carbonate fraction through the logged section at Angora Road.

6.4.4 Grain size results

Grain size data were gathered for uppermost M1b, M2b, M3, and S1 (Fig. 6.15). There is little variation in sand, silt and clay sized grains through the majority of the section. An increase in sand and decrease in silt and clay sized grains is associated with the brown weathered bed in M2b and the transition from M3 to S1.

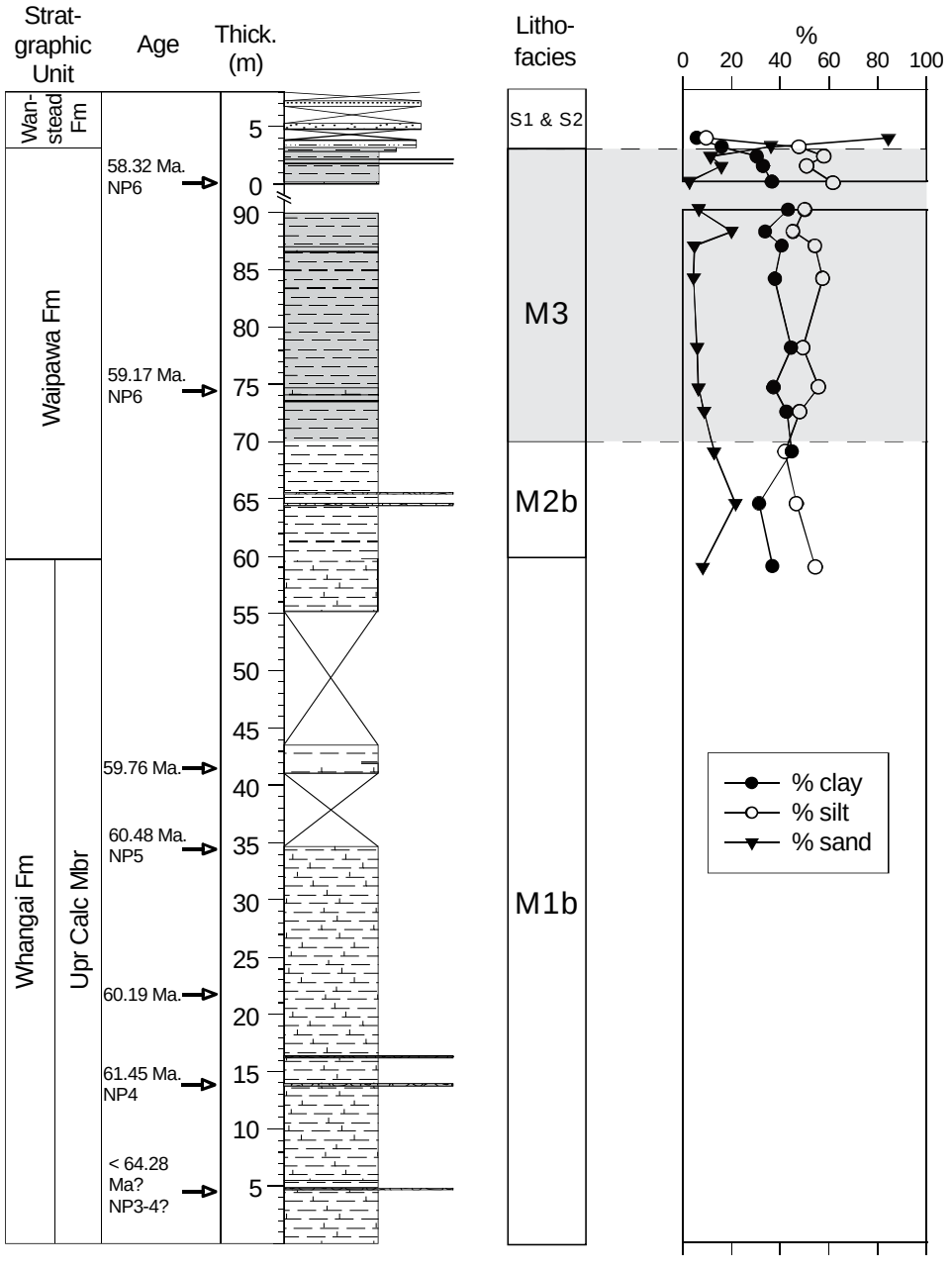

Figure 6.15: Variation in grain size through the upper half of the logged section at Angora Road determined using laser diffraction particle size analysis.

Chapter 7
TAWANUI

7.1 Location

The Tawanui section is near Tawanui in southern Hawke's Bay, located off Route 52 on Birch Road North very near the Tahuokaretu Road-Birch Road North junction. Weber is the nearest settlement and is located c. 6 km southwest from

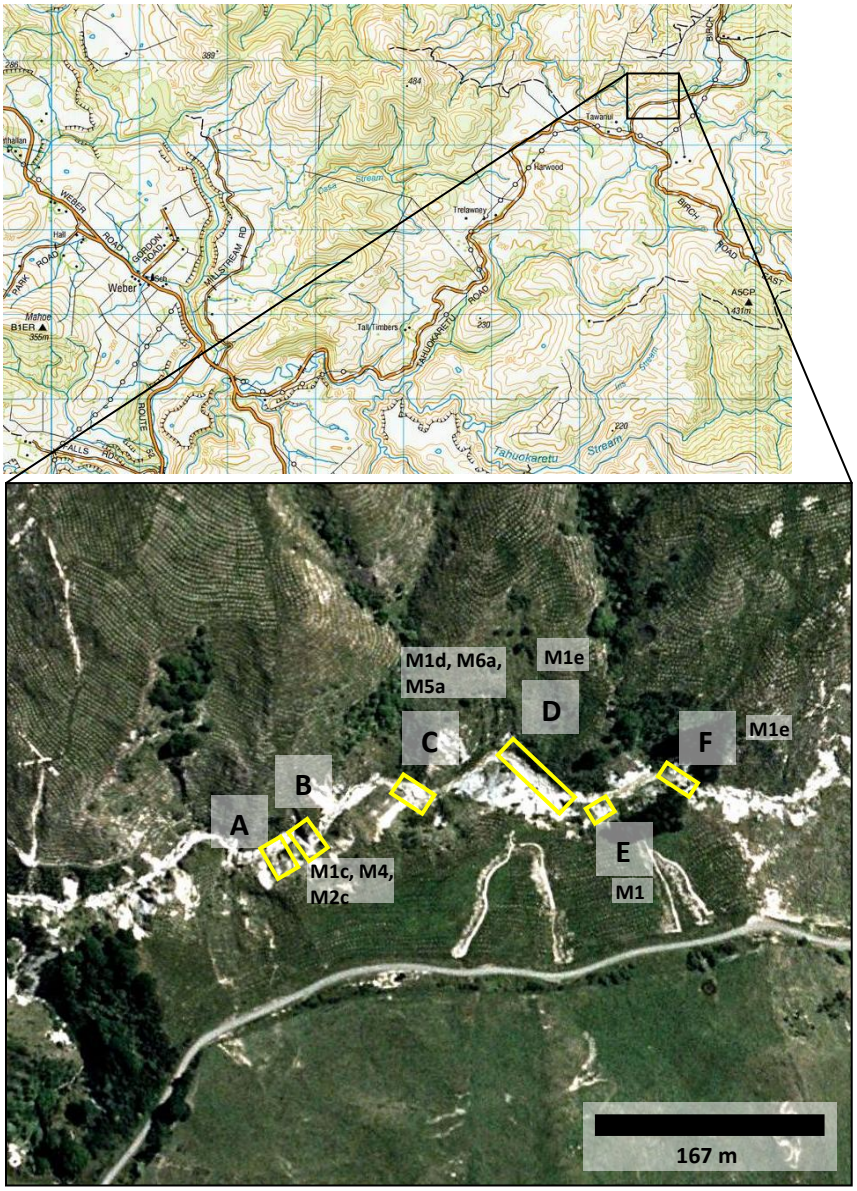

Figure 7.1: Location of the Tawanui section showing the six areas logged and the lithofacies observed within them (see Table 4.1). A and B = the "KTB" sections; C = "greensand" section; D = "mudstone" section; E = "PEB" section; F = mudstone above the "PEB" section. Lowermost strata described are at A and B, middle lithologies crop out at C and D, and the uppermost units are exposed at E and F.

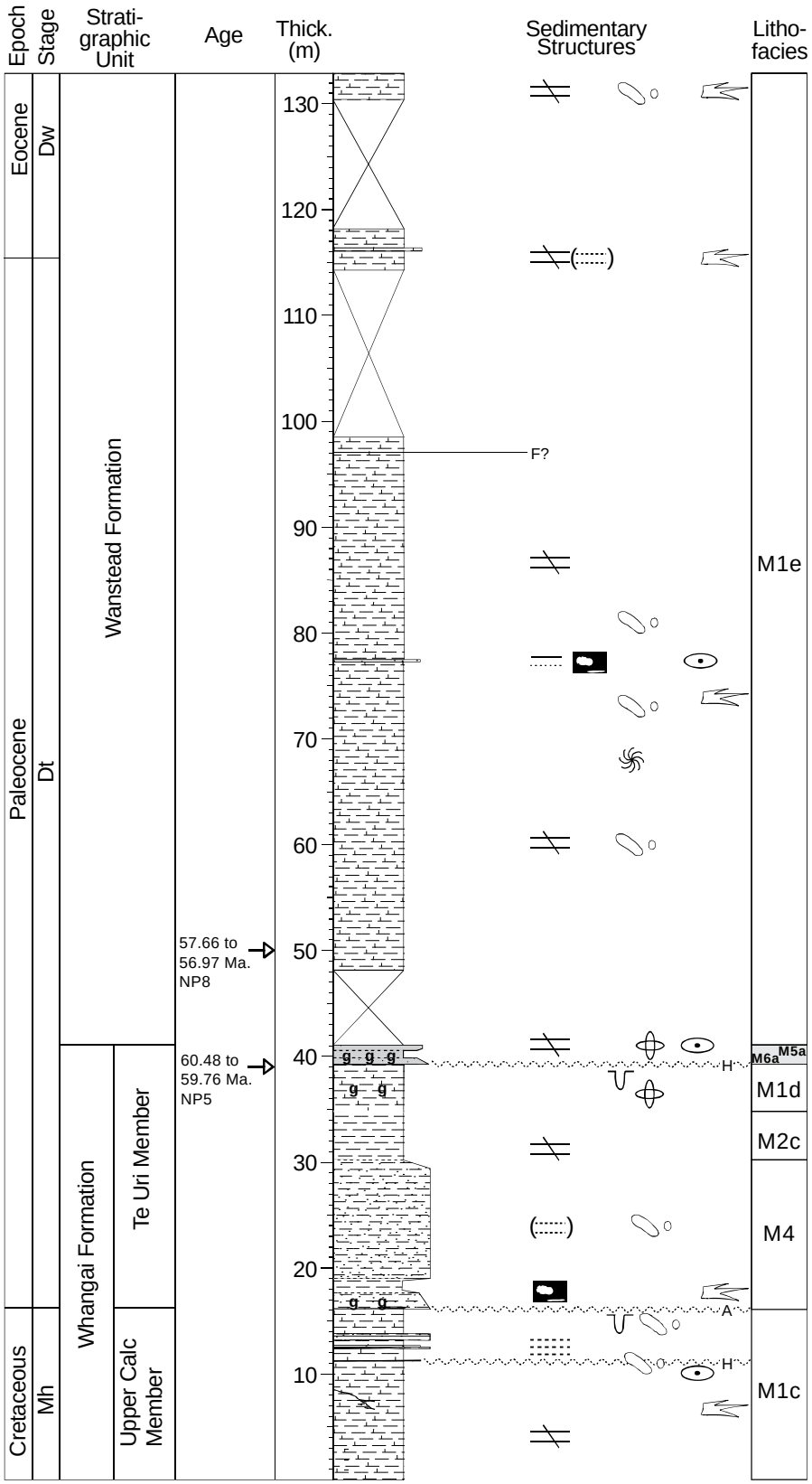

Figure 7.2: Stratigraphic column and lithofacies for the Tawanui section. Stratigraphic nomenclature and New Zealand stages shown are after Moore (1988), Stewart et al. (1999), and Rogers et al. (2001), with specific age data derived from nannofossil biostratigraphy (this study). Calcareous nannoplankton zones for the Paleogene (NP) are defined in Appendix A. Graphic log lithology and sedimentary structures symbols defined in Appendix B.

the section (Fig. 2.2 and 7.1). Six sections were logged at Tawanui to form a continuous stratigraphic column (Fig. 7.1 and 7.2). The lowermost strata described crop out at the "KTB" sections, middle units are accessible at the "greensand" and "mudstone" sections, and upper strata were logged at the "PEB" section and above (Fig. 7.1). Exposure through the sections is mostly good.

7.2 Facies characteristics

The sedimentary succession logged at Tawanui is presented in Fig. 7.2. The lithostratigraphic nonmenclature and New Zealand stages shown in the figure are after Moore (1988), Stewart et al. (1999), and Rogers et al. (2001) with the specific age data based on nannofossil biostratigraphy (this study).

The logged section at Tawanui consists of c. 16 m of calcareous mudstone (Upper Calcareous Member of the Whangai Formation) unconformably overlain by c. 19 m of non-calcareous sandy mudstone and mudstone (Te Uri Member of Whangai Formation). This succession is overlain by c. 4 m of calcareous mudstone, c. 2 m of highly glauconitic mudstone (both Te Uri Member of the Whangai Formation), and a further c. 90 m of calcareous mudstone (Wanstead Formation). Seven lithofacies have been identified in the succession (Fig. 7.2) and their field lithology, contacts, and petrography are described below, but first the textural classification scheme used in this study is briefly revisited to remind the reader of issues relating to classification of lithologies dominated by glaucony (see Section 3.4.1).

7.2.1 Glaucony and rock classification

In this study lithologic units rich in glaucony are named using their clastic grain size rather than their glaucony grain size so as to better reflect proximity of the paleoshoreline to the rocks depositional area in the rocks name. However, this classification system poorly describes the in-field character of lithologies dominated by glaucony, and consequently images presented in this chapter of samples with high proportions of sand sized glaucony grains, that normally would be classified as sandstones, are named glauconitic sandy mudstones due to the classification scheme excluding the grain size of the glaucony portion of the rock. To aid the reader, where a glaucony dominated lithology is referred to in the text

using this "new" classification scheme, the approximate percent glaucony and its conventional name are also given in square brackets (e.g. [c. 80% glc – muddy greensand]).

See Section 3.4.1 for further information on this topic

7.2.2 Calcareous mudstone lithofacies (M1c, d, e)

M1 occurs at four of the studied sections in the East Coast Basin (Table 4.1) and dominates the Tawanui sedimentary succession (Fig. 7.2). Three variants of the lithofacies occur at the Tawanui section (M1c, d, e) and details of the character of each of these is given below.

M1c

Field lithology

M1c consists of light grey, moderately well indurated, jointed, massive in outcrop, calcareous mudstone (Fig. 7.3A) with vague wispy laminations and possible burrows evident in slabbed samples. The lithofacies weathers to a frittery surface with pale yellow joint surfaces (Fig.7.3A). A glauconitic sandy mudstone [c. 20% glc – muddy sandstone] dike and three sandy mudstone [c. 20% glc – muddy sandstone] beds break up the succession.

The dike is composed of light green-grey, moderately well indurated, glauconitic, calcareous mudstone [muddy sandstone] (Fig. 7.3B). The main vein of the dike appears to cut down into the mudstone and splits up into long slender fingers that run away from the main vein at low and high angles. Its thickness varies from a few millimetres to 2 cm and the source of the dike is not visible in the section.

The sandy mudstone [muddy sandstone] beds consist of grey, well indurated, faintly to prominently laminated (Fig. 7.3C), glauconitic, calcareous sandy mudstone [muddy sandstone]. Laminations occur in the upper and/or lower portions of the beds and occasionally bed thickness appears to pinch and swell. The lower contacts are sharp and may undulate while the upper contacts grade into mudstone. There are prominent and unusually large glauconitic and pyrite infilled mudstone [c. 20% glc – muddy sandstone] burrows up to depths of 30 cm

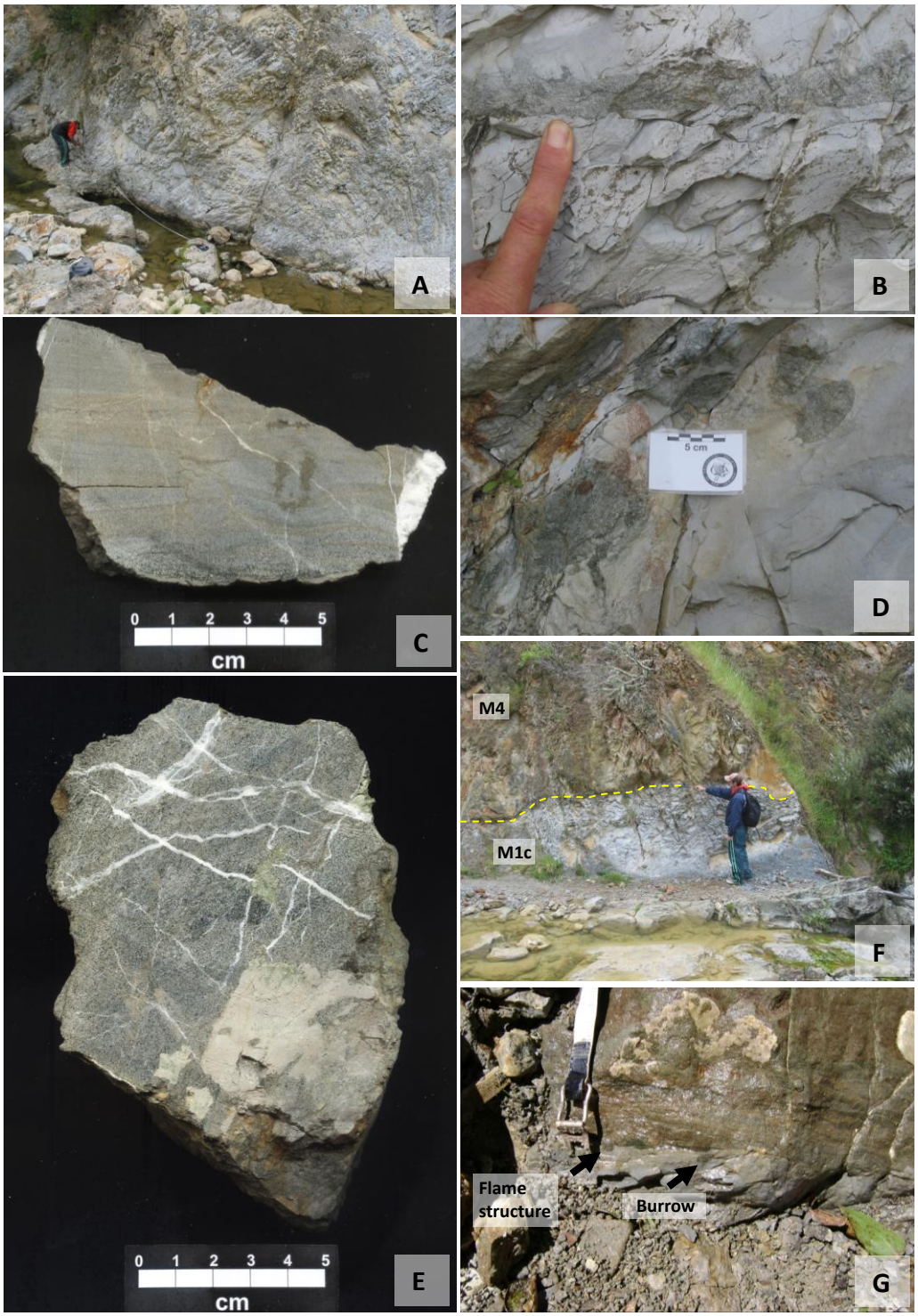

Figure 7.3: Features of the lowermost calcareous mudstone lithofacies (M1c) at Tawanui. A = Outcrop of M1c at the "KTB" section; B = glauconitic mudstone dike within calcareous mudstone [muddy sandstone] in M1c; C = laminations in, and normal grading of, a sandy mudstone bed in the M1c lithofacies; D = large ovoidal burrows underlying a thin sandy mudstone [muddy sandstone] bed; E = mudstone clasts and calcite veins within the sandy mudstones [muddy sandstone] of basal M4 at, and immediately above, the M1c-M4 contact; F = undulating Cretaceous-Tertiary contact involving the contact between M1c with overlying M4; G = slightly undulating upper contact of M1c with a small flame structure at the contact point, small ovoidal burrow in the underlying mudstone, and laminations within the overlying sandy mudstone.

below the lowermost sandy mudstone [muddy sandstone] bed (Fig. 7.3D). The burrows involve 3 - 8 cm diameter tubes which are subcircular in cross section. Smaller burrows, 0.5 - 1 cm in across are also present. Scattered ?pyrite nodules are present along the base of the sandy mudstone [muddy sandstone] bed, with locally intensive limonite staining in the vicinity of the nodules.

Contacts

The lower contact of M1c is not within the logged area. The upper contact of M1c occurs at the Cretaceous-Tertiary boundary (Fig. 7.2). The contact is sharp, appears to undulate slightly in some areas and can support small flame structures, and occasional vague ovoidal and tubular burrows (a few mm to 2 cm across) occur in M1c mudstone up to c.10 cm below the contact (Fig. 7.3F, G). Mudstone clasts and calcite veins are set within the sandy mudstone of basal M4 at, and immediately above, the contact (Fig. 7.3E).

Petrography

Description (MT1.14): Description of M1c is based on one sample. The lithofacies is composed of some very fine sand sized clastic grains set in a dark muddy (argillaceous) matrix with some shreds of muscovite and subrounded opaque minerals scattered throughout the rock (Fig. 7.4). The visible clastic component is moderately to poorly sorted and angular to subrounded. The mineral assemblage is dominated by clay and quartz, but feldspar is also a significant component (Fig. 7.5). Some fine sand sized glaucony grains are dispersed though the matrix and planktic and benthic foraminiferal tests (generally intact) are rare.

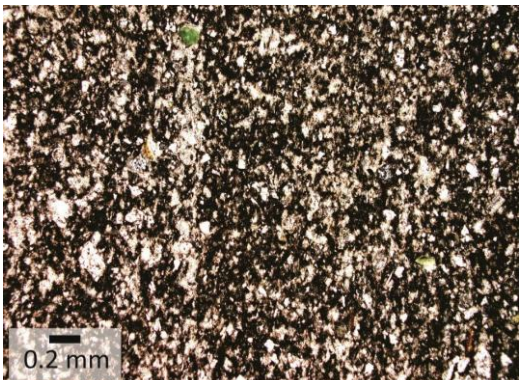

Figure 7.4: Typical mudstone of the M1c lithofacies with silt-sized and very fine sand-sized clastics, and some glaucony grains, set in a dark argillaceous matrix (MT1.14)

Classification: Immature to submature very slightly glauconitic quartzose argillutite (Fig. 3.11 and 7.5).

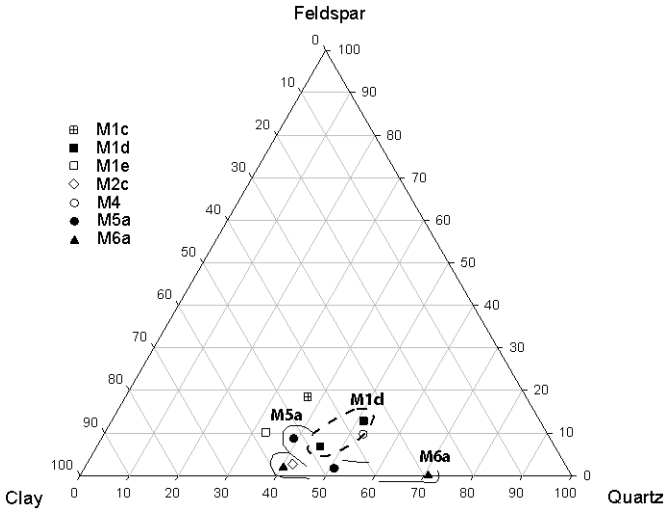

Figure 7.5: Ternary diagram of relative proportions of feldspar, clay minerals and quartz in the mudstone lithotype (M) at the Tawanui section.

M1d

Field lithology

M1d strata were logged at the "greensand" section (Fig. 7.6A). M1d is composed of light to dark grey, moderately to moderately well indurated, massive, variably burrowed, very slightly to slightly glauconitic, calcareous mudstone with faint laminations evident in some slabbed samples (Fig. 7.6C), and rare nodules. Most of the mudstone weathers to a light grey colour (Fig. 7.6B) but this becomes orange brown close to the lithofacies upper contact (Fig. 7.6D). A 40 cm thick horizon of prominent, glaucony infilled burrows occur c. 20 cm below the M1d-M6a contact (Fig. 7.6D, F). The burrows are finger like, 6 to 20 cm long and 2 to 3 cm across, penetrate down into the underlying strata approximately perpendicular to bedding, and fill the majority of the horizon. There are smaller (5 cm long and 1 cm across) less distinctive burrows in the top 7 cm of the horizon. These are separated from the larger burrows by a very thin bed of wispy glauconitic mudstone interbedded with non-glauconitic mudstone, and capped with a thinner layer of massive mudstone (c. 5 cm total thickness).

Contacts

The lower contact of M1d was discussed when describing the upper contact of the M2c lithofacies in Section 7.2.3. The upper contact of M1d with M6a is sharp,

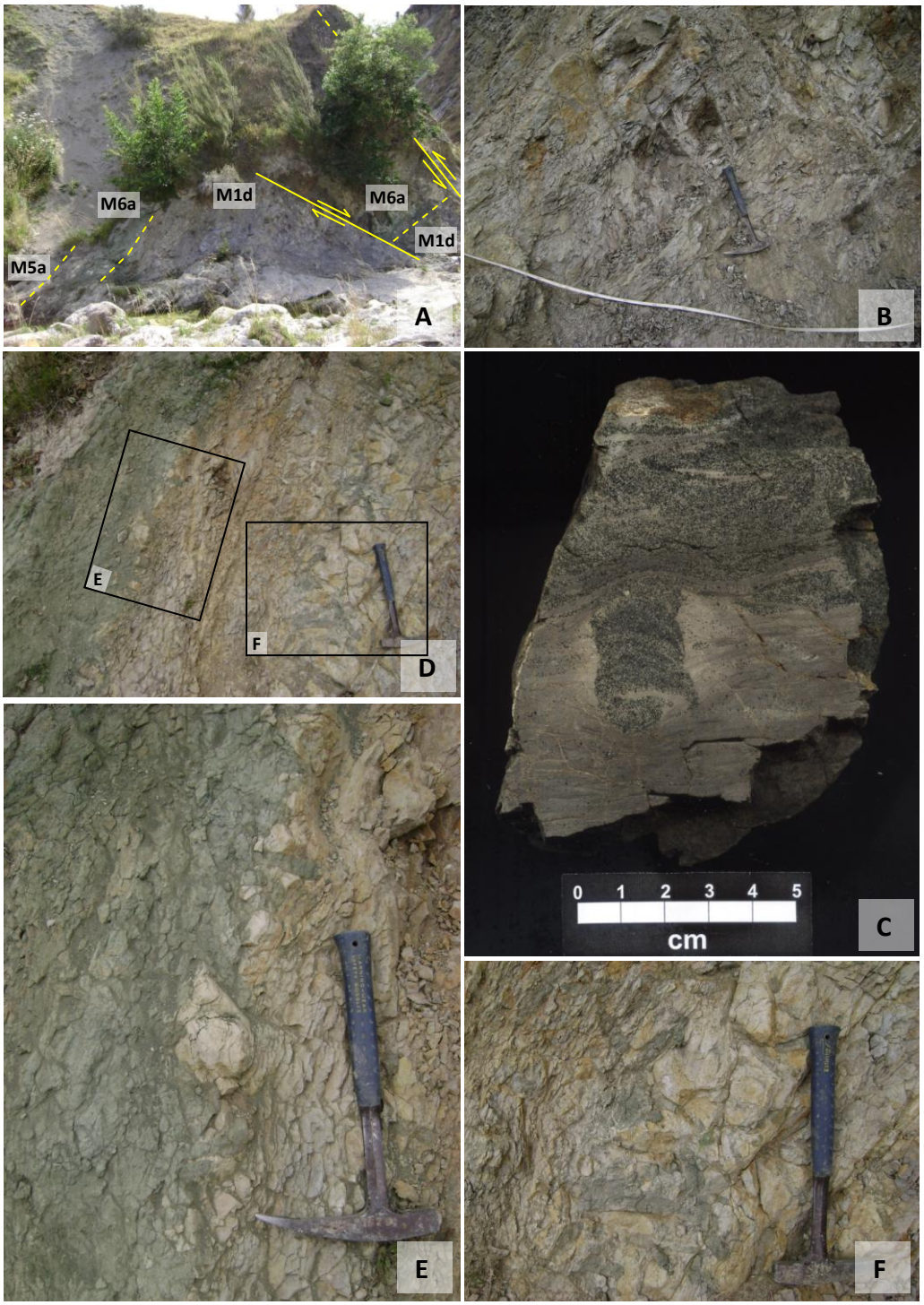

Figure 7.6: Features of the M1d lithofacies. A = Outcrop of M1d mudstone at the "greensand" section showing the location of lithofacies, and inferred faults and repeated strata; B = appearance in outcrop of typical M1d mudstone; C = slabbed example of M1d mudstone with relatively high glaucony contents and burrowing; D to F = the uppermost portion of M1d with orange-brown weathered surfaces (D-F), highly burrowed upper contact (E), and a prominent burrowed horizon near the upper contact (F).

with distinct 3 to 7 cm long and 2 cm wide finger like burrows penetrating into the underlying mudstone approximately perpendicular to bedding (Fig. 7.6D, E). The burrows are infilled with very highly glauconitic mudstone [c. 75% glc – muddy greensand] from the overlying lithology.

Petrography

Description (MT1.30, MT1.34, MT1.37, MT1.40): Description of M1d is based on four representative samples. The lithofacies is composed of some to many fine and very fine sand sized clastic grains set in a dark argillaceous matrix with some shreds of muscovite and opaque minerals dispersed through the rock (Fig. 7.7A). The visible clastic grains are poorly sorted and angular to rounded. Quartz and clay appear to be the dominant minerals present (Fig. 7.5) but calcite can also be a major constituent. Feldspar and rock fragments are minor components (Fig. 7.5). Many to common very fine and fine sand-sized glaucony grains occur through the succession (Fig. 7.7A). Planktic foraminiferal tests are generally rare but become common towards the upper contact (Fig. 7.7B).

Classification: Submature very slightly to slightly glauconitic quartzose argillutite and argillaceous quartzlutite (Fig. 3.11 and 7.5). Burrows are infilled with moderately glauconitic sandy mudstone [c. 20% glc – muddy sandstone].

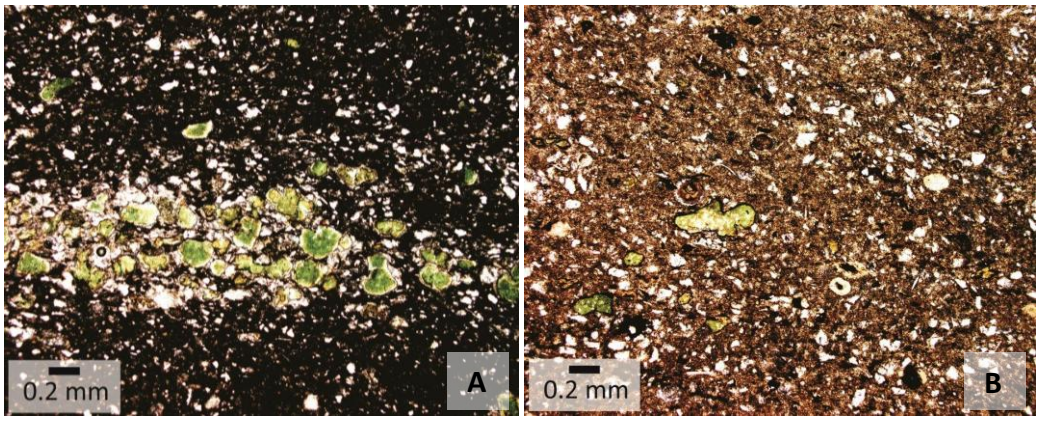

Figure 7.7: Photomicrographs of representative samples from the M1d lithofacies. A = Typical M1d mudstone composed of many glaucony grains (concentrated in a burrowed horizon) and some silt-sized and very fine sand-sized clastics set in a dominant dark argillaceous matrix (MT1.30); B = lighter coloured mudstone from the uppermost portion of M1d (see Fig. 7.6D-F) with a greater abundance of planktic microfossil tests compared with the underlying M1d mudstones (MT1.40).

M1e

Field lithology

Light to medium grey, poorly to well indurated, occasionally jointed, generally massive, calcareous mudstone (Fig. 7.8A-D) with vague burrowing and *Zoophycos* trace fossils sometimes evident in slabs (Fig. 7.8C). Weathering of the M1e mudstones varies with some areas developing a "popcorn" surface morphology (Fig. 7.8B), other units weathering to light grey frittered surfaces, and at the "PEB" section the mudstones are deeply weathered and have developed a light brown colouration (Fig. 7.8D). Changes in lithology are usually gradational.

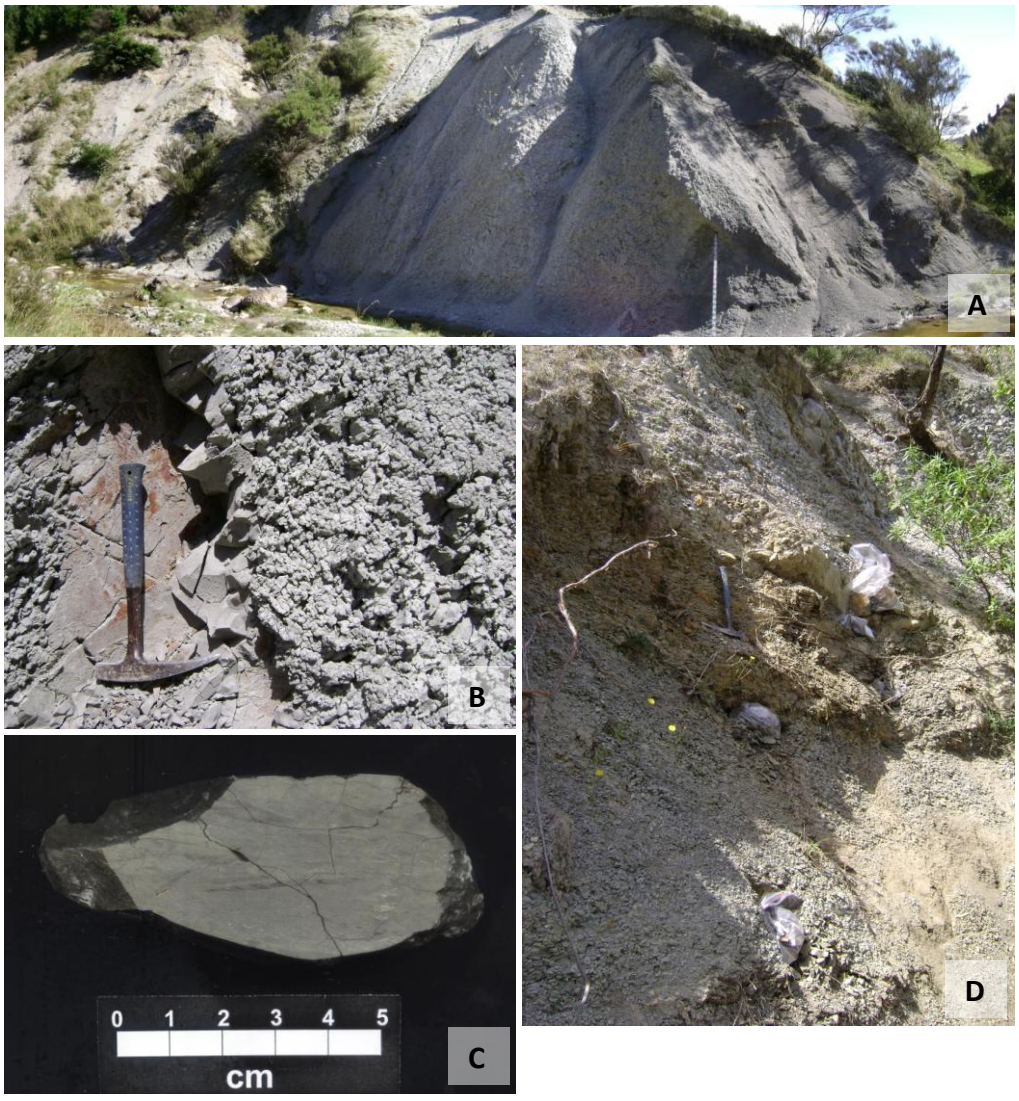

Figure 7.8: Some features of the M1e lithofacies. A = massive M1e mudstone cropping out at the "mudstone" section; B = mudstone unit with "popcorn" weathered surface; C = light grey mudstone, typical of M1e, with Z*oophycos* trace fossils; D = deeply weathered mudstone at the "PEB" section.

Contacts

The upper and lower contacts of M1e are not exposed.

Petrography

Description (MT1.50): Description is based on one sample. M1e consists of rare sand sized clastics set in a dark argillaceous matrix with some shreds of muscovite and opaque minerals dispersed through the rock (Fig. 7.9). Sorting is poor and the visible clastics are angular to subangular in shape. The rocks mineral assemblage is dominanted by clay with quartz secondary in abundance and feldspar and rock fragments minor constituents (Fig. 7.5). Glaucony grains and planktic microfossil tests are rare.

Classification: Immature quartzose argillutite (Fig. 3.11 and 7.5).

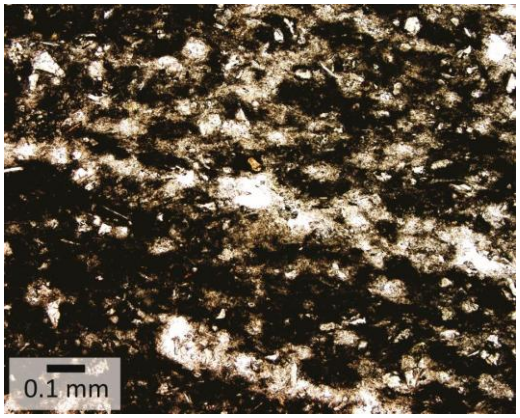

Figure 7.9: Example of an M1e mudstone composed predominantly of dark argillaceous matrix, with rare glaucony grains and sand-sized clastics.

7.2.3 Sandy mudstone lithofacies (M4)

Of the sections studied, M4 is only observed at Tawanui (Table 4.1). Description of this lithofacies follows.

Field lithology

M4 is composed of light grey, moderately well to well indurated, highly jointed, very slightly to slightly glauconitic, non-calcareous slightly sandy mudstone. The rock weathers to either a blocky or frittery surface with a light red-brown colour (Fig. 7.10A). In outcrop M4 is massive, but when slabbed there are faint wispy laminations and occasionally burrowing (Fig. 7.10B, C). The basal 3 m of the

succession appears to have rough bedding but the majority of the succession above this seems massive. Immediately above the lower contact there is c. 1.5 m thick light grey, well indurated, blocky, massive, slightly glauconitic, non-calcareous moderately sandy mudstone [10% glc – muddy sandstone] (Fig. 7.10B) that grades upwards into c. 1 m of mudstone. The abundance of glaucony decreases rapidly upwards through this basal bed and slabbed samples show that the lowermost portion of the bed is massive (Fig. 7.10B), the mid regions faintly laminated, and the upper mudstone massive. A moderately glauconitic, slightly sandy mudstone [30% glc – muddy sandstone] with a sharp undulating lower contact with flame structures (Fig. 7.10D) occurs about midway through the M4 succession. This bed, within M4, is visually difficult to distinguish from the surrounding rock and its upper contact was not observed.

Contacts

The lower contact of M4 was discussed previously when describing the upper contact of the M1c lithofacies in Section 7.2.1. The upper contact of M4 consists of slightly sandy mudstone of the M4 lithofacies grading upwards into the mudstone of M2c (Fig. 7.10A). In outcrop this is seen as a frittery rock grading upwards into a more coherent rock, and in some places the mudstone protrudes out, overhanging the slightly sandy mudstone (Fig. 7.10A).

Petrography

Description (MT1.16, MT1.15, MT1.17, MT1.18, MT1.69): Description of M4 is based on five samples. The majority of the lithofacies consists of many very fine sand sized grains set in a dark muddy (argillaceous) matrix with some muscovite shreds and opaque minerals dispersed through the rock (Fig. 7.11A). The rock is poorly sorted and the visible grains are angular to subangular in shape. Quartz is the dominant mineral present with clay secondary in abundance and feldspar and rock fragments minor (Fig. 7.5). Near the lithofacies lower contact calcite is a major component of the mineral assemblage. Generally glaucony grains are rare but towards the base of the succession they are more abundant. Planktic and benthic microfossil tests are absent.

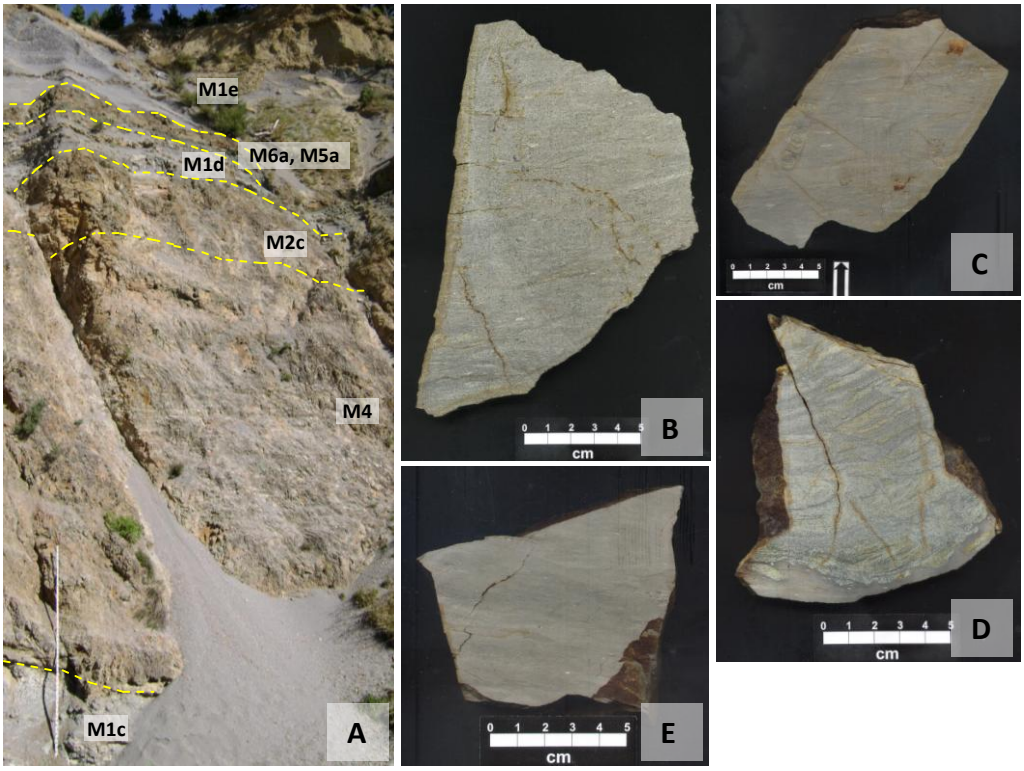

Figure 7.10: Some features of the M4 and M2c lithofacies. A = Character of the M4 and M2c lithofacies in outcrop and their relative position to other lithofacies identified at the Tawanui section; B = mostly massive moderately sandy mudstone [muddy sandstone] of basal M4; C = typical slightly sandy mudstone of M4 with burrowing and faint laminations; D = glauconitic sandy mudstone [muddy sandstone] with a sharp undulating lower contact with flame structures, within M4; E = example of an M2c mudstone in hand specimen. The rock is mostly massive with very faint laminations in areas.

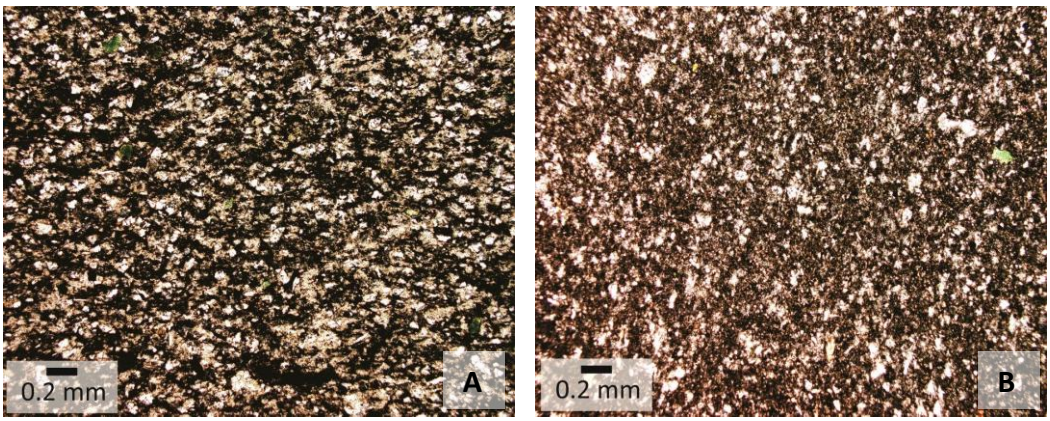

Figure 7.11: Photomicrographs of representative samples from the M4 and M2c lithofacies. A = Typical slightly sandy mudstone of M4 composed of many very fine and coarse silt-sized clastic grains, and some glaucony grains, set in a dark argillaceous matrix (MT1.69); B = example mudstone from M2c composed of some sand and coarse silt-sized clastics and rare glaucony grains, scattered through the dominantly muddy matrix (MT1.71).

Classification: Immature to submature very slightly glauconitic slightly to moderately sandy argillaceous quartzlutite (Fig. 3.11 and 7.5) with occasional burrows infilled with sandier more glauconitic mudstone [5% glc – muddy sandstone].

7.2.4 Siliceous mudstone lithofacies (M2c)

M2 occurs at four of the studied sections in the East Coast Basin (Table 4.1). The Tawanui variant of the lithofacies (M2c) is difficult to access and sample. Consequently description is from afar and based on one sample.

M2c

Field lithology

M2c appears to be similar to M4 except for a reduced sand component and an apparent better resistance to weathering, leading to it slightly protruding out over the underlying M4 (Fig. 7.10A).

Contacts

The lower contact of M2c was discussed previously when describing the upper contact of the M4 lithofacies in Section 7.2.2. The upper contact was not accessible so its nature could not be described.

Petrography

Description (MT1.71): Description is based on one sample collected from the base of the lithofacies. M2c is composed of some sand sized clastics set in a dark argillaceous matrix with some mica and opaque minerals scattered throughout the rock (Fig. 7.11B). M2c is poorly sorted and visible clastic grains are subangular in shape. Clay dominates the mineral assemblage with quartz secondary in abundance and feldspar a minor component (Fig. 7.5). Some glaucony grains are scattered through the muddy matrix and planktic and benthic microfossil tests are absent.

Classification: Immature to submature quartzose argillutite (Fig. 3.11 and 7.5).

7.2.5 Muddy 'greensand' lithofacies (M6a)

M6 is logged at two of the studied sections in the East Coast Basin (Table 4.1) and its characteristics at Tawanui (M6a) are described below.

M6a

Field lithology

The basal c. 0.6 m of M6a consists of green, poorly indurated, massive, burrowed, very highly to extremely glauconitic, non-calcareous moderately sandy mudstone [c. 75% glc - muddy greensand] (Fig. 7.12A, C, D). The basal lithology rapidly grades upwards into a very dark green, well indurated, massive, burrowed, highly glauconitic, mostly non-calcareous mudstone [c. 80% glc – muddy greensand] (Fig. 7.12A, E). The upper lithology is calcareous in burrowed areas and non-calcareous in glauconitic areas. When weathered the upper lithology is very dark grey and looks like a grey mudstone with abundant glaucony grains.

Contacts

The lower contact of M6a was discussed previously when describing the upper contact of the M1d lithofacies in Section 7.2.1. The upper contact is poorly exposed but may possibly be sharp. There may be a 10 cm thickness of softer muddier green mudstone at the contact but this could be a weathering affect.

Petrography

Description (MT1.45, 43, 44, 46, 47): Description of M6a is based on five samples. Immediately above the M6a lower contact the rock is composed of many very fine sand sized clastic grains in grain to grain contact with glaucony grains, with muddy matrix infilling pore spaces. Some opaque minerals are present and mica is rare – a reduction in the abundance of mica from the underlying lithologies. The rock is poorly sorted and the visible clastics are subangular to subrounded in shape. Glaucony is the dominant mineral present, with quartz secondary in abundance. Calcite and rock fragments are also present in lesser quantities. Glaucony grains mostly range in size from very fine sand to medium sand but can be up to very coarse sand in size. They are angular to subrounded in shape and some have cracks developed into their periphery. Benthic and planktic microfossil tests are absent.

Through the lower 0.6 m of M6a visible clastic grains fine upwards and in the uppermost portion of this bed there is an increase in muddy matrix. There is initially a slight increase in the abundance of glaucony above the basalmost horizon, followed by a decrease in the uppermost part of the lower bed. Rare glauconitised benthic and planktic microfossil tests may occur in this part of the lithofacies but it is difficult to tell for certain. A significant portion of the glaucony grains have a "popcorn" morphology, with cracks propagating from their edges towards their centres.

Through the remaining c. 0.7 m of M6a there appears to be no further decrease in the abundance of sand sized clastics or the abundance of glaucony, the proportion of muddy matrix appears to remain the same, no planktic microfossil tests were observed, and grains displaying "popcorn" morphology are rare or absent.

Classification: Immature to submature, highly to extremely glauconitic mudstone and moderately sandy mudstone [75-80% glc – muddy greensand]. M6a is an argillaceous quartzlutite in its lower sandier portion and a quartzose argillutite in its upper muddier portion (Fig. 3.11 and 7.5).

7.2.6 Glauconitic mudstone lithofacies (M5a)

M5 was observed at three of the study sites in the East Coast Basin and differs slightly at each (Table 4.1). The lithofacies particular characteristics at Tawanui (M5a) are described below.

M5a

Field lithology

M5a is composed of dark grey and black, poorly to well indurated, massive, moderately glauconitic, non-calcareous slightly sandy mudstone with abundant hard, ovoidal, possibly pyrite cemented nodules (Fig. 7.12B, F). The largest nodule seen is 9 cm × 6 cm in size.

Contacts

The lower contact of M5a was discussed previously when describing the upper

Figure 7.12: Features of the M6a and M5a lithofacies. A = The lower, more glauconitic bed of M6a is separated from the upper, less glauconitic and better indurated bed of the lithofacies by a rapidly gradational contact; B = hard ovoidal nodules within the poorly exposed M6a lithofacies; C to D = very highly glauconitic sandy mudstone [c. 75-80% glc – muddy greensand] with burrows infilled with non-glauconitic mudstone in the lowermost (C) and upper portion (E) of the lithofacies; F = cross section through a hard, glauconitic, ovoidal sandy mudstone nodule from M5a in hand specimen.

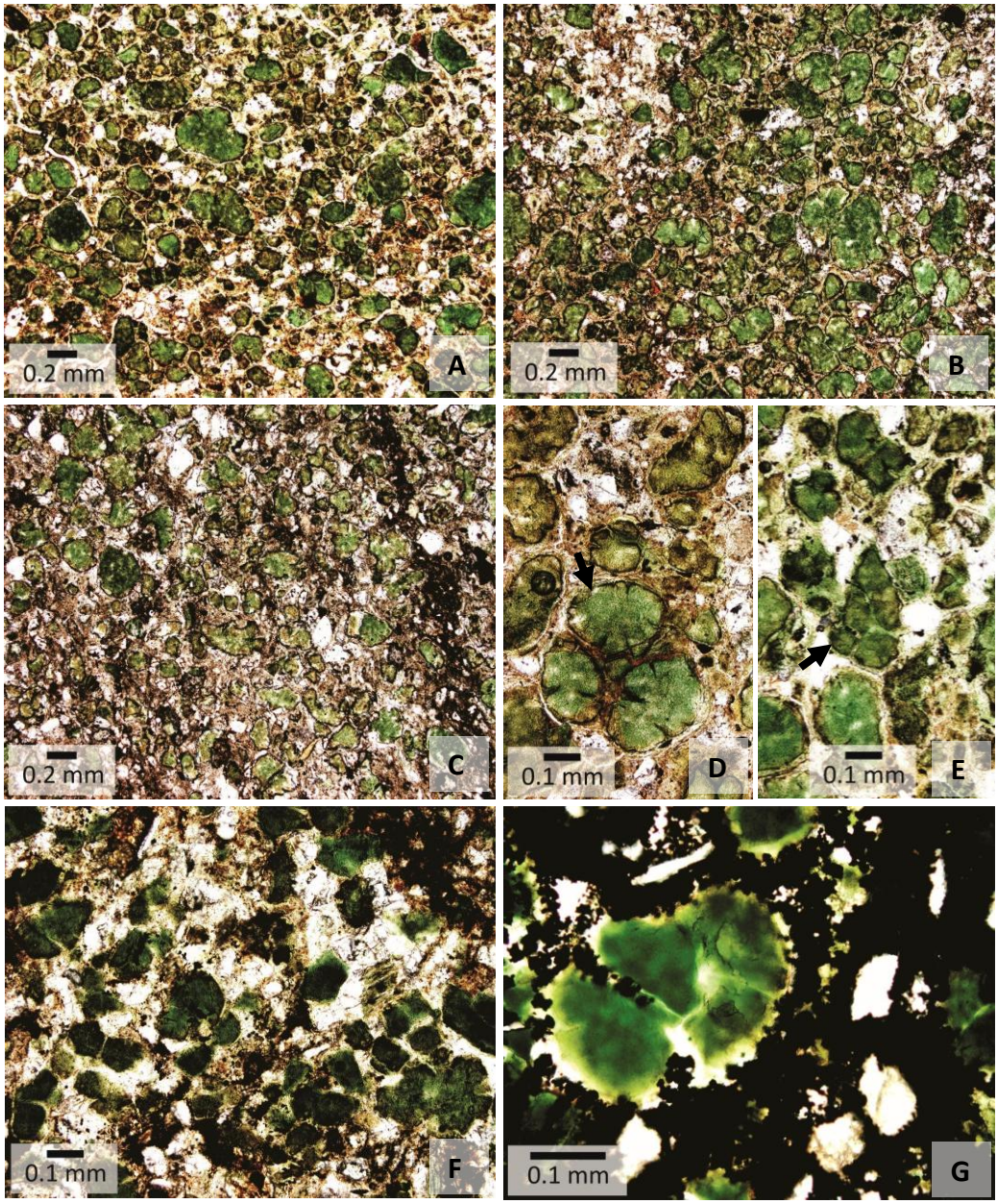

Figure 7.13: Photomicrographs of representative samples from the M6a and M5a lithofacies. A to C = decrease in the abundance of glaucony and sand-sized clastic grains and increase in muddy matrix from lower M6a (A, B) to the upper portion of M6a (C) (see Fig. 7.12A) – also evident is the "popcorn"-like irregular morphology of some glaucony grains in the lower portion of M6a (B) (A: MT1.45, B: MT1.44, C: MT1.46); D and E= glaucony possibly infilling the chambers of a planktic (D) and benthic (E) foraminiferal test (position of both indicated by arrows); F and G = many fine sand sized clastic grains and common glaucony grains set in either a muddy (F) or pyrite matrix (G) in a nodule from M5a (MT1.72). Pyrite appears to have eaten into the outer margins of glaucony and quartz (and ?feldspar) grains resulting in their "nibbled" morphology (G).

contact of the M6a lithofacies in Section 7.2.4. The upper contact of the M5a lithofacies is not exposed and inaccessible were it is exposed.

Petrography

Description (MT1.72): Petrographic description was performed on a nodule from the lithofacies. The nodule is composed of many fine sand sized clastic grains and common glaucony grains set in either a muddy (Fig. 7.13F) or pyritised matrix (Fig. 7.13G). The rock is poorly sorted and the visible clastic grains are angular to subrounded. Clay minerals (including glaucony) are the most abundant minerals present, with quartz second in abundance (Fig. 7.5). Some feldspar and common pyrite also occur, with minor rock fragments. Most glaucony grains are of medium sand size, moderately sorted, and angular to rounded in shape (Fig. 7.13F, G). Angular grains occur when the glaucony grains sit in pyrite "matrix". It appears that the pyrite eats into the outside of the glaucony grains, giving the grain edges multiple "bite marks" (Fig. 7.13G).

Classification: Immature to submature, moderately glauconitic and pyritic, slightly sandy argillaceous quartzlutite (Fig. 3.11 and 7.5).

7.3 Mineralogical trends

Quartz increases slightly from M1c to M4 and remains steady through the lithofacies before decreasing through M2c and M1d. It seems to increase through M6a and possibly through M5a and then either decreases or remains similar in content through into M1e. Clay decreases from M1c to M4 then gradually increases through M4 and into M2c. It decreases through M1d and increases through M6a, then decreases in M5a before increasing once again in M1e. There is little variation in feldspar but it reaches minima in M2c, M6a, and possibly M6b. Planktic microfossil tests are rare in M1b and lowermost M4 and absent up through the rest of M4 and M2c. Their abundance gradually increases up through M1c then possibly drops or is masked by glauconitisation in M6a. They become absent once again in M5a then increase up into M1d.

7.4 Geochemistry and palynofacies results

Geochemical and palynofacies proxies used in this study were introduced in

Chapter 3 (Sections 3.3.2 to 3.3.4) and are presented here for the Tawanui section. Fig. 7.14 and 7.15 present the up section trends for carbonate carbon and organic carbon stable isotopes (a), and also elemental proxies for ocean surface water biological productivity (b-d), seawater nutrient availability (e), bottom water oxygen levels (f), aeolian sediment supply (g), glaucony (h), and terrigenous sediment supply (i). Up section variations in ocean surface water biological productivity and bottom water oxygen levels are also indicated by the average percent organic carbon plot (j). Included in the figures are palynofacies proxies for the proximity of depositional areas to the paleoshoreline (k-q).

Fig. 7.14 displays up section trends of the above mentioned proxies for the entire Tawanui section, whereas Fig. 7.15 is an enlargement of the same data for a small portion of the section centred on M6a and M5a. M6a and M5a are focused on in this figure because the units span the Late Paleocene event (LPE) – a period of inferred climate cooling. Preliminary interpretations of geochemical and palynofacies trends are offered in this section, even though this is a results chapter, to aid later interpretations (see Chapter 10).

7.4.1 Elemental geochemistry and organic carbon proxies

In this section the results for elemental geochemistry and organic carbon proxies (Fig. 14b-j and 15b-j) are described. However, first the ocean surface water biological productivity proxies are tested for biogenic association using the methods outlined in Chapter 3. This is done in order to assess their reliability as paleoproductivity indicators for the logged area of the Tawanui section. If a productivity proxy is found to have no biogenic association its trends will not be described in any detail.

Testing for productivity proxy biogenic association

Ba[exc] co-varies with Ba/Ti and has poor correlation with TRG through all but the uppermost lithofacies at Tawanui (M1e) and therefore appears to have a biogenic association through most of the logged succession (Fig. 7.14b). Correlation between Ba[exc] and TRG through M1e is variable so there may be a mixed biogenic and terrigenous association with Ba[exc] through the lithofacies (Fig. 7.14b, i). Mo indicates that limited parts of the succession at Tawanui were

deposited under slightly to highly suboxic, or rarly Mo-limited euxinic or intermittently euxinic conditions (Fig. 7.14f). The majority of the succession was deposited under oxic conditions (Fig. 7.14f) and consequently Ba[exc] is used as the primary productivity indicator. U[ef] appears to broadly co-vary with Ca[exc] and Si[exc] (Fig. 7.14c, d) and is used in conjunction with, or without, Ba[exc] when there is evidence for sediment deposition in oxygen depleted conditions (Fig. 7.14c, f).

Proxy results

Entire section

Productivity proxies (Fig. 7.14b, c, d) indicate a combination of calcareous and siliceous productivity through M1c, with three spikes of high calcareous productivity suggested by coincident high U[ef] and Ca[exc] values. U[ef] values are favoured over the unvarying Ba[exc] values in this case because they coincide with high seawater nutrient levels (P[ef]). One of the spikes occurs at the Cretaceous-Tertiary boundary. Productivity levels through M4 and M2c are similar to levels through the majority of the underlying M1c lithofacies, but calcareous productivity is reduced to very low levels, and siliceous productivity dominates through the interval (Fig. 7.14b, c, d). Ba[exc] values suggest a slight decrease in productivity from M2c into M1d while U[ef] indicates an initial increase followed by a drop back to M4 and M2c levels (Fig. 7.14b, c). It is possible that Ba preservation in the sediments has been reduced by low oxygen levels at the time of sediment deposition, as shown by the Mo spike at the same time. Consequently the UEF record of increased productivity is used in preference to the Ba[exc] record. The base of M1c thus may have been marked by an increase in calcareous productivity followed by a sharp decrease. The remainder of M1d is characterised by gradually increasing calcareous productivity (Fig. 7.14d). Siliceous productivity decreases from the transition from M2c to M1d, after which it remains at a steady level (Fig. 7.14d). M6a is marked by a very slight increase in siliceous productivity and a sharp and drastic drop in calcareous productivity (Fig. 7.14d). Whether the drop in calcareous productivity is genuine or not is unknown. Glauconitised benthic and planktic foraminiferal tests may be present in the lithofacies, so the drop may be a reflection of glauconitisation of tests, rather than a drop in calcareous productivity. Ba[exc],

Ca[exc], and Si[exc] suggest that M1e is characterised by high, broadly or rapidly fluctuating calcareous and siliceous productivity, with a peak coinciding with the mudstone having a "popcorn" weathered crust (Fig. 7.8B), and a second peak in the vicinity of the Paleocene-Eocene boundary (Fig. 7.14b,c). Productivity lows occur in the middle of the lithofacies and in the Paleocene-Eocene boundary zone. There is some limited correlation between Ba[exc] and TRG through this lithofacies so a mixed terrigenous-biogenic association may be inferred (Fig. 7.14b, i). The transition from M5a to M1e is also complicated by the transition coinciding with a shift from oxygen depleted to normal oxygen levels (Fig. 7.14f). Because Ba[exc] concentration is depleted under low oxygen conditions the dramatic increase from M5a to M1e may not be as large (or even an increase) if M5a had rather been under oxygenated conditions during its deposition. Similarly, U[ef] is affected by oxygen depletion and its decrease in M1e may be a reflection of changed bottom water oxygen levels (Fig. 7.14c). Consequently any relative productivity differences between M5a and M1e are difficult to assess.

Seawater nutrient levels spike and fluctuate in M1c and at the Cretaceous-Tertiary boundary (Fig. 7.14e), possibly in association with increased calcareous productivity (Fig. 7.14d). Nutrient levels are at their lowest in the logged section through M4 and M2c, slightly elevated in M1d, M6a, and M5a, and remain relatively steady, and very slightly enriched above average shale values, through M1e.

Oxygen levels during deposition of sediments through the majority of the logged section are generally at the boundary between oxic and suboxic conditions, with very slightly suboxic conditions evident through limited areas of M1c, M4, M6a and M1e (Fig. 7.14f). Stronger oxygen depletion appears to have occurred during deposition of basal M1d, upper M6a, and M5a. Oxygen depletion is not always correlated with productivity, so other processes may be involved in its development.

Ti/Al is elevated above the 0.04 threshold throughout the logged area at Tawanui, but is generally higher pre-M1e (Fig. 7.14g). There is a gradual decrease in Ti/Al through M1c leading into the Cretaceous-Tertiary boundary, a sharp increase

through the boundary, and gradually decreasing but fluctuating values through M4 into M2c. The values spike at the base and top of M1d, then decrease in M6a and M5a. Ti/Al remains unchanged between M5a and basal M1e, and there is little variation through most of M1e. There is a slight increase mid M1e associated with low Ba[exc] productivity values (Fig. 7.14b, g), and a positive excursion in the vicinity of the Paleocene-Eocene boundary. The Ti/Al spikes may indicate increased offshore wind strength, invigorated currents, and/or sediment starvation. In some cases the Ti/Al values are negatively correlated with TRG, suggesting sediment starvation as the cause in those cases.

The glaucony proxy shows Fe[ef] spikes through M1c, at the Cretaceous-Tertiary boundary, and the base of M1d, and an increasing Fe[ef] trend through M1d, a large increase in M6a and M5a, and a small spike in the vicinity of the Paleocene-Eocene boundary (Fig. 7.14h). K[ef] values show definite covariance with Fe[ef] at the base of M1d and through M6a and M5a and it is likely that this signifies an increase in glaucony, which is not unexpected for M6a and M5a which are obviously rich in glaucony in hand specimen. For the Fe[ef] spikes of small amplitude it is difficult to determine if the very small deviations in K[ef] are associated with glaucony content or normal slight deviations associated with analytical background "noise". Field and petrographic data tend to support a glaucony relationship for all the trends except perhaps for some of those in M1c.

TRG remains relatively unchanged through M1c, M4, and M2c apart from decreases through the middle of M1c and at the Cretaceous-Tertiary boundary (Fig. 7.14i). There is a decrease from M2c into M1d, followed by an immediate and sharp increase and a more gradual fluctuating decrease through the rest of M1d. There is relatively little variation through M6a and M5a. The majority of M1e generally has higher TRG than the underlying lithofacies and there is an initial increase in TRG values at its base from M5a. The remainder of the facies shows little variation apart from a positive excursion in the vicinity of the Paleocene-Eocene boundary followed by a gradual decrease.

The average percent organic carbon appears to decrease slightly from the centre of M4 to upper M4, and remains unchanged through M2c and basalmost M1d (Fig.

7.14j). The values then fluctuate through M1d. There is a gradual increase in average percent of organic carbon values up through the M6a and into M5a. Values decrease from M5a to M1e.

The M6a and M5a succession

Closer examination of the succession leading into, through, and out of M6a and M5a is given in this section because these lithofacies are suspected to represent deposition during a time of climate change in the late Paleocene. Fig. 7.15 presents the results for this portion of the section, which includes M2c, M1d, M6a, M5a, and the base of M1e.

Based on the productivity proxies there generally appears to be a gradual increase in calcareous productivity up through M1d, with a collapse through M6a and M5a, followed by a slight increase up into M1e (Fig. 7.15b, c, d). Siliceous productivity seems to remain relatively constant through M1d then increases slightly in M6a and M5a, before decreasing into M1e.

P[ef] (sea water nutrient level) appears to follow the same general trends as calcareous productivity, but is also high at the top of M6a and in M5a when siliceous productivity is relatively high (Fig. 7.15d, e).

The Mo proxy shows suboxic depositional conditions at the base of M1d and in the upper part of M6a (Fig. 7.15f). In M5a suboxic to Mo-limited and intermittently euxinic conditions existed during deposition of the lithofacies.

Ti/Al is relatively high through M1d and peaks near the lithofacies upper contact (Fig. 7.15g). The peak is associated with the prominent burrowed horizon that occurs in the upper part of M1d (Fig. 7.6D, F). Ti/Al values decrease after the spike, then increase slightly into basal M6a. Ti/Al has a generally decreasing trend through M6a and M5a, apart from a slight increase in uppermost M6a. M5a Ti/Al values are the lowest for the entire section and remain low in basal M1e.

Covariance between Fe[ef] and K[ef] in the glaucony proxy indicate increased glaucony contents at the base of M1d, the base of M6a, and M5a (Fig. 7.15h).

There is a slight decrease in glaucony in uppermost M6a but relative to the majority of the section the values are still very high. Glaucony contents decrease in M1e.

TRG shows limited variation through this part of the succession (Fig. 7.15i). Initially it increases from a low at the base of M1d, to create a broad peak that corresponds with an area with a low degree of, or no, burrowing in the outcrop. From this peak there is a general decline in TRG through the rest of M1d, M6a, and M5a. TRG increases in M1e.

Percent organic carbon values fluctuate in M1d and the peaks and troughs do not appear to co-vary with any other proxies (Fig. 7.15j). Values then decrease into the base of M6a, followed by a gradual increase up through the lithofacies and into M5a where the highest values for the Tawanui section are recorded. This corresponds with high Mo values and possibly high productivity. Values decrease from M5a to M1e.

7.4.2 Palynofacies

Entire section

The palynofacies proxies used in this study and their significance to paleodepositional environments are outlined in Chapter 3 (Section 3.3.2). The percent palynomorphs fluctuates through the section (Fig. 7.14k). Peaks occur at the Cretaceous-Tertiary boundary, in M2c, and near the base of M1d. Lower values occur in uppermost M1c, through the centre of M4, at the base of M1d, and through upper M1d and M6a and M5a. The proxy appears for the most part to have a negative correlation to the Mo proxy, but some localised exceptions exist.

The percent amorphous organic matter (AOM) proxy suggests that the shoreline becomes more distal through the lower portion of M4, coincident with decreasing TRG and slightly increased siliceous productivity (Fig. 7.14l). The shoreline begins becoming more proximal through the upper half of M4 and in M2c in association with increasing TRG and decreasing siliceous productivity. Fluctuations in the proxy are larger through M1d, M6a, and M5a, with the highest

and lowest values recorded through these lithofacies. The details of these fluctuations are discussed below in "The M6a and M5a succession".

The percent phytoclasts, log black:brown phytoclasts, log marine algae/sporomorphs, and percent dinoflagellate cysts show a different trend through M4 and M2c compared with the percent AOM. The former group suggest that the shoreline becomes more distal across the Cretaceous-Tertiary boundary, then becomes more proximal through the lower half of M4 with more distal conditions developing through the upper half of the lithofacies (Fig. 7.14m-p). The transition between M4 and M2c records the shoreline becoming more distal. However, like the percent AOM poxy, the percent phytoclasts and log black:brown phytoclasts proxies also show an increased amplitude in fluctuations through M1d, M6a, and M5a.

The M6a and M5a succession

As stated in Section 7.4, M6a and M5a are of particular interest because they may record a climate episode in the late Paleocene. Palynofacies trends leading into, through, and out of these lithofacies are described in this section.

Percent AOM and percent phytoclasts (Fig. 7.15l, m) suggest that between M2c and the base of M1d the shore line becomes more distal, coincident with decreasing TRG (Fig. 7.15i), increasing glaucony (Fig. 7.15h), increasing Ti/Al (Fig. 7.15g), suboxia (Fig. 7.15f), and an increase in calcareous productivity (Fig. 7.15d). Log black:brown phytoclasts show a weak trend towards either more distal conditions or proximal turbulence (Fig. 7.15n). Log marine algae/sporomorphs and dinoflagellate cysts appear to show a shift to more proximal conditions through the interval (Fig. 7.15o, p).

Percent AOM and phytoclasts (Fig. 7.15l, m) suggest proximal conditions near the base of M1d, coinciding with increased TRG (Fig. 7.15i) and low or no burrowing. Log black:brown phytoclasts, log marine algae/sporomorphs, and percent dinoflagellate cysts indicate distal conditions through the same interval (Fig. 7.15n-p). All the palynofacies proxies generally indicate distal conditions in the upper portion of M1d (Fig. 7.15l-p), coincident with decreasing TRG (Fig. 7.15i)

and an increase in burrowing seen in outcrop. Most of the proxies indicate more proximal conditions near the upper contact of M1d (Fig. 7.15l-p), occurring in association with the upper part of a burrowed horizon.

Percent AOM and phytoclasts suggest a shift to more distal conditions across the M1d-M6a contact and into lower M6a, coincident with burrowing and an increase in glaucony (Fig. 7.15l, m). However, Log black:brown phytoclasts, log marine algae/sporomorphs, and percent dinoflagellate cysts indicate a shift to more proximal conditions over the same interval (Fig. 7.15n-p). On the basis of the field observations of burrowing and abundant glaucony the percent AOM and phytoclast suggestion of a shift to more distal conditions is favoured here. All the palynofacies proxies indicate that the shore line becomes more proximal through the upper half of M6a and in M5a. This coincides with a slight increase then decrease in TRG (Fig. 7.15i), an increase in oxygen deficiency (Fig. 7.15f), increased seawater nutrient levels (Fig. 7.15e), increasing average percent organic carbon (Fig. 7.15j), and decreasing Ti/Al (Fig. 7.15g).

All the palynofacies proxies suggest a shift to more distal conditions in M1e (Fig. 7.15l-p).

7.4.3 Stable isotopes

Stable carbonate carbon isotope values increase in the lead up to the Cretaceous-Tertiary boundary (Fig. 7.14a). The higher values are retained through most of M1d then decrease slightly in M6a. They are slightly higher in M1e.

Organic carbon values display little variation through the upper half of M4 and in M2c (Fig. 7.14a). They increase into M1d and continue to increase up through M1d, M6a, and M5a. The highest values for Tawanui occur in M5a, above which the values decrease in M1e.

Stable oxygen isotope trends are similar to stable carbonate isotope trends so may be diagenically altered (Fig. 7.16). However, there is a significant negative trend in oxygen isotope values at the top of M1c and into basal M6a which would indicate warming when associated with unaltered sediment. This trend coincides

with increased burrowing, slightly reduced terrigenous input (TRG) and high glaucony contents, which are characteristics associated with transgressions.

Figure 7.14: Variations for the entire Tawanui section in carbon isotopes (a), ocean surface water productivity proxies (b, c, d, j), proxies for seawater nutrient availability (e), bottom water oxygen levels (f, j), aeolian sediment input (g), glaucony (h), and terrigenous sediment input (i), and various palynofacies proxies for shoreline proximity to the site of deposition (k – q).

Figure 7.15: Enlargement of Fig. 7.14 to focus on vaiations for M2c, M1d, M6a, M5a, and M1e lithofacies at the Tawanui section in carbon isotopes (a), ocean surface water productivity proxies (b, c, d, j), proxies for seawater nutrient availability (e), bottom water oxygen levels (f, j), aeolian sediment input (g), glaucony (h), and terrigenous sediment input (i), and various palynofacies proxies for shoreline proximity to the site of deposition (k – q).

Fig. 7.14

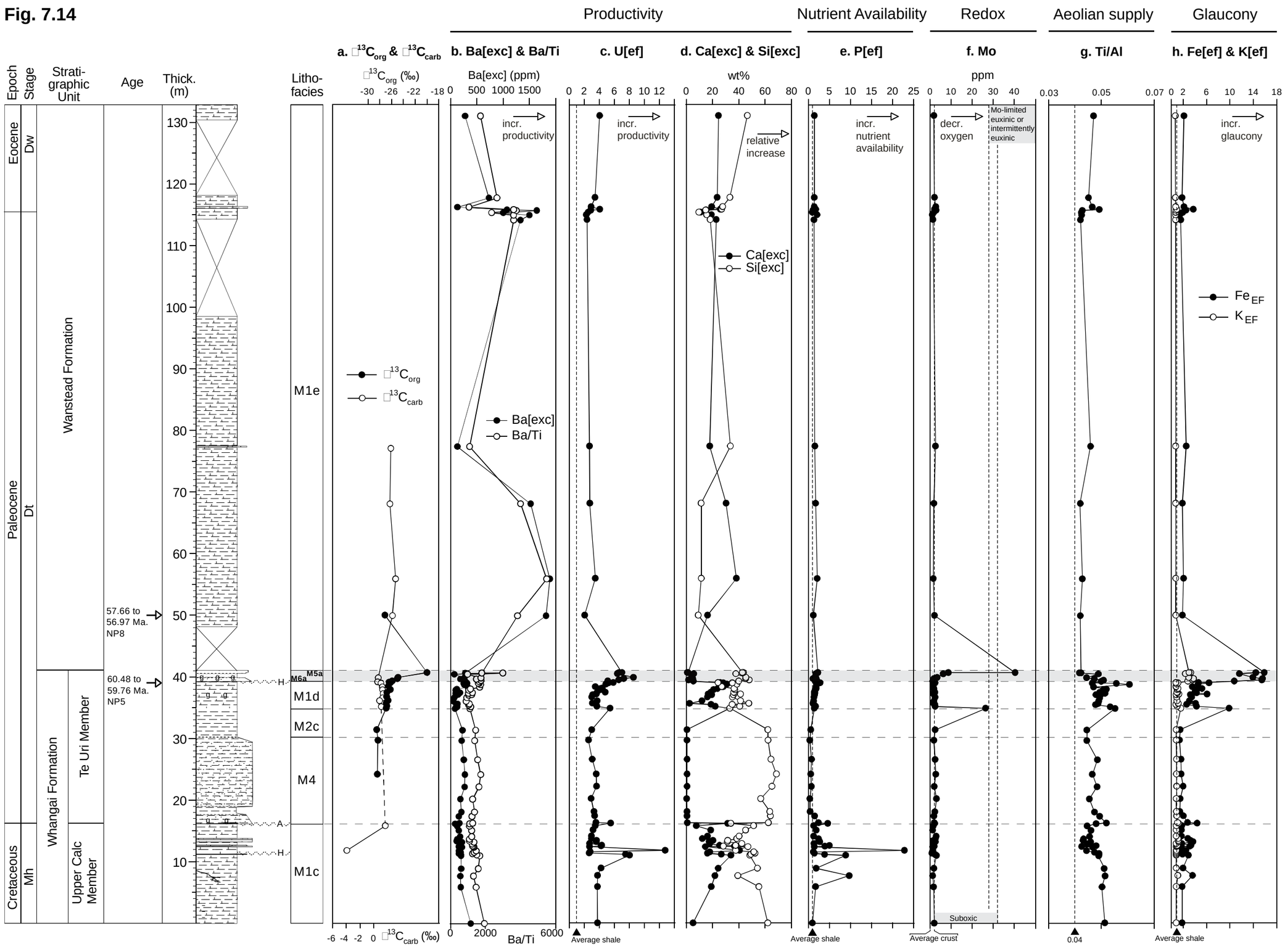
Productivity
Nutrient Availability
Redox
Aeolian supply
Glaucony
Epoch
Stage
Strati-graphic Unit
Age
Thick. (m)
Litho-facies
a. δ13Corg & δ13Ccarb
b. Ba[exc] & Ba/Ti
c. U[ef]
d. Ca[exc] & Si[exc]
e. P[ef]
f. Mo
g. Ti/Al
h. Fe[ef] & K[ef]
Eocene
Paleocene
Cretaceous
Dw
Dt
Mh
Wanstead Formation
Whangai Formation
Te Uri Member
Upper Calc Member
57.66 to 56.97 Ma. NP8
60.48 to 59.76 Ma. NP5
M1e
M5a
M6a
M1d
M2c
M4
M1c
δ13Corg (‰)
Ba[exc] (ppm)
wt%
ppm
incr. productivity
relative increase
Ca[exc]
Si[exc]
incr. nutrient availability
decr. oxygen
Mo-limited euxinic or intermittently euxinic
incr. glaucony
Fe EF
K EF
Ba[exc]
Ba/Ti
δ13Ccarb
Ba/Ti
Average shale
Average shale
Average crust
Suboxic
0.04
Average shale

Fig. 7.14 cont.

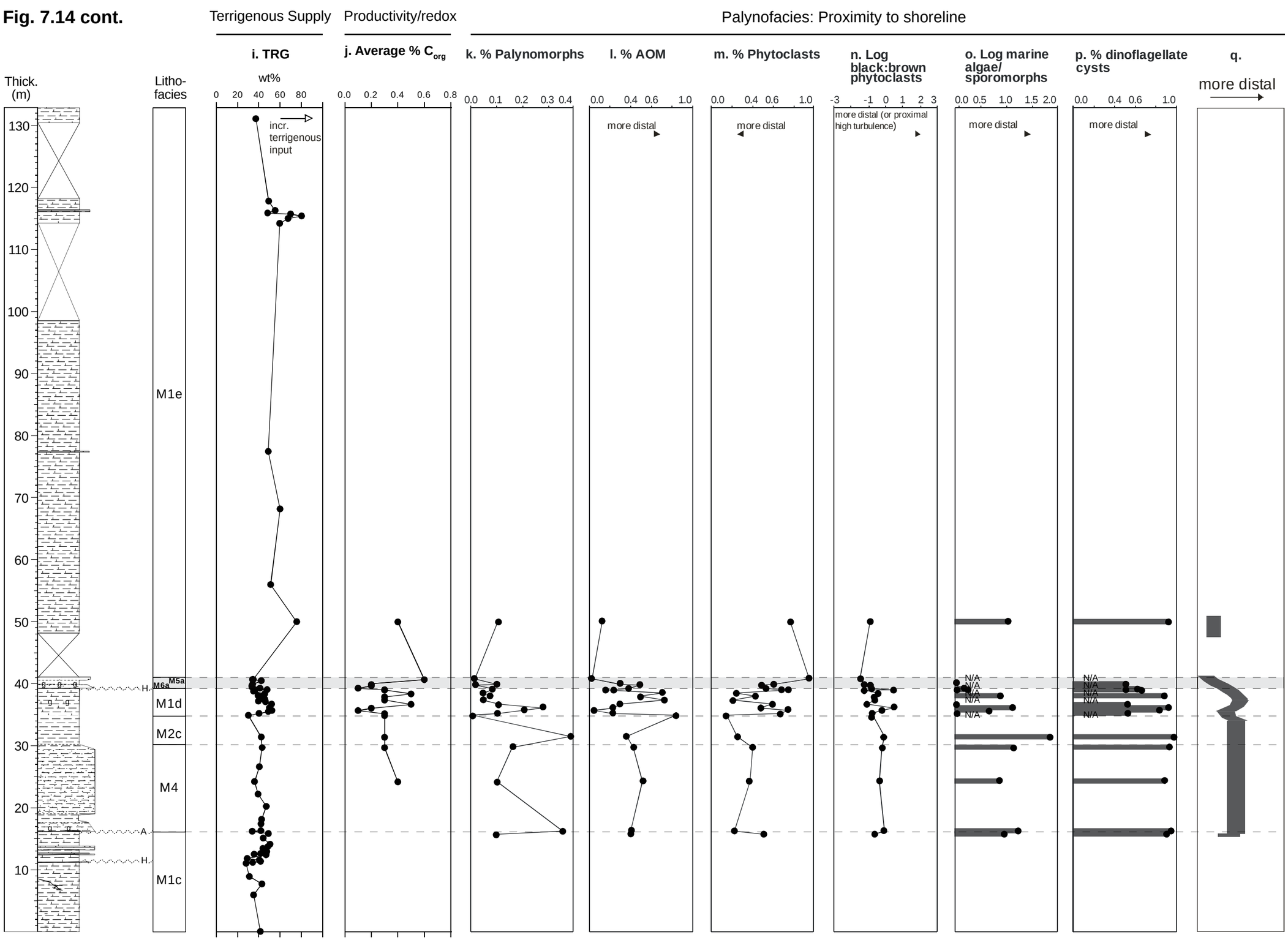
Terrigenous Supply
Productivity/redox
Palynofacies: Proximity to shoreline
Thick. (m)
Litho-facies
i. TRG
wt%
0 20 40 60 80
incr. terrigenous input
j. Average % C org
0.0 0.2 0.4 0.6 0.8
k. % Palynomorphs
0.0 0.1 0.2 0.3 0.4
l. % AOM
0.0 0.4 0.6 1.0
more distal
m. % Phytoclasts
0.0 0.4 0.6 1.0
more distal
n. Log black:brown phytoclasts
-3 -1 0 1 2 3
more distal (or proximal high turbulence)
o. Log marine algae/ sporomorphs
0.0 0.5 1.0 1.5 2.0
more distal
p. % dinoflagellate cysts
0.0 0.4 0.6 1.0
more distal
q.
more distal
130
120
110
100
90
80
70
60
50
40
30
20
10
M1e
M5a
M6a
M1d
M2c
M4
M1c
H
A
H
N/A

Fig. 7.15

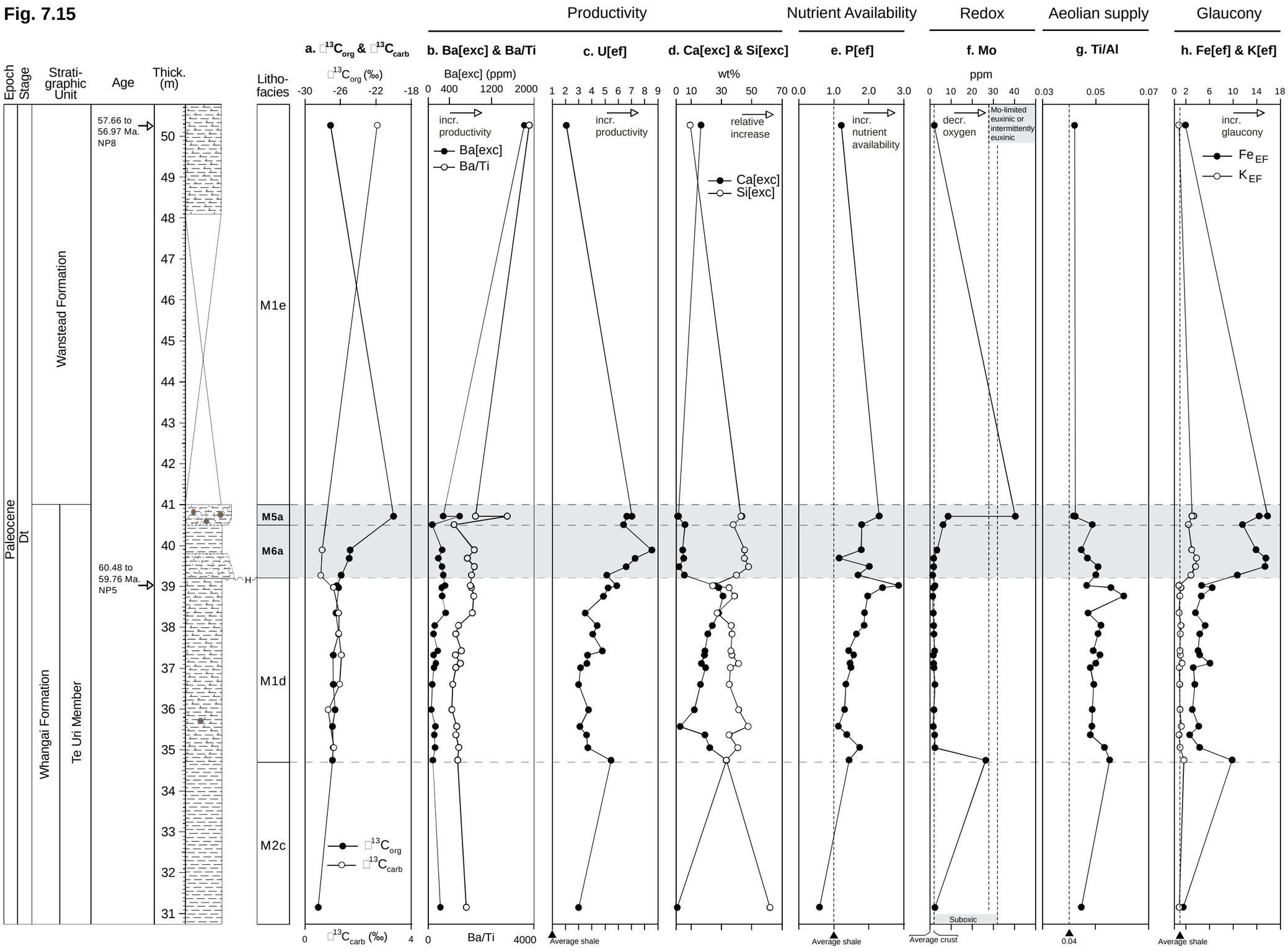
Productivity
Nutrient Availability
Redox
Aeolian supply
Glaucony
Epoch
Stage
Strati-graphic Unit
Age
Thick. (m)
Litho-facies
a. δ13Corg & δ13Ccarb
b. Ba[exc] & Ba/Ti
c. U[ef]
d. Ca[exc] & Si[exc]
e. P[ef]
f. Mo
g. Ti/Al
h. Fe[ef] & K[ef]
δ13Corg (‰)
Ba[exc] (ppm)
wt%
ppm
Paleocene
Dt
Wanstead Formation
Whangai Formation
Te Uri Member
57.66 to 56.97 Ma. NP8
60.48 to 59.76 Ma. NP5
M1e
M5a
M6a
M1d
M2c
incr. productivity
Ba[exc]
Ba/Ti
relative increase
Ca[exc]
Si[exc]
incr. nutrient availability
decr. oxygen
Mo-limited euxinic or intermittently euxinic
incr. glaucony
FeEF
KEF
δ13Corg
δ13Ccarb
Suboxic
Average shale
Average crust
0.04

Fig. 7.15 cont.

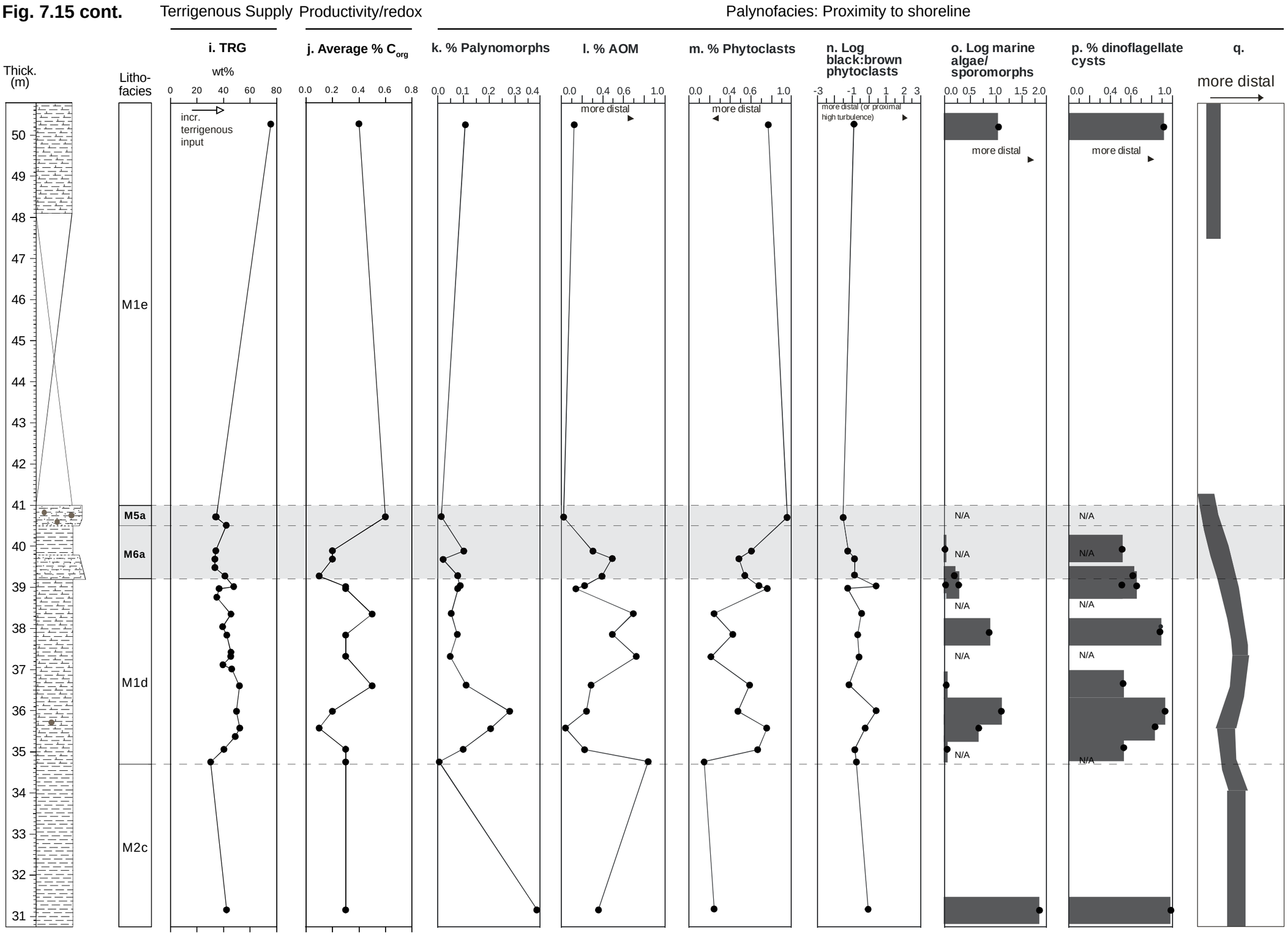
Terrigenous Supply
Productivity/redox
Palynofacies: Proximity to shoreline
Thick. (m)
Litho-facies
i. TRG
wt%
0 20 40 60 80
incr. terrigenous input
j. Average % C org
0.0 0.2 0.4 0.6 0.8
k. % Palynomorphs
0.0 0.1 0.2 0.3 0.4
l. % AOM
0.0 0.4 0.6 1.0
more distal
m. % Phytoclasts
0.0 0.4 0.6 1.0
more distal
n. Log black:brown phytoclasts
-3 -1 0 1 2 3
more distal (or proximal high turbulence)
o. Log marine algae/ sporomorphs
0.0 0.5 1.0 1.5 2.0
more distal
p. % dinoflagellate cysts
0.0 0.4 0.6 1.0
more distal
q.
more distal
50
49
48
47
46
45
44
43
42
41
40
39
38
37
36
35
34
33
32
31
M1e
M5a
M6a
M1d
M2c
N/A

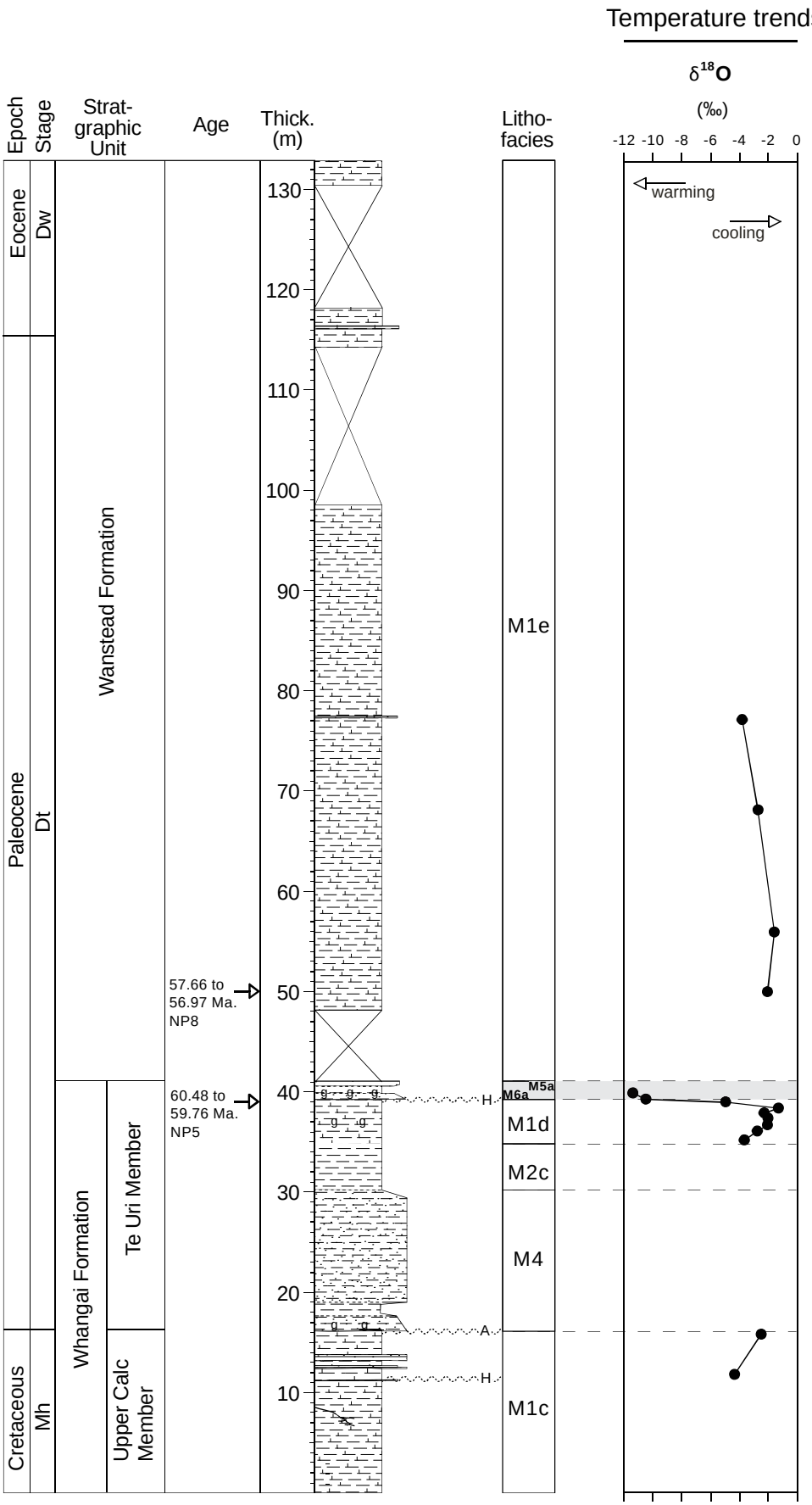

Figure 7.16: Variation in stable oxygen isotopes of the carbonate fraction through the entire logged section at Tawanui.

7.4.4 Grain size results

Laser grain size data were obtained for M1c, M6a, M5a, and basal M1d (Fig. 7.17A). These show reverse grading through M6a and M5a. Petrographic data demonstrate normal grading of the maximum siliciclastic and glaucony grain sizes (Fig. 7.18B).

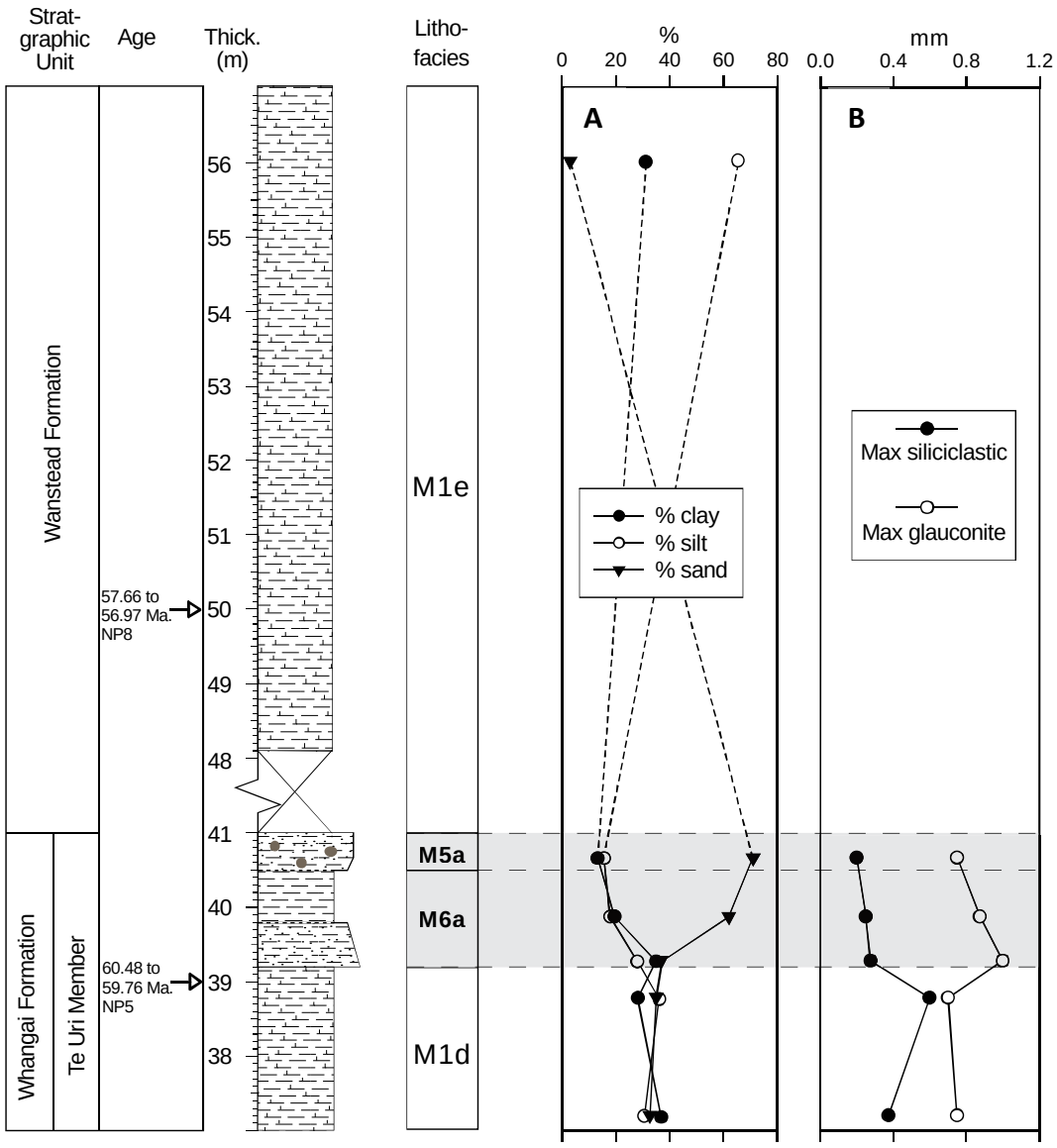

Figure 7.17: Variation in grain size through M1d, M6a, M5a, and M1d lithofacies at the Tawanui section determined using laser diffraction particle size analysis (A), and petrography (B).

Chapter 8
LOWER MANGAHOUANGA STREAM

8.1 Location

The lower Mangahouanga Stream section is located in northern Hawke's Bay, about 20 km southwest of Lake Waikaremoana (Fig. 2.2 and 8.1). The section

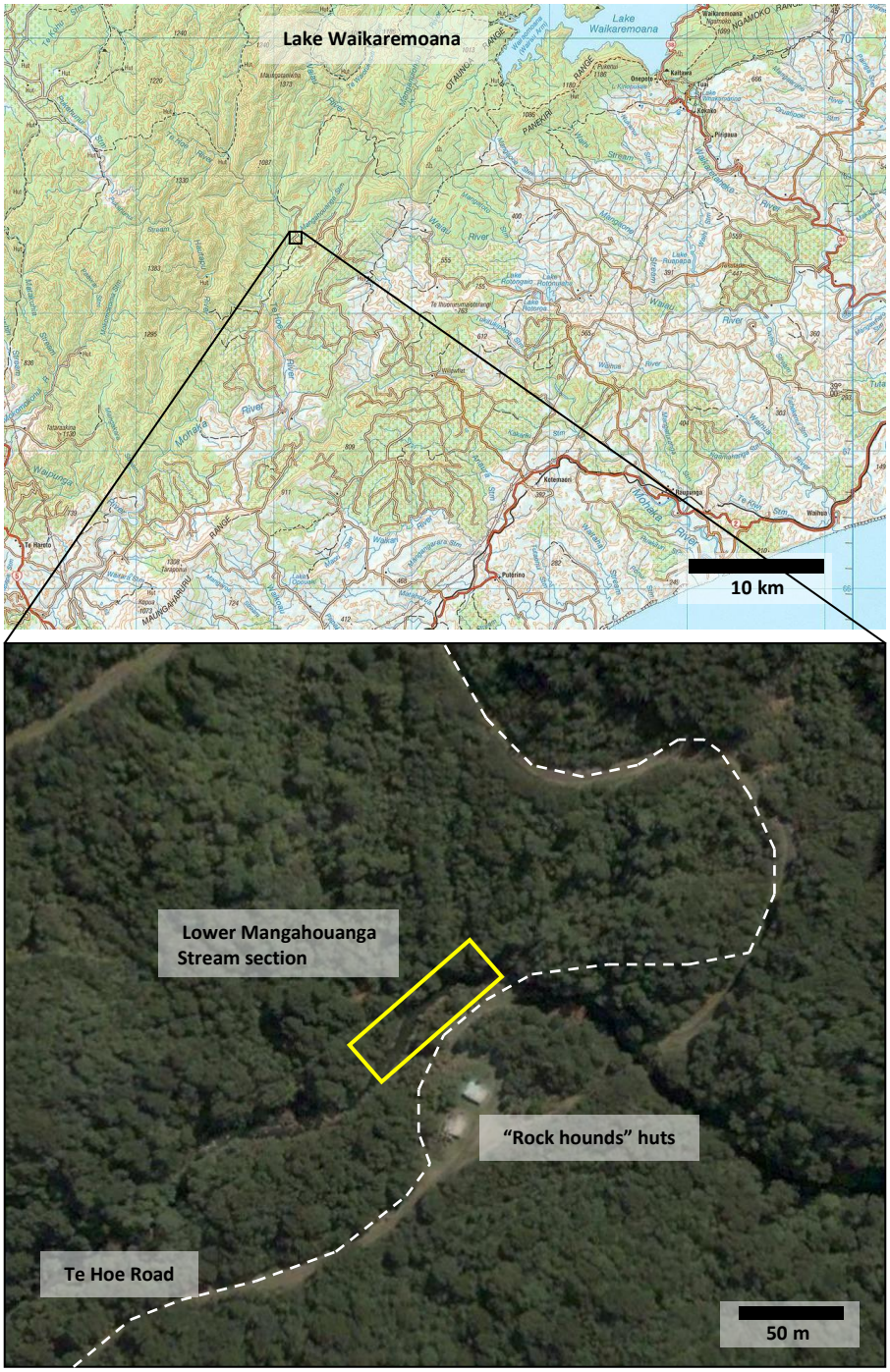

Figure 8.1: Location of the lower Mangahouanga Stream section in relation to Lake Waikaremoana and, at a finer scale, the "Rock hounds" huts and Te Hoe Road.

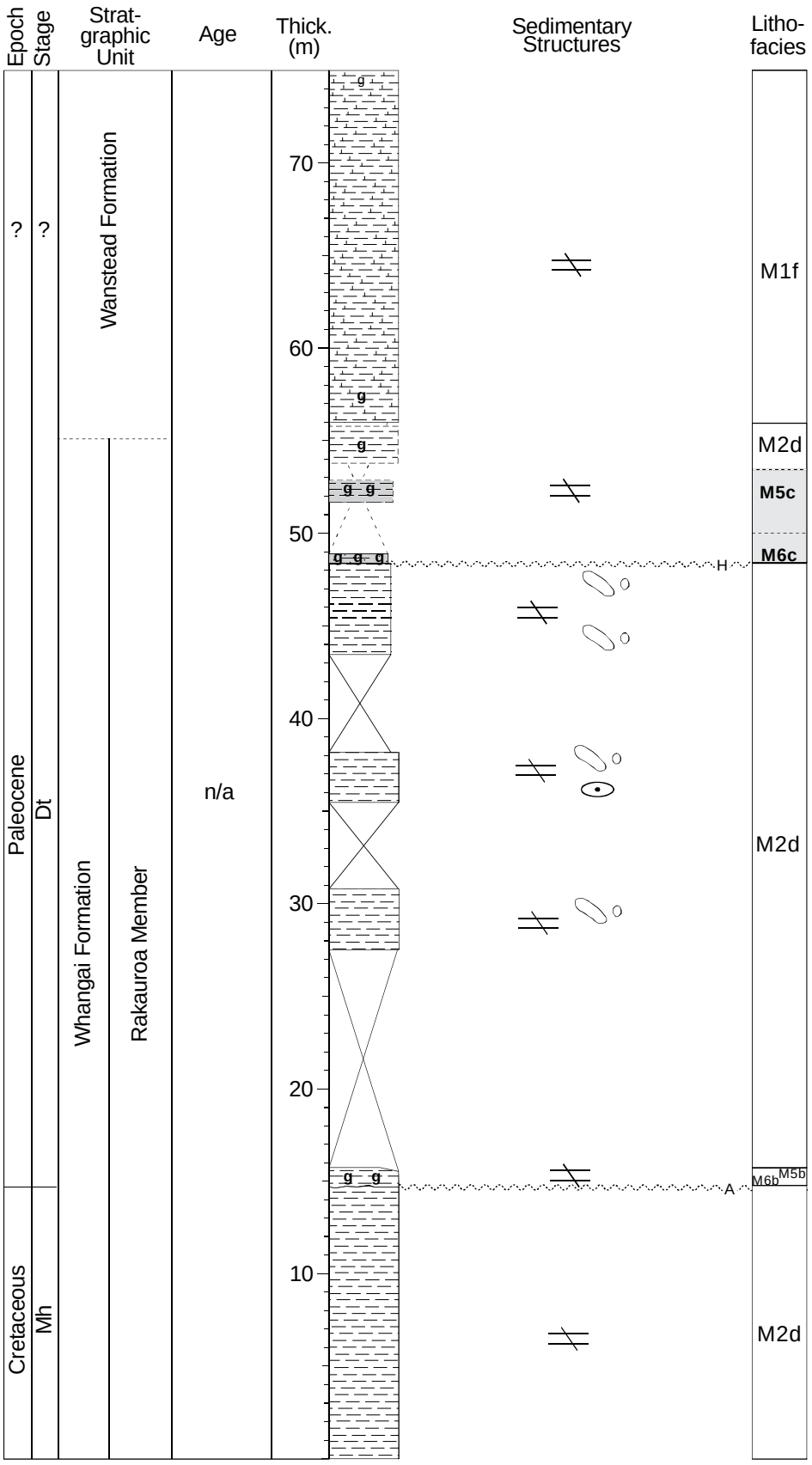

Figure 8.2: Stratigraphic column and lithofacies for the lower Mangahouanga Stream section. Stratigraphic nomenclature and New Zealand stages shown are sourced from unpublished stratigraphic columns produced by P. Moore in 1982, and from C. Hollis (pers. comm. 2010). Graphic log lithology and sedimentary structures symbols are defined in Appendix B.

studied crops out in the lower portion of the Mangahouanga Stream, a tributary of the Te Hoe River. The portion of the stream logged is close to Te Hoe Road and near the "Rock hounds" huts (Fig. 8.1). The section is mostly moderately to poorly exposed, although exposure improves during periods of low stream water level. During periods of high water levels it is likely that much of the section would be unexposed and inaccessible.

8.2 Facies characteristics

The sedimentary succession logged at the lower Mangahouanga Stream section is presented in Fig. 8.2. The lithostratigraphic nomenclature and New Zealand stages shown in Fig. 8.2 are sourced from unpublished stratigraphic columns produced by P. Moore in 1982, and from C. Hollis (pers. comm. 2010).

As mentioned above, the lower Mangahouanga Stream section was only moderately to poorly exposed at the time of logging. Consequently description of lithofacies at this section is less comprehensive compared to those from other sections investigated in this study. Petrographic and mineralogical analyses have not been undertaken due to time constraints.

The logged strata at the lower Mangahouanga Stream section consist of c. 56 m of non-calcareous mudstone with two glaucony rich intervals (Rakauroa Member of the Whangai Formation) conformably overlain by calcareous mudstone (Wanstead Formation). Six lithofacies have been identified in the succession (Fig. 8.2) and their field lithology and contacts are described in the following sections but first this studies textural classification scheme is briefly revisited to remind the reader of issues relating to classification of lithologies dominated by glaucony (see Section 3.4.1).

8.2.1 Glaucony and rock classification

As noted in Section 7.2.1, in this study glaucony rich units are named using their clastic grain size rather than their glaucony grain size so as to better reflect paleoshoreline proximity to the rocks depositional area in the rocks name. However, this classification system poorly describes the in-field character of lithologies dominated by glaucony, and consequently images presented in this

chapter of samples with high proportions of sand sized glaucony grains, that normally would be classified as sandstones, are often named glauconitic mudstones due to the classification scheme excluding the grain size of the glaucony portion of the rock. To aid the reader, where a glaucony dominated lithology is referred to in the text using this "new" classification scheme, the approximate percent glaucony and its conventional name are also given in square brackets (e.g. [c. 80% glc – muddy greensand]).

See section 3.4.1 for further information on this topic.

8.2.2 Siliceous mudstone lithofacies (M2d)

Variations of the M2 lithofacies occur at four of the studied sections in the East Coast Basin (Table 4.1). Description of the lower Mangahouanga Stream variety (M2d) follows.

M2d

Field lithology

The M2d lithofacies generally consists of medium grey or brown-grey (Fig. 8.3C, D), moderately to poorly indurated, massive, non-calcareous mudstone with occasional nodules and infrequent burrows sparsely infilled with glaucony. The rock weathers to a red brown, homogenous surface (Fig. 8.3A, B) and occasionally has a light dusting of yellow powder. Two glauconitic intervals occur within M2d and have been defined in this study as muddy greensand (M6b, c) and glauconitic mudstone (M5b, c) lithofacies (see Section 4.3 for use of the lithofacies name "muddy greensand". These lithofacies are described below in Sections 8.2.2 and 8.2.3. The clay content in the M2d mudstones appears to increase in the 4 m (at least) interval leading up towards the M2d-M6c contact (Fig. 8.3A, D).

Contacts

Upper and lower contacts between the M2d lithofacies and the muddy greensand and glauconitic mudstone lithofacies are described below in Sections 8.2.2 and 8.2.3. When M2d is considered as a continuous unit, with the contacts associated with the glaucony rich lithofacies ignored, the lower contact of M2d is not within

Figure 8.3: Features of the siliceous mudstone lithofacies (M2d) at the lower Mangahouanga Stream section. A = Outcrop of M2d with and M6c with more clay rich interval of M2d labeled; B = typical character of M2d in outcrop; C = an unweathered example of an M2d mudstone; D = example of a more clay rich mudstone from the upper part of M2d, nearing the M2d-M6c contact (mudstone has been encased in resin); E = contact area between M2d and M1f showing a gradual decline in glaucony.

the logged section and its upper contact with the M1f lithofacies is gradational. The upper contact appears to consist of a gradual decline in glaucony over c. 0.6 m (Fig. 8.3E), followed by a shift from the non-calcareous mudstone of M2d to the calcareous mudstone of M1f. The upper contact is very poorly exposed in the logged section.

8.2.3 Muddy greensand lithofacies (M6b, M6c)

M6 is logged at two of the studied sections the East Coast Basin (Table 4.1). Two slight variations of the lithofacies occur at the lower Mangahouanga Stream section (M6a, M6b) and are described below.

M6b

Field lithology

M6b occurs immediately above the Cretaceous-Tertiary boundary and consists of green, poorly to well indurated, massive, highly glauconitic, non-calcareous mudstone [c. 70% glc – muddy greensand] (Fig. 8.4A, B).

Contacts

The lower contact of lithofacies M6b with underlying M2d mudstone corresponds with the Cretaceous-Tertiary boundary, and is sharp and appears to undulate slightly (Fig. 8.4B). The underlying mudstone possibly contains lined burrows (?*Palaeophycus*) up to c. 10 cm below the contact (Fig. 8.4C). There appears to be a thin layer of clay at the contact but this may be a weathering affect. The upper contact of M6b with M5b shows a gradual decline in glaucony.

M6c

Field lithology

The M6c lithofacies occurs c. 6 m below the base of the Wanstead Formation and is poorly exposed (Fig. 8.4E). It consists of brown-green-grey, moderately indurated, massive, highly glauconitic, non-calcareous mudstone [c. 70% glc - muddy greensand] (Fig. 8.4D). In outcrop M6c appears to be finer grained than the underlying M2d mudstone and judging from its texture may have a higher clay content.

Contacts

Leading up into the lower contact of the M6c lithofacies the underlying siliceous mudstone of M2d becomes blue-grey and burrows infilled with glaucony are more prevalent (Fig. 8.4F). The lower contact of M6c appears to be sharp. The upper contact of M6c with M5c is not exposed.

8.2.4 Glauconitic mudstone lithofacies (M5b, c)

M5 occurs at three of the study sites in the East Coast Basin (Table 4.1). At the Lower Mangahouanga Stream section there are two variants of the lithofacies (M5b, M5c) and the characteristics of each are described below.

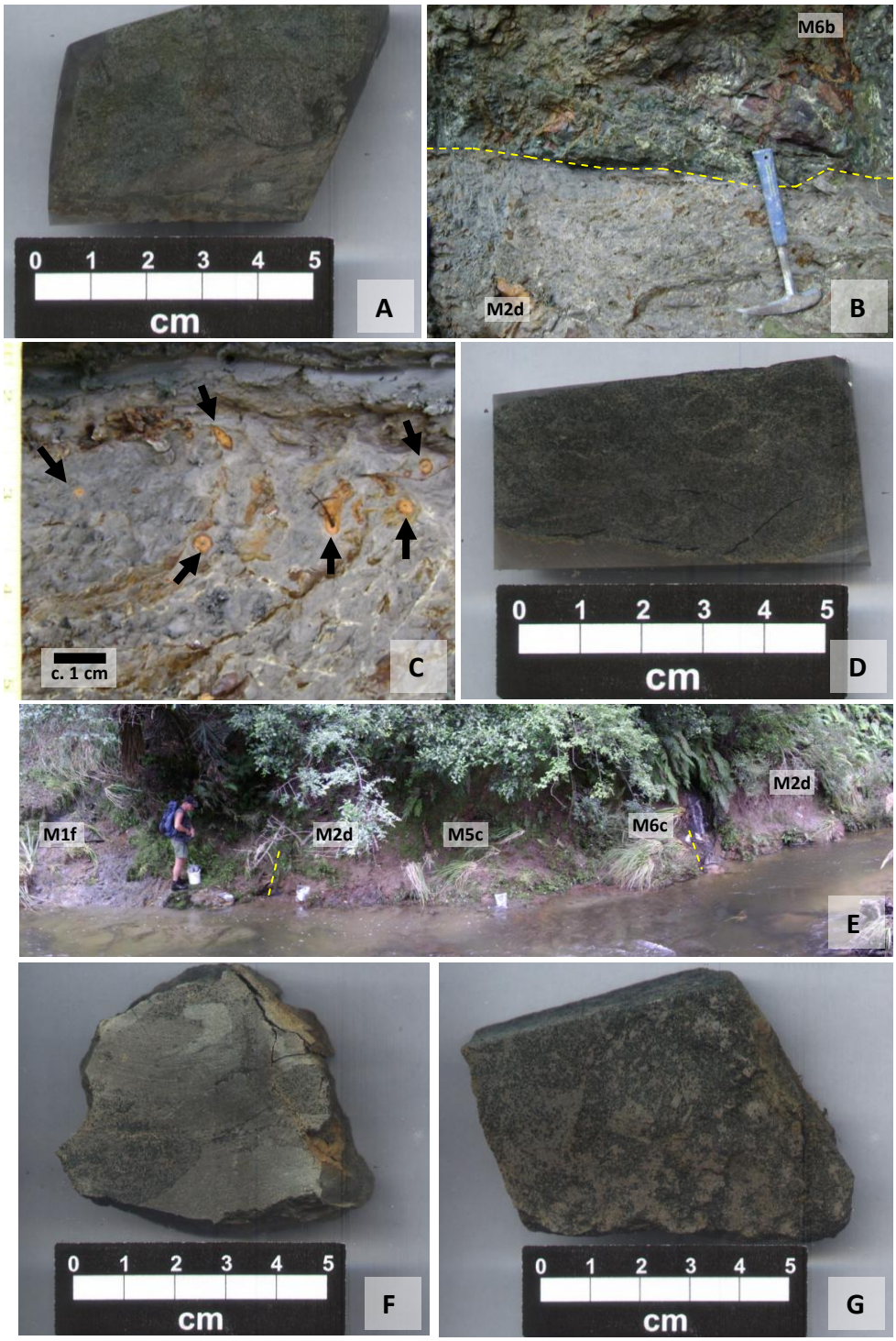

Figure 8.4: Characteristics of the muddy greensand (M6b, M6c) and glauconitic mudstone (M5c) lithofacies at the lower Mangahouanga Stream section. A = An unweathered example of the highly glauconitic mudstone [c. 70% glc – muddy greensand] of M6b (sediment is in-cased in resin); B = sharp and possibly slightly undulating contact between M2d and M6b (Cretaceous-Tertiary boundary); C = possible burrows (?*Palaeophycus*) in mudstone underlying M2d-M6b contact (indicated by arrows); D = an unweathered example of the highly glauconitic mudstone [c. 70% glc – muddy greensand] of M6c (sediment is encased in resin); E = position of the poorly exposed M6c and M5c lithofacies relative to M2d and M1f; F = burrows in the mudstone underlying the M2d-M6c contact; G = unweathered example of M5c.

M5b

M5b consists of grey-brown, moderately to well indurated, massive with burrows, very slightly glauconitic, non-calcareous mudstone. The lithofacies appears to be a transitional phase between the glaucony rich M6b and glaucony poor M2d. It weathers to a red-green fritter or blocky surface.

Contacts

Both the upper and lower contacts of the lithofacies appear to be gradational and show an upwards decrease in glaucony content of the mudstone.

M5c

The M5c lithofacies is poorly exposed at the lower Mangahouanga Stream section but appears to consist of brown-green-grey, moderately indurated, massive, moderately glauconitic, non-calcareous mudstone (Fig. 8.4G). It weathers to a red-brown surface.

Contacts

Both the upper and lower contacts of the lithofacies are not exposed.

8.2.5 Calcareous mudstone lithofacies (M1f)

M1 was logged at most of the East Coast Basin study sections (Table 4.1). The features of the lower Mangahouanga Stream variety of this lithofacies (M1f) are given below.

M1f

Field lithology

The M1f lithofacies consists of grey or green-grey, moderately to moderately well indurated, massive, mainly calcareous mudstone (Fig. 8.5). The basal c. 2 m of the lithofacies is non-calcareous, with the majority of the logged succession calcareous.

Contacts

The lower contact of M1f was discussed previously when describing the upper

contact of the M2d lithofacies (Section 8.2.1). The lithofacies upper contact is not within the logged area.

Figure 8.5: Example of a mudstone from the M1f lithofacies.

8.3 Geochemistry and palynofacies results

Geochemical and palynofacies proxies used in this study were introduced in Chapter 3 (Sections 3.3.2 to 3.3.4) and are presented here for the Lower Mangahouanga Stream section. Fig. 8.6 presents the up section trends for organic carbon stable isotopes (a) and elemental proxies for ocean surface water biological productivity (b, c, d, j), seawater nutrient availability (e), bottom water oxygen levels (f), aeolian sediment supply (g), glaucony (h), and terrigenous sediment supply (i). Up section variations in ocean surface water biological productivity and bottom water oxygen levels are also indicated by the average percent organic carbon plot (j). Included in Fig. 8.6 are palynofacies proxies for the depositional areas proximity to the paleoshoreline (k-q). Preliminary interpretations of geochemical and palynofacies trends are offered in this section, even though this is a results chapter, to aid later interpretations (see Chapter 10).

8.3.1 Elemental geochemistry and organic carbon proxies

In this section the results for elemental geochemistry and organic carbon proxies (Fig. 8.6b-j) are described. However, first the ocean surface water biological productivity proxies are tested for biogenic association using the methods outlined in Chapter 3. This is done in order to assess their reliability as paleoproductivity indicators for the logged area of the Angora Road section. If a productivity proxy is found to have no biogenic association its trends will not be described in any detail.

Testing for productivity proxy biogenic association

Ba[exc] mostly co-varies with Ba/Ti through the entire section, with the exception of at the lower contact of the M6b lithofacies (at the Cretaceous-Tertiary boundary) and in M5c (Fig. 8.6b). Ba[exc] also appears to have poor correlation with TRG (Fig. 8.6i) which, combined with Ba/Ti covariance, suggests that Ba[exc] has a biogenic association. However, Mo and U[ef] values may indicate varying degrees of suboxic oxygen deficiency at the time of deposition of the lithofacies below M6c, and oxic to very slightly suboxic conditions during deposition of lithofacies above M6c (Fig. 8.6c, f). Consequently, Ba[exc] values may be unreliable through the lower parts of the section. Ba[exc] values are depressed to negative values throughout the Lower Mangahouanga section, possibly reflecting oxygen deficient bottom waters (see Section 3.3.4), and/or a combination of anomalously low Ba values and high TiO_2 values for the section (Appendix M, and see Ba[exc] equation – Section 3.3.4). Low Ba[exc] values can be caused by reduced Ba preservation in sediments due to suboxic conditions (see Section 3.3.4). However, Mo values suggest the upper portion of the section was deposited under oxygenated conditions and these sediments also displays negative Ba[exc] values. It is more likely that the negative values reflect a combination of anomalously low oceanic productivity and high TiO_2 concentrations compared to regional levels. TRG levels for the section are some of the highest of all the study sections – a greater input of terrestrial TiO_2 at the lower Mangahouanga Section is possibly the source of the extra TiO_2.

U[ef] (Fig. 8.6c) appears to broadly covary with Si[exc] (Fig. 8.6d) and P[ef] (Fig. 8.6e) suggesting it is associated with siliceous biogenic productivity. U[ef] is therefore used as the primary productivity indicator through the section, with Ba[exc] also used through the upper portion of the section. Ba values for the Lower Mangahouanga Stream section are comparable to Ba values for the lower half of the Tawanui section (Digital Appendix M). However, at the Lower Mangahouanga Stream section Ba[exc] values are negative (Fig. 8.6b) whereas at Tawanui Ba[exc] values are positive (Fig. 7.14). The difference may be due to much higher TiO_2 values at Lower Mangahouanga Stream, compared with Tawanui (Digital Appendix M), depressing the Ba[exc] values.

Proxy results

The productivity proxies indicate a spike in siliceous productivity at the contact between M2d and M6b (Cretaceous-Tertiary boundary) and a second increase in siliceous productivity through M6c and M5c, with a subsequent decrease through the overlying M2d lithofacies (Fig. 8.6b-d). A spike in siliceous productivity c. 31 m above the base of the logged is not associated with an increase in U[ef], but is associated with a slight increase in Ba[exc].

Seawater nutrient levels spike at the contact between M2d and M6b (Cretaceous-Tertiary boundary), then decrease in the overlying M2d lithofacies (Fig. 8.6e). Values increase through M6c and M5c, and continue to increase through M1f. All increases in nutrient availability are associated with increased siliceous productivity, as indicated by U[ef] and Si[exc]. A Si[exc] spike c. 31 m above the base of the log is associated with a decrease in seawater nutrient levels (Fig. 8.6d, e).

Mo values suggest suboxic bottom water conditions in lithofacies below M6c (Fig. 8.6f). There is a sharp increase in values at the contact between M2d and M6b (Cretaceous-Tertiary boundary) followed by a broad increase peaking at c. 28 m above the base of the log in M2d. Subsequently, values decrease through the rest of the logged section and by M5c values are consistently oxic or very slightly suboxic. Trends in bottom water oxygen levels do not appear to co-vary with productivity or ocean water nutrient trends.

Ti/Al is slightly elevated above the 0.04 threshold throughout the section (Fig. 8.6g). Increases in Ti/Al values occur at the contact between M2d and M6b (Cretaceous-Tertiary boundary) and c. 31 m above the base of the log. The lower of the two increases is associated with increased siliceous productivity and the higher is associated with increased Si[exc] (Fig. 8.6d) and little change in other productivity proxies (Fig. 8.6b, c). A decrease in Ti/Al values occurs immediately below the M2d-M6c contact.

The glaucony proxy shows an increase in Fe[ef] and K[ef] at the contact between M2d and M6b (Cretaceous-Tertiary boundary) and through the M6c, M5c and overlying M2d lithofacies, which agrees with field observations (Fig. 8.6h).

There are decreases in TRG at the contact between M2d and M6b (Cretaceous-Tertiary boundary), c. 31 m above the base of the log in M2d, and immediately below and through the M6c and M5c lithofacies (Fig. 8.6i). Based on U[ef] and Si[exc] the decreases are associated with increased siliceous productivity, or increases in only Si[exc] (Fig. 8.6d.f). TRG values increase from M5c into the overlying M2d lithofacies.

Average percent organic carbon values broadly co-vary with Mo values and occasionally with TRG values, showing decreases at the M2d-M6b contact (Cretaceous-Tertiary boundary) and a broad trough through the majority of the section, centred on the M6c-M5c interval (Fig. 8.6j). An increase occurs c. 28 m above the base of the log and is associated with maximum oxygen deficiency for the section (Fig. 8.6f, j).

8.3.2 Palynofacies proxies

The palynofacies proxies used in this study and their significance to paleodepositional environments are outlined in Chapter 3 (Section 3.3.2). The percent palynomorphs proxy peaks at the contact between M2d and M6b (Cretaceous-Tertiary boundary), and through M6c, M5c, and overlying M2d (Fig. 8.6k).

The remaining palynofacies proxies (Fig. 8.6l-q) indicate that the shoreline becomes more distal through the M2d-M6b contact (Cretaceous-Tertiary boundary). This coincides with a reduction in TRG and percent organic carbon, increase in glaucony and Ti/Al, increasingly lower levels of oxygen in bottom waters (increased Mo values), increased nutrient availability, and an increase in siliceous productivity (Fig. 8.6b-j).

Above M5b there is c. 12 m of no exposure so it is problematic to connect M5b with the overlying M2d lithofacies. However, from the data obtained,

palynofacies proxies suggest that after becoming more distal in M6b, the shoreline at first remains at about the same position, then gradually becomes slightly more proximal through the overlying M2d mudstone (Fig. 8.6l-q). This coincides with gradually decreasing percent organic carbon, gradually increasing TRG, decreasing Ti/Al, increasing bottom water oxygen (Mo), decreased nutrient availability and glaucony, and a general decrease in surface ocean water productivity (Fig. 8.6b-j).

Leading up into the M6c lithofacies, palynofacies proxies (Fig. 8.6l-q) indicate that the shoreline becomes increasingly more proximal, with a short period where it becomes more distal immediately below the M2d-M6c contact (Fig. 8.6l-m). This coincides with a continued decrease in average percent organic carbon, no significant change in TRG, slight increase in glaucony, decrease in Ti/Al, continued increase in bottom water oxygen levels (Mo), continued decrease in surface ocean water productivity (Fig. 8.6b-j), and increased burrowing (Fig. 8.4f).

Palynofacies proxies suggest that the shoreline becomes more proximal from M2d to M6c then remains relatively proximal in M5c and the base of the overlying M2d lithofacies (Fig. 8.6l-q). This coincides with continued decreasing average percent organic carbon, a decrease then increase in TRG, an increase then decrease in glaucony and siliceous productivity, gradual decrease in Ti/Al, development of oxygenated bottom water conditions (Mo), and an increase in nutrient availability (Fig. 8.6b-j).

In the upper part of the M2d lithofacies overlying M5c, and across its contact with M1f, palynofacies proxies suggest that the shoreline becomes more distal (Fig. 8.6l-q). This coincides with decreasing TRG, increasing Ti/Al, oxic bottom water conditions, low productivity, and a slight increase in nutrient availability (Fig. 8.6b-i).

Palynofacies proxies suggest that through the M1f lithofacies the shoreline position remains relatively steady and becomes more proximal in the uppermost part logged (Fig. 8.6l-q). The trend through M1f coincides with gradually increasing average percent organic carbon, a gradual slight decrease in TRG,

oxygenated to very slightly suboxic bottom water conditions, gradually increasing surface ocean water nutrient supply, and possibly a slight increase in siliceous productivity (Fig. 8.6b-j).

8.3.3 Stable isotopes

Organic carbon stable isotopes do not show any strong trends. From the M2d-M6b contact (Cretaceous-Tertiary boundary) values show a gradual decline through the overlying M2d lithofacies after which they show a slight gradual increase through the remaining lithofacies (Fig. 8.6a).

Figure 8.6: Variations for the lower Mangahouanga Stream section in organic carbon isotopes (a), ocean surface water productivity proxies (b, c, d, j), proxy for seawater nutrient availability (e), bottom water oxygen levels (f, j), aeolian sediment input (g), glaucony (h), and terrigenous sediment input (i), and various palynofacies proxies for shoreline proximity to the site of deposition (k - q).

Fig. 8.6

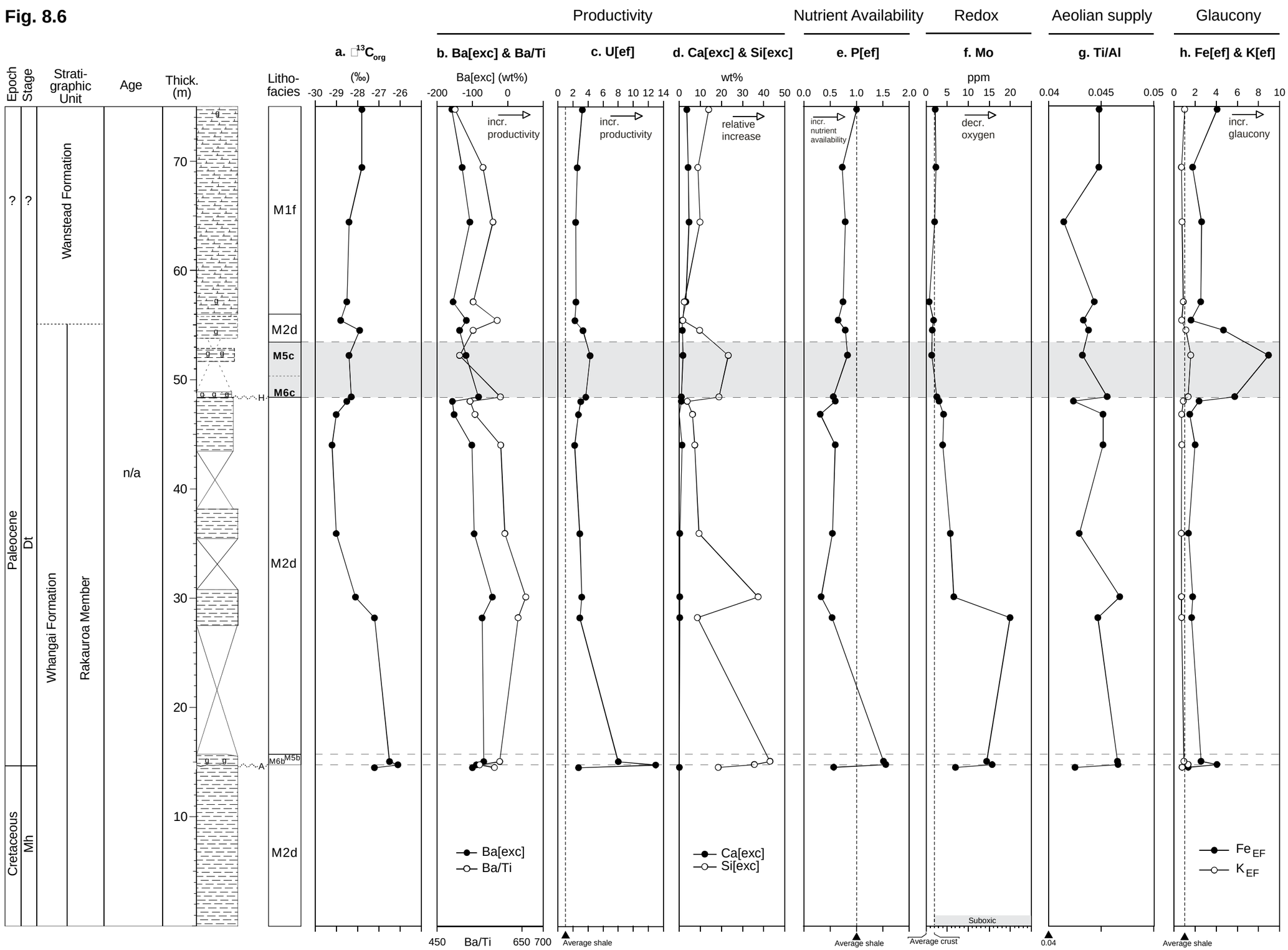
Productivity
Nutrient Availability
Redox
Aeolian supply
Glaucony
a. δ13Corg
b. Ba[exc] & Ba/Ti
c. U[ef]
d. Ca[exc] & Si[exc]
e. P[ef]
f. Mo
g. Ti/Al
h. Fe[ef] & K[ef]
Epoch
Stage
Strati-graphic Unit
Age
Thick. (m)
Litho-facies
(‰)
Ba[exc] (wt%)
wt%
ppm
incr. productivity
incr. productivity
relative increase
incr. nutrient availability
decr. oxygen
incr. glaucony
Paleocene
Cretaceous
Dt
Mh
Wanstead Formation
Whangai Formation
Rakauroa Member
n/a
M1f
M2d
M5c
M6c
M2d
M6b
M5b
M2d
Ba[exc]
Ba/Ti
Ca[exc]
Si[exc]
Fe EF
K EF
450
Ba/Ti
650
700
Average shale
Average shale
Average crust
Suboxic
0.04
Average shale

Fig. 8.6 cont.

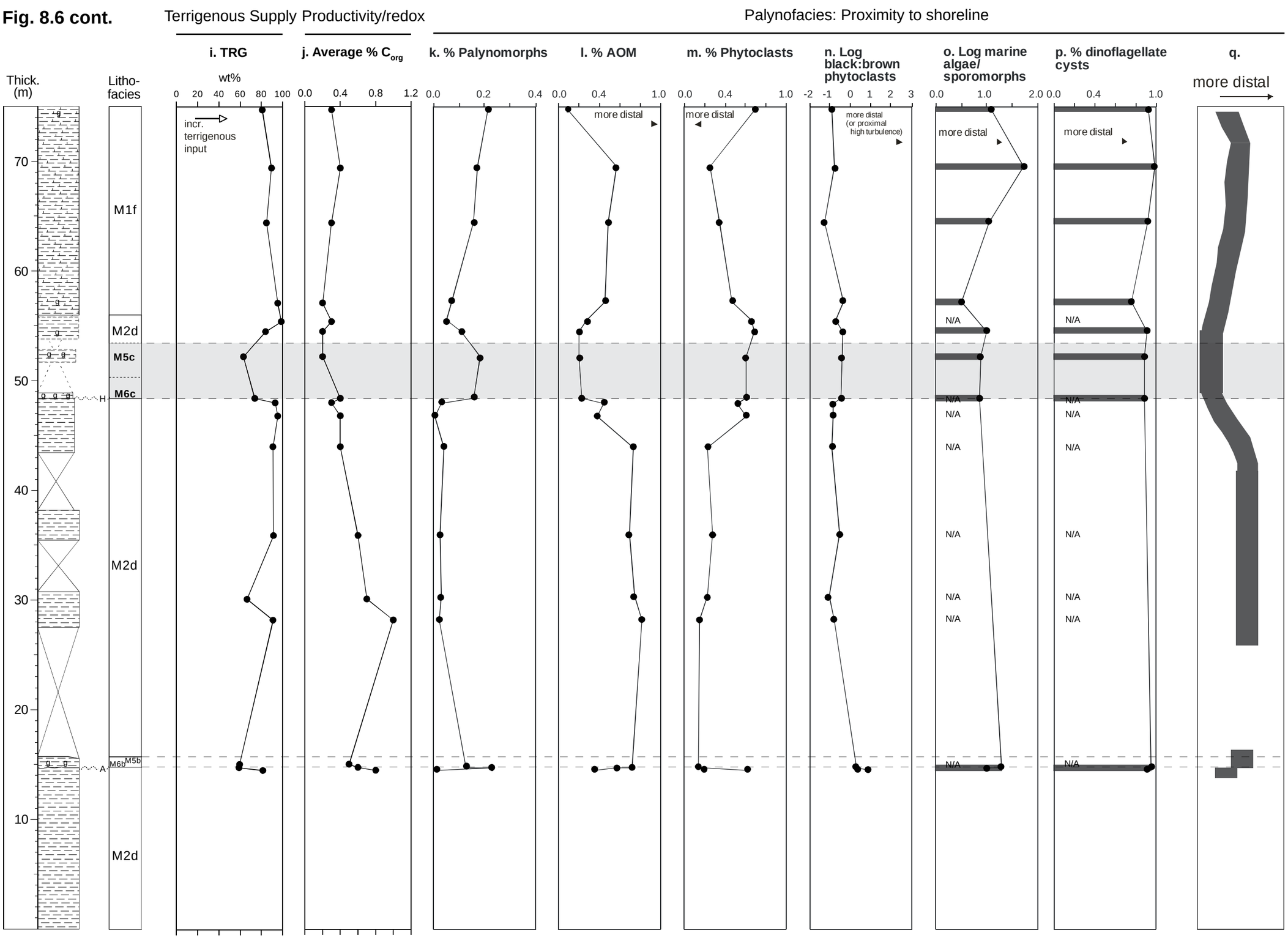
Terrigenous Supply
Productivity/redox
Palynofacies: Proximity to shoreline
Thick. (m)
Litho-facies
i. TRG
wt%
0 20 40 60 80 100
incr. terrigenous input
j. Average % C org
0.0 0.4 0.8 1.2
k. % Palynomorphs
0.0 0.2 0.4
l. % AOM
0.0 0.4 1.0
more distal
m. % Phytoclasts
0.0 0.4 1.0
more distal
n. Log black:brown phytoclasts
-2 -1 0 1 2 3
more distal (or proximal high turbulence)
o. Log marine algae/ sporomorphs
0.0 1.0 2.0
more distal
p. % dinoflagellate cysts
0.0 0.4 1.0
more distal
q.
more distal
70
60
50
40
30
20
10
M1f
M2d
M5c
M6c
M2d
M6b
M5b
M2d
N/A

Chapter 9
AKITIO RIVER

9.1 Introduction

The Akitio River section is younger (late Paleogene or Oligocene) than the other sections investigated in this study. It has been included in this research topic because it may record a North Island equivalent of the Marshall Unconformity (see Section 1.2) and thus could be used as a lithological and geochemical template for deposition during a period of cooling climate.

9.2 Location

The Akitio River section is located in southern Hawke's Bay about 2.5 km north-northwest of the small settlement of Weber, near Weber Road (Fig. 9.1). The section comprises strata that crop out along a small portion of the Akitio River. The section is well exposed and access is river level dependent, being best during periods of low flow.

9.3 Facies characteristics

The sedimentary succession logged at the Akitio River section is presented in Fig. 9.2. The lithostratigraphic nonmenclature and New Zealand stages shown in the figure are after Stewart et al. (1999) and C. Hollis (pers. comm. 2009).

The logged section at Akitio River consists of c. 15 m of muddy limestone (marl) with an c. 1 m thickness of glauconitic sandy mudstone [c. 8-15% glc – muddy sandstone (see Section 9.3.1 for explanation)] in the middle of the succession (Weber Formation) (Fig.9.3A). Two lithofacies have been identified in the succession (Fig. 9.2) and their field lithology, contacts, and petrography are described below but first this studies textural classification scheme is briefly revisited to remind the reader of issues relating to classification of lithologies dominated by glaucony (see Section 3.4.1).

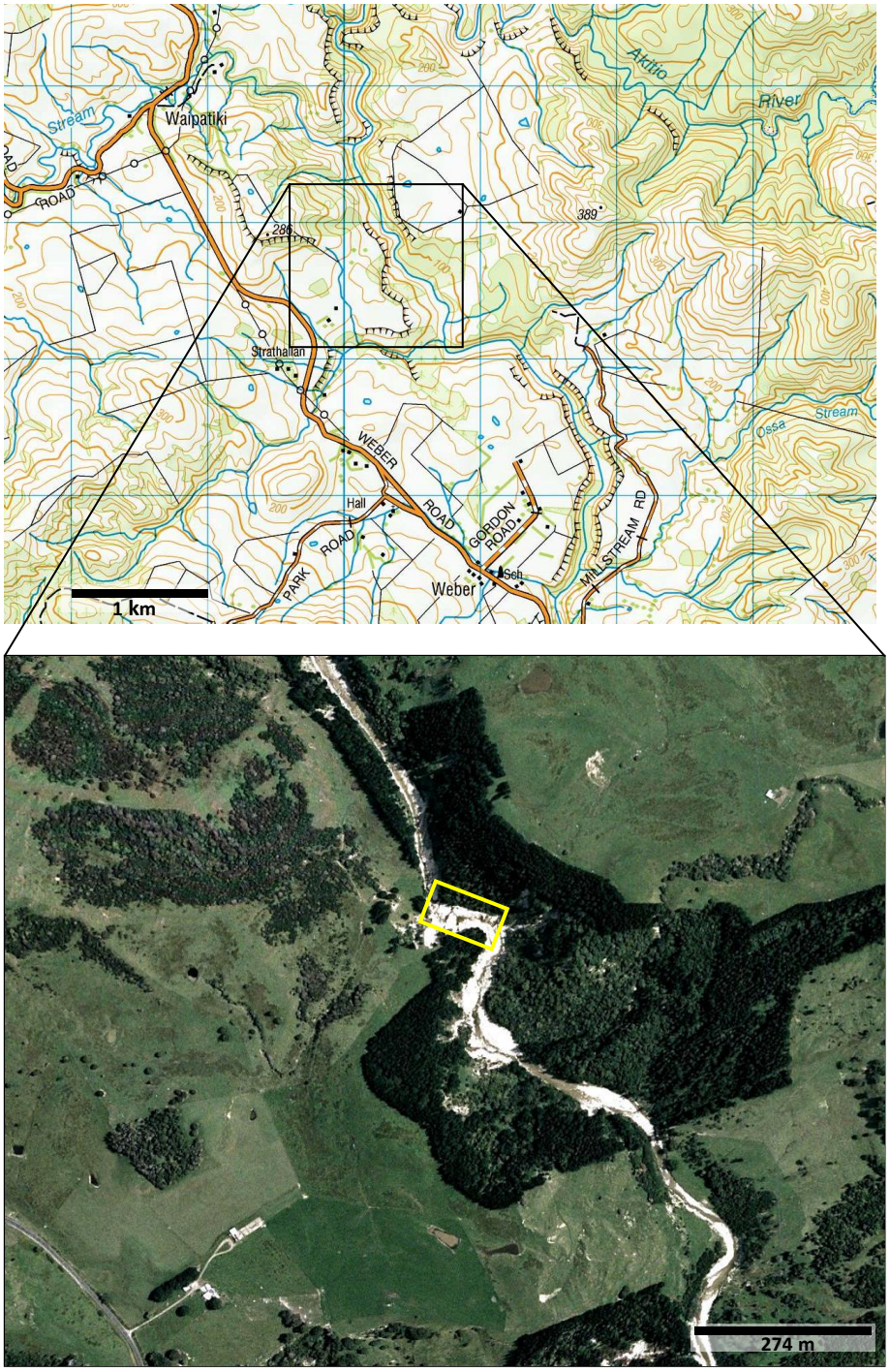

Figure 9.1: Location of the Akitio River section (rectangle in satellite image) with relation to Weber and Weber Road.

9.3.1 Glaucony and rock classification

As noted in Sections 7.2.1 and 8.2.1, in this study lithologic units rich in glaucony are named using their clastic grain size rather than their glaucony grain size so as to better reflect proximity of the paleoshoreline to the rocks depositional area in the rocks name. However, this classification system poorly describes the in-field character of lithologies dominated by glaucony, and consequently images

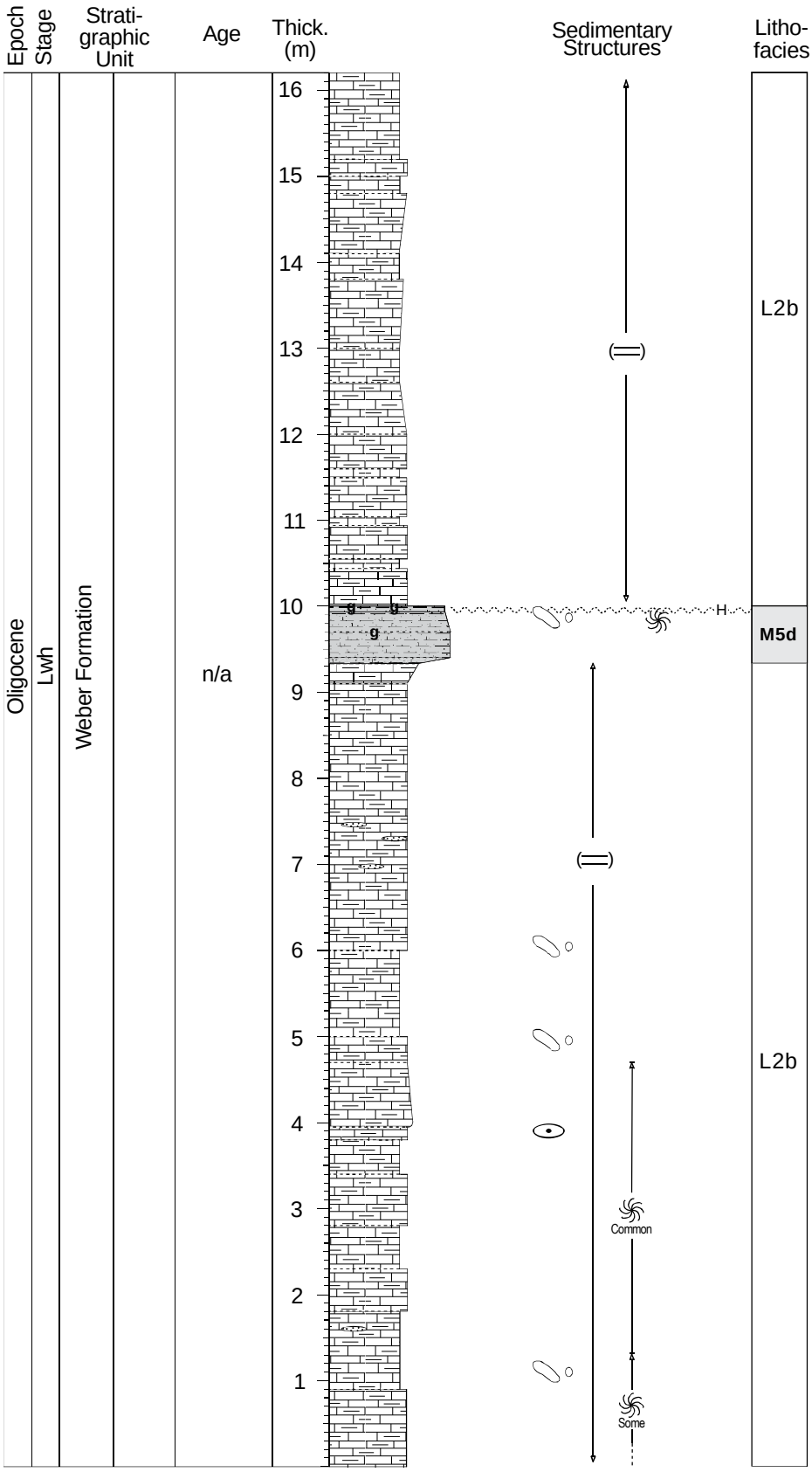

Figure 9.2: Stratigraphic column and lithofacies for the Akitio River section. Stratigraphic nomenclature and New Zealand stages shown are sourced from Stewart et al. (1999) and C. Hollis (pers. comm. 2009). Graphic log lithology and sedimentary structures symbols are defined in Appendix A.

presented in this chapter of samples with high proportions of sand sized glaucony grains, that normally would be classified as sandstones, are named glauconitic sandy mudstones due to the classification scheme excluding the grain size of the glaucony portion of the rock. To aid the reader, where a glaucony dominated lithology is referred to in the text using this "new" classification scheme, the approximate percent glaucony and its conventional name are also given in square brackets (e.g. [c. 80% glc – muddy greensand]).

See Section 3.4.1 for further information on this topic

9.3.2 Muddy limestone lithofacies (L2b)

The muddy limestone lithofacies is identified at the Akitio River section and one other study locality in the East Coast Basin (Table 4.1). Its characteristics at Akitio River are given below.

Field lithology

The L2b lithofacies consists of light grey, moderately to well indurated, moderately well bedded, massive in hand specimen, occasionally burrowed, calcareous muddy limestone (Fig. 9.3B-F). The lithofacies looks like a mudstone or siltstone in outcrop but $CaCO_3$ contents are between 54 and 77% (Appendix M), so the lithofacies is here considered to be a limestone (marl). Bedding appears to have formed as a result of different weathering susceptibility between horizons through the outcrop and *Zoophycos* and ?*Chondrites* trace fossils are seen to occur through the lower half of the succession (Fig. 9.3B-F).

Contacts

The L2b lithofacies lower contact and upper contact are not within the logged area. Its contacts with the M5d lithofacies are described below in Section 9.3.2.

Petrography

Description (MT5.02, MT5.12, MT5.15): Description of L2b is based on three samples. The lithofacies is composed of rare to some, mostly subangular, poorly sorted, very fine sand-sized and silt-sized quartz (and ?feldspar) grains set in a dark argillaceous (and/or ?micritic) matrix (Fig. 9.4). Calcite is the dominant

Figure 9.3: Some field characteristics of the Akitio River section. A = Overview of the section showing the position of inferred faults and lithofacies; B = moderately well bedded muddy limestone of the L2b lithofacies with the glauconitic mudstone lithofacies (M5d) residing in the middle of the L2b succession (5 m long Jacob staff for scale); C and D = examples of *Zoophycos* and ?*Chondrites*trace fossils in hand specimen (C) and *Zoophycos* in outcrop (D) (*Zoophycos* are the long burrows and ?*Chondrites* the tiny blebs within the matrix); E and F = possible *Chondrites* trace fossils in hand specimen (E) and in outcrop (F).

mineral present with quartz and feldspar minor components (Fig. 9.5). Some glaucony occurs within the succession and rarely has a "popcorn" morphology. Many planktic and occasionally benthic microfossils occur in the succession. Most of the planktic microfossils are broken up.

Classification: Muddy sparse biomicrite with a quartzose argillutite to argillaceous feldslutite clastic component.

Figure 9.4: Example of L2b lithofacies muddy limestone. It is composed of very fine sand-sized and silt sized clastic grains, coarse silt to medium sand-sized glaucony grains, many broken up planktic microfossil tests, and rare benthic microfossil tests, all set within a dark argillaceous and/or micritic matrix. A coarser area near the base of the image is likely the infill of a burrow (MT5.15).

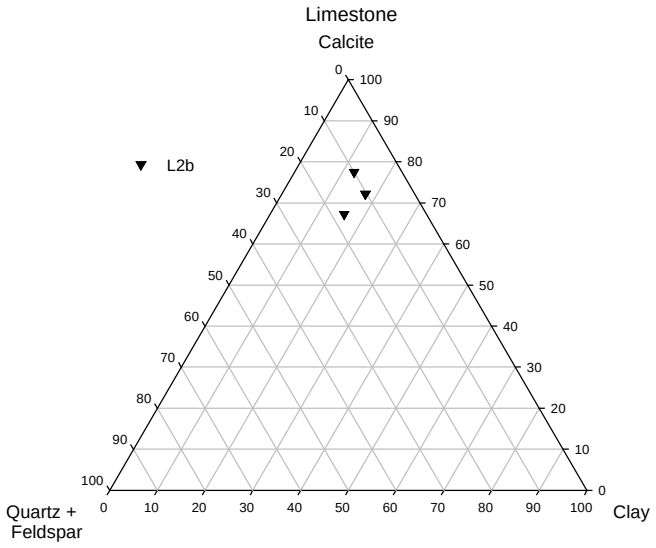

Figure 9.5: Ternary diagram of relative proportions of calcite, combined quartz and feldspar, and clay minerals in the muddy limestone lithofacies at the Akitio River section (L2b).

9.3.3 Glauconitic mudstone lithofacies (M5d)

The glauconitic mudstone lithofacies was identified at the Tawanui (Chapter 7), lower Mangahouanga (Chapter 8), and Akitio River sections (Table 4.1). The characteristics of the Akitio River variety of the lithofacies (M5d) are given below.

Field lithology

The M5d lithofacies consists of poorly to moderately indurated, massive, occasionally burrowed, slightly glauconitic, calcareous sandy mudstone [c. 8 glc – muddy sandstone] (Fig. 9.6C, D). Through the lower portion of the lithofacies grain size appears to coarsen upwards (Fig. 9.6B). Through the middle of the unit the grain size appears to remaining unchanged, and then fines upwards in the upper part of the lithofacies (Fig. 9.6B). This succession is capped by an c. 5 cm thick bed of more glauconitic mudstone [c. 15% glc – sandy mudstone to muddy sandstone] (Fig. 9.6D).

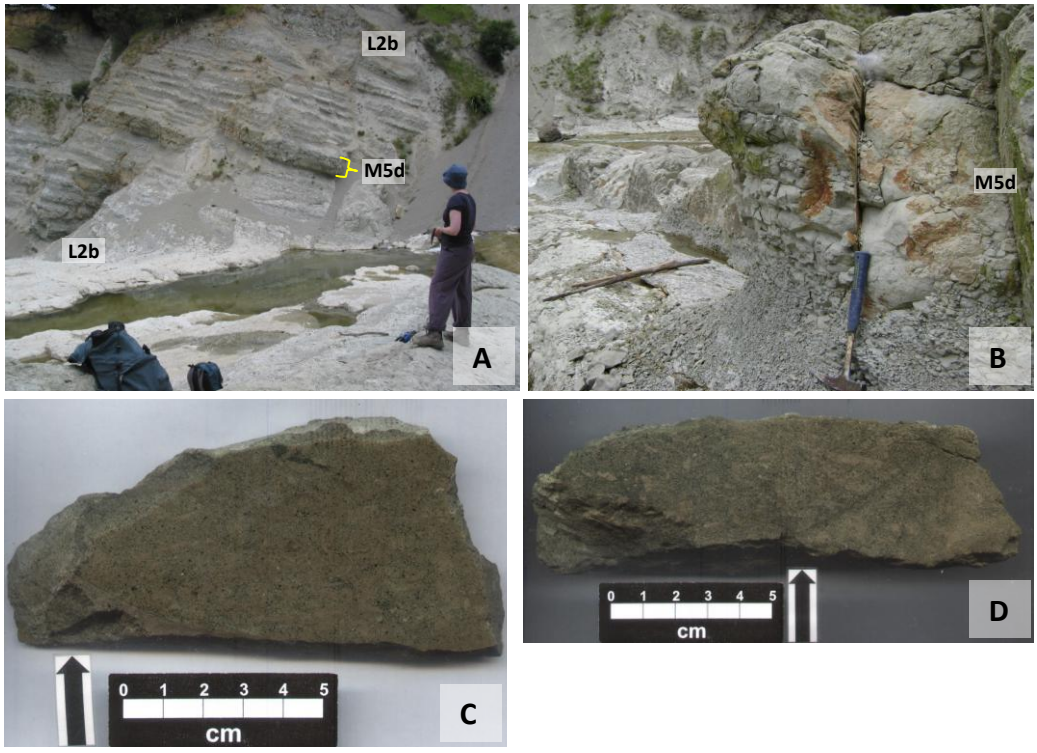

Figure 9.6: Features of the M5d lithofacies at Akitio River. A = Bed of M5d predominantly glauconitic sandy mudstone [muddy sandstone] midway up the face of the exposure; B = gradational lower contact of the M5d lithofacies with underlying L2b; C and D = hand specimens of the the M5d lithofacies glauconitic mudstone from the middle of the lithofacies [muddy sandstone] (C) and from the uppermost more glauconitic bed [sandy mudstone] (D).

Contacts

The lithofacies lower contact with underlying L2b appears rapidly gradational (Fig. 9.6B) and its upper contact is difficult to determine due to either poor exposure or poor access (Fig. 9.6A), but may be rapidly gradational or sharp.

Petrography

Description (MT5.05, MT5.07): Description of the lithofacies is based on two samples. M5d is composed of many to common, poorly sorted, angular to subangular, very fine sand-sized quartz and ?feldspar grains set in a dark argillaceous matrix (Fig. 9.7). Of the clastic fraction, quartz, feldspar, and clay minerals share relatively equal abundances in the succession, although quartz and clay dominate feldspar slightly (Fig. 9.8). Many to common angular to subrounded glaucony grains occur within the succession (Fig. 9.7). Some planktic microfossil tests, most broken up, and rare benthic microfossil tests occur in the lithofacies.

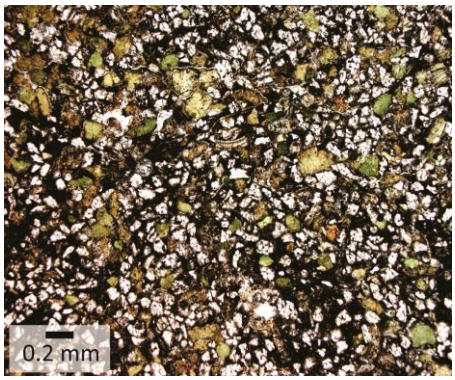

Figure 9.7: Microscopic features of the uppermost more glauconitic bed within the M5d lithofacies. It is composed of many very fine sand-sized clastics, many medium sand-sized glaucony grains, and some broken up planktic microfossil tests, all set in a dark argillaceous matrix (MT5.05).

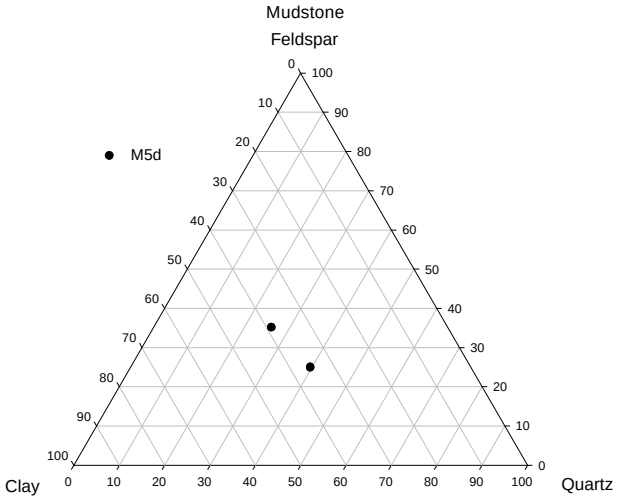

Figure 9.8: Ternary diagram of relative proportions of feldspar, clay minerals and quartz in the glauconitic mudstone lithofacies (M5d) at the Akitio River section.

9.4 Geochemistry results

Geochemical proxies used in this study were introduced in Chapter 3 (Section 3.3.4) and are presented here for the Akitio River section. Fig. 9.9 presents the up

section trends for carbonate carbon and oxygen stable isotopes (a) and elemental proxies for ocean surface water biological productivity (b-c), seawater nutrient availability (d), bottom water oxygen levels (e), aeolian sediment supply (f), glaucony (g), and terrigenous sediment supply (h). Preliminary interpretations of geochemical trends are offered in this section, even though this is a results chapter, to aid later interpretations (see Chapter 10).

First the ocean surface water biological productivity proxies are tested for biogenic association using the methods outlined in Chapter 3. This is done in order to assess their reliability as paleoproductivity indicators for the logged area of the Akitio River section. If a productivity proxy is found to have no biogenic association its trends will not be described in any detail.

9.4.1 Testing for productivity proxy biogenic association

Ba[exc] co-varies with Ba/Ti, Ca[exc], and seawater nutrient availability P[ef], and Mo values suggest the entire logged section was deposited under oxygenated bottom water conditions (Fig. 9.9b-e). Thus Ba[exc] is considered to have a biogenic association at the Akitio River section. One data point is negative however, apparently a result of a TiO_2 value slightly higher than all other TiO_2 values for the section (Appendix M).

9.4.2 Proxy results

Productivity, seawater nutrient availability, and glaucony proxies indicate an increase in siliceous productivity, nutrient availability, and glaucony through the M5d lithofacies, peaking in the thin, more glauconitic bed that caps the succession, then dropping sharply into the overlying L2b lithofacies (Fig. 9.9b-d, g). Mo values suggest oxygenated conditions during deposition of the entire logged section at Akitio River (Fig. 9.9e). Ti/Al values are generally slightly above the 0.04 threshold and show little variation through the section (Fig. 9.9f). TRG values gradually increases through the entire section (Fig. 9.9h).

9.4.3 Stable isotopes

Stable carbonate carbon isotopes show a small excursion in M5b and a positive trend at the top of the logged section (Fig. 9.9a). Stable oxygen isotopes tend to

co-vary with carbonate carbon isotopes for the majority of the succession, suggesting the values have been diagenetically altered (Fig. 9.9a). However, through the c. 1m of L2b below M5d, and in the lower half of M5d, the oxygen isotope record does not co-vary with the carbonate carbon record. In this interval the oxygen record suggests warming leading into M5d, with cooling during the deposition of the lower half of M5d.

Figure 9.9: Variations for the Akitio River section in carbonate carbon and oxygen isotopes (a), ocean surface water productivity proxies (b, c), proxy for seawater nutrient availability (d), bottom water oxygen levels (e), aeolian sediment input (f), glaucony (g), and terrigenous sediment input (h).

Fig. 9.9

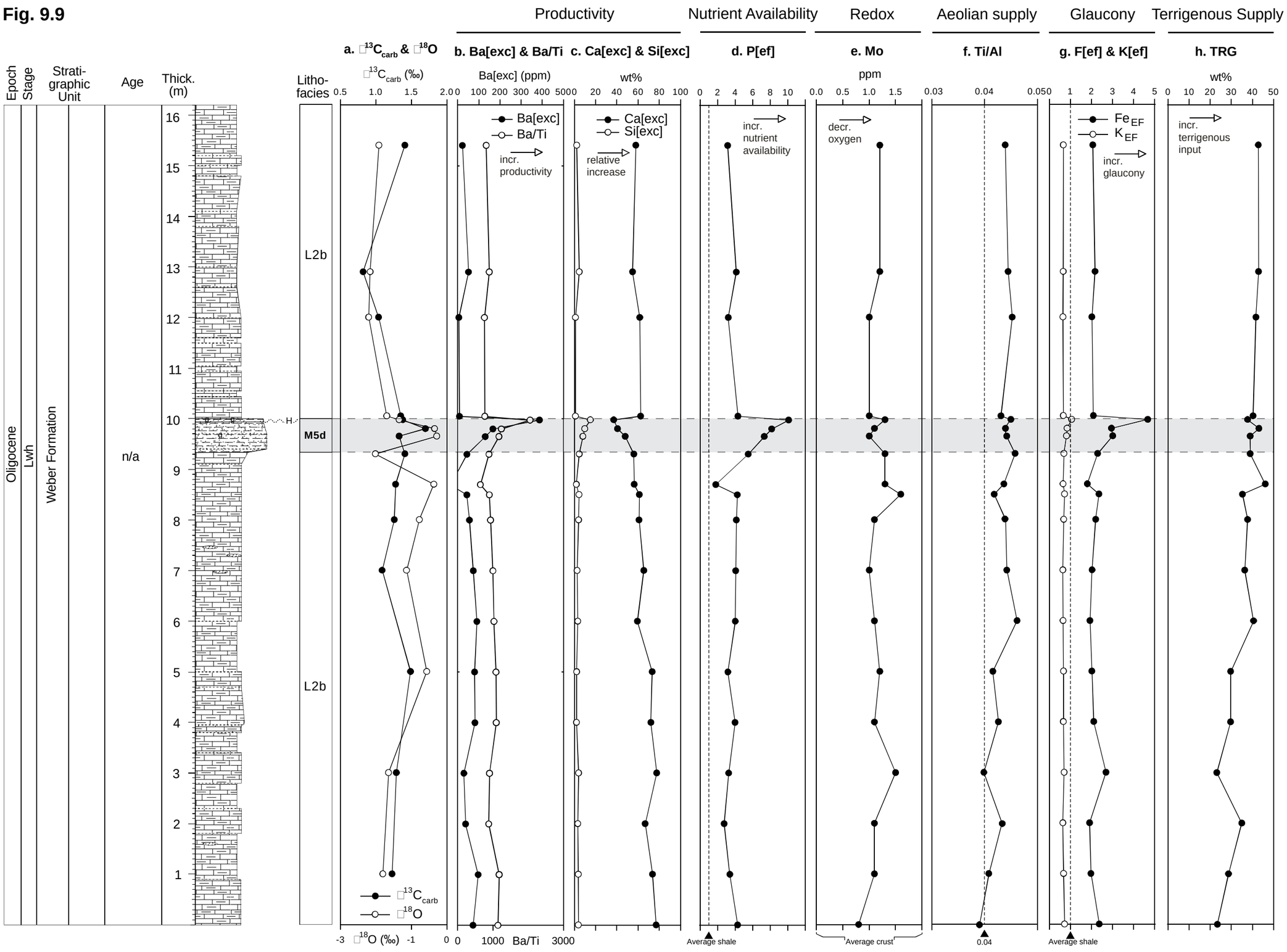
Productivity
Nutrient Availability
Redox
Aeolian supply
Glaucony
Terrigenous Supply
Epoch
Stage
Strati-graphic Unit
Age
Thick. (m)
Litho-facies
Oligocene
Lwh
Weber Formation
n/a
M5d
L2b
a. δ13Ccarb & δ18O
b. Ba[exc] & Ba/Ti
c. Ca[exc] & Si[exc]
d. P[ef]
e. Mo
f. Ti/Al
g. F[ef] & K[ef]
h. TRG
δ13Ccarb (‰)
Ba[exc] (ppm)
wt%
ppm
Ba[exc]
Ba/Ti
incr. productivity
Ca[exc]
Si[exc]
relative increase
incr. nutrient availability
decr. oxygen
FeEF
KEF
incr. glaucony
incr. terrigenous input
δ18O (‰)
Ba/Ti
Average shale
Average crust
0.04
Average shale

Chapter 10
DISCUSSION

10.1 Introduction

Sections 10.2 to 10.4 of this chapter discuss results from this study that are of significance to general eastern North Island geology, but of less relevance to the "Ice in the greenhouse" project (see Section 1.1). Topics discussed include issues raised in the preceding chapters regarding the naming of certain formations and placement of formation boundaries (see Sections 5.2 and 6.2), interpretions of the mode and environment of deposition of the lithofacies described, and specific issues relating to characteristics of some strata described in this study. Section 10.5 is devoted to discussing results directly relevant to the "Ice in the greenhouse" project. These include paleoproductivity trends, regional relative sea level, the significance of "dropstones" in the study area, and the significance of the Akitio River section. Lastly, the implications of the study's findings to the wider project – "Ice in the Greenhouse: a Paleocene record of Antarctic deep-water flow" – are considered.

10.2 Formation names and boundaries

In this section the formation names given to sedimentary successions at the Pahaoa section (Fig. 5.2) and the placement of the lower boundary of the Waipawa Formation at the Angoara Road section (Fig. 6.2) are discussed.

10.2.1 Formation names - Pahaoa

Two formation names have been tentatively proposed for the unnamed sedimentary successions at Pahaoa, namely the "Awhea Formation" and "Waipawa Formation". As indicated in Section 5.2, the flaggy micritic limestone at Pahaoa has previously been identified as Kaiwhata Limestone (Nelson, 1968), and this used here to correlate underlying and overlying lithologies with formations from other sections.

Awhea Formation

The structural subdivisions of the eastern North Island of Moore (1988) (Fig. 2.2)

portray the Tora block as divided into a northern and southern block, separated by a finger of Pongaroa block. The Pahaoa section occurs at the southernmost part of the northern Tora block (Fig. 2.2). The Kaiwhata Limestone at Pahaoa is considered to be the northern Tora block equivalent of the southern Tora block Mungaroa Formation (Field et al., 1997).

In the southern Tora block the Mungaroa Formation is underlain by Awhea Formation. Descriptions of the Awhea Formation from Waterhouse and Bradley (1957), Field et al. (1997), and Laird et al. (2003) resemble descriptions of the interbedded sandstone-mudstone lithofacies (M7a) underlying the Kaiwhata Limestone in this study. A combined description of the Awhea Formation from the above authors indicates that the Awhea Formation comprises blue-grey, cm-bedded, ungraded fine sandstone, and interbedded blue-grey calcareous and glauconitic very fine sandstone and thin black mudstone. This description resembles the field lithology descriptions of the interbedded sandstone-mudstone lithofacies (M7a) at the Pahaoa section (Section 5.2.1), illustrated in Fig. 5.3A, B and 5.4B. Additionally, Laird et al. (2003) noted that the Awhea Formation is highly bioturbated (see Fig. 5.3C, G for M7a example), parallel laminated (see Fig. 5.3D) and occasionally cross laminated (see Fig. 5.3D, E). Based on these similarities the interbedded sandstone-mudstone lithofacies (M7a) underlying the Kaiwhata Limestone at Pahaoa has been named the Awhea Formation.

However, it must be emphasised that assigning lithofacies M7a at Pahaoa this formation name is *tentative*. Field et al. (1997) states that the Awhea Formation is only present in the southern part of Tora block, and in the north Kaiwhata Limestone instead overlies Whangai Formation. Thus, the M7a lithofacies could alternatively be well bedded Whangai Formation (possibly a lateral equivalent of the Porangahau Member, see Section 2.2.1 for description). However, given the strong similarities of the M7a lithofacies to descriptions of the Awhea Formation, naming the succession Awhea Formation is favoured over Whangai Formation. Additionally, because the Pahaoa section resides at the southernmost tip of the northern Tora block it is possible that the section holds relatively more similarities to the southern Tora block lithologies compared with more northern, northern Tora block sections.

Waipawa Formation

Based on the description of Waipawa Formation at Mead Stream in Marlborough by Hollis et al. (2005) and Andrew (2010), the siliceous mudstone (M2a) at the Pahaoa section has tentatively been named "Waipawa Formation". The similarities between the description of the Waipawa Formation at Mead Stream and the M2a lithofacies at Pahaoa are their dark grey colour, fissile nature (Fig. 5.15A), laminations, burrowing (Fig. 5.15D, E), sharp burrowed lower contact (Fig. 5.15A), variable thickness due to wavy bedding (Fig. 5.16A), abundance of radiolarian microfossils (Fig. 5.17D, E), and a large positive $\delta^{13}C$(org) isotopic excursion through the interval (Fig. 5.20A).

The siliceous mudstone lithofacies at Pahaoa (M2a) has lower organic carbon contents (max. 0.3 wt%; Fig. 5.20i) than the Waipawa Formation at Mead Stream (>2 wt%; Hollis et al., 2005) and of the Waipawa Formation in general (1.8 to 12.3 wt%; Moore, 1989). Despite this difference, the many similarities between the M2a lithofacies at Pahaoa and the Mead Stream occurrence of Waipawa Formation are tentatively considered here to indicate that the lithofacies is equivalent to Waipawa Formation.

10.2.2 Lower boundary of Waipawa Formation – Angora Road

At the Angora Road section (Chapter 6) the lower boundary of the Waipawa Formation has tentatively been placed at the transition from dominantly calcareous to dominantly non-calcareous lithologies (Fig. 6.2). This is despite more traditional Waipawa Black Shale type lithologies (Moore, 1989) not occurring for a further c. 10 m above the proposed lower boundary. Reasons for placement of the boundary at this position are based on organic carbon contents, the organic carbon isotope record, and the calcareousness of the lithology.

Organic carbon contents increase from 0.7 wt% in the lower part of the logged section to 1.7 to 2.2 wt% at the calcareous to non-calcareous transition point (Fig. 6.13j). Additionally, $\delta^{13}C$(org) isotope values show a positive shift from -25.5‰, in the lower part of the logged succession, to -22 to -21‰ at the calcareous to non-calcareous transition point (Fig. 6.13a). High organic carbon contents and heavy $\delta^{13}C$(org) isotope values are characteristic of Waipawa Formation (Killops

et al., 2000) and suggest that the calcareous to non-calcareous transition is of that formation.

Data for organic carbon contents and $\delta^{13}C$(org) isotope values underlying the calcareous to non-calcareous transition are sparse, so the point at which there is an increase in organic carbon and a positive shift in $\delta^{13}C$(org) isotope values is unknown. The degree of sharpness to the shifts is also unknown. Given these uncertainties the calcareous to non-calcareous transition point has tentatively been selected as the lower boundary for the Waipawa Formation in order to avoid including non-calcareous lithologies in the underlying Upper Calcareous Member of the Whangai Formation whilst still remaining in accordance with elevated organic carbon contents and heavy $\delta^{13}C$(org) isotope values indicative of Waipawa Formation.

10.3 Environment and mode of deposition

Tentative interpretations of the environment and mode of deposition of lithologies at each of the studied sections are given in this section. The interpretations draw upon data from this study as well as from previous workers. Fig. 10.1 shows the approximate position of the early Paleogene study sections on the paleoshelf-slope during the Late Paleocene. All the sections appear to have resided in a slope environment at the time, which is reflected in their fine grained nature.

The identification of mass emplaced deposits and interpretation of the origin of glaucony rich deposits are important considerations in this section of the chapter and so are briefly introduced here.

Mass emplaced deposits

Deposits interpreted to have been mass emplaced are classified based on the Gani (2004) classification scheme (Fig. 10.2). This scheme classifies sediment gravity flows and their deposits based on flow rheology. Flows with Newtonian fluid rheology are classified as turbidites, those with non-Newtonian fluid rheology are debris flows and slides and slumps. Some flows exhibit part Newtonian fluid and part non-Newtonian fluid rheology, and are classified as dense flows. Turbidity current deposits are turbidites, debris flow deposits debrites, and dense flow

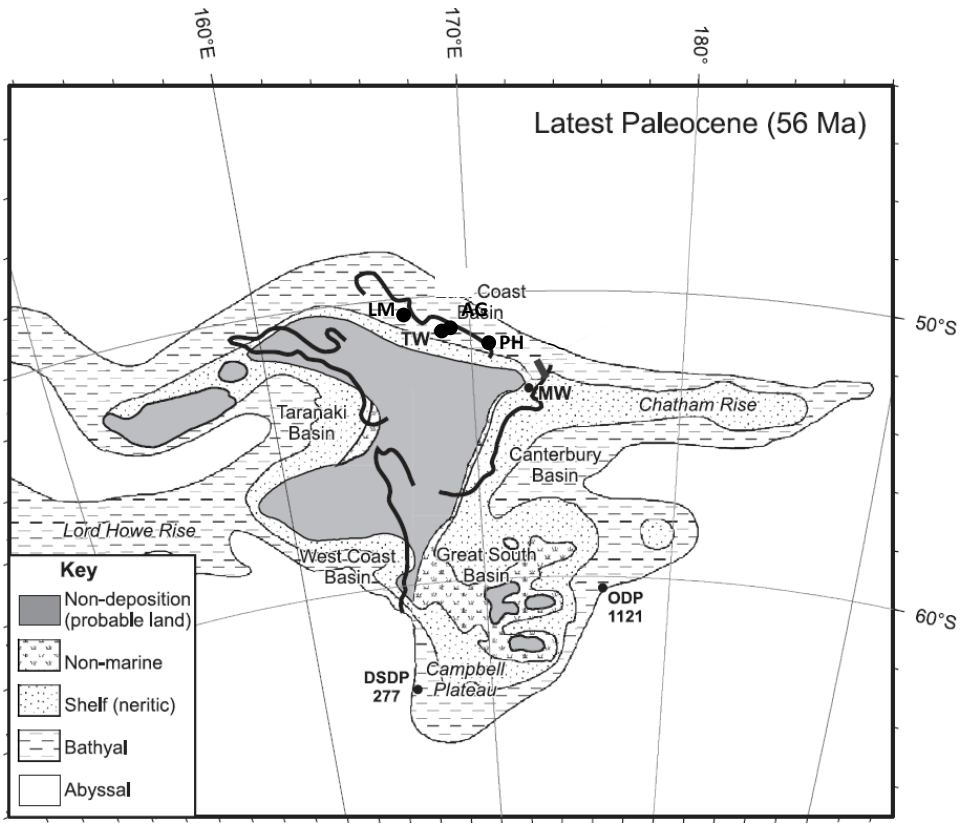

Figure 10.1: Paleogeographic reconstruction of Zealandia in the Late Paleocene showing the approximate position of land, the shelf slope break, and the dislocated elements of modern New Zealand (bold black lines) (modified from Hollis, et al., 2005). The approximate position of the study sections are shown as labelled black dots: PH = Pahaoa; AG = Angora Road; TW = Tawanui; LM = lower Mangahouanga Stream.

deposits densites. The diagnostic depositional features of each of the deposits are given in Fig. 10.2. "Gravite" is an umbrella term that incorporates all sediment gravity flow deposits.

Glaucony and glauconite

Glaucony is a broad term introduced by Odin and Matter (1981) for all green clay minerals, of which glauconite is the most common (Lewis and McConchie, 1994). Glauconite is formed in the marine environment, usually in the outer shelf and upper slope, at the sediment water interface under a low sedimentation rate (Lewis and McConchie, 1994). Glauconite can be authigenic, allogenic, or perigenic, where authogenic glauconite has never moved from its area of formation (*in situ*), allogenic glauconite is recycled from older sediments, and perigenic glaucony is locally redeposited (most glauconite is of this category) (Lewis and McConchie, 1994).

Deposit		Rheology	Flow Type			Dominant sediment support mechanism	Diagnostic depositional features
Gravite	Turbidite	Newtonian fluid	Turbidity current (mostly turbulent).	-	-	Fluid turbulence	Well sorted; no "floating" clasts; top part always shows normal distribution grading; can show inverse grading in lower portions if hyperpycnal flow; Bouma sequence.
	Densite	Variable (part Newtonian, part non-Newtonian).	Dense flow (part turbulent, part laminar).	-	-	Dispersive grain pressure, fluid turbulence, escaping pore fluid, matrix strength.	Consists of a lower non-cohesive (usually) debrite layer with upper turbidite layer with no bedding plane between the two; inverse grading or massive in lower parts; distribution grading in upper parts, dish and pillar structures; convolution.
	Debrite	Non-newtonian fluid	Debris flow (mostly laminar).	Dilatant fluid	Non-cohesive	Dispersive grain pressure.	Inverse grading; relatively mud free sandstones; generally have layer by layer accretion.
				Bingham plastic	Cohesive	Matrix strength.	No distribution grading; poor sorting with rare, if any, coarse tail grading; preserved flow morphology; matrix supported "floating" clasts in muddy matrix; sharp upper boundary; boulder projection through top.
	Slide and slump		Slide and slump.	Bingham plastic	Slide and slump	Matrix strength.	Matrix supported floating clasts; poor sorting.

Figure 10.2: Classification of sediment gravity flows and the diagnostic features of their deposits (adapted from Gani, 2004)

10.3.1 Pahaoa (Fig. 5.2)

The depth of deposition data reported for the Pahaoa section come from reconnaissance biostratigraphic assessment of foraminiferal samples by Hugh Morgans (GNS, pers. comm. 2010).

Interbedded sandstone-mudstone lithofacies (M7a) [lower in section]

The interbedded sandstone-mudstone lithofacies (M7a) at the base of the logged section at Pahaoa was deposited at mid to lower bathyal depths (probably c. 1000 m). The lithofacies is interpreted here to consist of beds deposited from gravity flows (gravites; Gani, 2004). This interpretation is based on some beds having semi-parallel or swaley and cross laminations (Fig. 5.3D, E), and/or sharp lower contacts with normal grading upwards from sandstone into mudstone in the uppermost portion of beds (Fig. 10.2). Mudstone beds may be the fine grained upper portion of normally graded gravites, and/or hemipelagic deposits, and/or distal gravites. The succession has the highest terrigenous input of the logged section at Pahaoa (Fig. 5.20h) and was mostly deposited under oxic conditions (Fig. 5.20e), with sharply decreasing terrigenous sediment input and isolated suboxic conditions occurring in its upper part, as indicated by the terrigenous supply and redox proxies (Fig. 5.20e, h), and an increase in burrowing (Fig. 5.2 and Fig. 5.4C, D).

In summary, the succession of M7a lithofacies at Pahaoa, coincident with the Awhea Formation, is interpreted as an ancient slope fan deposited at mid to lower bathyal depths (Fig. 10.3) in mostly oxic bottom waters, under a relatively high (for the section) sediment input regime. The influx of terrigenous sediment appears to decrease towards the top of the lithofacies (Fig. 5.20h).

Interbedded sandstone-limestone lithofacies (L1)

The "slope fan deposits" of the M7a lithofacies are overlain by the interbedded sandstone-limestone lithofacies (L1) consisting of micritic limestone with occasional interbeds of sandstone (Fig. 5.9). No depth of deposition for the L1 lithofacies was obtained for the Pahaoa section so depths are tentatively based on those suggested for the Kaiwhata Limestone (equivalent of L1) by Lee and Begg (2002), and in unpublished East Coast CCP reports for two sections to the north of Pahaoa that include Kaiwhata Limestone – the Kaiwhata River and the Huatokitoki Stream sections.

The interbedded sandstone-limestone lithofacies (L1) at Pahaoa may have been deposited at mid bathyal depths or deeper. Sandstone interbeds are interpreted as

gravites (possibly densites) based on the presence of occasional faint laminations, sharp occasionally undulating lower contacts with rare flame structures, and gradational upper contacts with limestone or mudstone (Fig. 5.9F) (Fig. 10.2). Nelson (1968) noted a number of similar features indicative of redeposition within the sandstone beds and also concluded a sediment gravity flow origin. The prominent c. 3 m thick sandstone bed midway through the lithofacies is interpreted as a gravite based on the presence of laminations in the upper third of the bed (Fig. 5.9H) and its sharp lower contact. The thin mudstone that caps the bed may represent the fine grained portion of the flow. However, the contact between the two beds is more abrupt than gradational, although this may simply reflect a strongly bimodal grain size distribution involving sand and mud without intermediate sizes, and so a lack of grading. If the depth of deposition inferred for this lithofacies is correct, the *in situ* formation of glaucony as a cement/matrix in the pores of the sandstone bed (Fig. 5.11) represents formation of the mineral at the lower end of its "normal" depth range (60 to 1000 m), although it is known to have formed at up to 2400 m water depth (Odin and Fullagar, 1988).

The Kaiwhata Limestone (equivalent to L1) is part of the Amuri Limestone in Marlborough (Lee and Begg, 2002). The Amuri Limestone is suggested to have been deposited far from the paleoshoreline under oxic bottom water conditions as a pelagic rain of sand to clay sized planktonic debris, which formed a soupy soft sediment (ooze) on the seafloor (Andrew, 2010). Redeposition of portions of this calcareous ooze in the form of turbulent gravity flows has been proposed for the Mungaroa Limestone and Kaiwhata Limestone (equivalent of L1) (Waterhouse and Bradley, 1956; Nelson, 1968).

In summary, the L1 lithofacies succession is interpreted as either: (1) a distal slope deposit consisting mostly of pelagic sedimentation of predominantly calcareous planktonic microbiota at middle bathyal depths (Fig. 10.3) with normal sedimentation occasional interrupted by sandy sediment gravity flows; or (2) a slope fan deposit consisting of redeposited micritic limestone and sandstone beds (Fig. 10.3). Regardless of the mode of deposition the lithofacies was deposited under oxic conditions under generally very low terrigenous input apart from the occasional sudden emplacement the sandstone interbeds (Fig. 5.20e, h).

Muddy limestone lithofacies (L2a)

The L2a lithofacies is likely similar to L1 in its depositional environment (Fig. 10.3) apart from the depositional site receiving greater terrigenous input compared to L1 (Fig. 5.20h). This could have been in the form of an increased number and frequency of siliciclastic sediment gravity flows or an increase in sediment reworking off the shelf.

Siliceous mudstone lithofacies (M2a)

Depth of deposition data for the siliceous mudstone lithofacies at Pahaoa (M2a) have not been obtained in this study. During deposition of M2a the lithofacies depositional area was under a higher terrigenous sediment influence compared with the underlying limestone (L1), and at least as high as that of the muddy limestone lithofacies (L2a) (Fig. 5.20h). Pelagic sedimentation of planktonic debris continued during deposition of the siliceous mudstone, but there was an abrupt change from the underlying limestone where predominantly calcareous microbiota (foraminifera, nannofossils) are preserved, to the siliceous mudstone where siliceous microbiota (radiolaria) dominate (Fig. 5.17D).

Near the base of the lithofacies the change in style of sedimentation was interrupted by a sandy sediment gravity flow or gravite. This interpretation is based on the sharp undulating lower contact and vague laminations in the gravite (Fig. 5.15B). Some degree of sediment starvation of the depositional area at the start of deposition of M2a is inferred by relatively low terrigenous supply proxy values (Fig. 5.20h) and colonisation and burrowing by benthic organisms of the base of the lithofacies, including the gravite and bounding siliceous mudstone beds (Fig. 5.2 and 5.15D, E).

Most of the succession was deposited under a mix of oxic and suboxic conditions with suboxic conditions more prevalent in the lower portion of the lithofacies and associated with an enrichment of organic matter (Fig. 5.20e, i). The upper portion of the lithofacies becomes green-grey (Fig. 5.15c) which could be associated with finely divided glauconite or a decrease in organic sedimentation (Potter et al., 2005), and/or possibly a decrease in sedimentation rate (Jansa and Hu, 2009). The

glaucony proxy does not indicate enrichment in glaucony (Fig. 5.20g) but the percent organic matter and terrigenous input proxies do show a decreasing trend up through the upper part of the lithofacies (Fig. 5.20h, i), suggesting the green-grey colour of the mudstone is due to a decrease in organic matter content and/or the rate of terrigenous sedimentation.

In summary, the siliceous mudstone lithofacies (M2a), coincident with the Waipawa Formation, is interpreted as being deposited under a higher influx of terrigenous sediment than the limestone of L1, and residing under a water column dominated by siliceous productivity. It appears that the beginning of deposition of the lithofacies was associated with decreased terrigenous input, with increased levels in its lower portion associated with lower oxygen levels and higher organic matter contents. The cessation of deposition seems to coincide with deceasing terrigenous sediment input and organic matter contents.

Calcareous mudstone lithofacies (M1a)

The calcareous mudstone lithofacies at Pahaoa (M1a) was deposited at lower bathyal to abyssal depths (1000-2000 m+), and most likely the latter. Red beds similar to those of lithofacies M1a at Pahaoa have been interpreted by other workers as being deposited under highly oxic, oligotropic, probably low-productivity conditions (with low organic carbon burial), with low clastic input, low sedimentation rates, and increasing paleowater depth (e.g. Wagreich et al., 2009; Wang et al., 2009). Green beds have been interpreted as being deposited under similar conditions but under a higher sedimentation rates (Jansa and Hu, 2009). The reason for this is that under low sedimentation rates the rate of diffusion of oxygen into the sediment exceeds its consumption during degradation of organic matter and the sediments become oxidised and red coloured (Jansa and Hu, 2009). However under higher sedimentation rates the sediment is exposed to oxygen diffusion for a shorter time and consequently attains a green colour (Jansa and Hu, 2009).

On this basis the M1a lithofacies should show a decreasing sediment influx up through the succession to mirror the gradual increase in red mudstones, and the colour of individual samples should mirror the terrigenous input. However, this is

not the case and red mudstone samples show higher TRG values than the green and mixed green and red mudstones (Fig. 5.20h). This conflict may be a result of the relatively small number of samples collected from each coloured bed while the uppermost part of the section that includes the most red mudstones were excluded from sampling due to time constraints. However, if the results do give a true reflection of the terrigenous input during the deposition of the red and green mudstones, then the colour is interpreted to be primarily the result of fluctuations in oxygen conditions during sediment deposition, rather than fluctuations in terrigenous supply.

Much of the upper third of the lithofacies is interpreted to be submarine slump deposits based on the common occurrence of foreign clasts, disrupted and broken up sandstone beds, and the twisted and contorted nature of the mudstone through the interval (Fig. 5.18H).

In summary, the calcareous mudstone lithofacies is interpreted to have been deposited at lower bathyal to abyssal depths (Fig. 10.3) under fluctuating well oxygenated conditions and during a period of relatively high (for the section) sediment input to the depositional area. The upper portion of the lithofacies is interpreted to be submarine slump deposits (Fig. 10.3).

Interbedded sandstone-mudstone lithofacies (M7b)[upper in section]

Limited information is available for the uppermost interbedded sandstone-mudstone lithofacies at Pahaoa, but based on the available data the lithofacies is interpreted to have been deposited at lower bathyal depths as one, or more likely, multiple olistrostrome type deposits (Fig. 10.3). This interpretation is based on common foreign clasts, some of which are twisted and folded back upon themselves (Fig. 5.8D-F), appearing to be concentrated to horizons within the lithofacies, and the erosional lower contact consisting of broken up sandstone beds and sedimentary dikes (Fig. 5.18I).

10.3.2 Angora Road (Fig. 6.2)

The calcareous mudstone lithofacies (M1b), siliceous mudstone lithofacies (M2b) and “Waipawa Black Shale” lithofacies (M3) at the Angora Road section were

likely deposited at outer shelf to upper slope depths, with the "Waipawa Black Shale" lithofacies likely deposited near the slope break (Fig. 10.3) (Killops et al., 2000) under variable redox conditions ranging from slightly suboxic and bordering on oxic, to Mo-limited euxinic or intermittently euxinic (Fig. 6.13f). The depositional area is interpreted to have been receiving a relatively moderately high terrestrial sediment input compared to other studied sections (Fig. 6.13i) which consisted mostly of hemipelagic sedimentation of fine grained clastics (evidenced by a lack of gravites through the logged section). Terrestrial sediment input decreases towards the top of the "Waipawa Black Shale" lithofacies (M3), coincident with the beginning of deposition of the coarser grained sandstone lithotype (S) in oxic conditions (Fig. 6.13f, i). During deposition of the calcareous mudstone lithofacies (M1b) benthic foraminifera resided at the seafloor and variable amounts of calcareous planktic microbiota rained down onto the depositional area (Leckie et al., 1995). During deposition of the siliceous mudstone (M2b) and "Waipawa Black Shale" lithofacies (M3) benthic foraminifera became absent or rare and the influx of calcareous planktic microbiota to the seafloor all but ceased and was replaced by an increased input of algal and terrestrial organic material (Killops et al., 2000).

10.3.3 Tawanui (Fig. 7.2)

Calcareous mudstone (M1c) [lower in section], and sandy mudstone (M4) lithofacies

The calcareous mudstone lithofacies (M1c) and basal sandy mudstone lithofacies (M4) at Tawanui were deposited at upper to middle bathyal depths (Fig. 10.3) (Culver, 2003). Both lithofacies are interpreted to have accumulated in a mostly oxic environment with moderately low sedimentation rates (Fig. 7.14f, i) under a water column normally dominated by siliceous productivity, but with calcareous productivity influential in the calcareous mudstone lithofacies (Fig. 7.14d). Benthic burrowers were common and normal hemipelagic sedimentation occasionally was interrupted by mass gravity flows – identified by their coarser texture, normal grading, laminations, and sharp undulating lower contacts (Fig. 7.3C and 7.10D). The contact between the M1c and M4 lithofacies (Cretaceous-Tertiary boundary) is interpreted to mark the base of one such mass flow and is interpreted as such due to the presence of rip up clasts, normal grading, faint

laminations, and an undulating lower contact with small flame structures (Fig. 7.3E, G). Alternatively the deposit represents a hiatus were sediment was initially reworked and eroded by a gradually waning bottom current.

Siliceous mudstone lithofacies (M2c)

From the sparse data available for the siliceous mudstone lithofacies (M2c) it is interpreted as having much the same depositional environment as the sandy mudstone lithofacies (M4), but its finer grain size may indicate it was more distal from the paleoshoreline.

Calcareous mudstone lithofacies (M1d) [middle in section]

Depth data for the M1d lithofacies were not obtained. It is interpreted to have been deposited under mostly oxic conditions as hemipelagic mud and planktonic debris fell to the sea floor during a general decline in terrigenous sediment input, and increasing calcareous and steady siliceous productivity (Fig. 7.14d, f, h). Benthic organisms colonised and burrowed areas of the lithofacies and glaucony grains occasionally accumulated in the burrowed intervals (Fig. 7.6C).

Muddy greensand lithofacies (M6a)

The muddy greensand lithofacies (M6a) was deposited at bathyal depths (Rogers et al., 2001) during a period of sediment starvation of the sea floor in initially oxic, but becoming suboxic, conditions (Fig. 7.14f, i and 7.15f, i). This interpretation is based on distinctive finger-like burrowing at its lower contact (Fig. 7.6D, E, F), abundant burrowing through the lithofacies itself (Fig. 7.12C, E), and its high glaucony content (Fig. 7.12D, E, F). The overlying water mass at the time appears to have been dominated by siliceous productivity (Fig. 7.14dand 7.15d).

The mode of emplacement is unclear. Laser diffraction particle size analysis suggests reverse grading of the lithofacies, whereas petrographic observations tend to indicate normal grading (Fig. 7.17A and B). This is important when considering whether the unit is a gravite. The petrographic observation of normal grading is favoured slightly here due to the possibility of incomplete disaggregation of the upper, better cemented portion of the lithofacies in the lead up to laser size analysis (see Section 3.3.5). Normal grading is a characteristic of

turbidites and the upper portion of densites (Gani, 2004; Fig. 10.2), however no features resembling the Bouma T_{B-D} divisions were obvious in outcrop, so it is considered unlikely the deposit is a turbidite. A densite does not necessarily show laminations but may have floating outsized clasts in the lower portion of the bed (Gani, 2004). Outsized floating clasts were not observed within the lithofacies, but this could simply be because they were either rare or absent from the flow. Some grains within the lithofacies are quite angular and others have "popcorn" morphology (Fig. 7.13D, E), but it would be expected that these grains would become rounded (Amorosi, 1997) or broken up during transport if they were deposited via a gravity flow mechanism. However, if the transport distance was short it may have been possible for the grains to escape much abrasion. Thus there is evidence in support and in opposition for a sediment gravity flow origin for the greensand lithofacies. To further complicate matters, the deposit could also be the result of a waning bottom current with burrowing responsible for reworking and abrading some, but not all, of the glaucony grains.

A conclusion as to the mode of emplacement of the muddy greensand lithofacies has not been reached based on the results of this study. However, the high concentration of glaucony in the lithofacies coupled with observations outlined above tends to suggest that if the glaucony was not formed *in situ*, then the source area of the glaucony was not far from where it was deposited. Odin and Fullagar (1988) consider the optimum depth for glaucony formation to be at about 200 m, near the top of the slope. They also state that "a common characteristic of glaucony on stable margins and in tectonically active areas is the fact that in both cases it is located at or near the top of a topographic high with a deep-sea basin nearby". On this basis, and on the inference that the glaucony in the lithofacies is at or near its site of formation, the muddy greensand lithofacies may have been deposited on the top or flanks of a topographic high near the upper part of the continental slope.

In summary, the muddy greensand lithofacies is interpreted to have possibly been deposited at bathyal depths upon, or on the flanks of, a submarine high near the top of the slope (Fig. 10.3) as authigenic or perigenic glaucony (see Section 10.3)

during a period of sediment starvation of the sea floor in initially oxic, but becoming suboxic, conditions (Fig. 10.3).

Glauconitic mudstone lithofacies (M5a)

The glauconitic mudstone lithofacies (M5a) is interpreted to have been deposited under moderately low rates of terrigenous sedimentation under a water mass dominated by siliceous productivity (Fig. 7.14d, i and 7.15d, i). Corrosion of the rims of glaucony grains by pyrite (Fig. 7.13G) either indicate that the sediment was deposited under Mo-limited euxinic or intermittently euxinic conditions, and that perigenic glaucony was transported into the depositional area where it began to be corroded, or that Mo-limited euxinic or intermittently euxinic conditions developed after the glaucony grains were deposited (Fig. 7.14f and 7.15f). Deposition upon or near the top of a submarine high on the upper slope (Fig. 10.3) is inferred for this lithofacies based on its close relationship with the underlying muddy greensand lithofacies (M6a).

Calcareous mudstone lithofacies (M1e)[upper in section]

The uppermost calcareous mudstone lithofacies (M1e) is inferred to have been deposited on a continental slope in upper middle bathyal depths of 500-1000 m (Fig. 10.3), proximal to the coastline (Crouch et al., 2003; Sluijs et al., 2008) in conditions bordering between oxic and suboxic as an accumulation of hemipelagic mud and siliceous and calcareous planktonic debris that fell to the sea floor under moderately high terrigenous sediment input (Fig. 7.14f, i).

10.3.4 Lower Mangahouanga Stream (Fig. 8.2)

No paleodepth data were obtained for the lower Mangahouanga Stream section. The depositional environment of this section is difficult to interpret because of the scarcity of good exposure at the time of logging (see Section 8.2) and a lack of micropaleontological data. While all the interpretations of the environments of deposition made in this study are tentative, those of the lower Mangahouanga stream are especially so due to these reasons. Further study of this site is warranted to better illuminate its depositional environment.

The succession is interpreted to have been deposited as hemipelagic fallout of

muddy clastic sediment under some of the highest terrigenous sedimentation rates of all the studied sections, although this drops through the muddy greensand (M6c) and glauconitic mudstone (M5c) lithofacies (Fig. 8.6i). Deposition was initially in suboxic bottom water conditions, but as sedimentation progressed bottom waters became more oxygenated, and eventually oxic (Fig. 8.6f). Surface ocean water productivity above the depositional site is inferred to have been low during the depositional period (Fig. 8.6b).

10.3.5 Akitio River (Fig. 9.2)

The late Paleogene Akitio River section may record a North Island equivalent of the Marshall Unconformity – a prominent hiatus in many Early Oligocene sedimentary sections in the wider New Zealand region that has been linked to major ice build up on the Antarctic continent (see Section 1.2). Paleodepth data for the Akitio River section was not obtained in this study. The section is interpreted to have been deposited under oxic conditions under moderately low, but steadily increasing, terrigenous sediment input. The poor preservation of calcareous planktic microfossils in the section brings into question whether the overlying water column was the source of calcareous the planktic debris, or whether it was transported into the depositional area from elsewhere.

10.4 Specific issues

Data and observations from Chapters 5 to 9 and interpretations from Section 10.3 are used here in an attempt to explain specific characteristics of some of the strata studied.

10.4.1 Deposition of the Waipawa Formation – Angora Road

The Angora Road section has the best exposure of Waipawa Formation of the study sections and its lithologic and geochemical characteristics are used here in an attempt to explain what caused the lithology to become enriched in organic matter (OM). Enrichment of OM in sediments is dependent on a number of contributing factors such as, the presence of a permanently stratified water column in which anoxic bottom water conditions can develop and cause OM enrichment by enhancing OM preservation, changes in biogeochemical cycling, relative sea level, primary productivity, and climate (Werne et al., 2002).

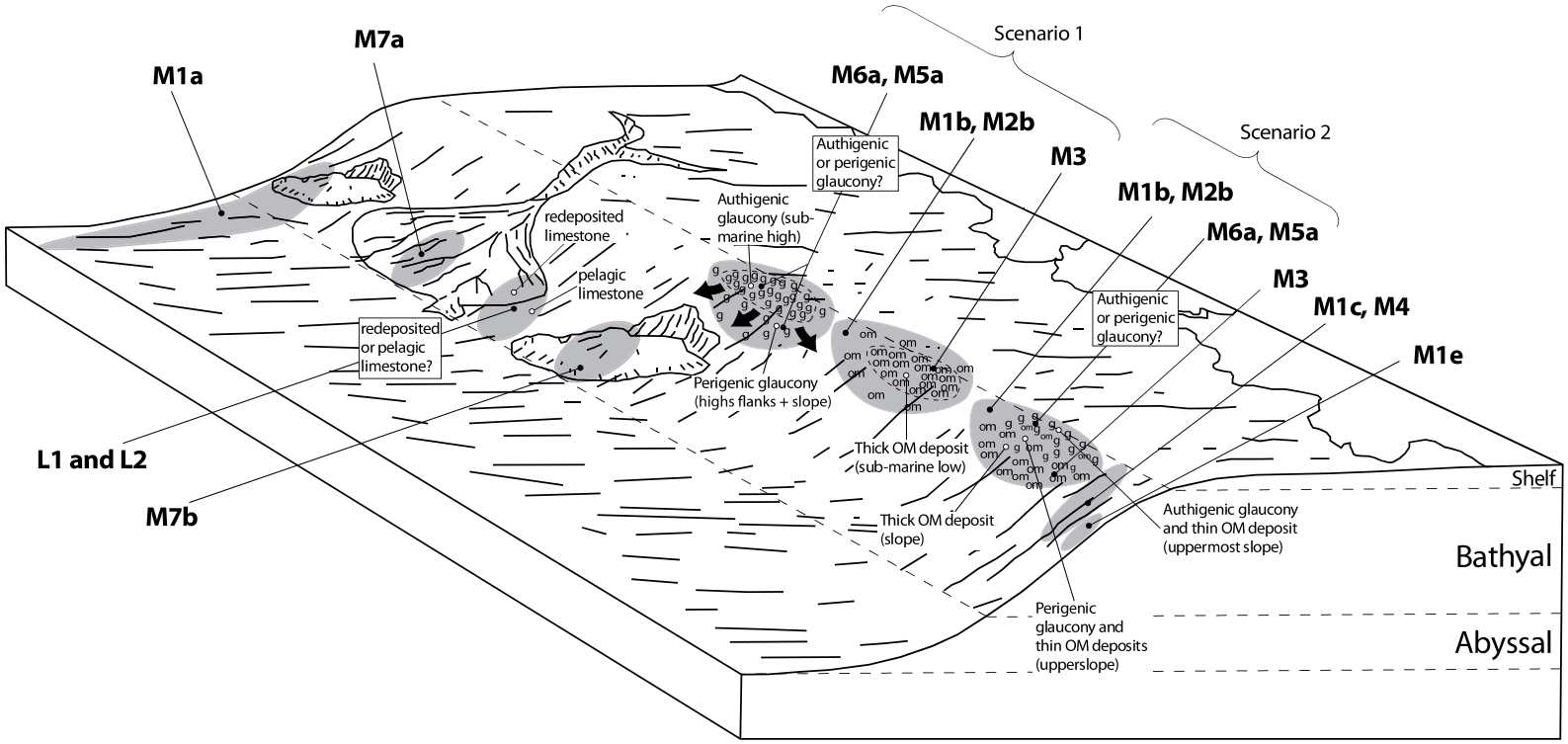

Figure 10.3: The interpreted position of some of the early Paleogene lithofacies identified in this study on the paleoshelf and slope (modified from Selley 1982). Two potential positions are shown for the L1 lithofacies, reflecting the possibility of the unit resulting from either pelagic sedimentation or from redeposition. Two scenarios that attempt to explain the relationship between the organic rich lithologies (M3 lithofacies) and the glauconitic units are shown, and are elaborated on in Fig. 10.5. See Table 4.1 for explanation of lithofacies codes.

Many organic rich lithologies are deposited during transgressions where sediment starvation during rising sea levels can cause condensation of OM rich sediments, which significantly elevates OM concentrations (Werne et al., 2002). Under such conditions the basin can periodically become anoxic and release P preferentially to C, increasing primary production in the surface waters. N is released during oscillations between oxic and anoxic conditions, further stimulating primary productivity. Increased productivity increases the supply of OM, which in turn increases anoxia and nutrient regeneration, so feeding and replenishing the system. Consequently, OM becomes enriched in the accumulating sediments (Werne et al., 2002).

Other organic rich lithologies are deposited under areas of the ocean with high surface water productivity which drives benthic oxygen demand to exceed oxygen resupply, thus causing oxygen depleted conditions and allowing greater preservation of OM (Murphy et al., 2000).

Fig. 10.4 summarises how OM is concentrated in sediment with relation to relative sea level and primary productivity. Variations in relative sea level change sedimentation rates which in turn affect how well preserved or how concentrated OM is in accumulating sediment. As mentioned above, sediment starvation elevates OM concentration but must develop low oxygen conditions and regenerate nutrients order to preserve and enhance the OM concentration (Werne et al. 2002). The process is accompanied by a rise in relative sea level. High sedimentation rates quickly bury the OM, protecting it from near surface degradation but also diluting it (Werne et al., 2002; Potter et al., 2005). High primary production increases OM concentration in sediment but must be accompanied with enhanced preservation under anaerobic conditions in order to maintain high levels of enrichment. Glaciation can enhance upwelling of nutrient rich water, increasing primary productivity, the influx of OM to the seafloor, and expanding the oxygen minimum zone as a result of oxidation of organic carbon (Keller et al., 2001). The combination of processes leads to OM enrichment and the event is accompanied by a eustatic fall in sea level.

At the Angora Road section (Fig. 6.2) deposition of the organic rich mudstone of the Waipawa Formation (equivalent to lithofacies M3) coincides with a low interpreted relative sea level (Fig. 10.6) and a shift from slightly increasing terrigenous sediment input to slightly decreasing terrigenous sediment input (Fig. 6.13i) . This shift in terrigenous sediment input is interpreted as a shift from a falling stage systems tract where terrigenous input increases, to a lowstand systems tract where terrigenous input begins to decrease in the lead up to the transgressive systems tract (Fig. 10.4). The dominant source of OM in the Waipawa Formation at Angora Road is suggested to be from upwelling of nutrient rich waters associated with the Late Paleocene event (LPE), a period of inferred cooling in the Late Paleocene (see Section 1.3). OM enrichment through this part of the succession may be because the climate had insufficiently warmed to have shut off upwelling so that primary production remained high, and the slight decrease in terrigenous sediment supply diluted the sediment less but still was at a sufficient rate to preserve the OM (Fig. 10.4).

The higher content of OM through the middle of the M3 lithofacies may be caused by the degree of surface ocean water productivity and the influx of terrigenous sediment to the seafloor reaching their most favourable ratio for maximising organic matter enrichment in sediments, through maintaining oxygen depletion and OM supply with sufficient primary productivity, and minimising dilution while optimising preservation with a suitable terrigenous supply rate relative to OM influx (Fig. 10.4). Below this optimal ratio the terrigenous sediment influx may have been too high relative to the productivity, leading to progressively more dilution of OM. Above the optimal ratio terrestrial input may have been too low relative to productivity, leading to progressively poorer preservation of OM.

Thus, organic enrichment of the Waipawa Formation at Angora Road is interpreted here to have not been a result of *only* sediment starvation during rising sea level, or *only* high productivity, but rather a combination of the two processes.

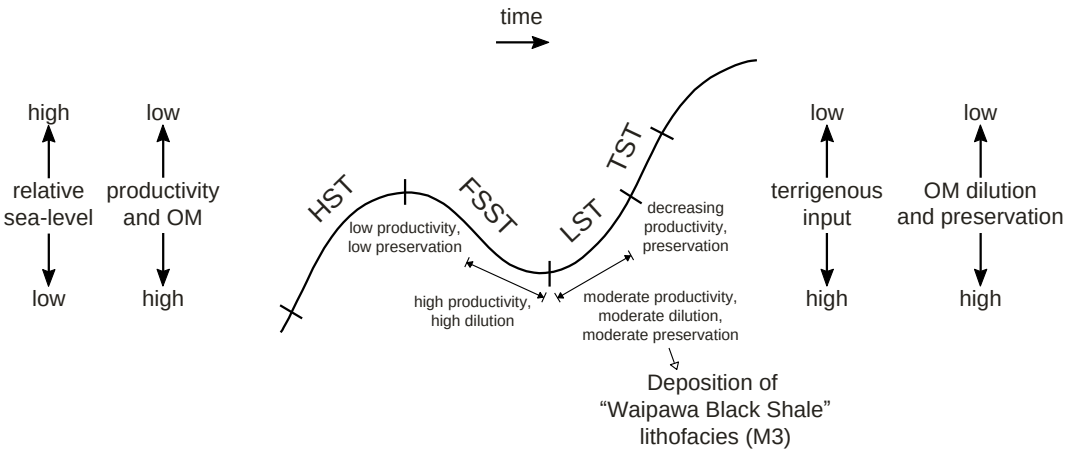

Figure 10.4: Schematic diagram illustrating how organic matter (OM) enrichment in the Waipawa Formation may occur. The effect sea level has on the level of productivity, OM accumulation, terrigenous input, and dilution and preservation of organic matter is also shown (modified from Coe, 2003). HST = highstand systems tact; FSST = falling stage systems tract; LST = lowstand systems tract; TST = transgressive systems tract.

10.4.2 Lateral variations of lithology and redox

All the early Paleogene study sites showed variation between them regarding lithologies, depositional thickness, and sometimes bottom water oxygenation. Specifics singled out for discussion here are the differences in lithology and depositional thickness though the LPE (see Section 1.3) at Angora Road and Tawanui, and differences in redox trends between lower Mangahouanga Stream strata and those at the other "early" Paleogene sections.

Organic matter to glaucony – Angora Road and Tawanui correlative lithologies

Tens of metres of organic rich mudstones of the Waipawa Formation at Angora Road (M2b and M3; Fig. 6.8A) are represented by c. 2 m (exposed) of glaucony rich lithologies with lower organic carbon contents at Tawanui (M6a and M5a; Fig. 7.6A). Rogers et al. (2001) suggested this lateral facies change may be due to deposition of the organic mudstone in areas of dysaerobia and the glaucony rich greensands "in slightly higher energy areas with increased oxygenation and intense bioturbation to provide a mechanism for digestion of OM". This proposal is elaborated on here based on this study's results.

Fine material such as mud and organic matter tends to settle in submarine lows, by-passing highs (Potter et al., 2005). Additionally, Potter (2005) considers oxygen depleted bottom waters to first form in topographic lows because these most readily isolate oxygen-deficient bottom waters from well mixed and oxygenated surface waters. From these points of generation oxygen-deficient bottom waters can expand outwards. In Section 10.3.3 it was suggested that the muddy greensand lithofacies at Tawanui (M6a) was deposited high on the flanks of a submarine high at the top of the continental slope (Fig. 10.3). It is suggested here that the increased concentration of terrigenous and marine organic matter within the siliceous mudstone lithofacies (M2b) and "Waipawa Black Shale" lithofacies (M3) at Angora Road, and the difference in organic matter concentration and deposit thickness of the correlative strata at Tawanui (M6a and M5a), is in part a result of submarine topography.

The depositional area for the "Waipawa Black Shale" lithofacies (M3) at Angora Road (see Section 10.3.2) and for the Waipawa Formation as a whole, may have been outer shelf to upper slope (Fig. 10.3; Killops et al., 2000). Thicker deposits of the formation may be the result of greater accumulation and preservation of OM in topographic lows along the outer shelf and upper slope (Fig. 10.3: Scenario 1; and Fig. 10.5A). Alternatively, thicker deposits may indicate deposition on the upper slope with thinner deposits occurring on the topographically higher outer shelf (Fig. 10.3: Scenario 2; and Fig. 10.5B).

The glauconitic mudstone at Tawanui (M5a) may have been deposited on top of, or on the flanks of, a submarine high near the top of the slope (Fig. 10.3: Scenario 1; and Fig. 10.5A) or it may have been deposited on the outer shelf to uppermost slope (Fig. 10.3: Scenario 2; and Fig. 10.5B). The lithofacies has relatively high organic carbon contents compared to strata from the rest of the Tawanui section (Fig. 7.14j) and it was deposited under Mo-limited euxinic or intermittently euxinic conditions (Fig. 7.14f). This may reflect either that OM accumulated at this location synchronous with its accumulation at the Angora Road site, but there was much less accumulation due to poorer preservation of OM and OM by-passing the topographic high, or low oxygen conditions in topographic lows/upper

slope expanded and advanced up the high and caused a gradual decrease in the oxygenation of bottom waters and an increase in OM preservation (Fig. 10.5A).

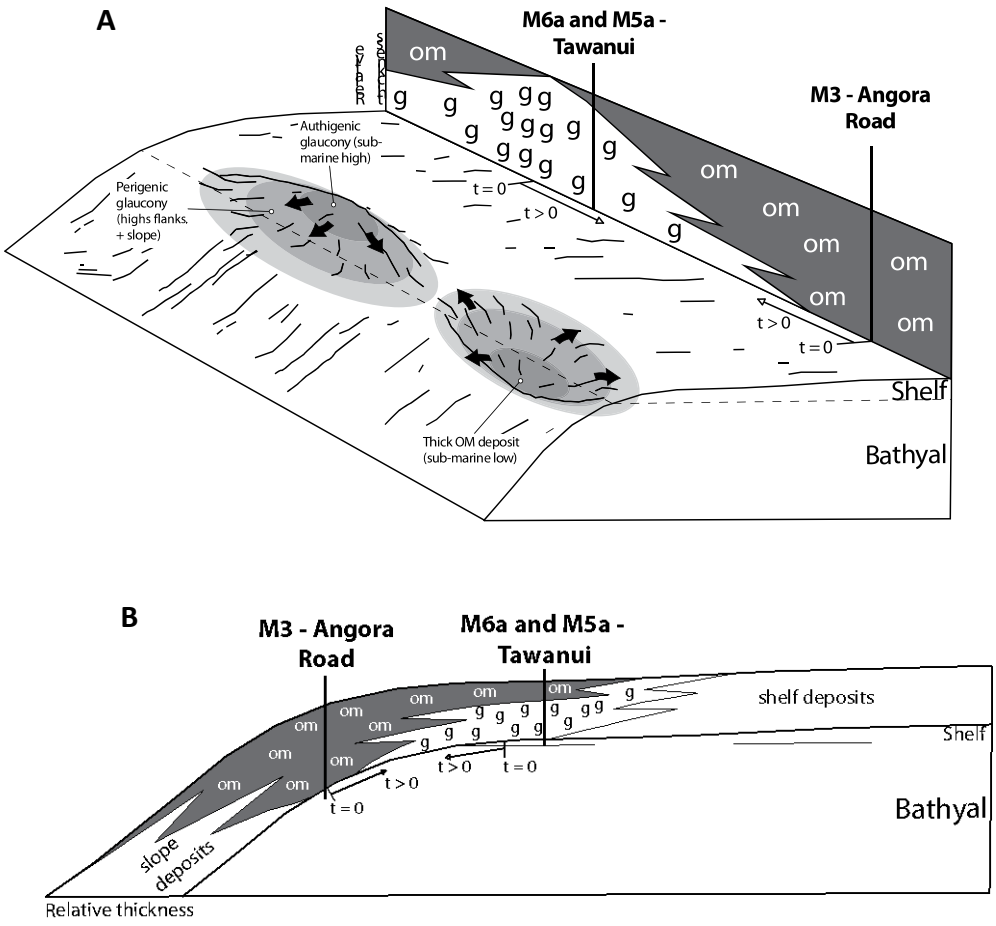

Figure 10.5: Two possible scenarios to account for the lateral transition from thick organic mudstones of the M3 lithofacies to thin, less organic rich, glauconitic lithologies. In "A" thick deposits of organic mudstones accumulate in submarine lows near the top of the slope with glauconitic lithologies accumulating on an adjacent high. Increased oxygen deficiency in the submarine lows causes organic rich deposits to expand out and up the high, prograding over perigenic or authogenic glaucony deposits. The same process occurs in "B" except the topographic low is the upper slope and the adjacent high is the outermost shelf.

Redox conditions at lower Mangahouanga Stream

Discussion involving comparison of strata at lower Mangahouanga Stream with "correlative" strata at other sections is inferred from stratigraphic correlation, not ages, and thus is speculative. This is represented in text by setting the word "correlative" within inverted commas. At lower Mangahouanga Stream the redox trends through the lower two thirds of the section are in stark contrast to trends

observed through "correlative" strata at other study sections. The lower two thirds of the section (M2d, M6b, and M5b) were deposited under suboxic conditions and the strata deposited during the LPE (M6c and M5c) were mostly under oxic conditions during deposition (Fig. 8.6f). At the other study sections the opposite trend is apparent, with lithologies deposited during the LPE experiencing oxygen deficiency during depositon, and the underlying strata being deposited under mostly oxic conditions (e.g. Fig. 7.14f)

The contrasting trends may be a reflection of differences in sedimentation rate and the submarine topography of depositional sites. Like the Angora Road section, the lower Mangahouanga Stream succession may have been deposited in a topographic low on the sea floor and thus was subjected to oxygen deficiency (see above). However, inferred relative falls in sea level during the LPE (see Section 10.5.2) may have enhanced circulation of oxygenated water in the low areas due to well mixed and oxygenated surface waters shifting closer to the sea floor, leading to oxic conditions in strata deposited during the LPE. "Correlative" strata at the Angora Road section are also inferred to have been deposited in a submarine topographic low, yet these lithologies were deposited under oxygen depleted conditions. The conflicting trends may be due to a difference in ocean surface water productivity and the rate of terrigenous input between the two sites, with lower Mangahouanga Stream interpreted to have had a lower productivity water mass overlying it and a higher sediment input compared with Angora Road. Low surface ocean water productivity over the lower Mangahouanga Stream depositional site would produce a low influx of organic matter, and high terrigenous sediment input would dilute the organic matter that did reach the seafloor, thus preventing organic overload and development of oxygen depletion during falls in relative sea level. At Angora Road, oxygen depletion could have been retained during falls in relative sea level because of a higher influx of organic matter to the sea floor, driven by comparatively higher productivity.

This suggested explanation for the redox trends observed at lower Mangahouanga Stream relies upon a comparison of productivity between strata under different oxygen conditions and at different localities to help explain the observed trends.

This is problematic (see Section 10.5.1), and consequently it is not considered a strong hypothesis.

An alternative explanation is that the glaucony rich lithologies deposited during the LPE at lower Mangahouanga Stream (M6c and M5c) are the result of winnowing of sediment by bottom currents. Some evidence for this occurs at the Tawanui section where the muddy greensand lithofacies (M6a) is associated with a decrease in terrigenous input and the palynofacies analyses indicate more distal conditions (Fig. 7.14i, l-q amd 7.15i, l-q). This is consistent with sediment starvation associated with transgression. Likewise, the overlying glauconitic mudstone lithofacies at Tawanui (M5a) is associated with slightly increased terrigenous input and more proximal conditions (Fig. 7.14i, l-q and 7.15i, l-q), which is consistent with increased sediment input during sea level fall and regression. At lower Mangahouanga Stream the LPE also consists of muddy greensand and glauconitic mudstone lithofacies. Palynofacies data suggest that the interval was deposited during a fall in sea level, which, based on observations made at Tawanui would be expected to result in an increase in terrigenous input. This does not occur through the lower half of the interval, and terrigenous input instead decreases with more proximal conditions (Fig. 8.6i, l-q). This trend is difficult to explain, but could reflect strengthening of bottom water currents and winnowing of fine grained terrigenous sediment from coarser glaucony grains, synchronous with lowering of relative sea level. However, in contradiction to this hypothesis, the unit appears to be composed of mainly finer grained material.

Two hypotheses have been given to attempt to explain the depositional characteristics of the lower two thirds of lower Mangahouanga Stream, but both have problems associated with them. Interpretation of the section would benefit from further study of the section and region.

10.4.3 Early Eocene olistrostromic deposits

Reconnaissance biostratigraphic assessment of a foraminiferal sample from the base of the uppermost interbedded sandstone-mudstone lithofacies at Pahaoa (M7b) suggests the lithofacies is Mangaorapan (Dm) in age (Fig. 5.2; H. Morgans pers. comm. 2010). This is similar in age to the base of the Pukemuri Siltstone at

other locations in the Tora block (Field et al., 1997). Consequently the M7b lithofacies may be a lateral equivalent of the Pukemuri Siltstone and, based on descriptions of the Pukemuri Siltstone by Waterhouse and Bradley (1957) and descriptions of M7b from this study, both share an apparent olistrostromic nature (Fig. 5.8D-F). The widespread mass wasting features that these deposits show strongly suggests a major tectonic influence in the region in the Early Eocene.

10.4.4 High terrigenous sediment input –Wanstead Formation

Terrigenous input to the depositional sites at the Pahaoa and Tawanui sections increases in basal Wanstead Formation, and possible redeposited units also occur in basal Wanstead Formation at the Angora Road section, which could suggest a prograding margin or falling relative sea level. However, palynofacies proxies indicate transgressive conditions with the shoreline becoming more distal from the depositional site. The same trend was reported by Sluijs et al. (2008) for the Paleocene-Eocene transition at the Tawanui section and six other sections of a similar age in the Arctic Ocean, Europe, Africa, and North America.

10.5 "Ice in the Greenhouse"

This section is devoted to discussing results directly relevant to the "Ice in the greenhouse" project. These include paleoproductivity trends, regional relative sea level, the significance of "dropstones" in the study area, and the significance of the Akitio River section. Lastly, the implications of the study's findings to the "Ice in the greenhouse" project are considered.

10.5.1 Paleoproductivity

As was touched upon in Chapters 5 to 9, there appears to be a problem associated with using the Ba[exc] and U[ef] paleoproductivity proxies in sections where units have been deposited under changing oxygenated or oxygen depleted conditions, due to the effect oxygen levels have on Ba preservation and U enrichment in sediment (see Section 3.3.4). The need to switch between using Ba[exc] and U[ef] through a section, due to variability in the reliability of each proxy with changing redox, makes it difficult to compare the level of productivity during oxic conditions with those during oxygen depleted conditions because the proxies use different measurement "units".

The LPE coincides with a change in oxygenation of bottom waters at all the "early" Paleogene sections studied. Consequently, the level of paleoproductivity in surface ocean waters for the LPE is difficult to directly compare with underlying and/or overlying strata. This limits the usefulness of the proxies as indicators of a possible increase in productivity associated with invigorated upwelling. Consequently, discussion of paleoproductivity in the early Paleogene sections focuses on the type of productivity (calcareous and siliceous) using the Ca[exc] and Si[exc] proxies.

The most distinctive surface ocean water productivity trend apparent at all the studied sections is that siliceous productivity dominates units deposited during the LPE. Relative increases in siliceous productivity occur at the lower Mangahouanga Stream and Pahaoa sections, with less definite increases occurring at the Tawanui and Angora Road sections because either siliceous productivity is low compared to earlier highs in siliceous productivity (Fig. 7.14D) or followed by an even greater high (Fig. 6.13D). At the Pahaoa section the relative increase and dominance of siliceous productivity appears to be associated with an increase in the abundance of radiolarians (Fig. 5.17D).

Hollis (2002) reported a biosiliceous bloom within Paleocene sediments – of a very similar age to those within the LPE – in a sedimentary succession at ODP Site 1121, on the eastern flanks of the Campbell Plateau. In the modern ocean biosiliceous sediments are usually found beneath relatively cool and productive surface waters (Hollis et al., 2005) and thus the biosiliceous bloom was interpreted as indicating an episode of global cooling, with enhanced upwelling promoting and sustaining widespread biosiliceous productivity. With regard to strata studied in this research, the dominance of siliceous productivity during the LPE is in support of a widespread biosiliceous bloom from 59 to 57 Ma, and may indicate global cooling.

At the Angora Road section there is an increase in siliceous productivity associated with a horizon with a "dropstone" in it (Fig. 6.13D). Based on the relative sea-level curves developed in this study for Angora Road the increase in

siliceous productivity occurs during a period of relatively high sea level (Fig. 10.6), suggesting deposition during a warm and humid climate (Keller et al., 2001). This is in contrast to the trends mentioned above and may be due to enhanced delivery of terrestrially derived nutrients by rivers (Murphy et al., 2000), although the nutrient availability proxy indicates a decrease in nutrient availability through the interval (Fig. 6.13E). These contradictory trends have not been resolved in this study.

10.5.2 Regional relative sea-level trends

Fig. 10.6 presents interpreted relative sea-level curves for the early Paleogene study sections alongside the Haq et al. (1987) eustatic sea-level curves for the Paleocene and part of the Eocene. Fig. 10.7 presents similar information but correlates the relative sea-level curves between sections and with the eustatic sea-level curve. The interpreted relative sea-level curves were constructed using combined field descriptions, sequence stratigraphy concepts, palynofacies data, and terrigenous supply (TRG) data. A brief description of the sequence stratigraphy concepts used and the relevant characteristics of the relative sea-level curves are described below.

Sequence stratigraphy concepts

The core sequence stratigraphic concepts used to interpret relative sea-level trends through the study sections are that periods of low sea level generally coincide with high detrital influx and periods of high sea level are generally characterised by increased carbonate production and low detrital influx (Keller et al., 2001) Sediment starvation during rising sea level results in a condensed bed that can be fossilliferous, bioturbated, and/or rich in glaucony (McRae, 1972; Coe and Church, 2003). Field descriptions were used in conjunction with the terrigenous supply proxy (TRG) to determine the relative level of detrital input.

Relative sea-level trends

All the study sections apart from lower Mangahouanga Stream appear to show three falls in sea level through the Paleocene, consistent with the global eustatic curve (Fig. 10.6 and 10.7). The lower Mangahouanga Stream section records one

fall in relative sea level, but others may be within the unexposed portions of the section (Fig. 10.6e).

At Pahaoa (Fig. 10.6b) the falls in relative sea level are represented by the interbedded sandstone-mudstone lithofacies (M7a), muddy limestone lithofacies (L2a), and siliceous mudstone lithofacies (M2a). More prominently burrowed lithologies are interpreted to represent transgressive conditions, and limestone lithologies (L1 and L2) and calcareous mudstone lithofacies (M1a) are interpreted as high relative sea level deposits.

At Angora Road (Fig. 10.6c) an inferred fall in sea level occurs at the base of the dark grey non-calcareous mudstone bed near the base of the section. Other inferred falls in sea level are associated with the uppermost calcareous mudstone lithofacies (M1b) and the "Waipawa Black Shale" lithofacies (M3). High sea levels are associated with the upper part of M1b and the brown weathered horizon with a "dropstone" in it within M2b (Fig. 6.6). The calcareous beds within the "Waipawa Black Shale" lithofacies are interpreted as recording brief rises in sea level, primarily based on palynofacies trends. The top of the "Waipawa Black Shale" lithofacies is interpreted to record a transgression.

At Tawanui (Fig. 10.6d) falls in relative sea level are associated with the sandy mudstone lithofacies (M4), unburrowed intervals in the M1d lithofacies, and the glauconitic mudstone lithofacies (M5a). Highstands occur immediately above the Cretaceous-Tertiary boundary, in the siliceous mudstone lithofacies (M2c), upper M1d, and in the muddy greensand lithofacies (M6a).

The lower Mangahouanga Stream section (Fig. 10.6e) records a fall in sea level in the M6c and M5c lithofacies followed by a transgression into the overlying calcareous mudstone lithofacies (M1f). A transgression is also interpreted to have occurred across the Cretaceous-Tertiary boundary.

Figure 10.6: Interpreted sea-level curves for the study sections. HS1, 2, 3, and 4 = high stand 1, 2, 3, and 4. LS1, 2, and 3 = lowstand 1, 2, and 3. Haq et al. (1987) eustatic sea-level curve is included for comparison.

Fig. 10.6

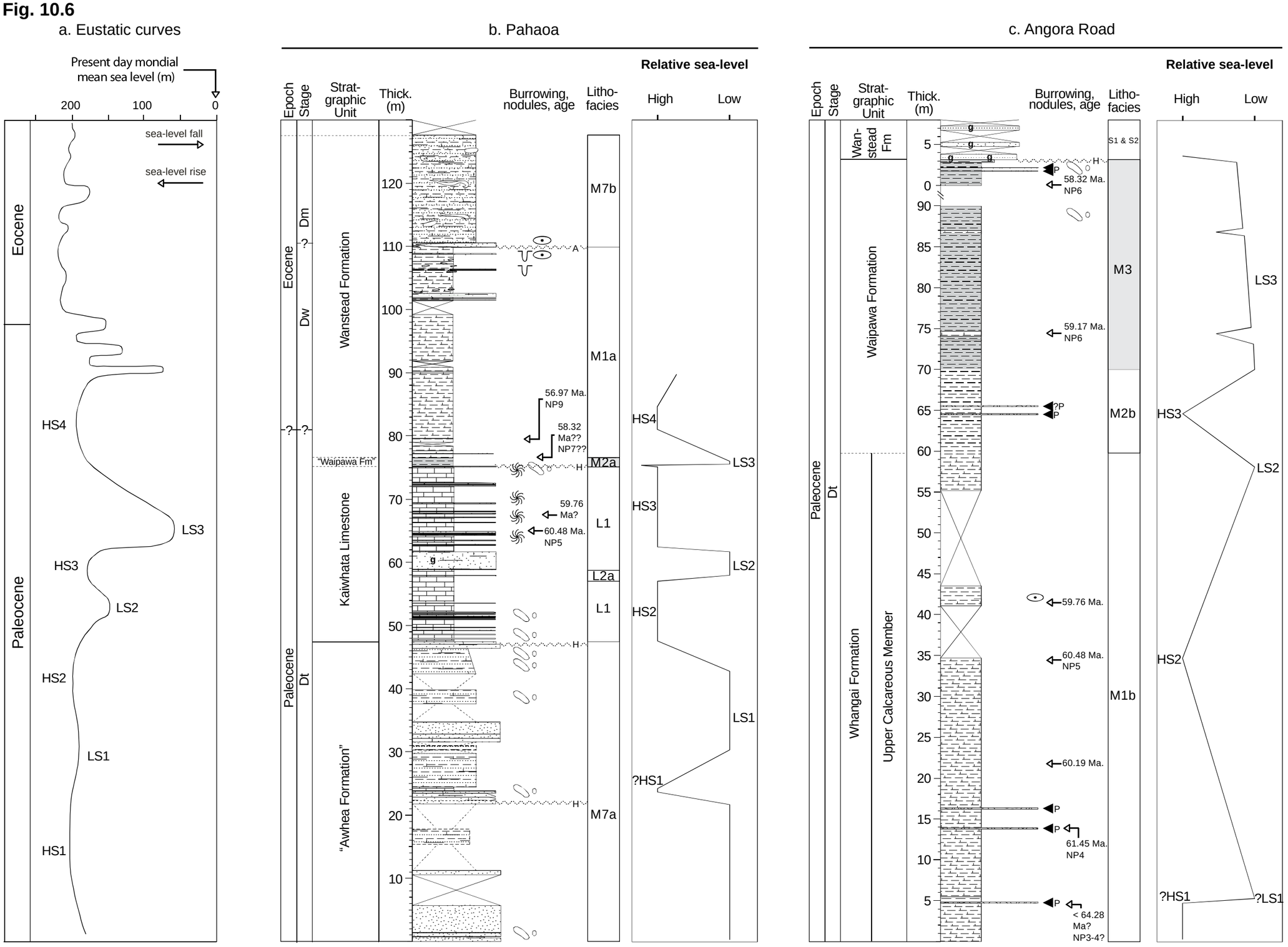
a. Eustatic curves
Present day mondial mean sea level (m)
200
100
0
sea-level fall
sea-level rise
Eocene
Paleocene
HS4
LS3
HS3
LS2
HS2
LS1
HS1
b. Pahaoa
Relative sea-level
Epoch
Stage
Strat-graphic Unit
Thick. (m)
Burrowing, nodules, age
Litho-facies
High
Low
Eocene
Dm
Dw
Wanstead Formation
"Waipawa Fm"
Kaiwhata Limestone
Paleocene
Dt
"Awhea Formation"
M7b
M1a
M2a
L1
L2a
L1
M7a
56.97 Ma.
NP9
58.32
Ma??
NP7??
59.76
Ma?
60.48 Ma.
NP5
A
H
g
HS4
LS3
HS3
LS2
HS2
LS1
?HS1
c. Angora Road
Relative sea-level
Epoch
Stage
Strat-graphic Unit
Thick. (m)
Burrowing, nodules, age
Litho-facies
High
Low
Paleocene
Dt
Wan-stead Fm
Waipawa Formation
Whangai Formation
Upper Calcareous Member
S1 & S2
M3
M2b
M1b
58.32 Ma.
NP6
59.17 Ma.
NP6
59.76 Ma.
60.48 Ma.
NP5
60.19 Ma.
61.45 Ma.
NP4
< 64.28
Ma?
NP3-4?
P
?P
H
g
LS3
HS3
LS2
HS2
?HS1
?LS1

Fig. 10.6 cont.

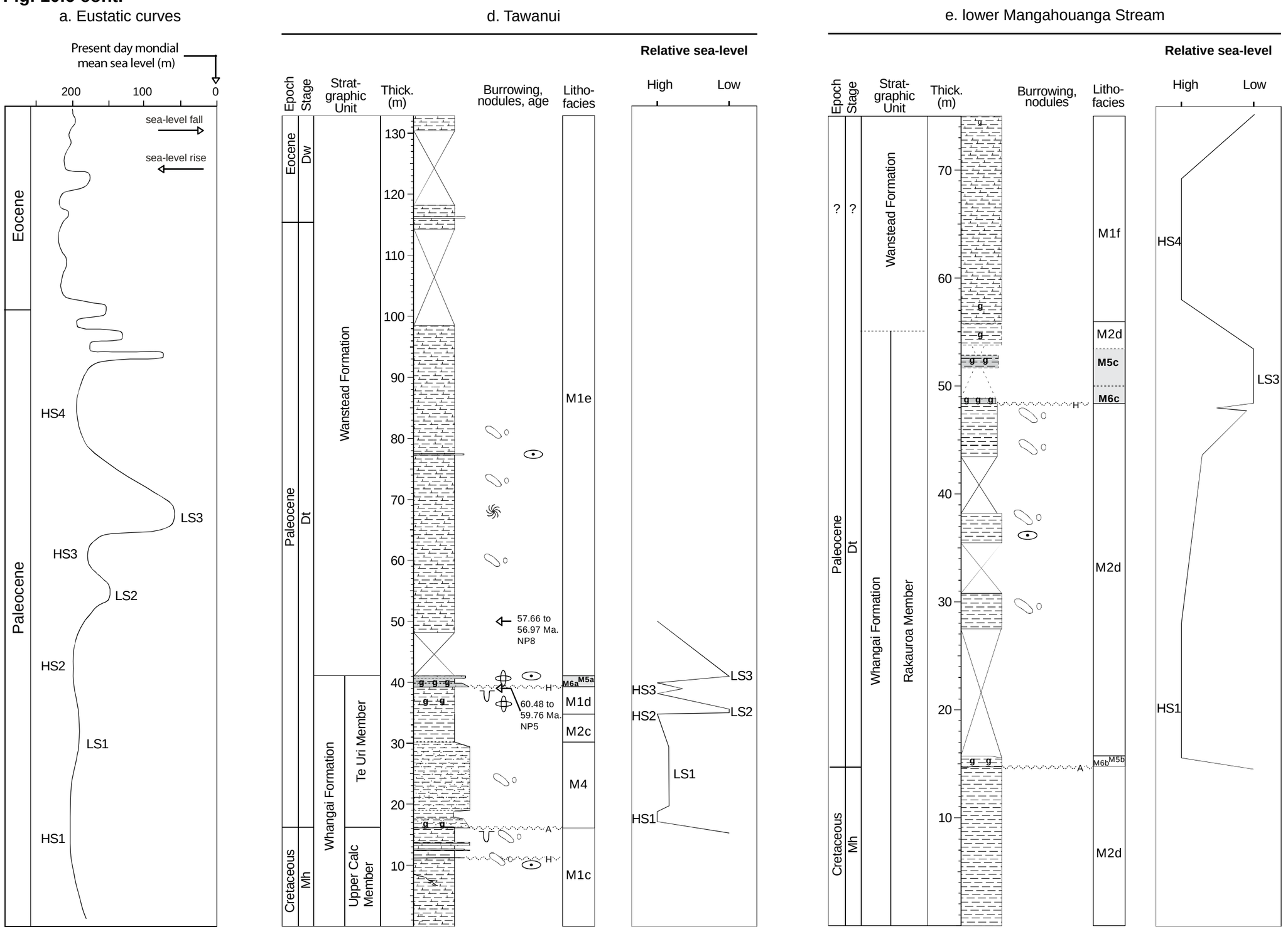
a. Eustatic curves
Present day mondial mean sea level (m)
200
100
0
sea-level fall
sea-level rise
Eocene
Paleocene
HS4
LS3
HS3
LS2
HS2
LS1
HS1
d. Tawanui
Relative sea-level
High
Low
Epoch
Stage
Strat-graphic Unit
Thick. (m)
Burrowing, nodules, age
Litho-facies
Eocene
Dw
Paleocene
Dt
Cretaceous
Mh
Wanstead Formation
Whangai Formation
Te Uri Member
Upper Calc Member
130
120
110
100
90
80
70
60
50
40
30
20
10
57.66 to 56.97 Ma. NP8
60.48 to 59.76 Ma. NP5
M1e
M5a
M6a
M1d
M2c
M4
M1c
LS3
HS3
LS2
HS2
LS1
HS1
e. lower Mangahouanga Stream
Relative sea-level
High
Low
Epoch
Stage
Strat-graphic Unit
Thick. (m)
Burrowing, nodules
Litho-facies
?
?
Wanstead Formation
Paleocene
Dt
Cretaceous
Mh
Whangai Formation
Rakauroa Member
70
60
50
40
30
20
10
M1f
M2d
M5c
M6c
M6b
M5b
M2d
M2d
HS4
LS3
HS1

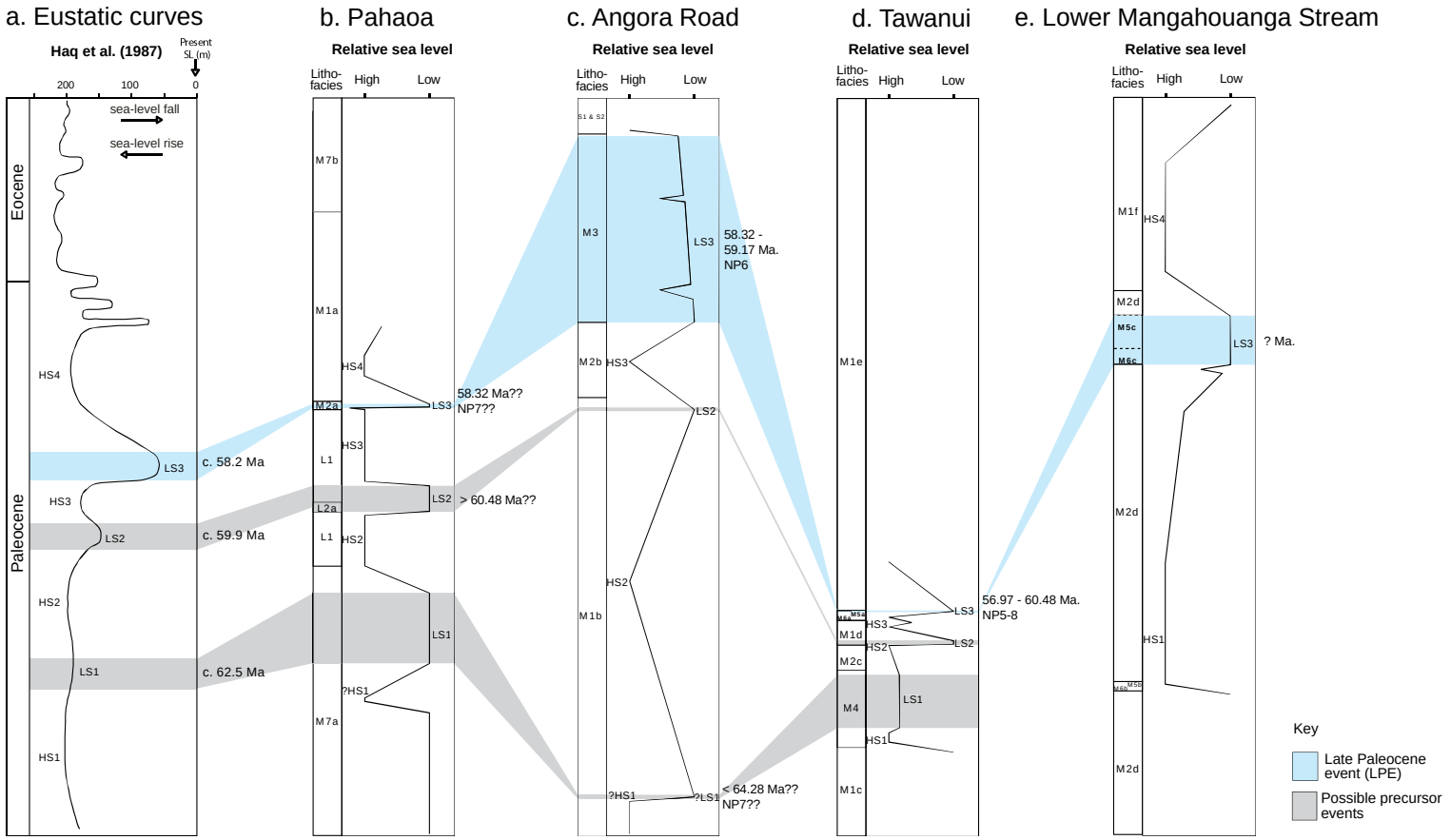

Figure 10.7: Correlation between the eustatic sea-level curve of Haq et al. (1987) and the interpreted sea-level curve for the study sections. Age data for the study sections is from calcareous nannofossil biostratigraphy (this study).

An important feature of the relative sea-level curves presented in Fig. 10.5 and 10.6 is that they all suggest that at all the study sections, lithologies deposited during the LPE were deposited during a time of low sea level. Additionally, at the Pahaoa, Angora Road, and Tawanui sections two earlier falls in sea level may have occurred.

10.5.3 Origin of "dropstones" – Angora Road

Leckie et al. (1995) suggested that "dropstones" observed at the Angora Road section were released to the seafloor from icebergs or ice flows during a period of cool climate or glaciation. They tended to favour an Antarctic derived iceberg origin for the "dropstones". The basis for these interpretations was a lack of evidence for deposition via sedimentary gravity flows or currents competent enough to transport the clasts, delicately preserved laminations that bow beneath the clasts, their exotic nature, evidence for Antarctic glaciation in the Eocene, Northern Hemisphere evidence for possible Paleocene cooling, and the closer proximity of Zealandia to Antarctica during the Paleocene.

Five to six additional pebbly zones have been identified at the Angora Road section in this study (Fig. 6.2). Observations at most of these pebbly zones either support, or don't conflict with, a "dropstone" origin for the clasts. Fig. 6.3H and 6.6B and C in particular support a "dropstone" origin. A possible exception is the lowermost pebbly zone identified in the logged area (Fig. 6.2) which occurs below a bed of differing lithology to the bounding mudstone (Fig. 6.3B, C), which may be a sedimentary gravity flow.

This interpretation of relative sea-level trends through the Angora Road section in this study (Fig. 10.5c) places the deposition of most of the pebbly zones during periods of rising sea level and once in a period of high sea level. This is in disagreement with Leckie et al. (1995) which placed deposition of the "dropstones" during a period of falling and low sea level. However, the occurrence of the pebbly horizons in periods of rising sea level and high sea level does not rule out an ice rafted origin for the clasts. A study of sediments from the Antarctic continental margin by Grobe and Mackensen (1992) indicated that sedimentation of ice rafted debris is higher during interglacials than during

glacials, with the highest rates of sedimentation occurring at the start of interglacials. If the relative sea-level curves presented in this study reflect eustatic sea-level variations then the deposition of "dropstones" during rising sea level and high sea level reflect the greater sedimentation of ice rafted debris during transition from glacial to interglacial conditions.

However, deposition of the "dropstones" from driftwood and floating algae cannot be ruled out and, additionally, Miller (1996) states that "no individual feature is uniquely diagnostic of glacial processes". The repeated occurrence of pebbly zones at the Angora Road section and apparent absence from the other studied sections also brings into question whether the "dropstones" are rather derived from a local source as opposed to ice bergs from Antarctica. Consequently, the full climatic implications of the "dropstones" at the Angora Road section remain uncertain.

10.5.4 Akitio River section – Marshall Unconformity

The probable Oligocene age Akitio River section (Fig. 9.2) was briefly studied because it may record a North Island equivalent of the Marshall Unconformity (see Section 1.2) and thus could possibly be used as a template recording the geochemical and depositional response to an inferred Antarctic glaciation event (Carter and Landis, 1972). Unfortunately, micropaleontologic analysis of calcareous nannofossils was unable to determine a specific Early Oligocene age for the section due to poor fossil preservation. Consequently, whether or not the inferred Marshall Unconformity interval is represented at the Akitio River section remains uncertain and the site cannot be used in this study as a template for Antarctic glaciation. However, it is worth while mentioning some of the trends apparent in the section because some are similar to those that occur in the Paleocene age lithologies deposited during the LPE at the early Paleogene study sections.

The most pronounced trends observed in the Akitio River section are a synchronous increase in siliceous productivity (similar to during the LPE), sea water nutrient availability, and glaucony through the glauconitic mudstone lithofacies (M5d). An increase in productivity associated with increased nutrient

availability is to be expected, but the increase in glaucony does not coincide with a decrease in terrigenous input as might be expected, and the clastic M5d lithofacies is not associated with an increase in terrigenous sediment input as would be expected.

The section as a whole has a low terrigenous sediment input so a decrease may not have been necessary for glaucony formation. Its association with increased productivity may reflect glauconitisation of faecal pellets. Deposition of the clastic glauconitic mudstone lithofacies (M5d) without an increase in terrigenous input may be caused by winnowing of sediment through strengthened bottom currents, where planktic tests could have been preferentially moved out of the depositional area leaving clastics behind. Additionally, the increase in siliceous productivity may indicate an episode of enhanced upwelling promoting and sustaining widespread biosiliceous productivity, which could be linked to cooling climate (Hollis, 2002).

Further investigation of the Akitio River section is needed to determine its significance to late Paleogene climate.

10.5.5 Implications for "Ice in the Greenhouse"

The main implication that this research has for the "Ice in the Greenhouse: a Paleocene record of Antarctic deep-water flow" project (see Section 1.1) stems from the interpretations of relative sea level fluctuations through the Paleocene, and in particular, during the Late Paleocene event (LPE) – a period of inferred cooling (Fig. 1.1). New Zealand was a passive margin at the time so short term sea level fluctuations are considered here to be the result of eustatic sea level changes. This inference is supported by an apparent correlation between the interpreted relative sea-level curves with the eustatic sea-level curves of Haq et al. (1987) (Fig. 10.7). Based on field observations, sequence stratigraphy principles, terrigenous supply, and palynofacies data, sea level is interpreted to have fallen during the LPE. A eustatic fall in sea level implies that water was being locked up on Antarctic as continental ice at this time, associated with a cooling climate.

Additionally, siliceous bioproductivity, organic rich lithologies, and oxygen depleted conditions dominate strata deposited during the LPE. Based on the distribution of biosiliceous sediments in modern oceans, this can be interpreted as indicative of an episode of global cooling, with enhanced upwelling, which promoted and sustained widespread siliceous primary productivity (Hollis, 2002), leading to oxygen depletion associated with degradation of large amounts of organic matter, and deposition of the siliceous and organic rich lithologies that dominate the LPE.

The "dropstones" at the Angora Road section could record episodes of ice rafted sedimentation during interglacials, however, their restricted distribution in the eastern North Island sections and the inability to rule out deposition from driftwood or floating algae means that their use as indicators of fluctuating climate is presently uncertain.

It was not possible to confirm the presence of the Early Oligocene Marshall Unconformity in the late Paleogene Akitio River section due to poor microfossil preservation, and consequently inconclusive definitive age. The section does however show some similarities to the early Paleogene study sections. The glaucony-bearing sandy mudstone unit that has been suggested to mark the Marshall Unconformity is similar to the M6 and M5 lithofacies deposited during, or close to the time of the LPE, and is associated with an episode of increased biosiliceous productivity supportive of climate cooling. The Marshall Unconformity has been linked to major ice build up on the Antarctic continent in the Early Oligocene and the similarities between the LPE lithofacies and the possible expression of the Marshall Unconformity at the Akitio River section lends support for a comparable interpretation to the LPE in the studied strata.

In addition to the interpreted eustatic fall in sea level associated with the LPE, two additional interpreted eustatic falls in sea level prior to the LPE in the study sections, but still within the Paleocene, can also be associated with dominant siliceous productivity and so may record precursor cooling events.

Andrew (2010) investigated the lithological features and geochemical expression of the LPE in sedimentary successions in Marlborough in the South Island and on Campbell Island to the south of New Zealand. He found evidence for increased siliceous productivity, reduced oxygen conditions, winnowing of sea-floor sediments, ice rafted debris, and a greater influx of terrigenous sediment during the LPE. Additionally, he suggests the Teredo Limestone to be a "skin drift" deposited under the influence of intermediate depth contour currents during the Late Paleocene to Early Eocene. He suggested that these features are indicative of a brief period of Antarctic ice sheet growth associated with an episode of global cooling during the LPE, where Antarctic ice sheets may have been responsible for transport and deposition of ice rafted debris, and cooling of surface waters adjacent to the Antarctic continent. Cooling of Antarctic surface waters could have resulted in downwelling and invigorated intermediate depth ocean currents with subsequent reworking of seafloor sediments and upwelling of nutrient rich waters, promoting primary production on the Marlborough paleo-platform.

In summary, the eastern North Island expression of the LPE in the studied sedimentary successions is dominated by siliceous and organic rich lithologies, and may record eustatic falls in sea level, dominance of siliceous bioproductivity, as well as possible "dropstones". These features, as well as lithologic and geochemical similarities to a possible occurrence of the Marshall Unconformity, suggests that the LPE may be associated with cooling and continental ice development on Antarctica. The findings of Andrew (2010) – for increased siliceous productivity, winnowing of sea-floor sediments, ice rafted debris, a greater influx of terrigenous sediment, and a possible "skin drift" in association with the LPE – in Marlborough and Campbell Island supports the interpretation for Antarctic continental ice sheet development during the LPE.

An episode of cooling climate in the "greenhouse world" of the Paleocene, well before the circum-Antarctic sea-way had widened sufficiently to allow thermal isolation of the Antarctic continent, suggests that Antarctic ice sheet growth is less reliant on ocean heat transport than what is currently believed. The LPE occurred during the Paleocene carbon isotope maximum (PCIM, Fig. 1.1), a period inferred to record increased burial of carbon. Andrew (2010) suggests that draw down of

atmospheric CO_2, in association with the PCIM, may be the driver responsible for brief Antarctic glaciation during the LPE, although he notes that the link between the LPE and PCIM requires further investigation.

Chapter 11
CONCLUSIONS

The primary aim of this research has been to investigate whether there is evidence in four early Paleogene eastern North Island sedimentary sections (Pahaoa, Angora Road, Tawanui, and lower Mangahouanga Stream) for marked cooling in New Zealand marine climate in the Late Paleocene, referred to in this study as the "Late Paleocene event" (LPE). The LPE is within the same period as the Paleocene carbon isotope maximum (PCIM; Fig. 1.1), a period inferred to record increased burial of carbon. A variety of techniques have been used in this study, including detailed descriptions of stratigraphy and sedimentology, petrography and mineral studies, elemental and stable isotope geochemistry, palynofacies, and micropalaeontology. The main outcomes relevant to determining New Zealand climate in the Paleocene are:

1) Stratigraphic descriptions and sequence stratigraphy concepts coupled with palynofacies and geochemical data have been used to formulate relative sea-level curves for the studied sections through the Paleocene. Three main falls in sea level are evident, the last of which coincides with the LPE and PCIM (Fig. 10.7). The eastern edge of continental Zealandia facing the paleo-Pacific ocean was a passive margin at this time and the inferred relative sea-level curves appear to correlate with global eustatic sea-level curves, suggesting the variations in sea level in eastern North Island were eustatic. This implies that the volume of water in the oceans decreased at these times, possibly due to the short-term build up of ice on the Antarctic continent.

2) Siliceous bioproductivity and organic rich lithologies dominate the period of inferred sea-level fall associated with the LPE and PCIM, supportive of cooling and widespread upwelling. Siliceous bioproductivity usually also dominates the Paleocene periods prior to the LPE that span the two earlier interpreted falls in sea level.

3) “Dropstone” horizons within Paleocene strata at the Angora Road study section may have been released to the seafloor from icebergs sourced from Antarctica and consequently could record fluctuations between glacial and interglacial conditions. However, the restricted distribution of the “dropstones” in the eastern North Island sections and the inability to rule out deposition from driftwood or floating algae means that their use as indicators of glacial-interglacial conditions is presently uncertain.

4) Because of poor microfossil preservation and consequently inconclusive definitive age, it was not possible to confirm the presence of the Early Oligocene Marshall Unconformity in the late Paleogene Akitio River section. Nevertheless, the glaucony-bearing sandy mudstone unit that has been suggested to mark the Marshall Unconformity is similar to the LPE facies associations in the Paleocene studied sections and is associated with an episode of increased biosiliceous productivity supportive of climate cooling. The Marshall Unconformity has been linked to major ice build up on the Antarctic continent in the Early Oligocene which lends support for a comparable interpretation to the LPE in the studied Paleocene strata.

5) In summary, an interpreted eustatic fall in sea level, dominance of siliceous bioproductivity and organic rich lithologies, as well as possible “dropstones” and lithologic and geochemical similarities to a possible occurrence of the Marshall Unconformity, suggest that the LPE may be associated with marked cooling and continental ice development on Antarctica. As has been noted by other workers, this event may be related to draw down of atmospheric CO_2 during the PCIM. The two interpreted eustatic falls in sea level prior to the LPE in the study sections, but still within the Paleocene, can also be associated with dominant siliceous productivity and so may record precursor cooling events.

Other results from this study of less relevance to interpreting New Zealand marine climate in the Paleocene, but of relevance to wider studies of the eastern North Island early Paleogene sedimentary succession, are as follows:

6) The production of high-resolution stratigraphic columns and accompanying sedimentological logs for the four main study sites between southern Wairarapa and northern Hawke's Bay. The formations represented include the Late Cretaceous to Paleocene aged Whangai Formation, the Paleocene aged Awhea Formation, Waipawa Formation, and Kaiwhata Limestone, and the dominantly Eocene aged Wanstead Formation.

7) The establishment of a comprehensive lithofacies classification for the Paleocene sedimentary deposits in eastern North Island which comprises eleven lithofacies, each of which falls under one of three lithotypes: limestone lithotype, mudstone lithotype, or sandstone lithotype (Table 4.1).

8) The suggested identification for the first time of the previously named Awhea Formation and Waipawa Formation at the well exposed Pahaoa coastal section in eastern Wairarapa.

9) Interpretations of the mode and environment of deposition of the Paleocene sedimentary successions at the study sections, which dominantly consist of hemipelagic upper to lower slope mudstone, but also occasional mass emplaced sandstone and pelagic limestone deposits.

10) A suggested mechanism that led to organic matter enrichment in the Waipawa Formation – a widespread mudstone that, inclusive of its lateral equivalents, is found in many New Zealand sedimentary basins and has been of particular interest in the past because of its high hydrocarbon source potential. Deposition of the unit occurred during low relative sea level, with enrichment of organic matter in the sediment controlled by the balance between the rate of organic matter input versus terrigenous sediment input. The ratio between these two factors seems to have been most favourable for organic matter preservation within the lowstand systems tract, during which terrigenous sedimentation rates were

beginning to decrease (Fig. 10.4) but primary productivity remained sufficient to provide adequate quantities of organic matter to the sediment.

11) A suggestion made by previous workers to explain a lateral facies shift is elaborated upon. The lateral facies shift is from thick deposits of organic rich mudstones of the Waipawa Formation at Angora Road, to relatively thin greensands and glauconitic mudstones of the upper Te Uri Member (Whangai Formation) at Tawanui, a distance of c. 10 km. The variations in thickness and lithology of these deposits are related to submarine topography and site location on the shelf and slope, with the thick organic rich deposits accumulating on the upper slope, or in topographic lows in the vicinity of the shelf-slope break, while thinner deposits enriched in glaucony formed on the top of the slope, or on or near highs at the top of the slope.

12) The proposal of two imperfect explanations for lateral variation in redox conditions at two of the study sections. At the lower Mangahouanga Stream section an interval of greensands and glauconitic mudstone was deposited under oxic conditions, while possible correlative strata at the Pahaoa, Tawanui, and Angora Road sections consist of organic rich mudstone and glauconitic mudstone deposited in oxygen depleted conditions. Possible explanations for the contrasting redox conditions involve either differences in submarine topography, terrigenous sediment input, and surface ocean water productivity at each of the sites, or differences in bottom current strength.

13) The correlation of a prominent Early Eocene olistrostromic unit at the coastal Pahaoa section with an olistrostomic unit farther south (Pukemuri Siltstone), implying widespread submarine mass wasting in the southern Wairarapa area at this time, presumably coincident with a major tectonic event.

14) Confirmation of an anomalous trend noted by previous workers at the Tawanui section, and several other international Paleocene-Eocene

sections, of increased terrigenous sediment input synchronous with the shoreline became more distal to the site of deposition. In this study such a trend was evident in the Wanstead Formation at Pahaoa and Tawanui.

REFERENCES

Amorosi, A. 1997, 'Detecting composition, spatial, and temporal attributes of glaucony: a tool for provenance research', *Sedimentary Geology*, vol. 109, no. pp. 135-153.

Andrew, B. 2010, Sedimentary facies and unconformity analysis of some Paleocene-Eocene sections, Marlborough and Campbell Island, New Zealand, Thesis, The University of Waikato.

Andrews, P. B. 1982, *Revised guide to recording field observations in sedimentary sequences. Report NZGS 102*, New Zealand Geological Survey, Lower Hutt, New Zealand.

Archer, D. & Maier-Reimer, E. 1994, 'Effect of deep-sea sedimentary calcite preservation on atmospheric CO2 concentration', *Nature*, vol. 367, no. pp. 260-263.

Barrett, P. J. 2003, 'Cooling a continent', *Nature*, vol. 421, no. 6920, pp. 221-223.

Bown, P. R. (ed) 1998, *Calcareous Nannofossil Biostratigraphy*, Cambridge University Press, Cambridge.

Carter, R. M. & Landis, C. A. 1972, 'Correlative unconformities in southern Australasia', *Nature*, vol. 237, no. pp. 12-13.

Coe, A. L. 2003, 'Division of the stratigraphical record and geological time', in A. L. Coe (ed.), *The sedimentary record of sea-level change*, Cambridge University Press, Cambridge, pp. 18-33

Coe, A. L. & Church, K. D. 2003, 'Sequence stratigraphy and sea-level change', in A. L. Coe (ed.), *The sedimentary record of sea-level change*, Cambridge University Press, Cambridge, pp. 57-98

Crouch, E. M. 2001, Environmental change at the time of the Paleocene-Eocene biotic turnover, Thesis, Utrecht University.

Crouch, E. M., Dickens, G. R., Brinkhuis, H., Aubry, M., Hollis, C. J., Rogers, K. M. & Visscher, H. 2003, 'The Apectodinium acme and terrestrial discharge during the Paleocene-Eocene thermal maximum: new palynological, geochemical and calcareous nannoplankton observations at Tawanui, New Zealand', *Palaeogeography, Palaeoclimatology, Palaeoecology*, vol. 194 no. pp. 387-403.

Culver, S. J. 2003, 'Benthic foraminifera across the Cretaceous-Tertiary (K-T) boundary: a review', *Marine Micropaleontology* vol. 47, no. pp. 177-226.

DeConto, R. M. & Pollard, D. 2003, 'Rapid Cenozoic glaciation of Antarctica induced by declining atmospheric CO2', *Nature*, vol. 421, no. pp. 245-249.

Field, B. D., Uruski, C. I. & others 1997, 'Cretaceous-Cenozoic geology and petroleum systems of the East Coast Region, New Zealand', *Institute of Geological and Nuclear Sciences monograph*, vol. 19, no. pp. 301 p, 7 enclosures. Lower Hutt, New Zealand: Institute of Geological and Nuclear Sciences Limited.

Folk, R. L. 1954, 'The distinction between grain size and mineral composition in sedimentary rock nomenclature', *Journal of Geology*, vol. 62, no. pp. 344-359.

Folk, R. L. 1962, 'Spectral subdivision of limestone types', in W. E. Ham (ed.), *Classification of carbonate rocks - a symposium*, American Association of Petroleum Geologists Memoir 1, Tulsa, OK, pp. 62-84.

Folk, R. L., Andrews, P. B. & Lewis, D. W. 1970, 'Detrital sedimentary rock classification and nomenclature for use in New Zealand', *New Zealand Journal of Geology and Geophysics*, vol. 13, no. pp. 937-968.

Gani, R. M. 2004, 'From turbid to lucid: a straightforward approach to sediment gravity flows and their deposits', *The Sedimentary Record*, vol. 2, no. 3, pp. 4 - 8.

Gipson, J. M. 1963, 'Ultrasonic disaggregation of shale', *Journal of Sedimentary Research*, vol. 33, no. pp. 955-958.

Grobe, H. & Mackensen, A. 1992, 'Late Quaternary climate cycles as recorded in sediments from the Antarctic continental margin', *The Antarctic paleoenvironment: a perspective on global change. Antarctic research series*, vol. 56, no. pp. 349-376.

Haq, B. U., Hardenbol, J. & Vail, P. R. 1987, 'Chronology of fluctuating sea levels since the Triassic', *Science*, vol. 235, no. pp. 1156-1167.

Henderson, G. M. 2002, 'New oceanic proxies for paleoclimate', *Earth and Planetary Science Letters*, vol. 203, no. pp. 1-13.

Hollis, C. 2002, 'Biostratigraphy and paleoceanographic significance of Paleocene radiolarians from offshore eastern New Zealand', *Marine Micropaleontology*, vol. 46, no. pp. 265-316.

Hollis, C. J., Beu, A. G., Crampton, J. S., Crundwell, M. P., Morgans, H. E. G., Raine, J. I. & Boyes, A. F. 2010, *Calibration of the New Zealand Cretaceous-Cenzoic Timescale to GTS2004*, GNS Science Report

Hollis, C. J., Dickens, G. R., Field, B. D., Jones, C. M. & Strong, C. P. 2005, 'The Paleocene-Eocene transition at Mead Stream, New Zealand: a southern Pacific record of early Cenozoic global change', *Palaeogeography Palaeoclimatology Palaeoecology*, vol. 215, no. pp. 313-343.

Hollis, C. J., Strong, C. P., Rogers, K. A. & Rogers, K. M. 2003, 'Paleoenvironmental changes across the Cretaceous/Tertiary boundary at Flaxbourne River and Woodside Creek, eastern Marlborough, New Zealand', *New Zealand Journal of Geology and Geophysics*, vol. 46, no. pp. 177-197.

Jansa, L. & Hu, X. 2009, 'Cretaceous pelagic black shales and red beds of the North Atlantic: origins, paleoclimate and paleoceanographic implications', in X. Hu, C. Wang, R. W. Scott, M. Wagreich & L. Jansa (ed.), *Cretaceous oceanic red beds: Stratigraphy, composition, origins, and paleoceanographic and paleoclimatic significance*, SEPM (Society for Sedimentary Geology), Tulsa, Oklahoma, pp. 59-72.

JCPDS 1980, *Mineral powder diffraction file: Data book*, International Centre for Diffraction Data, Pennsylvania, USA.

Katz, M. E., Pak, D. K., Dickens, G. R. & Miller, K. G. 1999, 'The source and fate of massive carbon input during the latest Paleocene thermal maximum', *Science*, vol. 286, no. pp. 1531-1533.

Keller, G., Han, Q., Adatte, T. & Burns, S. J. 2001, 'Palaeoenvironment of the Cenomanian-Turonian transition at Eastbourne, England', *Cretaceous Research*, vol. 22, no. pp. 391-422.

Killops, S., Morgans, H. E. G. & Leckie, D. A. 1996, 'The Waipawa Black Shale - A ubiquitous super source rock?' *New Zealand Petroleum Conference*, Ministry of Commerse, pp. 12-21.

Killops, S. D., Hollis, C. J., Morgans, H. E. G., Sutherland, R., Field, B. D. & Leckie, D. A. 2000, 'Paleoceanographic significance of Late Paleocene dysaerobia at the shelf/slope break around New Zealand', *Palaeogeography, Palaeoclimatology, Palaeoecology*, vol. 156, no. pp. 51-70.

King, P. R. 2000, 'New Zealand's changing configuration in the last 100 million years: plate tectonics, basin development, and depositional setting', *2000 New Zealand Petroleum Conference*, Ministry of Economic Development, Wellington, pp. 132-146.

Laird, M. G., Bassett, K. N., Schioler, P., Morgans, H. E. G., Bradshaw, J. D. & Weaver, S. D. 2003, 'Paleoenvironmental and tectonic changes across the Cretaceous/Tertiary boundary at Tora, southeast Wairarapa, New Zealand: a link between Marlborough and Hawke's Bay', *New Zealand Journal of Geology and Geophysics*, vol. 46, no. pp. 275-293.

Leckie, D. A., Morgans, H. E. G., Wilson, G. J. & Edwards, A. R. 1995, 'Mid-Paleocene dropstones in the Whangai Formation, New Zealand-evidence of mid-Paleocene cold climate?' *Sedimentary Geology*, vol. 97, no. pp. 119-129.

Lee, J. M., Begg, J. G. & (compilers) 2002, *Geology of the Wairarapa area*, Institute of Geological and Nuclear Sciences Limited, Lower Hutt, New Zealand.

Lewis, D. W. & McConchie, D. 1994, *Practical Sedimentology*, Chapman and Hall, New York.

Lyons, T. W., Anbar, A. D., Severmann, S., Scott, C. & Gill, B. C. 2009, 'Tracking euxinia in the ancient ocean: a multiproxy perspective and Proterozoic case study', *Science*, vol. 37, no. pp. 507-534.

Martin, W. R. & Sayles, F. L. 2005, 'The recycling of biogenic material at the seafloor', in F. T. Mackenzie (ed.), *Sediments, diagenesis, and sedimentary rocks*, Elsevier, Sydney, pp. 37-65.

Mazengarb, C., Speden, I. G. & (compilers) 2000, *Geology of the Raukumara area*, Institute of Geological and Nuclear Sciences Limited, Lower Hutt, New Zealand.

McManus, J., Berelson, W. M., Klinkhammer, G. P., Johnson, K. S., Coale, K. H., Anderson, R. F., Kumar, N., Burdige, D. J., Hammond, D. E., Brumsack, H. J., McCorkle, D. C. & Rushdi, A. 1998, 'Geochemistry of barium in marine sediments: Implications for its use as a paleoproxy', *Geochimica et Cosmochimica Acta*, vol. 62, no. 21/22, pp. 3453–3473.

McRae, S. G. 1972, 'Glauconite', *Earth-Science Reviews*, vol. 8, no. pp. 397-440.

Miller, J. M. G. 1996, 'Glacial sediments', in H. G. Reading (ed.), *Sedimentary environments: processes, facies and stratigraphy*, Blackwell Science, Oxford, pp. 454-484.

Moore, P. R. 1988, 'Stratigraphy, composition and environment of depostion of the Whangai Formation and associated Late Cretaceous-Paleocene rocks, eastern North Island, New Zealand', *New Zealand Geological Survey Bulletin 100*, vol. no. pp. 1-82

Moore, P. R. 1989, 'Stratigraphy of the Waipawa Black Shale (Paleocene), eastern North Island, New Zealand', *New Zealand Geological Survey record 38*, vol. no. pp. 1-19

Morrow, J. R., Schindler, E. & Walliser, O. H. 1995, 'Phanerozoic development of selected global environmental features', in O. H. Walliser (ed.), *Global events and event stratigraphy*, Springer, Berlin, pp. 53-61

Murphy, A. E., Sageman, B. B. & Hollander, D. J. 2000, 'Black shale deposition and faunal overturn in the Devonian Appalachian basin: Clastic starvation, seasonal water-column mixing, and efficient biolimiting nutrient recycling', *Paleoceanography*, vol. 15, no. pp. 280-291.

Nelson, C. S. 1968, 'Sedimentology of redeposited calcareous and glauconitic beds at Pahaoa, south-east Wellington', *Transactions of the Royal Society of New Zealand*, vol. 6, no. pp. 45-62.

Nelson, C. S. & Cooke, P. J. 2001, 'History of oceanic front development in the New Zealand sector of the Southern Ocean during the Cenozoic - a synthesis', *New Zealand Journal of Geology and Geophysics*, vol. 44, no. 4, pp. 535-553.

Nelson, C. S., Lee, D., Maxwell, P., Maas, R., Kamp, P. J. J. & Cooke, S. 2004, 'Strontium isotope dating the New Zealand Oligocene', *New Zealand Journal of Geology and Geophysics*, vol. 47, no. pp. 719-730.

Nelson, C. S. & Smith, A. M. 1996, 'Stable oxygen and carbon isotope compositional fields for skeletal and diagenetic components in New Zealand Cenozoic nontropical carbonate sediments and limestones: a synthesis and review', *New Zealand Journal of Geology and Geophysics*, vol. 39, no. pp. 93-107.

Odin, G. S. & Fullagar, P. D. 1988, 'Geological significance of glaucony facies', in G. S. Odin (ed.), *Green Marine Clays: oolitic ironstone facies, verdine facies, glaucony facies and celadonite-bearing facies - a comparative study*, Elsevier, Oxford, pp. 295-332

Odin, G. S. & Matter, A. 1981, 'De glauconiarum origine.' *Sedimentology*, vol. 45, no. 28, pp. 611-641.

Perch-Nielsen, K. 1985, 'Cenozoic calcareous nannofossils', in H. Bolli, K. Perch-Nielsen & J. B. Saunders (ed.), *Plankton Stratigraphy*, Cambridge University Press, New York, pp. 427-554.

Potter, P. E., Maynard, J. B. & Depetris, P. J. 2005, *Mud and mudstones: An introduction and overview*, Springer, Berlin, pp. 1-243

Prothero, D. R. & Schwab, F. 1996, *Sedimentary geology. An introduction to sedimentary rocks and stratigraphy*, W. H. Freeman, New York.

Rogers, A. D. 2000, 'The role of the oceanic oxygen minima in generating biodiversity in the deep sea', *Deep-Sea Research Part 2*, vol. 47, no. pp. 119-148.

Rogers, K. M., Morgans, H. E. G. & Wilson, G. S. 2001, 'Identification of a Waipawa Formation equivalent in the upper Te Uri Member of the Whangai Formation - implications for depositional history and age', *New Zealand Journal of Geology and Geophysics*, vol. 44, no. pp. 347-354.

Sageman, B. B., Murphy, A. E., Werne, J. P., Ver Straeten, C. A., Hollander, D. J. & Lyons, T. W. 2003, 'A tale of shales: the relative roles of production, decomposition, and dilution in the accumulation of organic-rich strata, Middle-Upper Devonian, Appalachian basin', *Chemical Geology*, vol. 195, no. pp. 229-273.

Salinger, J. 2001, 'Climate variation in New Zealand and the southwest Pacific', in A. Sturman & R. Spornken-Smith (ed.), *The physical environment - A New*

Zealand perspective, Oxford University Press, Melbourne; Oxford, pp. 131-148

Schiøler, P., Rogers, K., Sykes, R., Hollis, C. J., Ilg, B., Meadows, D., Roncaglia, L. & Uruski, C. 2010, 'Palynofacies, organic geochemistry and depositional environment of the Tartan Formation (Late Paleocene), a potential source rock in the Great South Basin, New Zealand', *Marine and Petroleum Geology*, vol. 27, no. pp. 351-369.

Scholle, P. A. & Ulmer-Scholle, D. S. 2003, 'A colour guide to the petrography of carbonate rocks: grains, textures, porosity, diagenesis', *AAPG Memoir 77*, vol. no. pp. 1-474.

Selley, R. C. 1982, *An introduction to sedimentology*, Academic Press, London, pp. 312.

Sluijs, A., Brinkhuis, H., Crouch, E. M., John, C. M., Handley, L., Munsterman, D., Bohaty, S. M., Zachos, J. C., Reichart, G., Schouten, S., Pancost, R. D., Damste, J. S. S., Welters, N. L. D., Lotter, A. F. & Dickens, G. R. 2008, 'Eustatic variations during the Paleocene-Eocene greenhouse world', *Paleoceanography*, vol. 23, no. pp. 1-18

Smith, A. G. & Pickering, K. T. 2003, 'Oceanic gateways as a critical factor to initiate icehouse Earth', *Journal of the Geological Society*, vol. 160, no. pp. 337-340.

Spielhagen, R. F. & Tripati, A. 2009, 'Evidence from Svalbard for near-freezing temperatures and climate oscillations in the Arctic during the Paleocene and Eocene', *Palaeogeography Palaeoclimatology Palaeoecology*, vol. 278, no. 1-4, pp. 48-56.

Stewart, B., Neall, V., Wallace, C., Palmer, J. & Palmer, A. 1999, 'Field Trip Guides', *Geological Society of New Zealand Inc. Annual Conference*, Geological Society of New Zealand Miscellaneous Publication 107A, Massey University, Palmerston North, New Zealand, pp. 230-248

Turgeon, S. & Brumsack, H. J. 2006, 'Anoxic vs dysoxic events reflected in sediment geochemistry during the Cenomanian-Turonian Boundary Event (Cretaceous) in the Umbria-Marche Basin of central Italy', *Chemical Geology*, vol. 234, no. pp. 321-339.

Tyson, R. V. 1995, *Sedimentary Organic Matter – Organic Facies and Palynofacies*, Chapman and Hall, London.

Vonhof, H. B., Smit, J., Brinkhuis, H., Montanari, A. & Nederbragt, A. J. 2000, 'Global cooling accelerated by early late Eocene impacts?' *Geology*, vol. 28, no. pp. 687-690.

Wagreich, M., Neuhuber, S., Egger, H., Wendler, I., Scott, R., Malata, E. & Sanders, D. 2009, 'Cretaceous oceanic red beds (CORBs) in the Austrian Eastern Alps: passive margin vs. active-margin depositional settings', in X.

Hu, C. Wang, R. W. Scott, M. Wagreich & L. Jansa (ed.), *Cretaceous oceanic red beds: Stratigraphy, composition, origins, and paleoceanographic and paleoclimatic significance*, SEPM (Society for Sedimentary Geology), Tulsa, Oklahoma, pp. 73-90.

Wang, C., Hu, X., Huang, Y., Scott, R. W. & Wagreich, M. 2009, 'Overview of Cretaceous oceanic red beds (CORBs): A window on global ocean and climate change', in X. Hu, C. Wang, R. W. Scott, M. Wagreich & L. Jansa (ed.), *Cretaceous oceanic red beds: Stratigraphy, composition, origins, and paleoceanographic and paleoclimatic significance*, SEPM (Society for Sedimentary Geology), Tulsa, Oklahoma, pp. 13-34.

Waterhouse, J. B. & Bradley, J. 1957, 'Redeposition and slumping in the Cretaceo-Tertiary strata of S.E. Wellington', *Transactions of the Royal Society of New Zealand*, vol. 84, no. pp. 519-548.

Wedepohl, K. H. 1971, 'Environmental influences on the chemical composition of shales and clays', *Physics and Chemistry of the Earth*, vol. 8, no. pp. 305-333.

Weedon, G. P. & Hall, I. R. 2004, 'Neogene palaeoceanography of Chatham Rise (Southwest Pacific) based on sediment geochemistry', *Marine Geology*, vol. 205, no. pp. 207-225.

Werne, J. P., Sageman, B. B., Lyons, T. W. & Hollander, D. J. 2002, 'An intergrated assessment of a "type euxinic" deposit: evidence for multiple controls on black shale deposition in the middle Devonian Oatka Creek Formation', *American Journal of Science*, vol. 302, no. pp. 110-143.

Zachos, J. C., Pagani, M., Sloan, L., Thomas, E. & Billups, K. 2001, 'Trends, rhythms, and aberrations in global climate 65 Ma to Present', *Science*, vol. 292, no. 686 (2001), pp. 686-693.

Appendix A

GEOLOGICAL TIMESCALE AND CALCAREOUS NANNOPLANKTON ZONES

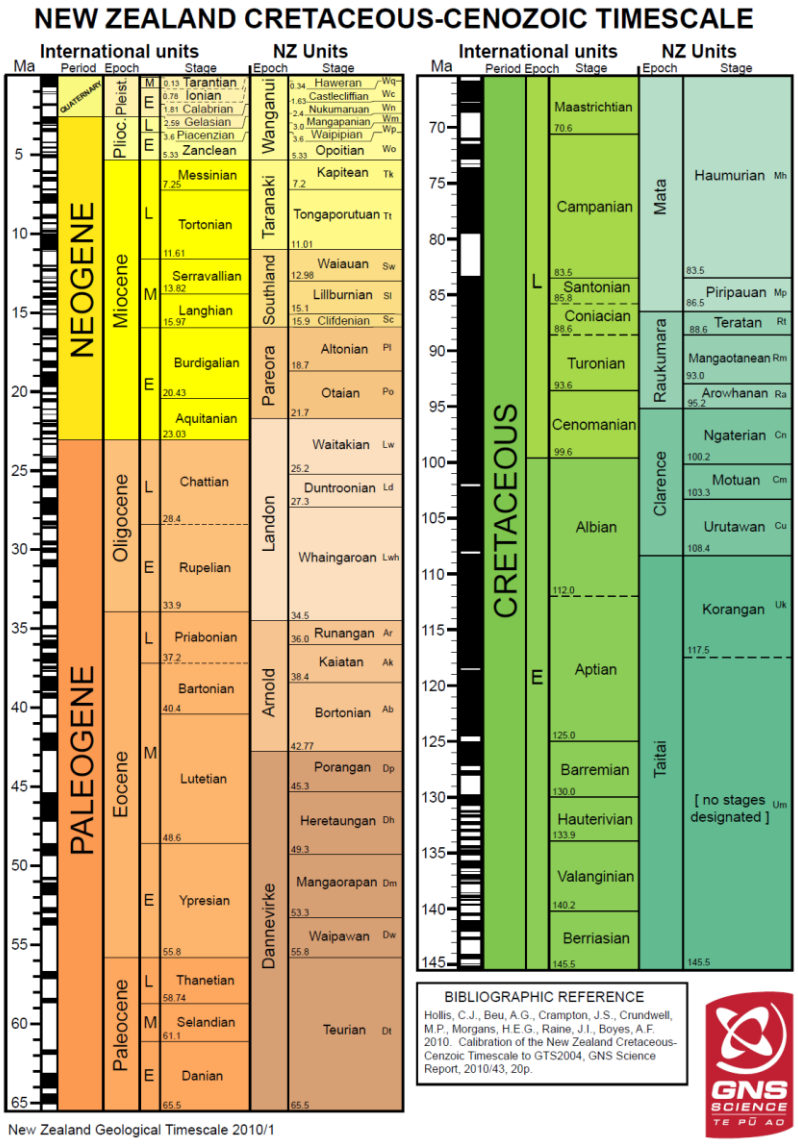

Figure A1: New Zealand Cretaceous-Cenozoic timescale (Hollis et al., 2010).

Note on nomenclature

In text use of official epoch subdivisions is denoted by capitalisation of the subdivisions leading letter e.g. Early Paleocene. The leading letter of New Zealand stage subdivisions are lower case e.g. lower Teurian. Unofficial subdivisions are set within inverted commas and are given a lower case leading letter e.g. "middle" Oligocene.

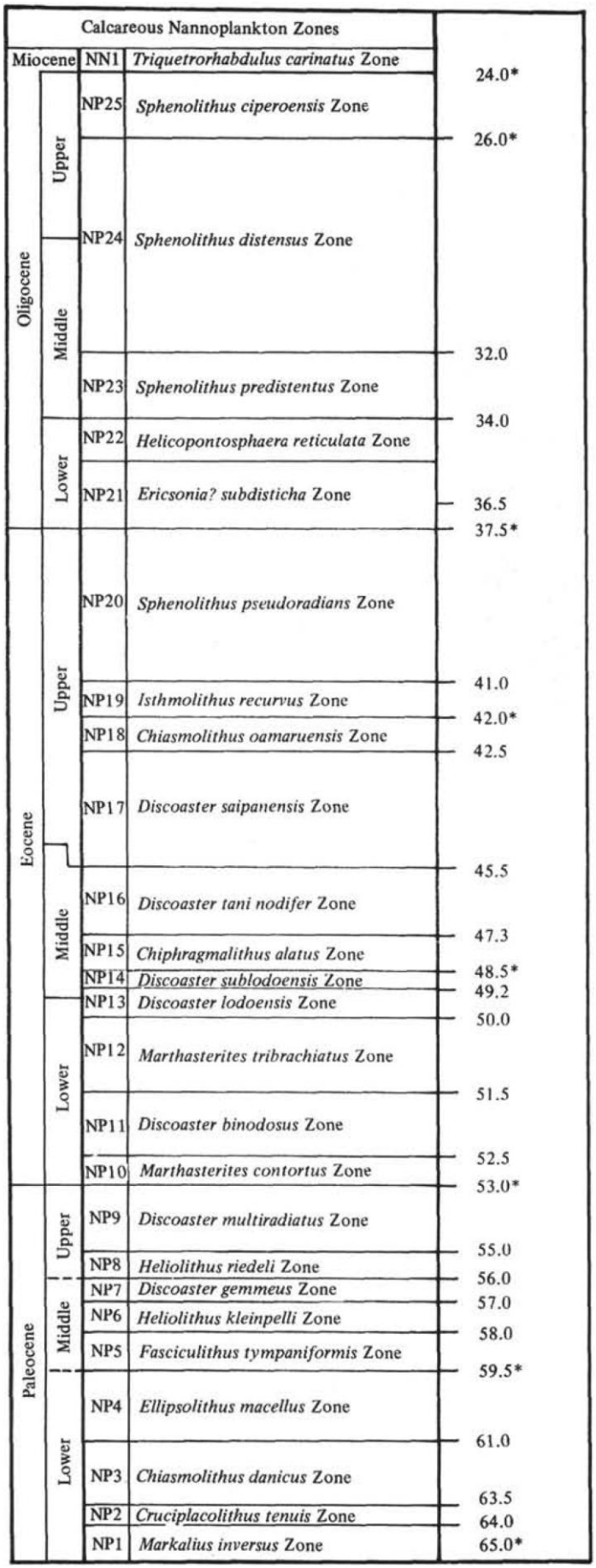

Figure A2: Calcareous nannoplankton zones used in this study (Martini, 1971).

Appendix B

STRATIGRAPHIC COLUMN KEY


Well bedded.


Faintly bedded.


Graded bedding.


Prominant laminations in general.


Faint laminations in general.


No apparent bedding; massive.


Churned, burrowing, mottling, bioturbation.


Burrowing.


Lensoidal/ovular burrows.


Zoophycus.


No burrowing.


Concretions and nodules in general.


Vein, dike.


Megaclasts, rafted blocks, etc; often associated with slumped sediments and debris flows.


Rip-up clasts, flame structures.


Flute casts.

Glauconitic lithology


Calcareous lithology


Micritic limestone.


Muddy limestone.


Mudstone.


Muddy Sandstone


Sandy mudstone.


Interbedded sandstone-mudstone


Massive Sandstone.


Pebbly mudstone.

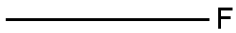

Fault

Sharp contact

Gradational contact

Inferred angular unconformity

Inferred hiatus

Appendix C

PAHAOA DETAILED STRATIGRAPHIC COLUMN

Stratigraphic Column: Pahaoa - Overview

Column No: 1:1

Region: Wairarapa, New Zealand

Location: PAHAOA. Measured sections located on coastal exposures North of Pahaoa River, on Glendhu Station.

Logged by: Michael Tayler, Carrie Hopkirk

Date: 13-17 (day) 12 (month) 2009 (year)

and:

GPS base:

GPS top:

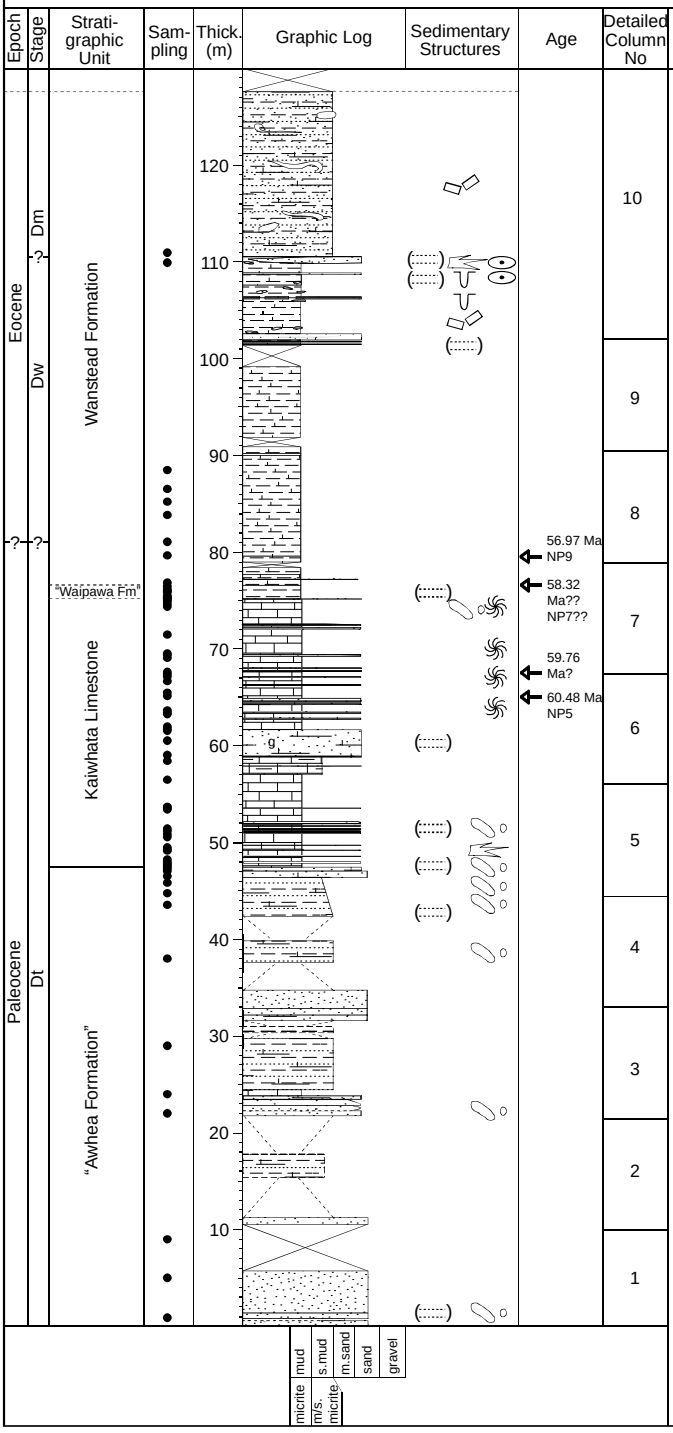

- 110.55 to ~127 m Interbedded calcareous sandstone-mudstone: Dark grey, well indurated, possibly glauconitic, calcareous, cm to mm interbedded sandstone-mudstone. The bedding has been folded in places and there are foreign clasts of various lithologies. Some clasts appear to be muddy mictritic limestones that have been compressed into lenses and smeared, twisted, and folded back over themselves. Other clasts appear to be of the same lithology as the matrix, and others are sandstones. Clasts can be very large (4.4 x 0.55 m). It appears that the areas of distorted matrix and clasts may form horizons beween non-distorted matrix. This would need to be verified.

- 89.04 m Transition from calcareous striped mudstone to interbedded calcareous sandstone-mudstone: The contact between the calcareous striped mudstones and the interbedded sandstone-mudstone is sharp and occurs above a thick broken up sandstone bed. A few phosphate/pyrite nodules are at the contact. Sedimentary dikes and broken up and distorted beds are present in the strata below the contact.

- 79.7 to 89.04 m Calcareous striped mudstone: The striped mudstones are dominantly red and green (with minor grey), moderately indurated, massive, and calcareous. The colours form continuous and semi-continuous parallel to semi-parallel alternating stripes. The contacts between some of the stripes undulate and within a single stripe thin streaks of another colour are occasionally observed. The stripes are sometimes patchy. The stripes are more distinct and patchier when they are within the inter-tidal zone. The colour and intensity of the stripes changes through the sequence, with a greater proportion of green mudstones at the base, more red to light red mudstones through the middle, and dark red mudstone dominate the upper portion. The redder upper portion of the succession is more susceptable to erosion, and it has a number of horizons where the coloured stripes had been folded and become inter-twined with one another. These horizons often include foreign clasts and appear slumped. Broken up and intact sandstone beds occur in the upper portion of the succession.

- 75.09 to 79.7 m Non-calcareous dark mudstone and transition to calcareous striped mudstone: The dark mudstones above the limestone are generally dark grey, dark green, or green grey in colour. They are non-calcareous, often laminated, and often have gradational contacts. Some beds have sharp contacts and of these some of the contacts undulated. It appears that there are slight variations in grainsize through the sequence, with some beds having a more frittery weathered surfaces that others. The upper part of the sequence grades into lighter coloured, calcareous mudstone which appears to grade into the striped calcareous mudstone sequence. The gradual transition is interrupted near the top of the calcareous mudstones by a short interval of highly distorted, slumped striped mudstones.

- 75.09 m Transition from limestone dominated sequence to non-calcareous dark mudstone: The transition from micritic limestone to the non-calcareous dark mudstone succession is sharp. The limestone flag immediately below the contact is burrowed to about the same degree as other underlying burrowed limestone flags. Immediately above the contact lies a 10 cm thick bed of non-calcareous slightly sandy mudstone and moderatly muddy sandstone. The bed has large voids infilled with white powdery loose sand (probably burrows) and a sharp upper contact with the overlying dark non-calcareous mudstones.

- 47.54 to 75.09 m Flaggy micritic limestone with occasional calcareous sandstone and mudstone beds: The limestone succession is generally white, well indurated, flaggy, massive with trace fossils common through some flags (especially at the base of the succession), calcareous, and micritic. Occassional beds of blue-green-grey, well to very well indurated, massive, glauconitic, calcareous fine sandstone are spread throughout the succession. Occassionally the sandstones grade upwards into mudstone. A thick, green-grey, well indurated, massive through its lower two thirds and laminated in its upper third, slightly glauconitic, calcareous fine sandstone bed occurs approximately midway throught the limestone succession.

- 44.27 to 48.1 m Transition from calcareous interbedded sandstone-mudstone to limestone dominated sequence: Towards the top of the bedded sandstone and mudstone succession the rock appears to fine upwards. This is accompanied by a gradual increase in the thickness of the bedding, a possible lighting of the rock colour, and an increase in the intensity of burrowing. This gradual change is abruptly interrupted by a coarser laminated sandstone which grades upwards into an intensely burrowed sandstone, which in turn grades into burrowed micritic limestone.

- 0 to 44.27 m Calcareous interbedded sandstone-mudstone: The succession consists of cm to dm bedded, well indurated, often calcareous, alternating light grey slightly glauconitic medium sandstone and dark grey mudstone. The medium sandstones have a brown weathered surface and the mudstones a dark grey weathered surface when wet. When dry they both have a light grey weathered surface. There are intervals of generally lighter grey sandstone and mudstone beds. Some beds are highly burrowed and others are laminated and can have sharp lower and gradational upper contacts. There are minor limestones near the base of the succession and a number of thick (up to ~4 m), non-calcareous, sandstone beds spread throughout the succession.

Stratigraphic Column: Pahaoa - Detailed Log

Column No: 1:10

Region: Wairarapa, New Zealand

Location: PAHAOA. Measured sections located on coastal exposures North of Pahaoa River, on Glendhu Station.

Logged by: Michael Tayler, Carrie Hopkirk

Date: 13-17 (day) 12 (month) 2009 (year)

and: (day) (month) (year)

GPS base:

GPS top:

Epoch	Stage	Strati-graphic Unit	Sample No	Thick. (m)	Graphic Log	Sedimentary Structures	Age	Description
Paleocene	Dt	"Awhea Formation"	MT4.31	1–9				**- 5.87 to 10.77 m Very poorly exposed.** **- 0 to 5.87 m Sandstone:** Thick beds of sandstone with a brown weathered surface. Thin dark moderately muddy sandstones overlie the two lower most sandstones. The lowest muddy sandstone is burrowed and the higher muddy sandstone is laminated.

mud | s.mud | m.sand | sand | gravel

micrite | m/s | micrite

Stratigraphic Column: Pahaoa - Detailed Log

Column No: 2:10

Epoch	Stage	Strati-graphic Unit	Sample No	Thick. (m)	Graphic Log	Sedimentary Structures	Age	Description
Paleocene	Dt	"Awhea Formation"		21 20 19 18 17 16 15 14 13 12 11	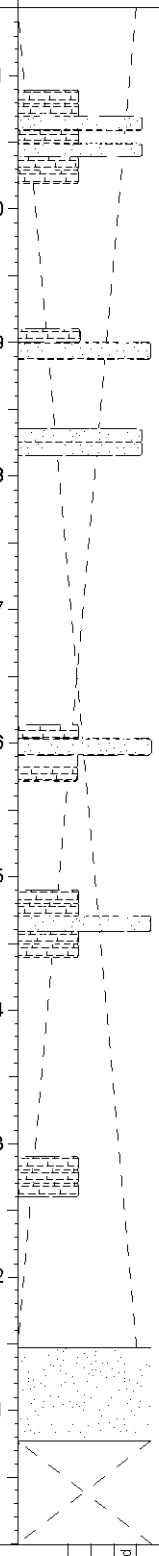			**- 10.77 to 22.17 m Poorly exposed:** Sequence appears to predominantly consists of dark, mudstones, with minor beds of weathered brown sandstones.

Stratigraphic Column: Pahaoa - Detailed Log

Column No: 3:10

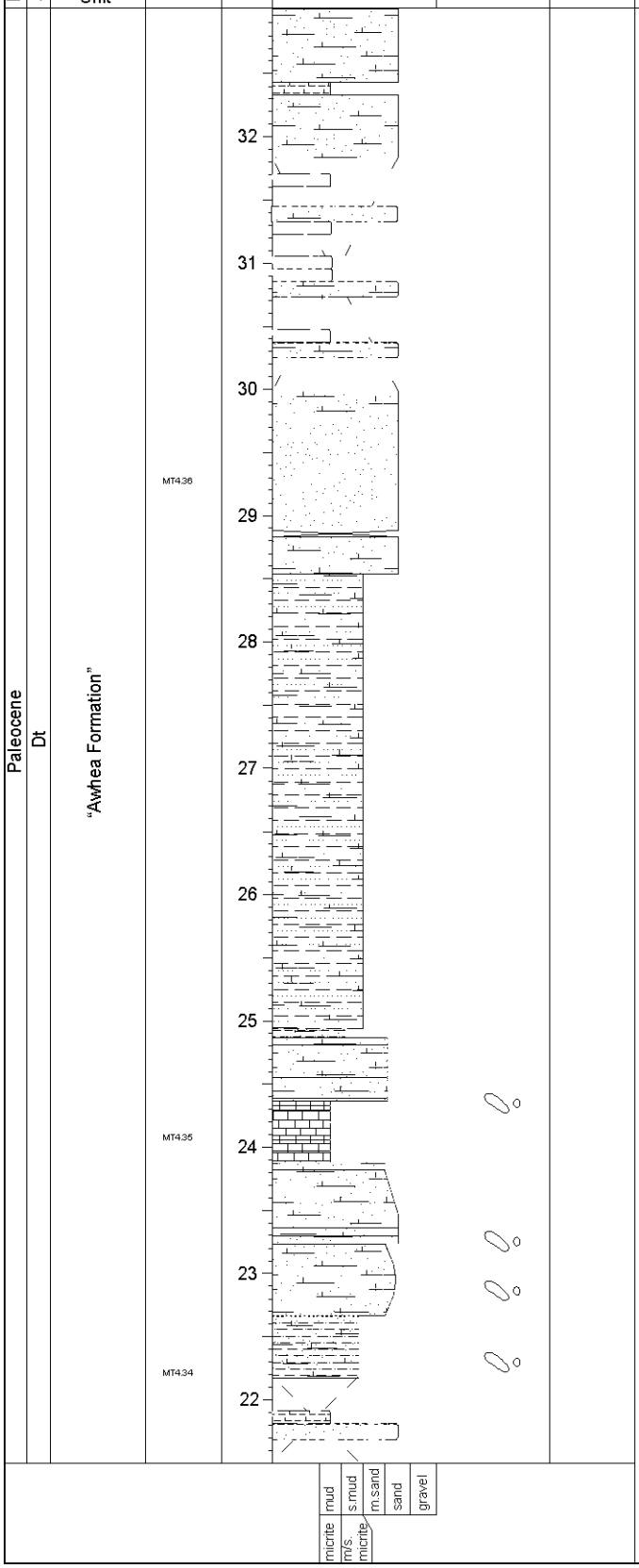

- 32.43 to 33.03 m Calcareous sandstone: Light grey, glauconitic, calcareous sandstone.

- 32.33 to 32.43 m Calcareous mudstone: Dark grey to black, calcareous mudstone.

- 31.83 to 32.33 m Calcareous sandstone: Light grey, glauconitic, calcareous sandstone.

- 29.98 to 31.83 m Poorly exposed: Sequence appears to predominantly consists of beds of dark grey to black, possibly calcareous mudstone, with minor beds of dark grey to black, calcareous sandstone.

- 28.54 to 28.84 m Mostly non-calcareous sandstone: Dark grey-green, glauconitic sandstone. The majority of the bed is non-calcareous. A relatively small portion of the upper part of the bed is calcareous. Upper and lower contacts are unexposed.

- 28.54 to 28.84 m Calcarous sandstone: Medium grey, calcareous, sandstone. Sharp lower and upper contacts.

- 24.94 to 28.54 m Bedded calcareous sandstone and mudstone: Succession of altemating beds of dark grey to black, calcareous mudstone and sandstone. The sandstone weathers to a brown colour throughout the unit. The mudstone weathers to a dark grey colour in the lower 2.3 m of the unit, a light grey colour for a 40 cm interval in the middle of the unit, and a greener colour through the upper part of the unit.

- 24.86 to 24.94 m Calcareous sandy mudstone: Light grey, calcareous, sandy mudstone. Sharp upper and lower contacts. The surface of the rock has distinctive web like veining/burrowing.

- 24.36 to 24.86 m Bedded calcareous sandstone: Interval of dark grey to black, calcareous sandstone. The interval consists of 8 beds with thicknesses of 2-17 cm. The thinner beds are greener in colour. The intervals lower contact is possibly burrowed. The upper contact is sharp.

- 23.88 to 24.36 m Limestone: Interval of light grey, calcareous limestone. The interval consists of 6 beds ranging in thickness from 9-14 cm. The interval has a sharp upper contact and possibly gradational lower contact. The surface of the rock has distinctive web like veining.

- 23.82 to 23.88 m Calcareous sandstone: Dark grey to black, calcareous sandstone. Sharp lower contact, and possibly a gradational upper contact.

- 23.36 to 23.82 m Calcareous sandstone: Dark grey to black, calcareous sandstone in the lower 10 cm. Grades upwards into a light grey, burrowed, calcareous, finer grained sandstone. Sharp lower and upper contacts.

- 23.3 to 23.36 m Calcareous sandstone: Dark grey, intensely burrowed, calcareous sandstone.

- 23.24 to 23.3 m Calcareous sandstone: Dark grey calcareous sandstone. Sharp lower, and possibly sharp upper contact. Upper contact is burrowed.

- 22.64 to 23.24 m Calcareous sandstone: Intensly burrowed, calcareous sandstone. Appears to get coarser throught the middle of the bed. Sharp upper contact and gradational lower contact.

- 22.17 to 22.64 m Calcareous sandy mudstone: Medium grey, well indurated, massive, burrowed, calcareous sandy mudstone. Gradational upper contact, lower contact is unexposed.

Stratigraphic Column: Pahaoa - Detailed Log

Column No: 4:10

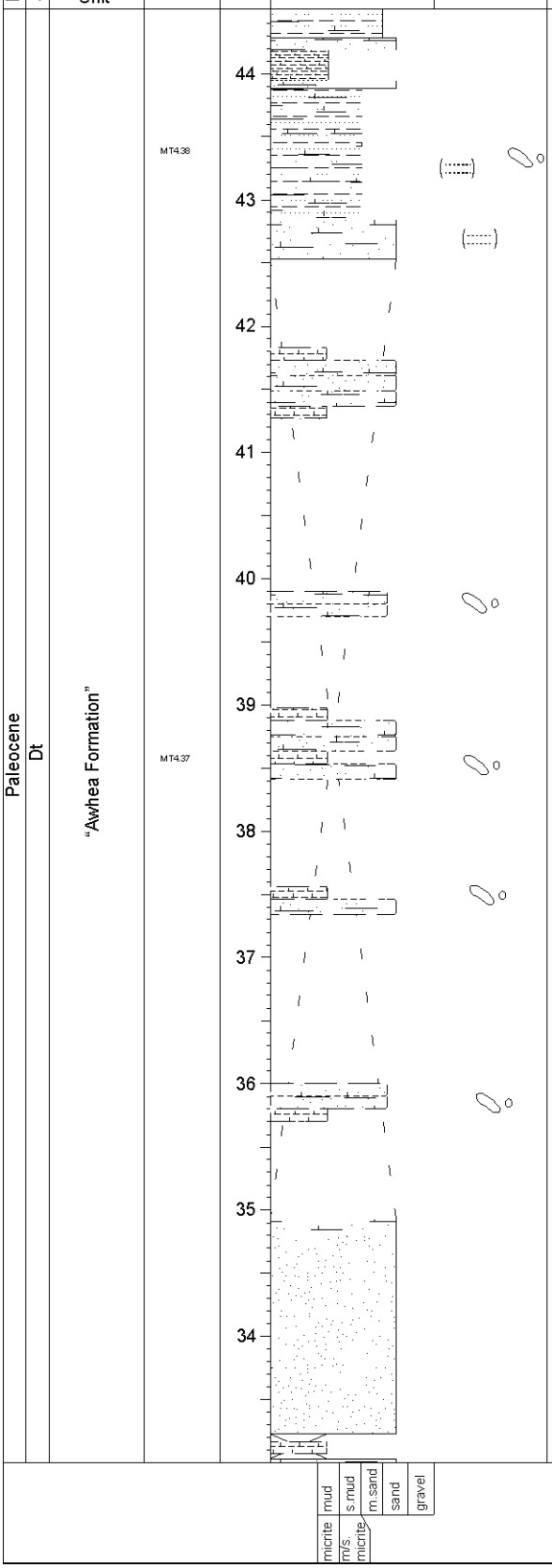

- 44.19 to 44.27 m Calcareous sandstone: Blue-grey to black, calcareous sandstone. Sharp lower contact and gradational upper contact.

- 43.94 to 44.19 m Calcareous mudstone: Dark grey to black, cm bedded, calcareous mudstone.

- 43.79 to 43.94 m Calcareous sandstone: Grey, calcareous sandstone. Sharp lower contact and gradational upper contact.

- 42.84 to 43.79 m Interbedded calcareous sandstone-mudstone: Succession of beds alternating between dark grey to black, calcareous mudstone, and medium grey, calcareous sandstone. The sandstone appears to have sharp lower contacts and gradational upper contacts. The thickest of the sandstone beds has laminations near the base of the bed and burrowing through its upper finer grained portion.

- 42.53 to 42.84 m Calcareous sandstone: Light grey, vaguely laminated, glauconitic, calcareous sandstone.

- 34.93 to 42.53 m Poorly exposed: Succession of beds alternating between dark grey to black, burrowed, calcareous mudstone, and grey to dark grey, laminated, calcareous sandstone. There appears to have been some folding through the interval.

- 33.23 to 34.93 m Mostly non-calcareous sandstone: Light grey, glauconitic sandstone. The majority of the bed is non-calcareous. A relatively small portion of the upper part of the bed is calcareous.

- 33.03 to 33.23 m Poorly exposed: Succession appears to consist of dark grey to black, calcareous mudstone.

Stratigraphic Column: Pahaoa - Detailed Log

Column No: 5:10

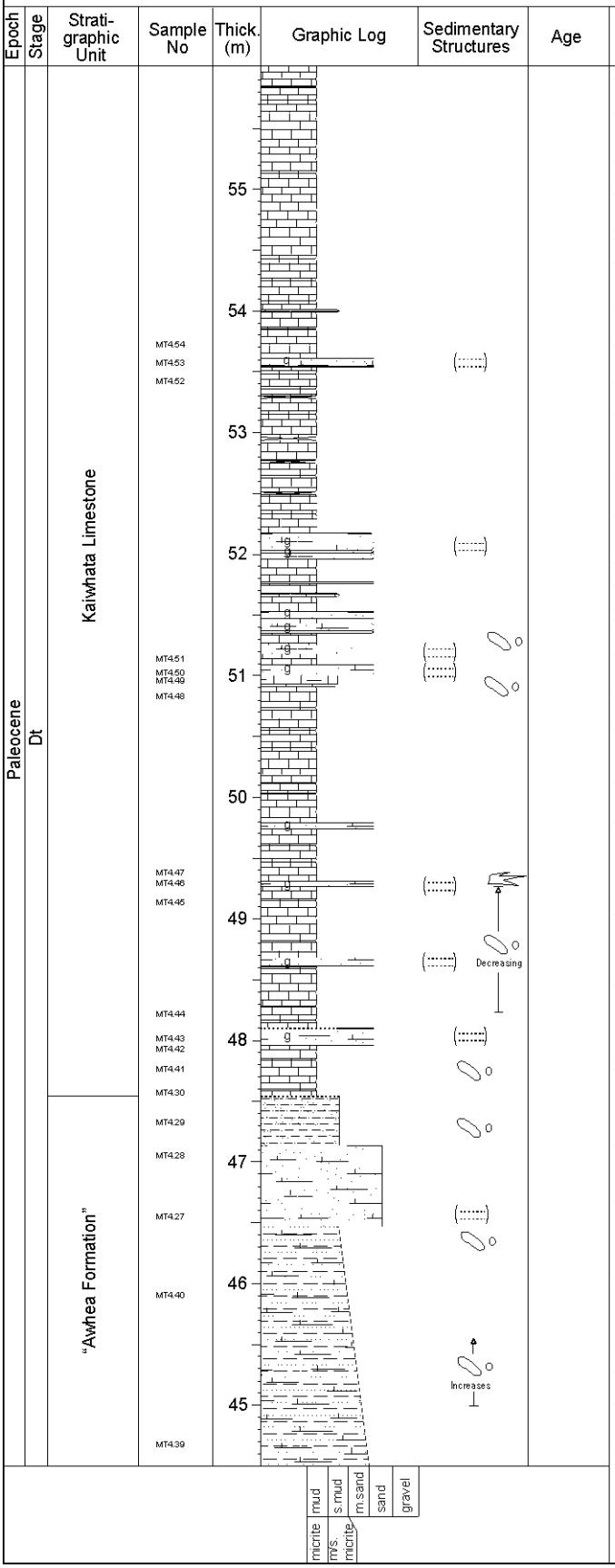

- **53.61 to 57.0 m Limestone:** Creamy white, well indurated, massive, flaggy, calcareous micritic limestone. Weathers to white with brown stains.

- **53.54 to 53.61 m Calcareous sandstone:** Blue-green-grey, well indurated at its base, mostly massive with possibly a laminated base, glauconitic, calcareous sandstone. Grades upwards into a finer grained rock.

- **52.17 to 53.54 m Limestone:** Creamy-white, well indurated, massive, flaggy, calcareous micritic limestone. Weathers to white with brown stains.

- **52.03 to 52.17 m Calcareous sandstone:** Blue-grey, well indurated, massive with a laminated base, calcareous sandstone. Grades upwards into a finer grained sandstone.

- **52.01 to 52.03 m Calcareous sandstone:** Blue-green-grey, well indurated, mostly massive with a possibly laminated base, glauconitic, calcareous sandstone.

- **51.96 to 52.01 m Calcareous sandstone:** Blue-green-grey, well indurated at its base, mostly massive with a possibly laminated base, glauconitic, calcareous sandstone. Grades upwards into a finer grained rock.

- **51.77 to 51.96 m Limestone:** Creamy-white, well indurated, massive, flaggy, calcareous micritic limestone. Weathers to white with brown stains.

- **51.76 to 51.77 m Calcareous sandstone:** Green-grey, poorly indurated, massive, glauconitic, calcareous sandstone.

- **51.53 to 51.76 m Limestone:** Creamy-white, well indurated, massive, flaggy, calcareous micritic limestone. Weathers to white with brown stains.

- **51.35 to 51.53 m Calcareous sandstone:** Three beds of blue-grey, moderately indurated, massive, calcareous sandstone. All beds grade upwards into finer grained rock. All have sharp undulating upper contacts (a micritic limestone bed sits in between the middle and upper beds).

- **51.25 to 51.35 m Limestone:** Creamy-white, well indurated, burrowed, calcareous micritic limestone. Weathers to white with brown stains.

- **51.17 to 51.25 m Calcareous sandstone:** Blue-grey, well indurated, mostly massive with possibly a laminated upper half, calcareous sandstone. Grades upwards into a muddier rock. Sharp undulating lower contact.

- **51.09 to 51.17 m Limestone:** Creamy-white, well indurated, calcareous micritic limestone. Sharp contacts. Appears to grade upwards into a muddy micritic limestone. Weathers to white with brown stains.

- **51.0 to 51.09 m Calcareous sandstone:** Blue-green-grey, well indurated, mostly massive with a laminated base, calcareous sandstone. Grades upwards into a softer rock. Sharp contacts.

- **50.91 to 51.0 m Muddy limestone:** Blue-grey, well indurated, burrowed, calcareous muddy micritic limestone. Sharp contacts. Erodes more easily at its base.

- **49.79 to 50.91 m Limestone:** Creamy-white, well indurated, massive, flaggy, calcareous micritic limestone. Sharp contacts. Weathers to white with brown stains.

- **49.74 to 49.79 m Calcareous sandstone:** Blue-green-grey, well indurated at its base, massive, glauconitic, calcareous sandstone. Grades upwards into a finer grained rock. Sharp lower contact and sharp undulating upper contact.

- **49.31 to 49.74 m Limestone:** Creamy-white, well indurated, massive, flaggy, calcareous micritic limestone. Sharp contacts. Weathers to white with brown stains.

- **49.26 to 49.31 m Calcareous sandstone:** Green-grey, moderately indurated, vaguely laminated in outcrop but massive when fresh, glauconitic, calcareous sandstone. Sharp lower contact and sharp undulating upper contact. Thin sedimentary dikes vein up into the overlying micritic limestone. The dikes extend < 2 cm into the overlying limestone and are approximately 6-7 cm long. They penetrate the overburden at an angle of c. 20 degrees.

- **48.67 to 49.26 m Limestone:** Creamy-white, well indurated, flaggy, variably burrowed (some flags do not appear to be burrowed), calcareous micritic limestone. Trace fossils appear as dark blue-grey to light blue-grey tubes and lenses. Sharp contacts. Weathers to white with brown stains. Burrows weather to a green-brown surface. The flags in this part of the outcrop appear disturbed in one area. Possibly due to faulting or seafloor slumping.

- **48.61 to 48.67 m Calcareous sandstone:** Blue-grey, well indurated, possibly laminated in outcrop but massive when fresh, calcareous sandstone. Sharp lower contact and gradational upper contact. Grades upwards into a blue-grey, poorly indurated, massive, calcareous mudstone. The upper 2 cm of the bed are mudstone.

- **48.1 to 48.61 m Limestone:** Creamy-white, well indurated, flaggy, variably burrowed (some flags are more burrowed), calcareous micritic limestone. Trace fossils appear as dark blue-grey to light blue-grey tubes and lenses. Sharp contacts. Weathers to white with brown stains. Burrows weather to a green-brown surface. One flag grades upwards into a sandier, more burrowed rock.

- **47.96 to 48.1 m Calcareous sandstone:** Blue-grey, well indurated, very vaguely laminated, calcareous, sandstone. Sharp lower contact and gradational upper contact. Upper contact is burrowed. Weathers to a green brown surface.

- **47.54 to 47.96 m Limestone:** Creamy-white, well indurated, flaggy, burrowed, calcareous micritic limestone. Trace fossils appear as dark blue-grey to light blue-grey tubes and lenses. Gradational lower contact, sharp upper contact. Weathers to white with brown stains. Burrows weather to a green-brown surface.

- **47.14 to 47.54 m Calcareous sandy mudstone:** Light blue-grey, well indurated, intensely burrowed, glauconitic, calcareous sandy mudstone. Burrows follow subparallel to the bedding. Gradational upper and lower contacts. Weathers to a light grey colour with patches of brown where the burrows are.

- **46.47 to 47.14 m Calcareous sandstone:** Light grey, well indurated, massive with laminations at the base, glauconitic, calcareous sandstone. The lower 60 cm of the bed weathers to a brown colour.

- **44.27 to 46.47 m Interedded calcareous sandstone-mudstone:** The lower 70 cm of the succession is centimeter bedded and consists of alternating beds of dark grey to black, burrowed, calcareous mudstone and beds of dark grey, sometimes laminated, calcareous sandstone. The succession grades upwards into a lighter coloured, thicker bedded version of the lower portion of the succession. The colour change may be due to this area of the outcrop spending gradually less time in the ocean because it is near the high tide mark, but slabbed samples do show a shift from dark grey/black near the base of the sequence to light green-grey near the top. The upper part of the succession is decimeter bedded and consists of alternating beds of medium to dark grey, intensely burrowed, calcareous mudstone, and blue-grey, calcareous sandstone. The sandstones appear to have sharp lower contacts, and gradational upper contacts with the mudstones. The upper contact of the succession is intensely burrowed.

Stratigraphic Column: Pahaoa - Detailed Log

Column No: 6:10

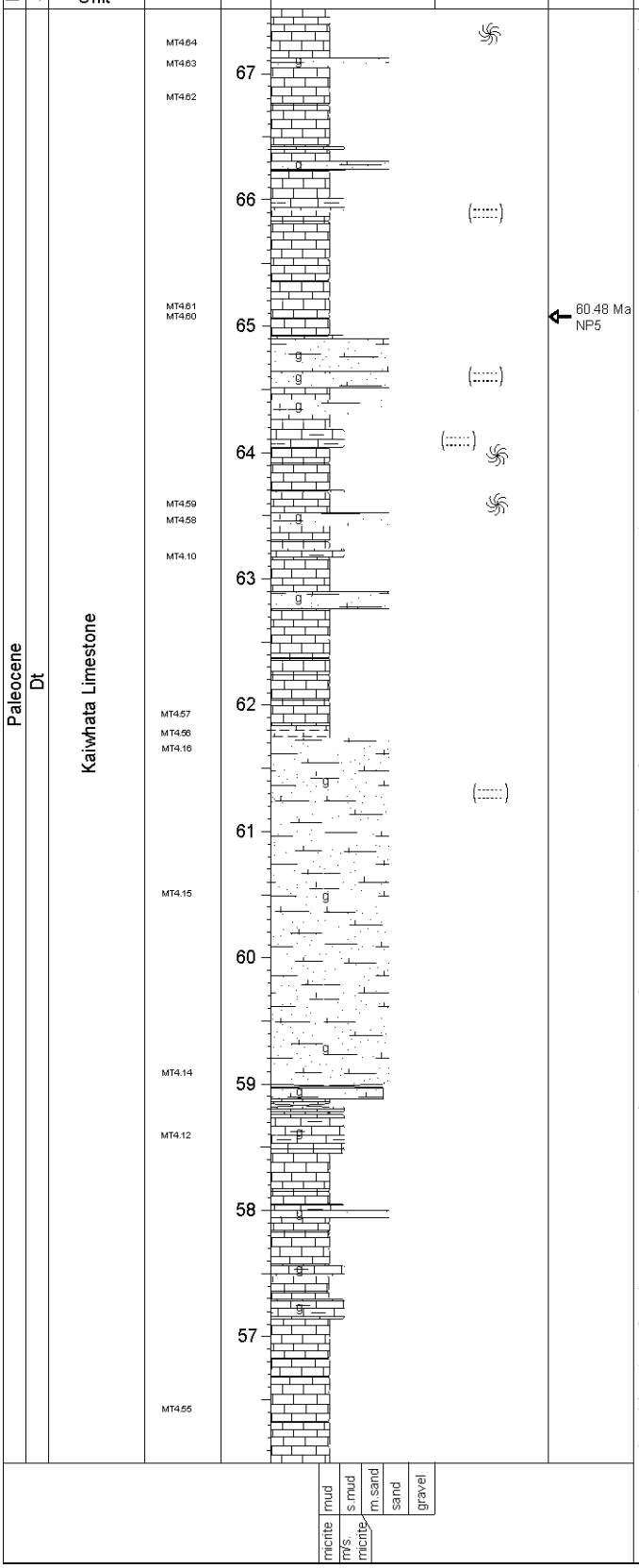

- **67.12 to 67.58 m Limestone:** Creamy-white, well indurated, massive with burrows in some flags, flaggy, calcareous micritic limestone. Weathers to white with brown stains and a light cover of black lichen.

- **67.05 to 67.12 m Calcareous sandstone and mudstone unit:** Blue-green-grey, very well indurated, massive, glauconitic, calcareous sandstone. Grades upwards into a white to light grey, moderately indurated, massive, glauconitic, calcareous mudstone. The unit has a sharp lower contact and a sharp to rapidly gradational upper contact. The sandstone weathers to a brown green colour and the mudstone weathers to a frittery surface.

- **66.31 to 67.05 m Limestone:** Creamy-white, well indurated, massive, flaggy, calcareous micritic limestone. Weathers to white with brown stains and a light cover of black lichen.

- **66.24 to 66.31 m Calcareous sandstone and mudstone unit:** Blue-green-grey, very well indurated, massive, glauconitic, calcareous sandstone. Grades upwards into a white to light grey, moderately indurated, massive, calcareous, glauconitic, mudstone. The unit has a sharp lower contact and a sharp to rapidly gradational upper contact. The sandstone weathers to a brown green colour and the mudstone weathers to a frittery surface.

- **66.01 to 66.24 m Limestone:** Creamy-white, well indurated, massive, flaggy, calcareous micritic limestone. Weathers to white with brown stains and a light cover of black lichen.

- **65.91 to 66.01 m Pale green white limestone:** Creamy-white in lower half, pale green-white in upper half, well indurated in lower most 7 cm, possible fine laminations in upper part of bed, calcareous micritic limestone. The top 3 cm of the flag is a white muddy limestone.

- **64.92 to 65.91 m Limestone:** Creamy-white, well indurated, mostly massive but with faint laminations in some flags, flaggy, calcareous micritic limestone. Weathers to white with brown stains and a light cover of black lichen.

- **64.9 to 64.92 m Muddy limestone:** White to light grey, moderately indurated, massive, glauconitic, calcareous muddy limestone.

- **64.64 to 64.9 m Calcareous sandstone:** Blue-green-grey, well indurated, massive, glauconitic, calcareous sandstone. Weathers to a brown green colour.

- **64.62 to 64.64 m Limestone:** Creamy-white, well indurated, massive with laminations at base, calcareous micritic limestone. Weathers to white with brown stains and a light cover of black lichen.

- **64.51 to 64.62 m Calcareous sandstone and mudstone unit:** Blue-green-grey, very well indurated, massive, glauconitic, calcareous sandstone. Grades upwards into a white to light grey, moderately indurated, massive, glauconitic, calcareous mudstone. The unit has a sharp lower contact and a sharp to rapidly gradational upper contact. The sandstone weathers to a brown green colour and the mudstone weathers to a frittery surface.

- **64.41 to 64.51 m Limestone:** Creamy-white, well indurated, massive, calcareous micritic limestone. Weathers to white with brown stains and a light cover of black lichen.

- **64.30 to 64.41 m Calcareous sandstone and mudstone unit:** Blue-green-grey, very well indurated, massive, glauconitic, calcareous sandstone. Grades upwards into a white to light grey, moderately indurated, massive, glauconitic, calcareous mudstone. The unit has a sharp lower contact and a sharp to rapidly gradational upper contact. The sandstone weathers to a brown green colour and the mudstone weathers to a frittery surface.

- **64.18 to 64.30 m Limestone:** Creamy white, well indurated, massive, calcareous micritic limestone. Weathers to white with brown stains with a light coverage of black lichen.

- **64.04 to 64.18 m Pale green-white muddy limestone:** Pale green-white, possibly laminated at the base, glauconitic, calcareous slightly muddy limestone. Sharp upper and lower contacts.

- **63.92 to 64.04 m Limestone:** Creamy-white, well indurated, burrowed, calcareous micritic limestone. Weathers to white with brown stains and a light cover of black lichen.

- **63.70 to 63.92 m Limestone:** Creamy-white, well indurated, massive, calcareous micritic limestone. Weathers to white with brown stains and a light cover of black lichen.

- **63.69 to 63.70 m Muddy limestone:** White to light grey, moderately indurated, massive, calcareous muddy limestone.

- **63.52 to 63.69 m Limestone:** Creamy white, well indurated, massive with trace fossils, calcareous micritic limestone. Trace fossils appear as dark blue-grey to light blue-grey criss crossing lines and lenses 0.5-8 mm thick. Weathers to white with brown stains and a light cover of black lichen.

- **63.42 to 63.52 m Calcareous sandstone and mudstone unit:** Blue-green-grey, well indurated, massive, glauconitic, calcareous sandstone. Grades upwards into a white to light grey, moderately indurated, massive, glauconitic, calcareous mudstone. The unit has sharp lower and upper contacts. The sandstone weathers to a brown green colour and the mudstone weathers to a frittery surface.

- **62.9 to 63.42 m Limestone:** Creamy-white, well indurated, massive, flaggy, calcareous micritic limestone. Weathers to white with brown stains and a light cover of black lichen.

- **62.76 to 62.9 m Calcareous sandstone:** Blue-green-grey, very well indurated, massive, glauconitic, calcareous sandstone. Sharp lower contact and gradational upper contact with limestone. Weathers to a brown-green colour and preferentially erodes along its upper contact.

- **61.84 to 62.76 m Limestone:** Creamy-white, well indurated, massive, flaggy, calcareous micritic limestone. Weathers to white with brown stains and a light cover of black lichen.

- **61.74 to 61.84 m Calcareous mudstone:** Dark grey to black mudstone with a gradational to rapidly gradational lower contact and an upper contact that appears sharp, however, the bed grades from a dark colour at its base to a light colour (similar to the overlying limestone) at its top. At its base it is soft, has a clay like texture, and is highly calcareous. Through the middle of the bed it is slightly calcareous in places. The top of the bed is calcareous.

- **59.0 to 61.74 m Calcareous sandstone:** Green-grey, well indurated, massive through its lower two thirds and laminated in its upper third, glauconitic, calcareous sandstone. The bed appears to have a gradational to rapidly gradational contact with a thin overlying mudstone. The lower contact is poorly exposed but looks like it may be sharp. Weathers to a brown green blocky surface.

- **58.88 to 58.97 m Calcareous sandstone:** Blue-grey, well indurated, massive, calcareous sandstone. Contacts poorly exposed.

- **58.0 to 58.88 m Limestone and slightly muddy limestone:** Creamy-white or with a green tint if slightly muddy, well indurated, massive, flaggy, calcareous micritic limestone and muddy limestone. Weathers to white with brown stains and a light cover of lichen.

- **57.94 to 58.0 m Calcareous sandstone:** Blue-green-grey, well indurated, massive, calcareous sandstone. Sharp lower contact, gradational upper contact.

- **57.14 to 57.94 m Limestone:** Creamy-white or with a green tint, well indurated, massive, flaggy, calcareous micritic limestone. Weathers to white with brown stains and a light cover of black lichen.

- **53.61 to 57.0 m Limestone:** Creamy-white, well indurated, massive, flaggy, calcareous micritic limestone. Weathers to white with brown stains.

Stratigraphic Column: Pahaoa - Detailed Log

Column No: 7:10

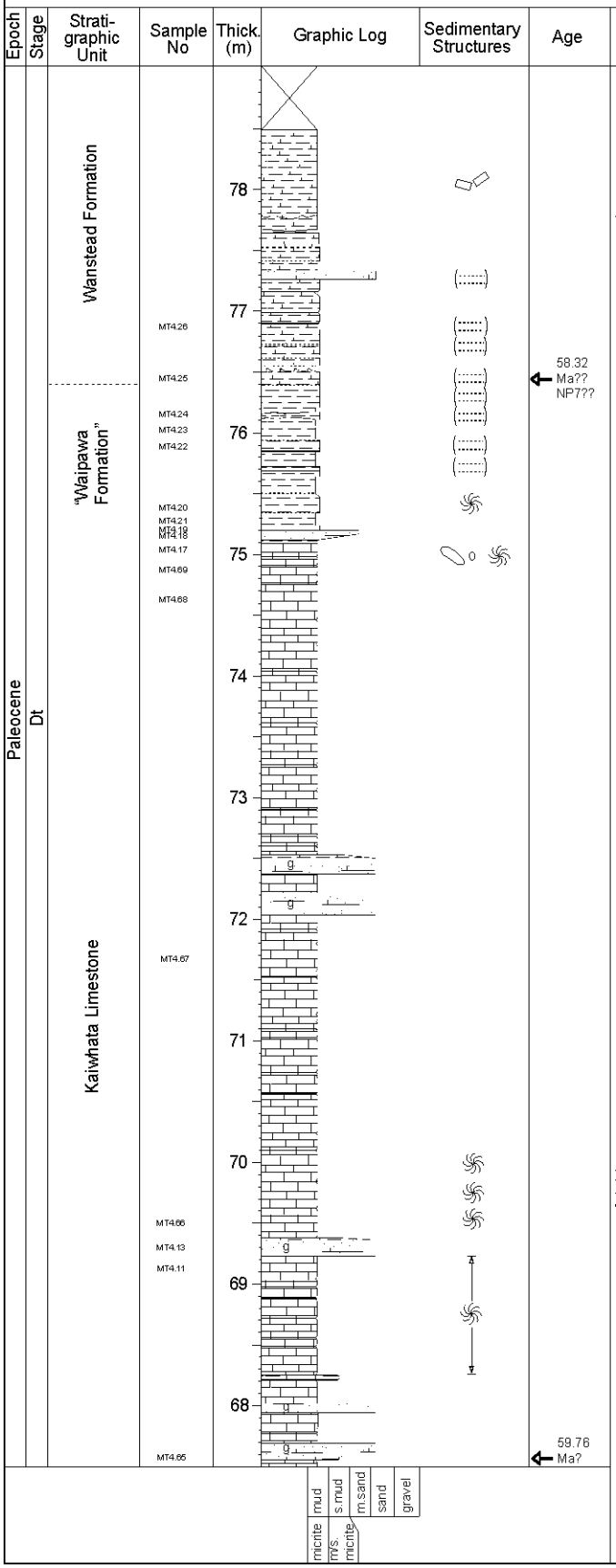

- **78.49 to 79.09 m Unexposed**
- **77.79 to 78.49 m Calcareous mudstone:** Red and light green, moderately indurated, highly distorted, calcareous mudstone. The colours of the mudstone are folded and inter-twined with one another. The lower contact undulates and appears to cut into the lower bed.
- **77.33 to 77.79 m Calcareous mudstone:** White or with green tint, moderately indurated, flaggy, massive, calcareous mudstone. Weathers to a relatively frittery surface.
- **77.26 to 77.33 m Calcareous sandstone:** Blue-grey, well indurated, faintly laminated, calcareous sandstone. Sharp lower contact and sharp to rapidly gradational upper contact. This bed is faulted but the overlying beds are not.
- **76.9 to 77.26 m Calcareous mudstone:** White, moderately indurated, flaggy, massive, calcareous mudstone. Weathers to a relatively frittery surface.
- **76.85 to 76.9 m Calcareous mudstone:** Dark green, laminated, possibly glauconitic, calcareous mudstone. Has a micritic limestone texture. Gradational contacts. This bed is used to correlate between outcrops.
- **76.5 to 76.85 m Calcareous mudstone:** Light grey, moderately indurated, calcareous mudstone. Alternates between frittery and less frittery beds. The upper most bed is less frittery and may be a muddy micritic limestone.
- **76.39 to 76.5 m Calcareous mudstone:** Medium grey, moderately indurated, laminated in the lower half of the bed and massive in the upper half, possibly glauconitic in the lower third, calcareous mudstone. Gradational lower contact and sharp upper contact that undulates in a saw tooth fashion.
- **76.2 to 76.39 m Non-calcareous mudstone:** The lower 7 cm of the bed is a dark green, moderately indurated, massive with possibly very vague laminations, non-calcareous, mudstone. It has the same texture as the micritic limestones. The rest of the bed consists of a gradational change to a lighter coloured, more frittery, mudstone/muddy limestone. Sharp lower contact.
- **76.16 to 76.2 m Non-calcareous mudstone:** Green-grey, poorly indurated, non-calcareous mudstone. Sharp contacts. Weathers to a frittery surface.
- **76.13 to 76.16 m Non-calcareous mudstone:** Dark green, moderately indurated, massive with possibly some very vague laminations, non-calcareous mudstone. Has the same texture as the micritic limestones. Sharp contacts.
- **75.93 to 76.13 m Non-calcareous mudstone:** Light grey with possibly a green tint, moderately indurated, massive, non-calcareous mudstone. Weathers to a frittery surface. Grades upwards into a dark grey, moderately indurated, laminated, non-calcareous, Mst with frittery weathering.
- **75.85 to 75.93 m Non-calcareous mudstone:** Dark green, moderately indurated, laminated, non-calcareous mudstone. Gradational upper contact, it is difficult to tell what the nature of the lower contact is - possibly rapidly gradational or sharp.
- **75.72 to 75.85 m Non-calcareous mudstone:** Dark grey, massive, non-calcareous mudstone. Sharp to rapidly gradational lower contact. Weathers to a frittery surface.
- **75.69 to 75.72 m Non-calcareous mudstone:** Dark grey, laminated, non-calcareous mudstone. Sharp to rapidly gradational contacts.
- **75.64 to 75.69 m Non-calcareous mudstone:** Dark grey, massive, non-calcareous, mudstone.
- **75.49 to 75.64 m Non-calcareous mudstone:** Medium grey, moderately indurated, massive or possibly very vaguely laminated, non-calcareous mudstone. Weathers to an intensely frittery surface.
- **75.34 to 75.49 m Non-calcareous mudstone:** Dark grey, moderately well to well indurated, massive, non-calcareous mudstone. Gradational upper contact. Has less frittery weathering than the underlying bed.
- **75.25 to 75.34 m Non-calcareous mudstone:** Medium to dark grey, moderately indurated, *Zoophycos* trace fossils, non-calcareous, mudstone. Gradational upper contact. Weathers to an intensely frittery surface with heavy rust staining in places.
- **75.22 to 75.25 m Non-calcareous mudstone:** Green-brown, moderately indurated, massive with occasional dark lenses and *Zoophycos* trace fossils, non-calcareous mudstone. Gradational upper contact.
- **75.09 to 75.22 Non-calcareous sandstone:** Light blue-green-grey, well indurated, vaguely laminated, burrowed, glauconitic, non-calcareous sandstone with nodules at base. The burrows are large (c. 7 cm wide) and infilled with white powdery sand. The lower contact is sharp. Weathers to a rusty colour.
- **74.98 to 75.09 m Limestone:** Creamy-white, well indurated, massive with trace fossils, calcareous, micritic limestone. Trace fossils appear as criss crossing *Zoophycos* traces, and lenses 0.5-8 mm thick. Burrowing is also evident on the top surface of the flag. Weathers to white with brown stains and a light cover of black lichen.
- **72.53 to 74.98 m Limestone:** Creamy-white, well indurated, flaggy, massive, calcareous micritic limestone. Weathers to white with brown stains and a light cover of black lichen.
- **72.37 to 72.53 m Calcareous sandstone and mudstone unit:** Blue-green-grey, very well indurated, massive, glauconitic, calcareous sandstone. Grades upwards into a white to light grey, moderately indurated, massive, glauconitic, calcareous mudstone. The unit has a sharp lower contact and a sharp to rapidly gradational upper contact. The sandstone weathers to a brown green colour and the mudstone weathers to a frittery surface.
- **72.22 to 72.37 m Limestone:** Creamy-white, well indurated, massive, calcareous micritic limestone. Weathers to white with brown stains and a light cover of black lichen.
- **72.03 to 72.22 m Calcareous sandstone and mudstone unit:** Blue-green-grey, very well indurated, massive, glauconitic, calcareous sandstone. Grades upwards into a white to light grey, moderately indurated, massive, glauconitic, calcareous mudstone. The unit has sharp lower contact and sharp to rapidly gradational upper contact. The sandstone weathers to a brown green colour and the mudstone weathers to a frittery surface.
- **70.1 to 72.03 m Limestone:** Creamy-white, well indurated, flaggy, massive, calcareous micritic limestone. Weathers to white with brown stains and a light cover of black lichen.
- **69.85 to 70.1 m Limestone:** Creamy-white, well indurated, massive with *Zoophycos* at the top of the bed, calcareous micritic limestone. Weathers to white with brown stains and a light cover of black lichen.
- **69.84 to 69.85 m Muddy limestone:** White to light grey, massive, calcareous muddy limestone.
- **69.38 to 69.84 m Limestone:** Creamy-white, well indurated, massive with trace fossils, flaggy, calcareous micritic limestone. Trace fossils appear as criss crossing *Zoophycos* traces, and lenses 0.5-8 mm thick and become more distinctive towards the top of each flag. Weathers to white with brown stains and a light cover of black lichen.
- **69.23 to 69.38 m Calcareous sandstone and mudstone unit:** Blue-green-grey, very well indurated, massive at the base, laminated through the middle, glauconitic, calcareous sandstone. Grades into a dark grey to black, soft, calcareous, mudstone in its upper 1-2 cm. Nodules are present along a horizon 10 cm above the base of the bed. The unit has sharp lower and upper contacts. The sandstone weathers to a brown-green colour and the mudstone weathers to a frittery surface.
- **69.04 to 69.23 m Limestone:** Creamy-white, well indurated, massive with distinct trace fossils, calcareous micritic limestone. Trace fossils appear as criss crossing *Zoophycos* traces and lenses 0.5-8 mm thick. The upper 5 cm of the flag grades into a grey micritic limestone. Trace fossils are particularly distinctive at the interface between the lower lighter and upper darker limestones. Weathers to white with brown stains and a light cover of black lichen.
- **68.01 to 69.04 m Limestone:** Creamy-white, well indurated, commonly burrowed, calcareous micritic limestone. Some flags appear to pinch and swell (either the upper contact is undulating or the lower flag is part of the upper flag). Weathers to white with brown stains and a light cover of black lichen.
- **67.94 to 68.01 m Calcareous sandstone and mudstone unit:** Blue-green-grey, very well indurated, massive, glauconitic, calcareous sandstone. Grades upwards into a white to light grey, moderately indurated, massive, glauconitic, calcareous mudstone. The unit has a sharp lower contact and a sharp to rapidly gradational upper contact. The sandstone weathers to a brown green colour and the mudstone weathers to a frittery surface.
- **67.69 to 67.94 m Limestone:** Creamy-white, well indurated, flaggy, massive, calcareous micritic limestone. Weathers to white with brown stains and a light cover of black lichen.
- **67.58 to 67.69 m Calcareous sandstone and mudstone unit:** Blue-green-grey, very well indurated, massive, glauconitic, calcareous sandstone. Grades upwards into a white to light grey, moderately indurated, massive, glauconitic, calcareous mudstone. The unit has a sharp lower contact and a sharp to rapidly gradational upper contact. The sandstone weathers to a brown green colour and the mudstone weathers to a frittery surface.

Stratigraphic Column: Pahaoa - Detailed Log

Column No: 8:10

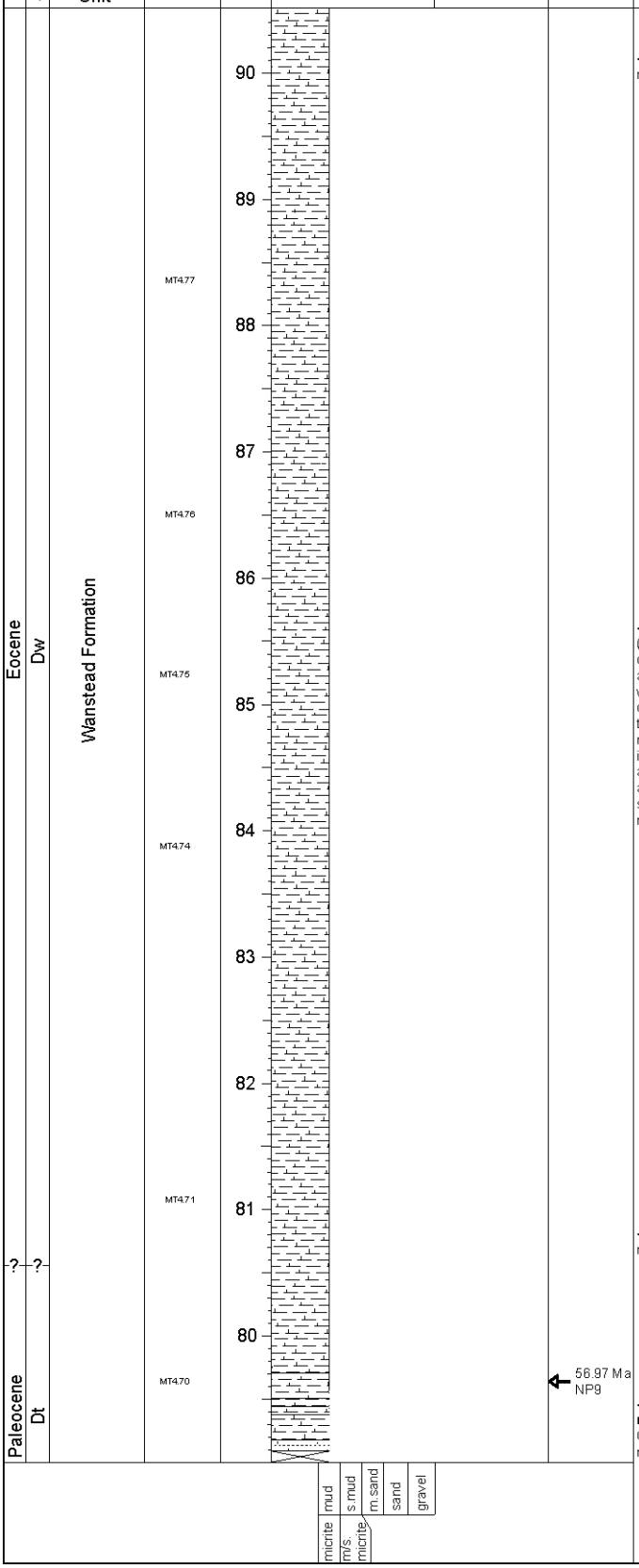

- 89.25 to 90.95 m Calcareous mudstone: Red with light green streaks, mudstone.

- 79.7 to 89.04 m Calcareous striped mudstone: Dominantly red and green (with minor grey), moderately indurated, massive, calcareous mudstone. The different colours form continuous and semi-continuous parallel to semi-parallel alternating stripes. The contacts between some of the stripes undulate and within a single stripe thin streaks of another colour can occasionally be observed. The stripes can also be patchy. The patchyness and distinction of the stripes appears to be affected by water. They become more distinct and more patchy when they are within the inter-tidal zone. When above the inter-tidal zone the stripes are more continuous but less distinct. The colour and intensity of the stripes changes through the sequence. The general trend appears to be of a greater proportion of green mudstones at the base of the sequence, with more red to light red mudstones through the middle, and dark red mudstones beginning to dominate the upper portion of the sequence.

- 79.56 to 79.7 m Calcareous mudstone: Dark grey, moderately indurated, massive, calcareous mudstone. Weathers to a relatively frittery surface.

- 79.09 to 79.56 m Calcareous mudstone grading into bedded calcareous mudstone: Red, moderately indurated, massive, calcareous mudstone. Grades into a white, moderately indurated, massive, bedded, calcareous mudstone. Weathers to a relatively frittery surface.

Stratigraphic Column: Pahaoa - Detailed Log

Column No: 9:10

Epoch	Stage	Strati-graphic Unit	Sample No	Thick. (m)	Graphic Log	Sedimentary Structures	Age	Description
Eocene	Dw	Wanstead Formation		101 – 91	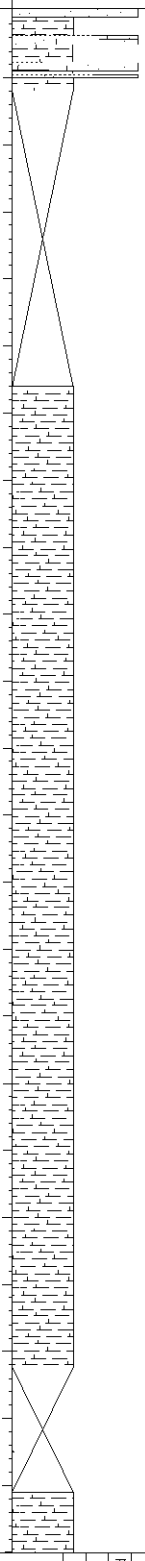			**- 101.74 to 101.95 m Calcareous sandstone and mudstone unit:** Green-grey, calcareous sandstone grading upwards into light green calcareous mudstone. The lower 2 cm is well indurated and massive. The overlying 4-5 cm has parallel laminations and this is followed by c. 4 cm of wavy laminations. The remainder of the unit is a frittery mudstone. The unit has sharp contacts. **- 101.57 to 101.74 m Calcareous sandstone and mudstone unit:** Light grey, calcareous sandstone grading upwards into calcareous mudstone. The lower 3-7 cm is well indurated and massive. The overlying 4-6 cm is poorly indurated and vaguely laminated. The remainder of the unit is a frittery mudstone. The unit has sharp contacts. **- 101.5 to 101.57 m Sandstone and mudstone unit:** Light green-blue-grey sandstone grading upwards into a medium grey, frittery mudstone. The unit has sharp contacts. The lower 3.5 cm is well indurated. **- 101.4 to 101.5 m Calcareous mudstone:** Frittery, calcareous mudstone. Sharp upper contact, unexposed lower contact. **- 99.2 to 101.4 m Unexposed** **- 96.81 to 99.2 m Calcareous mudstone:** Alternating stripes of dark red and light green, massive, calcareous mudstone. The sequence is softer between 97.34 and 97.94 m. Lenses of light green mudstone occur between 98.6 and 98.7 m. The sequence is poorly exposed between 96.81 and 97.94 m. **- 96.37 to 96.81 m Calcareous mudstone:** Grey-green, massive, calcareous mudstone. Weathers to a white frittery surface. Poorly exposed. **- 93.17 to 96.37 m Calcareous mudstone:** Light green with pale red streaks, dark red with flecks of green, and dark red, calcareous mudstone. The rock surface is discoloured due to weathering but it appears that the light green coloured mudstone with pale red streaks probably grades into the dark red mudstone with flecks of green, which in turn grades into the dark red (poorly exposed) mudstone. The colours within the beds do not seem to be continuous horizontal beds and seem to rather lense out and interweave with one another. **- 91.89 to 93.17 m Calcareous mudstone:** Alternating stripes of red and light green, massive, calcareous mudstone. Gradational upper contact. Planar or undulating contacts between colours. **- 90.95 to 91.89 m Unexposed**

Stratigraphic Column: Pahaoa - Detailed Log

Column No: 10:10

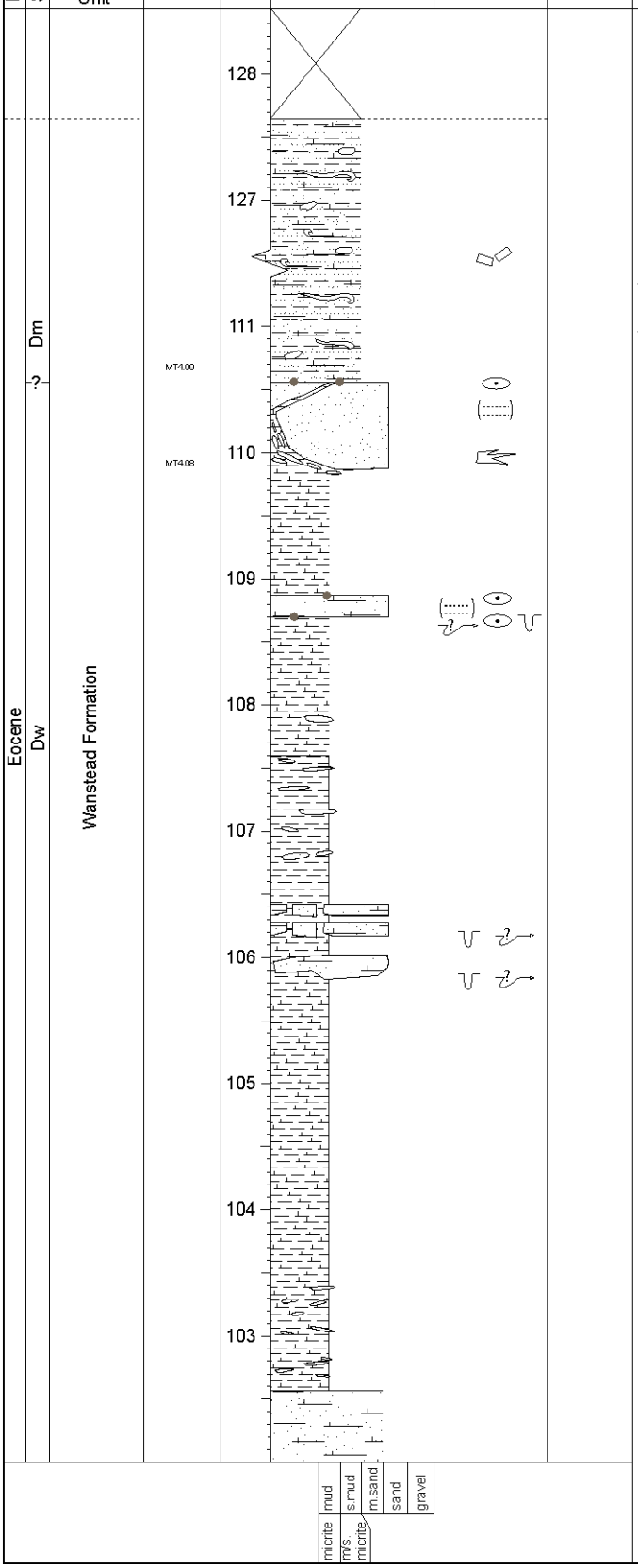

- 110.55 to ~127 m Interbedded calcareous sandstone-mudstone: Dark grey, well indurated, possibly glauconitic, calcareous, cm to mm interbedded sandstone and mudstone. The bedding has been folded in places and there are foreign clasts of various lithologies. Some clasts appear to be muddy micritic limestones that have been squashed into lenses and smeared, twisted, and folded back over themselves. Other clasts appear to be of the same lithology as the matrix, and others are blue-grey, well to very well indurated, massive to cm-dm bedded and some times highly burrowed, calcareous and non-calcareous, sandstones. Clasts can be very large (4.4 m long and 0.55 m wide). It appears that the areas of distorted matrix and clasts may form horizons beween non-distorted matrix. Further investigation is be needed to verify this.

- 109.87 to 110.55 m Non-calcareous sandstone: Brown-green, moderately indurated, massive with possible faint laminations in the upper half of the bed (may be a weathering affect), probably glauconitic, non-calcareous sandstone. Sharp undulating lower contact and sharp upper contact. The bed lenses off to a point of zero thickness. This bed probably correlates with a similar looking bed at the opposite side of the cove where it appears that the bed is broken up and mudstone resides within the fractures (sedimentary dikes?). A thin glauconitic sedimentary dike and broken up and distorted beds are in the strata underlying the contact in this area.

- 108.87 to 109.87 m Calcareous mudstone: Green-grey, poorly indurated, massive, calcareous mudstone. Sharp to rapidly gradational lower contact and sharp upper contact. Weathers to a highly frittery surface.

- 108.7 to 108.87 m Calcareous sandstone: Blue-grey, well indurated, laminated throughout, calcareous sandstone. Sharp lower contact with possible burrowing/flute casts, and a sharp to rapidly gradational upper contact with nodules. Weathers to an orange-brown colour.

- 108.44 to 108.7 m Calcareous mudstone: Green-grey to grey, moderately indurated, massive, calcareous mudstone. Gradational lower contact and sharp upper contact with nodules. Weathers to a frittery surface.

- 108.15 to 108.44 m Calcareous mudstone: Red-brown-grey, moderately indurated, massive, calcareous mudstone. Gradational contacts. Weathers to a frittery red and pink surface.

- 107.88 to 108.15 m Calcareous mudstone: Green-grey, poorly indurated, massive, calcareous mudstone. Gradational contacts. A blue-green-grey, well indurated, massive, calcareous sandstone clasts (27 cm long, 7 cm wide) is at the lower contact. The mudstone weathers to a muddy green frittery surface.

- 107.72 to 107.88 m Calcareous mudstone: Green-grey to grey, moderately indurated, massive, calcareous mudstone. The thickness of the bed varies greatly. The lower contact looks sharp, the upper contact is gradational to rapidly gradational. Weathers to a frittery surface.

- 107.6 to 107.72 m Calcareous mudstone: Red-brown, moderately indurated, massive, calcareous mudstone. Gradational contacts. Weathers to a frittery surface red and pink surface.

- 106.43 to 107.6 m Non-calcareous mudstone: Green-grey, very poorly indurated, massive, non-calcareous mudstone. Gradational upper contact. The bed is highly weathered and weathers to a brown-yellow-red muddy surface. When dug out there are red-brown faces on all the joint surfaces. Elongated clasts between 6-32 cm long and 2-2.5 cm wide are found within the mudstone. The clasts are blue-grey, well indurated, massive, calcareous, sandstone which weathers to a rusty surface.

- 106.33 to 106.43 m Calcareous sandstone: Blue-grey, well indurated, massive, calcareous sandstone. Sharp contacts. Weathers to a rusty brown surface. It is unclear if this is a broken up bed or a horizon of clasts.

- 106.28 to 106.33 m Non-calcareous mudstone: Green-grey, poorly indurated, massive, non-calcareous mudstone. Weathers to a frittery surface.

- 106.17 to 106.28 m Calcareous sandstone: Blue-grey, well indurated, massive, calcareous sandstone. Sharp contacts. Lower contact has burrows/possible flute casts. Weathers to a rusty brown surface. It is unclear if this is a broken up bed or a horizon of clasts.

- 106.03 to 106.17 m Calcareous mudstone: Green-grey, poorly indurated, massive, calcareous mudstone. Weathers to a frittery surface.

- 105.82 to 106.03 m Calcareous sandstone: Blue-grey, well indurated, massive, calcareous sandstone. Sharp upper contact and sharp undulating lower contact. The lower contact has burrows/possible flute casts. The entire bed appears to be a large clast (45 cm long) within the mudstone.

- 105.38 to 105.82 m Calcareous mudstone: Light green, poorly indurated, massive, calcareous mudstone.

- 104.82 to 105.38 m Calcareous mudstone: Alternating stripes of light green and light red, with overlying red-brown-pink, calcareous mudstone.

- 103.49 to 104.82 m Calcareous mudstone: Dark red with streaks of pale green, calcareous mudstone. Elongated foreign clasts arranged semi-parallel to the bedding are found in the bed.

- 102.88 to 103.49 m Calcareous mudstone: Alternating stripes of light green and light red, highly distorted, calcareous mudstone. The colours dont form semi-parallel bands but rather interweave and are distorted. Foreign clasts are found within the bed.

- 102.56 to 102.88 m Calcareous mudstone: Dark red with three thin light green streaks, calcareous, mudstone. The bed contains foreign clasts.

- 101.95 to 102.56 m Calcareous sandstone: Alternating stripes of dark red and light green, moderately indurated, calcareous sandstone. The lower most dark red band has patches of light green calcareous mudstone through it and a slightly undulating lower colour contact. All the contacts between the colours within the bed are sharp. Weathers to a less frittery surface.

Appendix D

ANGORA ROAD DETAILED STRATIGRAPHIC COLUMN

Stratigraphic Column: Lower Angora Rd - Overview

Column No: 1:1

Region: Southern Hawke's Bay, New Zealand

Location: LOWER ANGORA ROAD, WIMBLEDON. Measured section located at the lower quarry on Angora Rd and on exposures along Angora Stream, down stream from the quarry.

Logged by: Michael Tayler.

Date: 20-26 02 2010 (day month year)

GPS base: E2804969 N6078128

GPS top: E2804989 N6078004

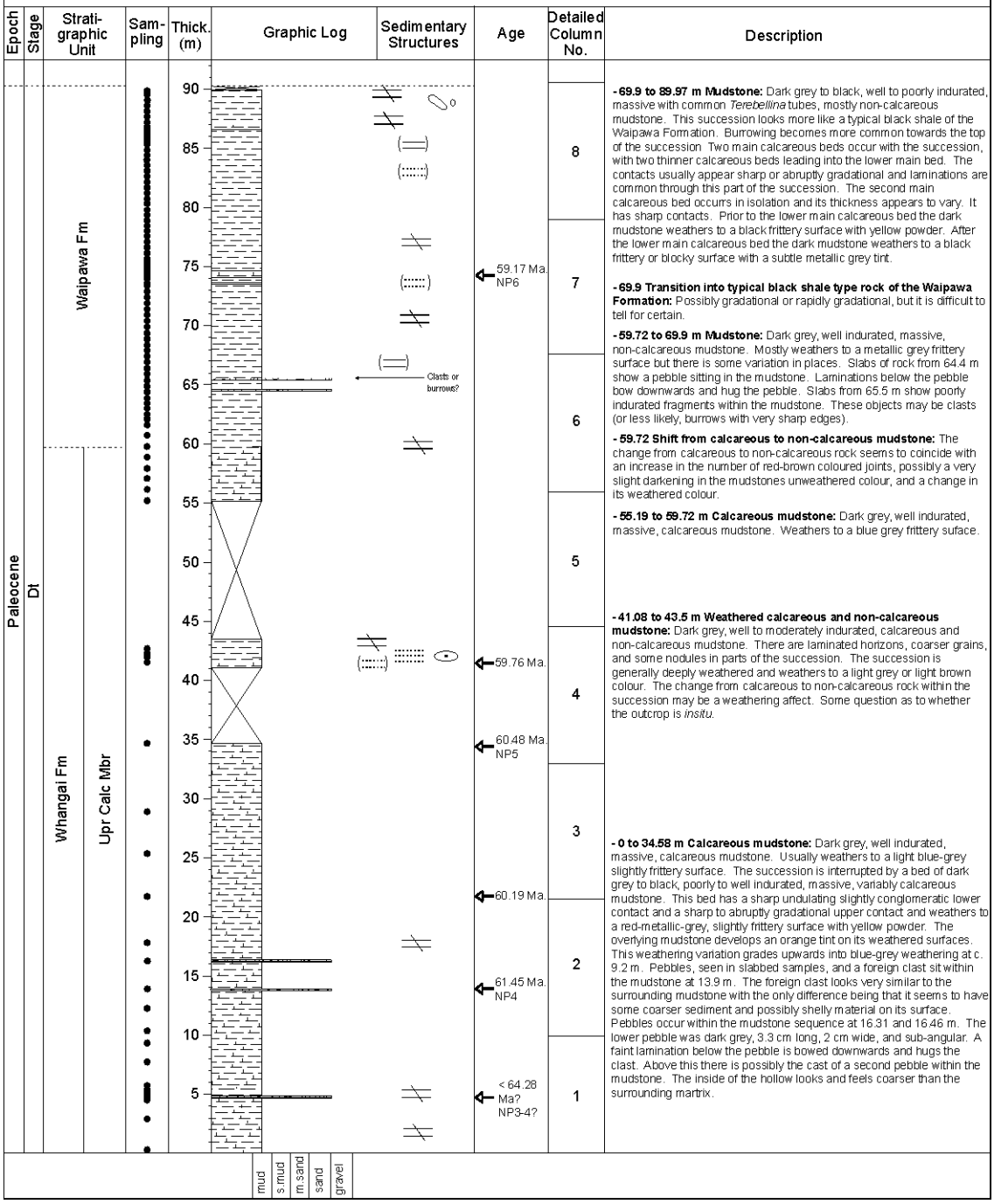

- 69.9 to 89.97 m Mudstone: Dark grey to black, well to poorly indurated, massive with common *Terebellina* tubes, mostly non-calcareous mudstone. This succession looks more like a typical black shale of the Waipawa Formation. Burrowing becomes more common towards the top of the succession. Two main calcareous beds occur with the succession, with two thinner calcareous beds leading into the lower main bed. The contacts usually appear sharp or abruptly gradational and laminations are common through this part of the succession. The second main calcareous bed occurs in isolation and its thickness appears to vary. It has sharp contacts. Prior to the lower main calcareous bed the dark mudstone weathers to a black frittery surface with yellow powder. After the lower main calcareous bed the dark mudstone weathers to a black frittery or blocky surface with a subtle metallic grey tint.

- 69.9 Transition into typical black shale type rock of the Waipawa Formation: Possibly gradational or rapidly gradational, but it is difficult to tell for certain.

- 59.72 to 69.9 m Mudstone: Dark grey, well indurated, massive, non-calcareous mudstone. Mostly weathers to a metallic grey frittery surface but there is some variation in places. Slabs of rock from 64.4 m show a pebble sitting in the mudstone. Laminations below the pebble bow downwards and hug the pebble. Slabs from 65.5 m show poorly indurated fragments within the mudstone. These objects may be clasts (or less likely, burrows with very sharp edges).

- 59.72 Shift from calcareous to non-calcareous mudstone: The change from calcareous to non-calcareous rock seems to coincide with an increase in the number of red-brown coloured joints, possibly a very slight darkening in the mudstones unweathered colour, and a change in its weathered colour.

- 55.19 to 59.72 m Calcareous mudstone: Dark grey, well indurated, massive, calcareous mudstone. Weathers to a blue grey frittery suface.

- 41.08 to 43.5 m Weathered calcareous and non-calcareous mudstone: Dark grey, well to moderately indurated, calcareous and non-calcareous mudstone. There are laminated horizons, coarser grains, and some nodules in parts of the succession. The succession is generally deeply weathered and weathers to a light grey or light brown colour. The change from calcareous to non-calcareous rock within the succession may be a weathering affect. Some question as to whether the outcrop is *insitu*.

- 0 to 34.58 m Calcareous mudstone: Dark grey, well indurated, massive, calcareous mudstone. Usually weathers to a light blue-grey slightly frittery surface. The succession is interrupted by a bed of dark grey to black, poorly to well indurated, massive, variably calcareous mudstone. This bed has a sharp undulating slightly conglomeratic lower contact and a sharp to abruptly gradational upper contact and weathers to a red-metallic-grey, slightly frittery surface with yellow powder. The overlying mudstone develops an orange tint on its weathered surfaces. This weathering variation grades upwards into blue-grey weathering at c. 9.2 m. Pebbles, seen in slabbed samples, and a foreign clast sit within the mudstone at 13.9 m. The foreign clast looks very similar to the surrounding mudstone with the only difference being that it seems to have some coarser sediment and possibly shelly material on its surface. Pebbles occur within the mudstone sequence at 16.31 and 16.46 m. The lower pebble was dark grey, 3.3 cm long, 2 cm wide, and sub-angular. A faint lamination below the pebble is bowed downwards and hugs the clast. Above this there is possibly the cast of a second pebble within the mudstone. The inside of the hollow looks and feels coarser than the surrounding martrix.

Stratigraphic Column: Lower Angora Rd - Detailed log

Column No: 1:8

Region: Southern Hawke's Bay, New Zealand

Location: ANGORA ROAD, WIMBLEDON. Measured section located at the lower quarry on Angora Rd and on exposures along Angora Stream, down stream from the quarry.

Logged by: Michael Tayler.

Date: 20-26 (day) 02 (month) 2010 (year)

and:

GPS base: E2804969 N6078128

GPS top: E2804989 N6078004

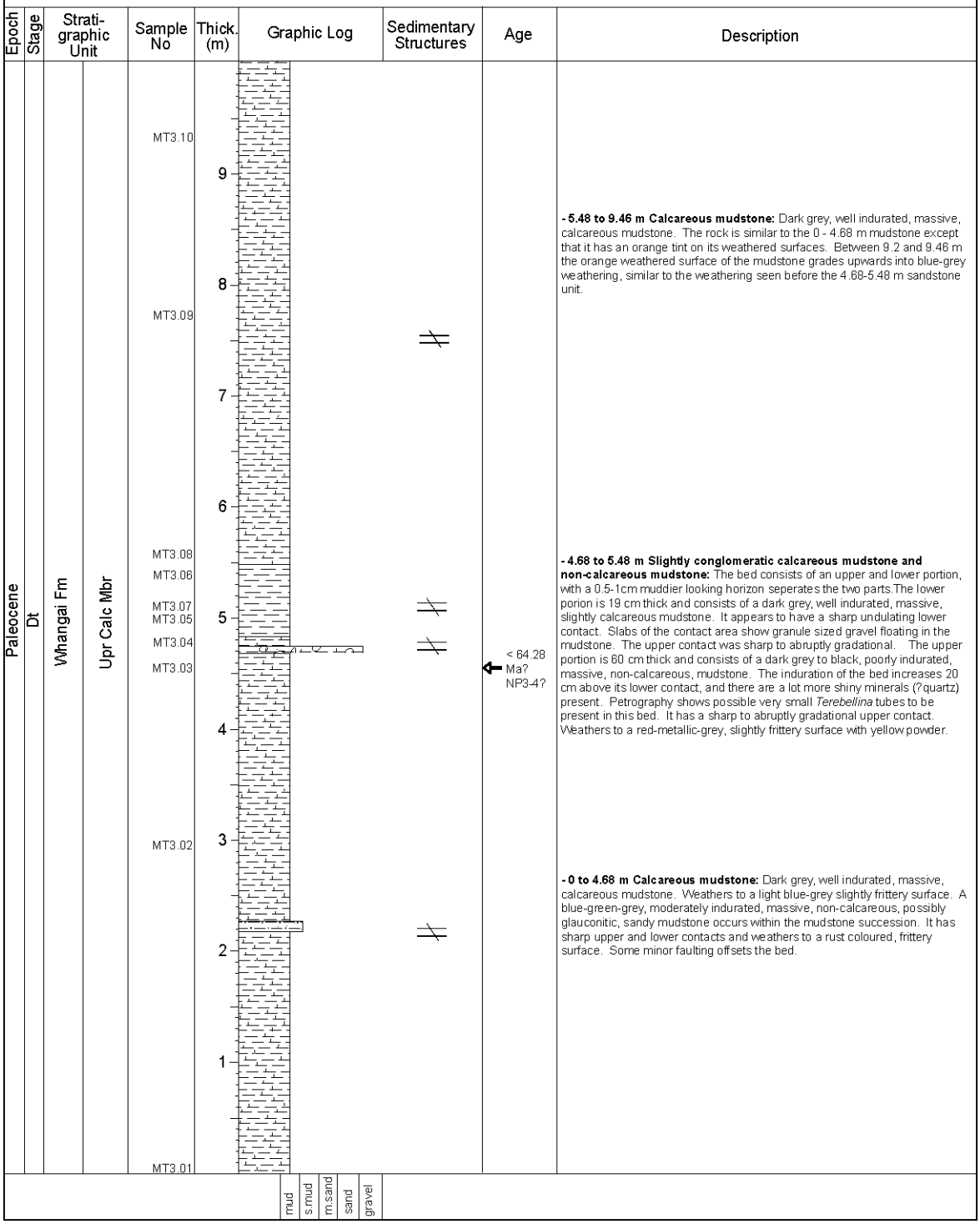

- 5.48 to 9.46 m Calcareous mudstone: Dark grey, well indurated, massive, calcareous mudstone. The rock is similar to the 0 - 4.68 m mudstone except that it has an orange tint on its weathered surfaces. Between 9.2 and 9.46 m the orange weathered surface of the mudstone grades upwards into blue-grey weathering, similar to the weathering seen before the 4.68-5.48 m sandstone unit.

- 4.68 to 5.48 m Slightly conglomeratic calcareous mudstone and non-calcareous mudstone: The bed consists of an upper and lower portion, with a 0.5-1cm muddier looking horizon seperates the two parts.The lower porion is 19 cm thick and consists of a dark grey, well indurated, massive, slightly calcareous mudstone. It appears to have a sharp undulating lower contact. Slabs of the contact area show granule sized gravel floating in the mudstone. The upper contact was sharp to abruptly gradational. The upper portion is 60 cm thick and consists of a dark grey to black, poorly indurated, massive, non-calcareous, mudstone. The induration of the bed increases 20 cm above its lower contact, and there are a lot more shiny minerals (?quartz) present. Petrography shows possible very small *Terebellina* tubes to be present in this bed. It has a sharp to abruptly gradational upper contact. Weathers to a red-metallic-grey, slightly frittery surface with yellow powder.

- 0 to 4.68 m Calcareous mudstone: Dark grey, well indurated, massive, calcareous mudstone. Weathers to a light blue-grey slightly frittery surface. A blue-green-grey, moderately indurated, massive, non-calcareous, possibly glauconitic, sandy mudstone occurs within the mudstone succession. It has sharp upper and lower contacts and weathers to a rust coloured, frittery surface. Some minor faulting offsets the bed.

Stratigraphic Column: Lower Angora Rd - Detailed Log

Column No: 2:8

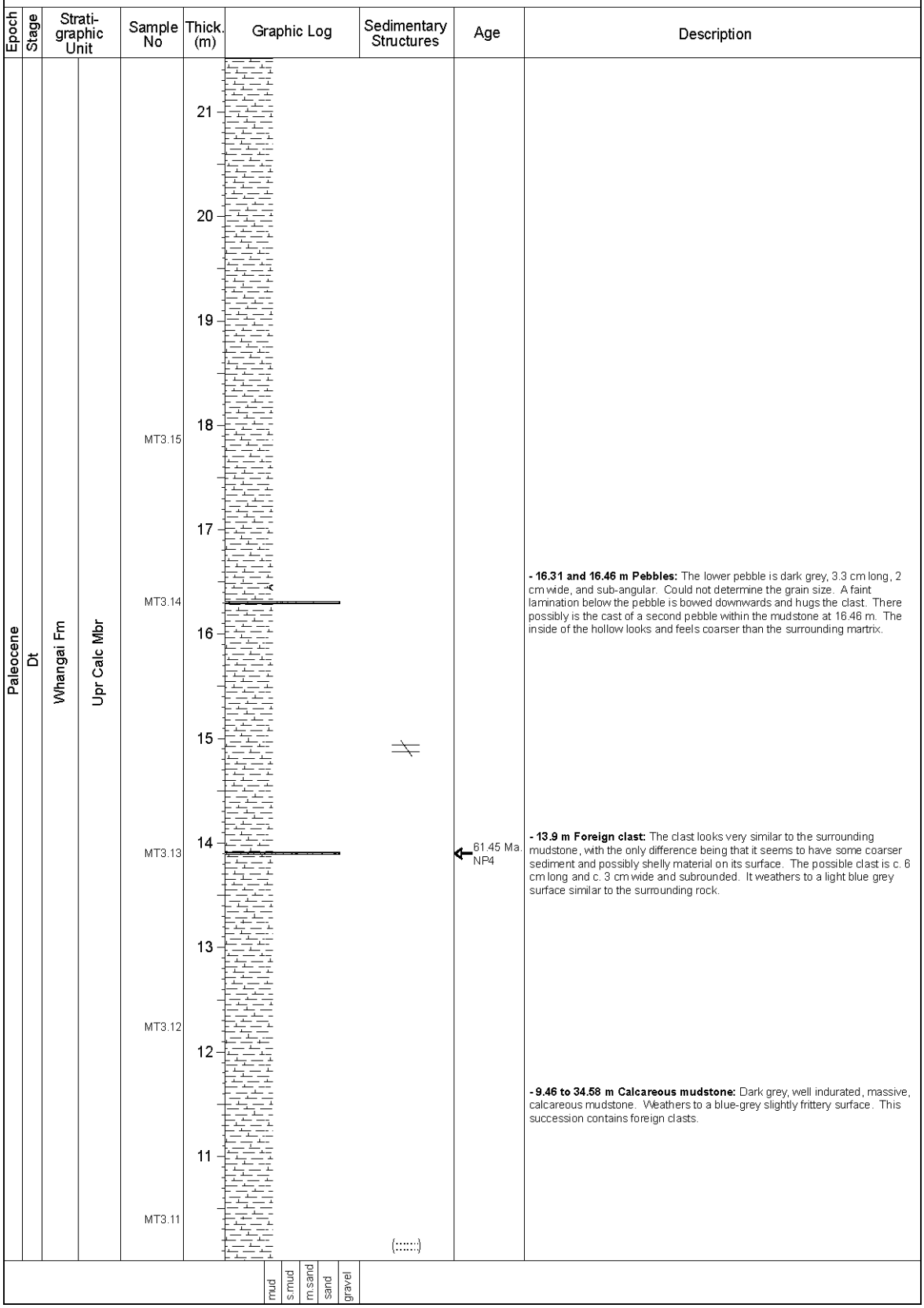

Stratigraphic Column: Lower Angora Rd - Detailed Log

Column No: 3:8

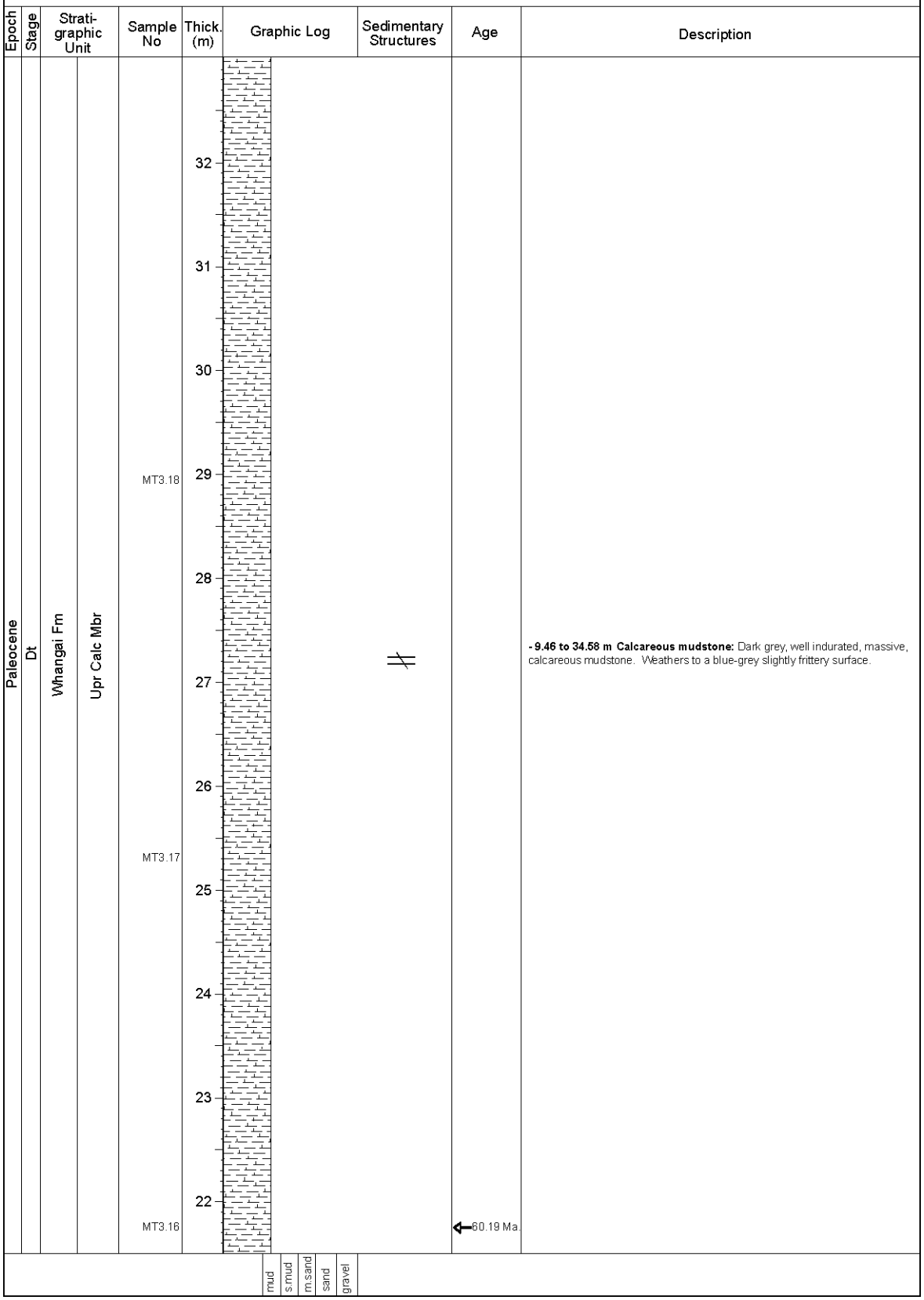

Stratigraphic Column: Lower Angora Rd - Detailed Log

Column No: 4:8

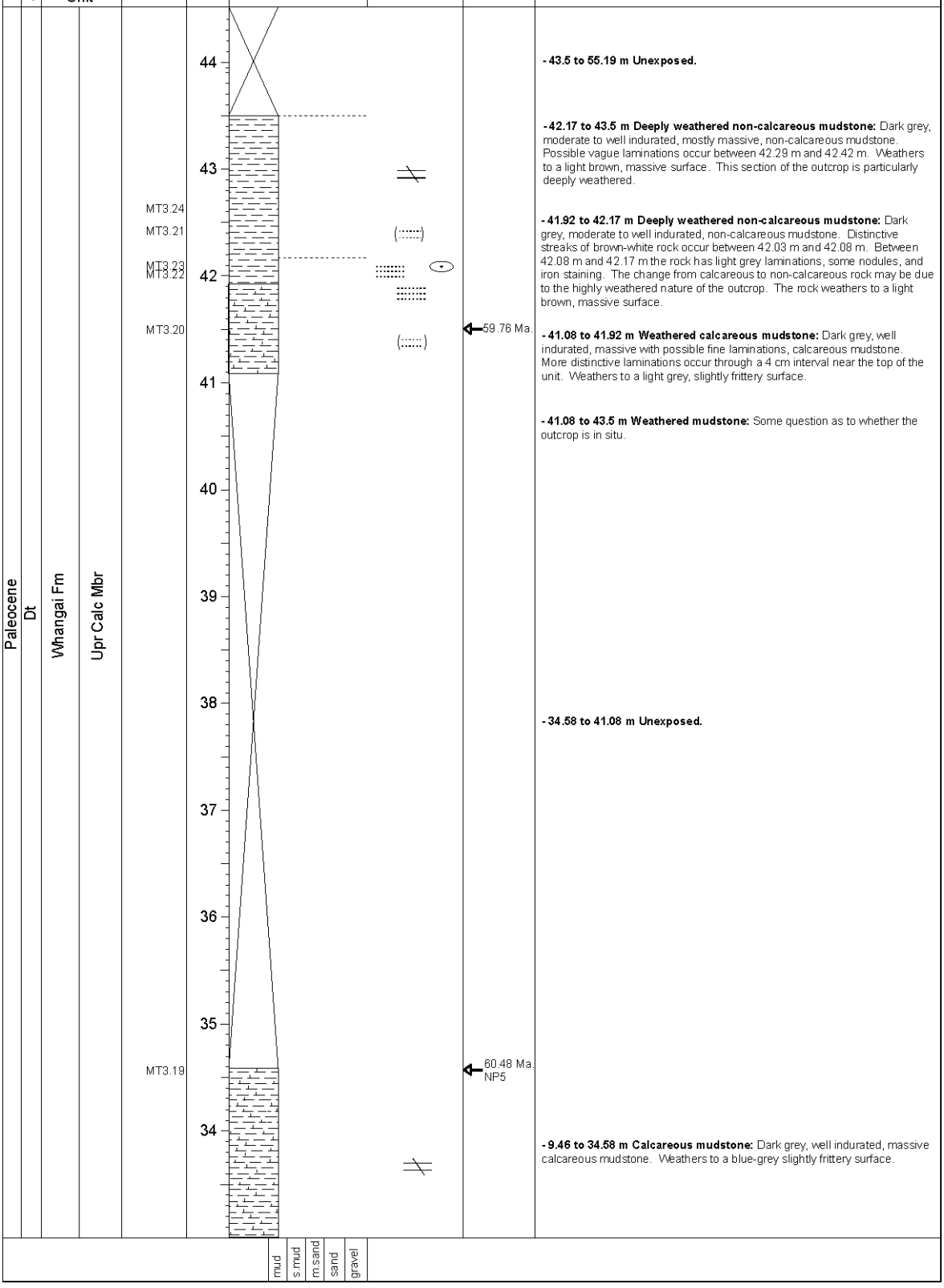

Stratigraphic Column: Lower Angora Rd - Detailed Log

Column No: 5:8

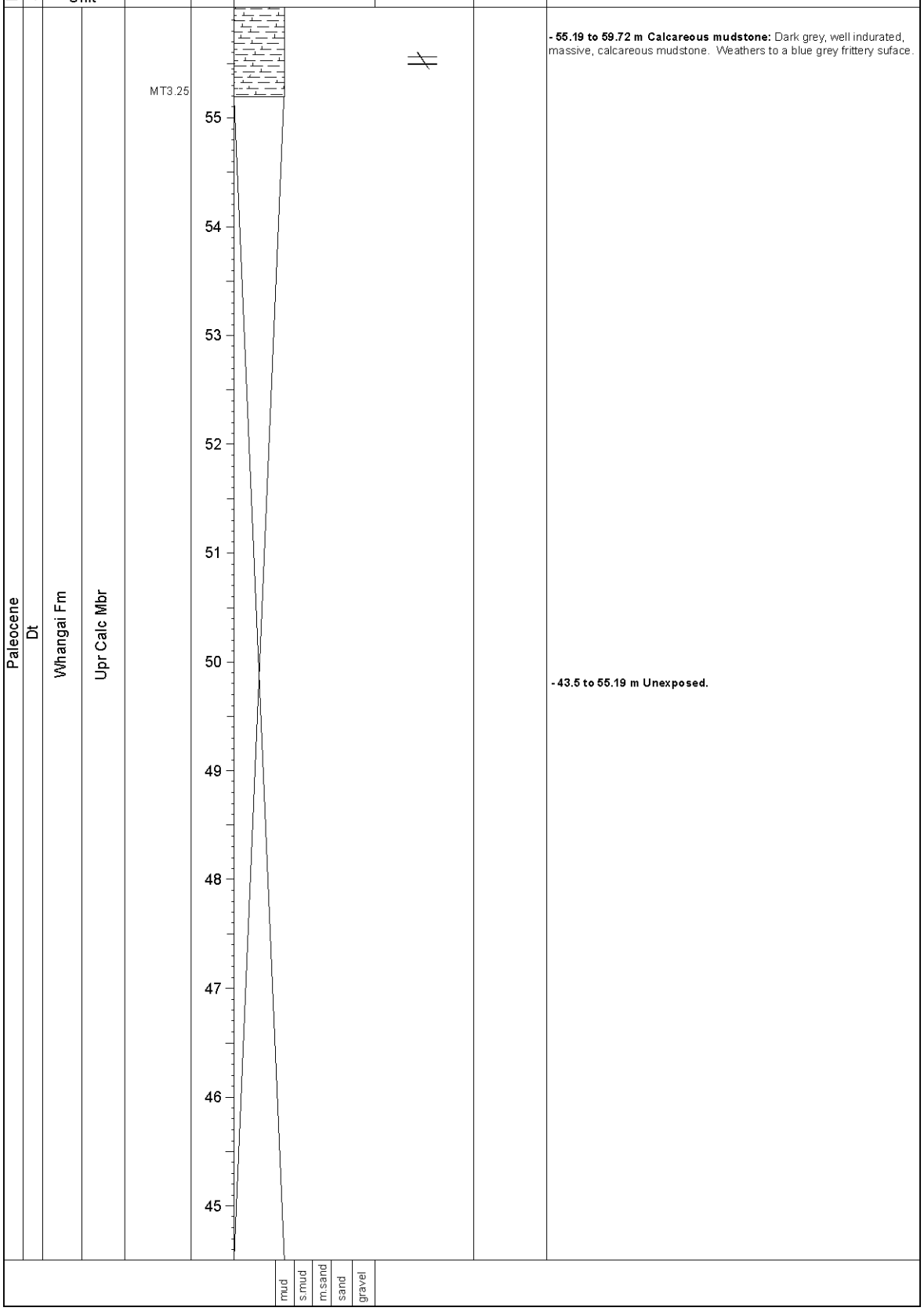

Stratigraphic Column: Lower Angora Rd - Detailed Log

Column No: 6:8

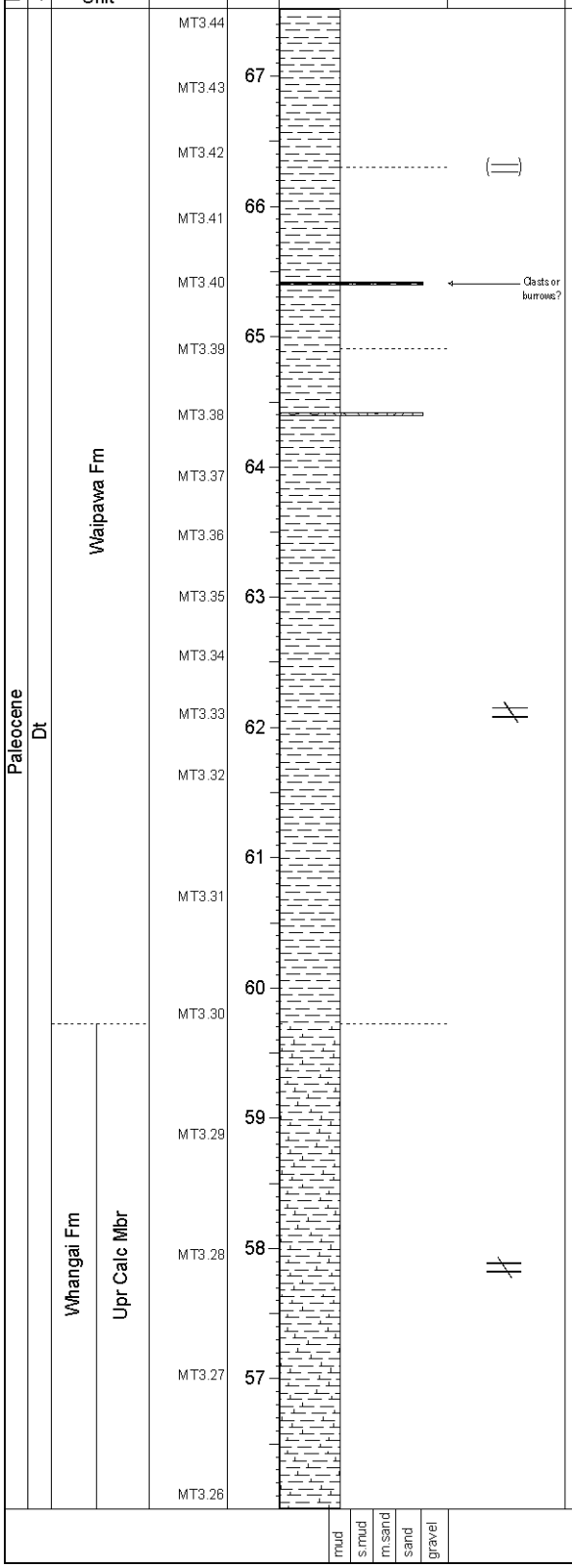

- 66.5 to 69.9 m Non-calcareous mudstone: Dark grey, well indurated, massive, non-calcareous mudstone. The rock seems to be sandy at 66.9 m. Weathers to a metallic grey frittery surface.

- 66.3 to 66.5 m Non-calcareous mudstone: Dark grey to black, moderately indurated, massive, non-calcareous mudstone. Weathers to a soft, black, frittery surface.

- 64.9 to 66.3 m Non-calcareous mudstone: Dark grey, well indurated, massive, non-calcareous mudstone. Slabs show poorly indurated fragments within the mudstone. These objects that may be clasts (or less likely burrows with very sharp edges?). Rock weathers to a metallic grey frittery surface.

- 63.7 to 64.9 m Non-calcareous mudstone: Dark grey, well indurated, massive, non-calcareous mudstone. Slabs show a pebble sitting in the mudstone. Underlying laminations are bowed downwards and hug the pebble. Rock weathers to a brown frittery surface.

- 62.3 to 63.7 m Non-calcareous mudstone: Dark grey, well indurated, massive, non-calcareous mudstone. Weathers to a metallic grey frittery surface.

- 59.72 to 62.3 m Non-calcareous mudstone: Dark grey, well indurated, massive, non-calcareous mudstone. The change from calcareous to non-calcareous mudstone seems to coincide with a possible very slight darkening in the fresh colour of the mudstone (if there is a darkening it is very subtle), more red-brown coloured joints, and a change in the weathered colour. Weathers to a metallic grey frittery surface but there are still patches of blue-grey weathered rock.

- 55.19 to 59.72 m Calcareous mudstone: Dark grey, well indurated, massive, calcareous mudstone. Weathers to a blue grey frittery suface.

Stratigraphic Column: Lower Angora Rd - Detailed Log

Column No: 7:8

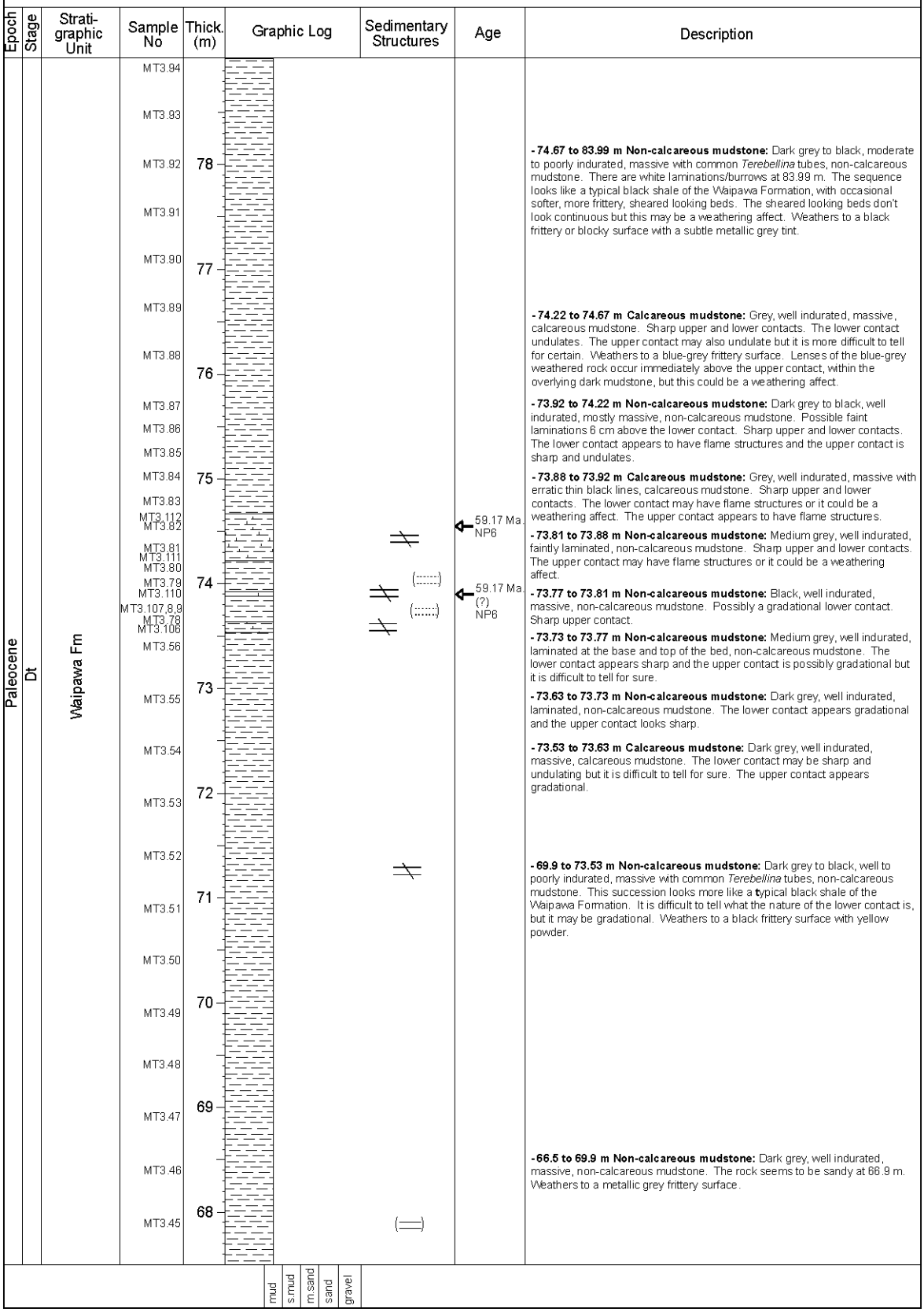

- 74.67 to 83.99 m Non-calcareous mudstone: Dark grey to black, moderate to poorly indurated, massive with common *Terebellina* tubes, non-calcareous mudstone. There are white laminations/burrows at 83.99 m. The sequence looks like a typical black shale of the Waipawa Formation, with occasional softer, more frittery, sheared looking beds. The sheared looking beds don't look continuous but this may be a weathering affect. Weathers to a black frittery or blocky surface with a subtle metallic grey tint.

- 74.22 to 74.67 m Calcareous mudstone: Grey, well indurated, massive, calcareous mudstone. Sharp upper and lower contacts. The lower contact undulates. The upper contact may also undulate but it is more difficult to tell for certain. Weathers to a blue-grey frittery surface. Lenses of the blue-grey weathered rock occur immediately above the upper contact, within the overlying dark mudstone, but this could be a weathering affect.

- 73.92 to 74.22 m Non-calcareous mudstone: Dark grey to black, well indurated, mostly massive, non-calcareous mudstone. Possible faint laminations 6 cm above the lower contact. Sharp upper and lower contacts. The lower contact appears to have flame structures and the upper contact is sharp and undulates.

- 73.88 to 73.92 m Calcareous mudstone: Grey, well indurated, massive with erratic thin black lines, calcareous mudstone. Sharp upper and lower contacts. The lower contact may have flame structures or it could be a weathering affect. The upper contact appears to have flame structures.

- 73.81 to 73.88 m Non-calcareous mudstone: Medium grey, well indurated, faintly laminated, non-calcareous mudstone. Sharp upper and lower contacts. The upper contact may have flame structures or it could be a weathering affect.

- 73.77 to 73.81 m Non-calcareous mudstone: Black, well indurated, massive, non-calcareous mudstone. Possibly a gradational lower contact. Sharp upper contact.

- 73.73 to 73.77 m Non-calcareous mudstone: Medium grey, well indurated, laminated at the base and top of the bed, non-calcareous mudstone. The lower contact appears sharp and the upper contact is possibly gradational but it is difficult to tell for sure.

- 73.63 to 73.73 m Non-calcareous mudstone: Dark grey, well indurated, laminated, non-calcareous mudstone. The lower contact appears gradational and the upper contact looks sharp.

- 73.53 to 73.63 m Calcareous mudstone: Dark grey, well indurated, massive, calcareous mudstone. The lower contact may be sharp and undulating but it is difficult to tell for sure. The upper contact appears gradational.

- 69.9 to 73.53 m Non-calcareous mudstone: Dark grey to black, well to poorly indurated, massive with common *Terebellina* tubes, non-calcareous mudstone. This succession looks more like a typical black shale of the Waipawa Formation. It is difficult to tell what the nature of the lower contact is, but it may be gradational. Weathers to a black frittery surface with yellow powder.

- 66.5 to 69.9 m Non-calcareous mudstone: Dark grey, well indurated, massive, non-calcareous mudstone. The rock seems to be sandy at 66.9 m. Weathers to a metallic grey frittery surface.

Stratigraphic Column: Lower Angora Rd - Detailed Log

Column No: 8:8

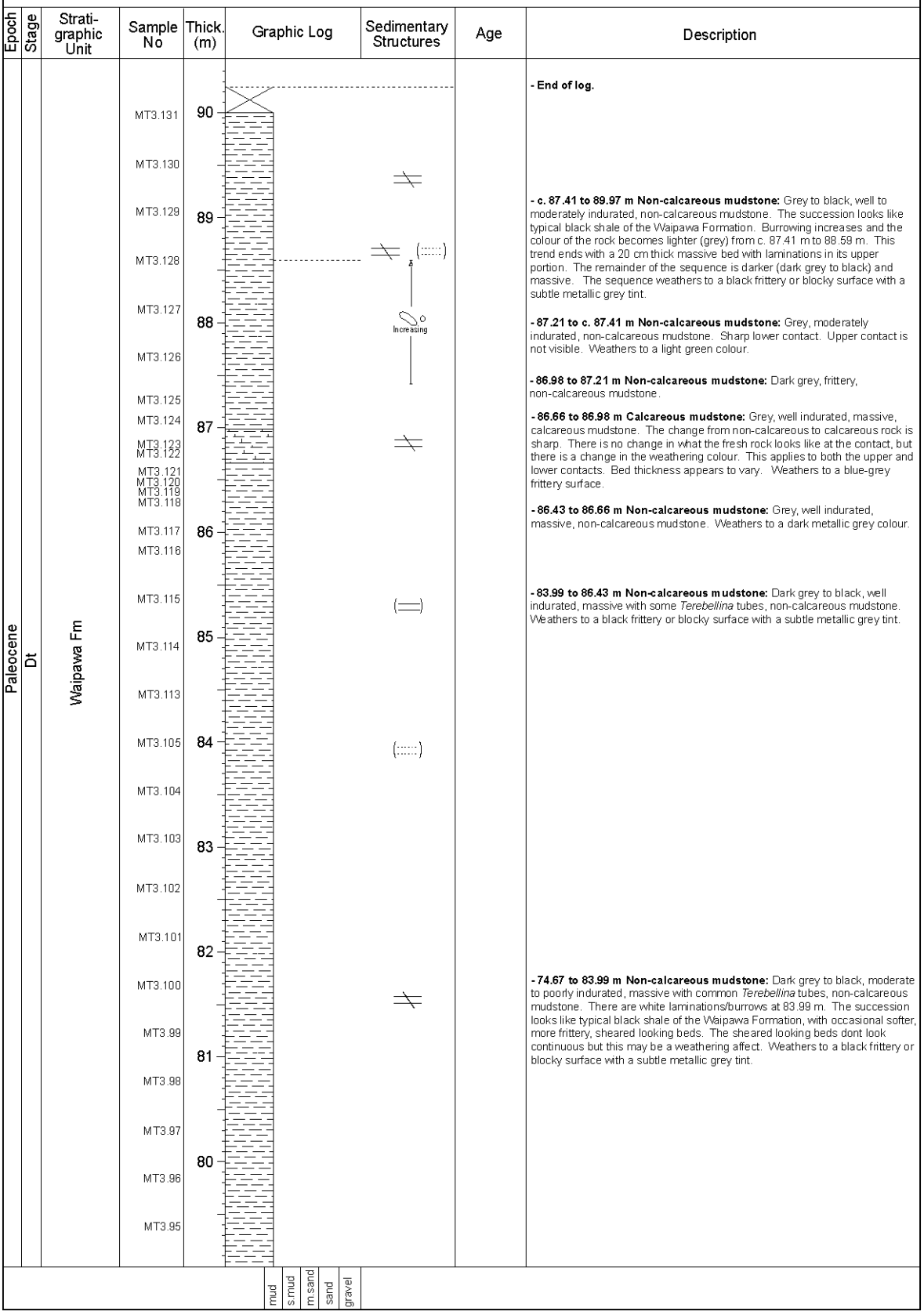

- End of log.

- c. 87.41 to 89.97 m Non-calcareous mudstone: Grey to black, well to moderately indurated, non-calcareous mudstone. The succession looks like typical black shale of the Waipawa Formation. Burrowing increases and the colour of the rock becomes lighter (grey) from c. 87.41 m to 88.59 m. This trend ends with a 20 cm thick massive bed with laminations in its upper portion. The remainder of the sequence is darker (dark grey to black) and massive. The sequence weathers to a black frittery or blocky surface with a subtle metallic grey tint.

- 87.21 to c. 87.41 m Non-calcareous mudstone: Grey, moderately indurated, non-calcareous mudstone. Sharp lower contact. Upper contact is not visible. Weathers to a light green colour.

- 86.98 to 87.21 m Non-calcareous mudstone: Dark grey, frittery, non-calcareous mudstone.

- 86.66 to 86.98 m Calcareous mudstone: Grey, well indurated, massive, calcareous mudstone. The change from non-calcareous to calcareous rock is sharp. There is no change in what the fresh rock looks like at the contact, but there is a change in the weathering colour. This applies to both the upper and lower contacts. Bed thickness appears to vary. Weathers to a blue-grey frittery surface.

- 86.43 to 86.66 m Non-calcareous mudstone: Grey, well indurated, massive, non-calcareous mudstone. Weathers to a dark metallic grey colour.

- 83.99 to 86.43 m Non-calcareous mudstone: Dark grey to black, well indurated, massive with some *Terebellina* tubes, non-calcareous mudstone. Weathers to a black frittery or blocky surface with a subtle metallic grey tint.

- 74.67 to 83.99 m Non-calcareous mudstone: Dark grey to black, moderate to poorly indurated, massive with common *Terebellina* tubes, non-calcareous mudstone. There are white laminations/burrows at 83.99 m. The succession looks like typical black shale of the Waipawa Formation, with occasional softer, more frittery, sheared looking beds. The sheared looking beds dont look continuous but this may be a weathering affect. Weathers to a black frittery or blocky surface with a subtle metallic grey tint.

Stratigraphic Column: Lower Angora Rd - Lower Calc Bed

Column No: 1:1

Region: Southern Hawke's Bay, New Zealand

Location: LOWER ANGORA ROAD, WIMBLEDON. Measured section located at the lower quarry on Angora Rd.

Logged by: Michael Tayler.

Date: 20-26 02 2010 (day month year)

and:

GPS base:

GPS top:

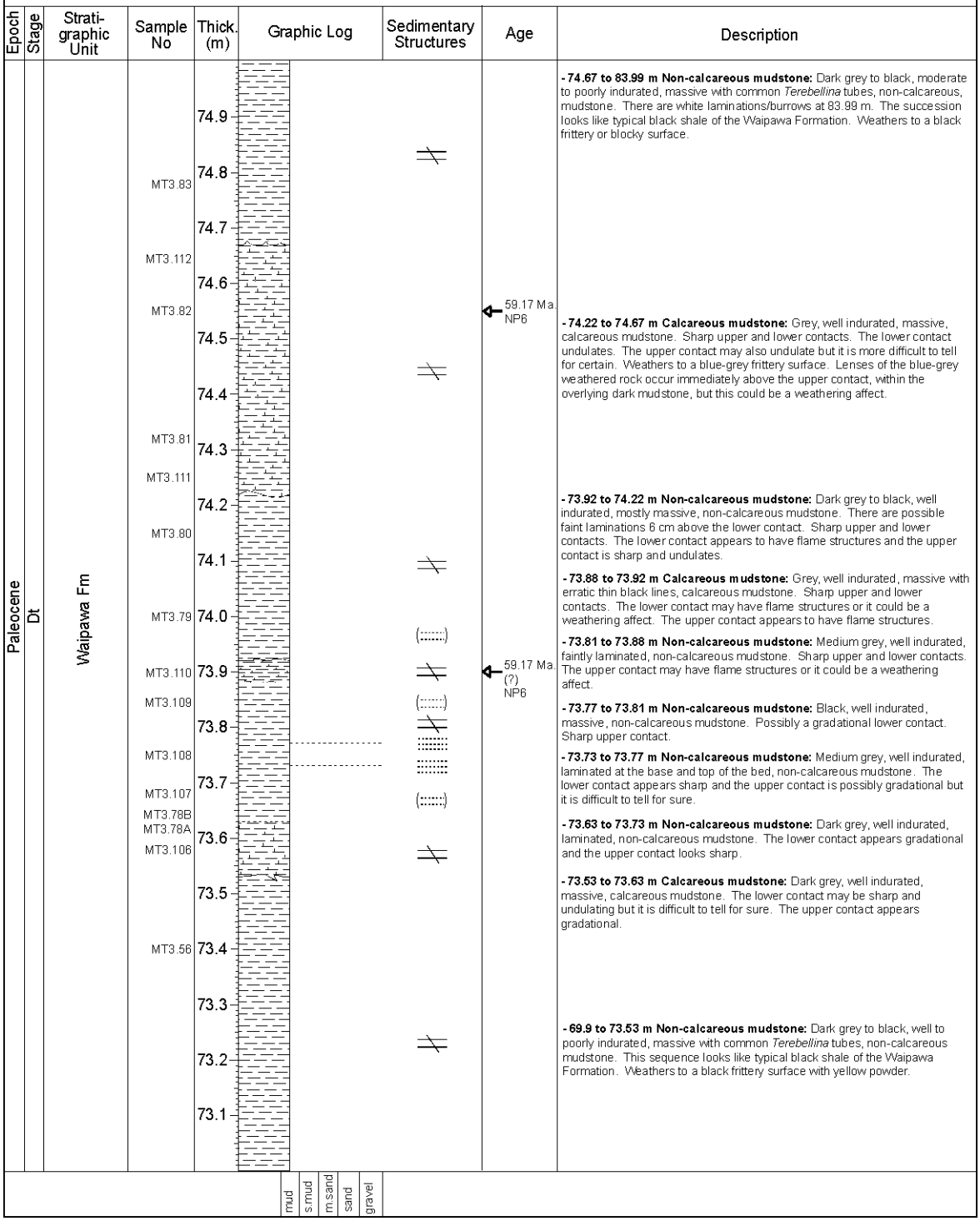

- 74.67 to 83.99 m Non-calcareous mudstone: Dark grey to black, moderate to poorly indurated, massive with common *Terebellina* tubes, non-calcareous, mudstone. There are white laminations/burrows at 83.99 m. The succession looks like typical black shale of the Waipawa Formation. Weathers to a black frittery or blocky surface.

- 74.22 to 74.67 m Calcareous mudstone: Grey, well indurated, massive, calcareous mudstone. Sharp upper and lower contacts. The lower contact undulates. The upper contact may also undulate but it is more difficult to tell for certain. Weathers to a blue-grey frittery surface. Lenses of the blue-grey weathered rock occur immediately above the upper contact, within the overlying dark mudstone, but this could be a weathering affect.

- 73.92 to 74.22 m Non-calcareous mudstone: Dark grey to black, well indurated, mostly massive, non-calcareous mudstone. There are possible faint laminations 6 cm above the lower contact. Sharp upper and lower contacts. The lower contact appears to have flame structures and the upper contact is sharp and undulates.

- 73.88 to 73.92 m Calcareous mudstone: Grey, well indurated, massive with erratic thin black lines, calcareous mudstone. Sharp upper and lower contacts. The lower contact may have flame structures or it could be a weathering affect. The upper contact appears to have flame structures.

- 73.81 to 73.88 m Non-calcareous mudstone: Medium grey, well indurated, faintly laminated, non-calcareous mudstone. Sharp upper and lower contacts. The upper contact may have flame structures or it could be a weathering affect.

- 73.77 to 73.81 m Non-calcareous mudstone: Black, well indurated, massive, non-calcareous mudstone. Possibly a gradational lower contact. Sharp upper contact.

- 73.73 to 73.77 m Non-calcareous mudstone: Medium grey, well indurated, laminated at the base and top of the bed, non-calcareous mudstone. The lower contact appears sharp and the upper contact is possibly gradational but it is difficult to tell for sure.

- 73.63 to 73.73 m Non-calcareous mudstone: Dark grey, well indurated, laminated, non-calcareous mudstone. The lower contact appears gradational and the upper contact looks sharp.

- 73.53 to 73.63 m Calcareous mudstone: Dark grey, well indurated, massive, calcareous mudstone. The lower contact may be sharp and undulating but it is difficult to tell for sure. The upper contact appears gradational.

- 69.9 to 73.53 m Non-calcareous mudstone: Dark grey to black, well to poorly indurated, massive with common *Terebellina* tubes, non-calcareous mudstone. This sequence looks like typical black shale of the Waipawa Formation. Weathers to a black frittery surface with yellow powder.

Stratigraphic Column: Upper Angora Rd - Overview

Column No: 1:1

Region: Southern Hawke's Bay, New Zealand

Location: UPPER ANGORA ROAD, WIMBLEDON. Measured section located on a road side exposure below the upper quarry on Angora Rd.

Date: 26 02 2010 (day month year)

GPS base: E2804372 N6076693

GPS top: E2804364 N6076637

Logged by: Michael Tayler (description partly from Column File: U24/c20b)

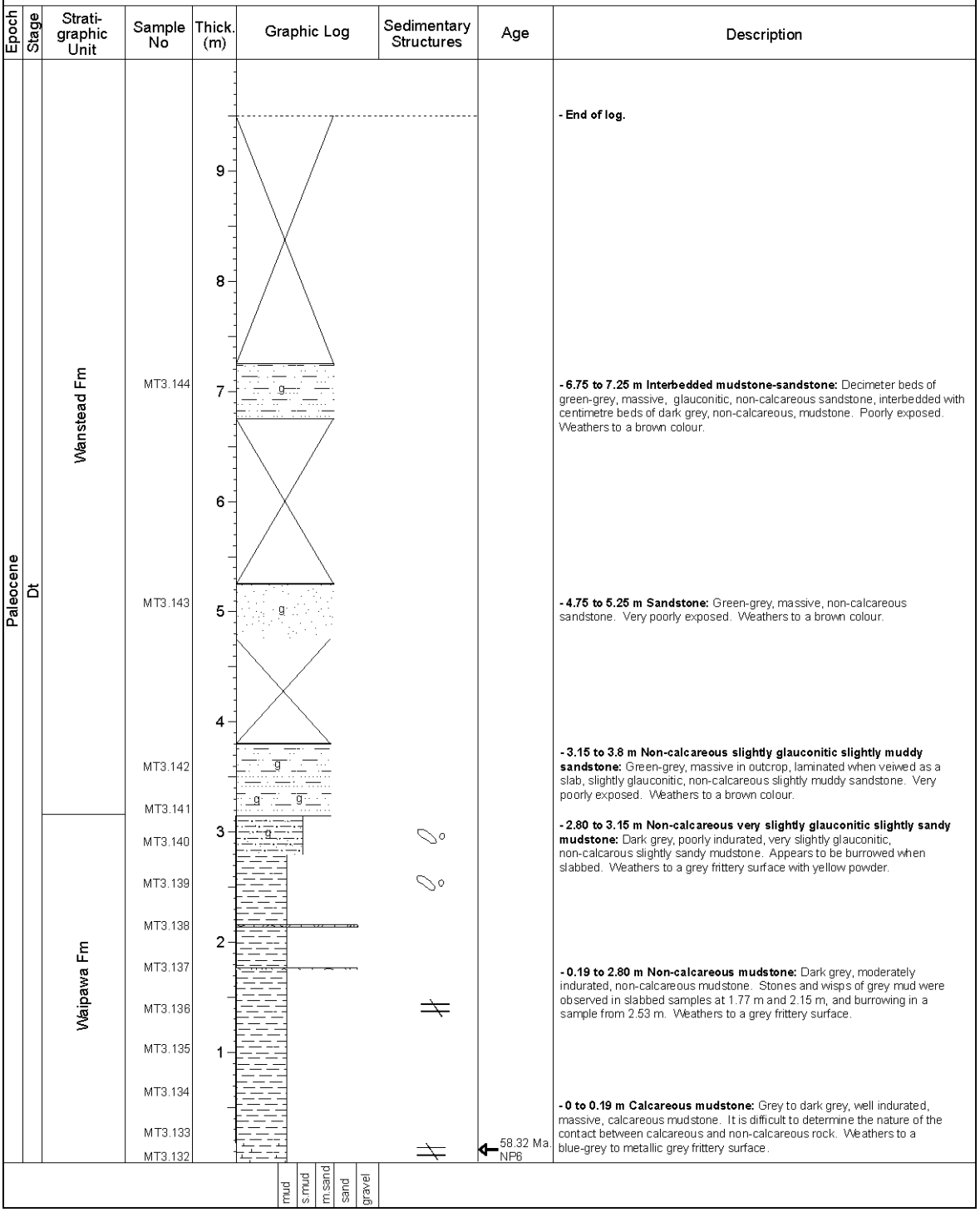

- End of log.

- 6.75 to 7.25 m Interbedded mudstone-sandstone: Decimeter beds of green-grey, massive, glauconitic, non-calcareous sandstone, interbedded with centimetre beds of dark grey, non-calcareous, mudstone. Poorly exposed. Weathers to a brown colour.

- 4.75 to 5.25 m Sandstone: Green-grey, massive, non-calcareous sandstone. Very poorly exposed. Weathers to a brown colour.

- 3.15 to 3.8 m Non-calcareous slightly glauconitic slightly muddy sandstone: Green-grey, massive in outcrop, laminated when veiwed as a slab, slightly glauconitic, non-calcareous slightly muddy sandstone. Very poorly exposed. Weathers to a brown colour.

- 2.80 to 3.15 m Non-calcareous very slightly glauconitic slightly sandy mudstone: Dark grey, poorly indurated, very slightly glauconitic, non-calcarous slightly sandy mudstone. Appears to be burrowed when slabbed. Weathers to a grey frittery surface with yellow powder.

- 0.19 to 2.80 m Non-calcareous mudstone: Dark grey, moderately indurated, non-calcareous mudstone. Stones and wisps of grey mud were observed in slabbed samples at 1.77 m and 2.15 m, and burrowing in a sample from 2.53 m. Weathers to a grey frittery surface.

- 0 to 0.19 m Calcareous mudstone: Grey to dark grey, well indurated, massive, calcareous mudstone. It is difficult to determine the nature of the contact between calcareous and non-calcareous rock. Weathers to a blue-grey to metallic grey frittery surface.

Appendix E

TAWANUI DETAILED STRATIGRAPHIC COLUMN

Stratigraphic Column: Tawanui Section - Overview

Column No: 1:1

Region: Southern Hawkes Bay, New Zealand

Location: TAWANUI. Measured section located in the head waters of the Akitio River. Base of log near Tawanui homestead beside Birch Road North. Log continues upstream for approximately 400m.

Logged by: Michael Tayler, Glen Treweek, Cam Nelson

Date: 03-04 (day) 12 (month) 2008 (year)

and: 04-06 (day) 01 (month) 2009 (year)

GPS base: E2796667 N6086293

GPS top: E2797032 N6086324

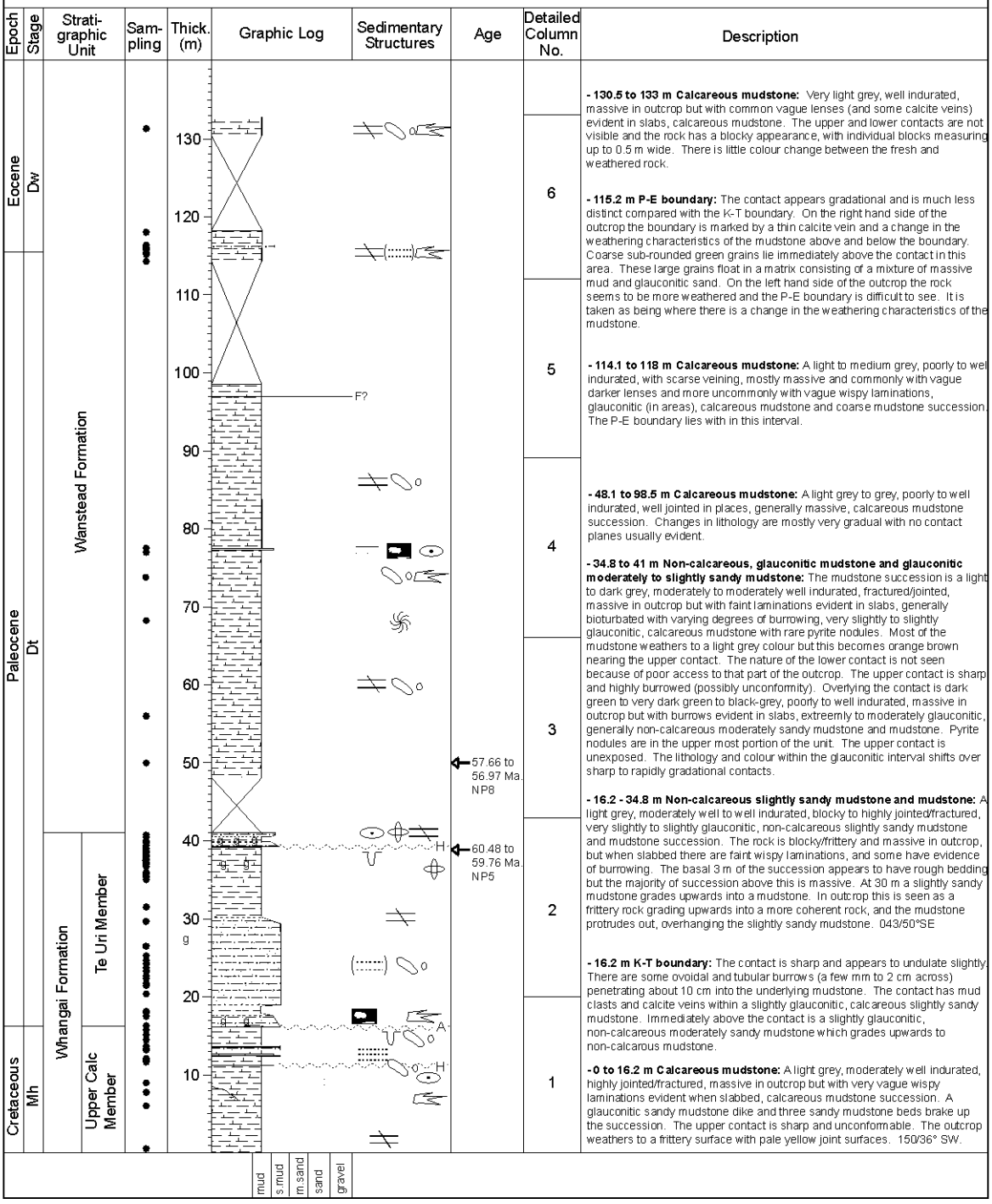

- 130.5 to 133 m Calcareous mudstone: Very light grey, well indurated, massive in outcrop but with common vague lenses (and some calcite veins) evident in slabs, calcareous mudstone. The upper and lower contacts are not visible and the rock has a blocky appearance, with individual blocks measuring up to 0.5 m wide. There is little colour change between the fresh and weathered rock.

- 115.2 m P-E boundary: The contact appears gradational and is much less distinct compared with the K-T boundary. On the right hand side of the outcrop the boundary is marked by a thin calcite vein and a change in the weathering characteristics of the mudstone above and below the boundary. Coarse sub-rounded green grains lie immediately above the contact in this area. These large grains float in a matrix consisting of a mixture of massive mud and glauconitic sand. On the left hand side of the outcrop the rock seems to be more weathered and the P-E boundary is difficult to see. It is taken as being where there is a change in the weathering characteristics of the mudstone.

- 114.1 to 118 m Calcareous mudstone: A light to medium grey, poorly to well indurated, with scarse veining, mostly massive and commonly with vague darker lenses and more uncommonly with vague wispy laminations, glauconitic (in areas), calcareous mudstone and coarse mudstone succession. The P-E boundary lies with in this interval.

- 48.1 to 98.5 m Calcareous mudstone: A light grey to grey, poorly to well indurated, well jointed in places, generally massive, calcareous mudstone succession. Changes in lithology are mostly very gradual with no contact planes usually evident.

- 34.8 to 41 m Non-calcareous, glauconitic mudstone and glauconitic moderately to slightly sandy mudstone: The mudstone succession is a light to dark grey, moderately to moderately well indurated, fractured/jointed, massive in outcrop but with faint laminations evident in slabs, generally bioturbated with varying degrees of burrowing, very slightly to slightly glauconitic, calcareous mudstone with rare pyrite nodules. Most of the mudstone weathers to a light grey colour but this becomes orange brown nearing the upper contact. The nature of the lower contact is not seen because of poor access to that part of the outcrop. The upper contact is sharp and highly burrowed (possibly unconformity). Overlying the contact is dark green to very dark green to black-grey, poorly to well indurated, massive in outcrop but with burrows evident in slabs, extreemly to moderately glauconitic, generally non-calcareous moderately sandy mudstone and mudstone. Pyrite nodules are in the upper most portion of the unit. The upper contact is unexposed. The lithology and colour within the glauconitic interval shifts over sharp to rapidly gradational contacts.

- 16.2 - 34.8 m Non-calcareous slightly sandy mudstone and mudstone: A light grey, moderately well to well indurated, blocky to highly jointed/fractured, very slightly to slightly glauconitic, non-calcareous slightly sandy mudstone and mudstone succession. The rock is blocky/frittery and massive in outcrop, but when slabbed there are faint wispy laminations, and some have evidence of burrowing. The basal 3 m of the succession appears to have rough bedding but the majority of succession above this is massive. At 30 m a slightly sandy mudstone grades upwards into a mudstone. In outcrop this is seen as a frittery rock grading upwards into a more coherent rock, and the mudstone protrudes out, overhanging the slightly sandy mudstone. 043/50°SE

- 16.2 m K-T boundary: The contact is sharp and appears to undulate slightly. There are some ovoidal and tubular burrows (a few mm to 2 cm across) penetrating about 10 cm into the underlying mudstone. The contact has mud clasts and calcite veins within a slightly glauconitic, calcareous slightly sandy mudstone. Immediately above the contact is a slightly glauconitic, non-calcareous moderately sandy mudstone which grades upwards to non-calcarous mudstone.

- 0 to 16.2 m Calcareous mudstone: A light grey, moderately well indurated, highly jointed/fractured, massive in outcrop but with very vague wispy laminations evident when slabbed, calcareous mudstone succession. A glauconitic sandy mudstone dike and three sandy mudstone beds brake up the succession. The upper contact is sharp and unconformable. The outcrop weathers to a frittery surface with pale yellow joint surfaces. 150/36° SW.

Stratigraphic Column: Tawanui Section - Detailed Log

Column No: 1:6

Region: Southern Hawkes Bay, New Zealand

Location: TAWANUI. Measured section located in the head waters of the Akitio River. Base of log near Tawanui homestead, beside Birch Road North. Log continues upstream for approximately 400m.

Logged by: Michael Tayler, Glen Treweek, Cam Nelson

Date: 03-04 (day) 12 (month) 2008 (year)

and: 04-06 (day) 01 (month) 2009 (year)

GPS base: E2796667 N6086293

GPS top: E2797032 N6086324

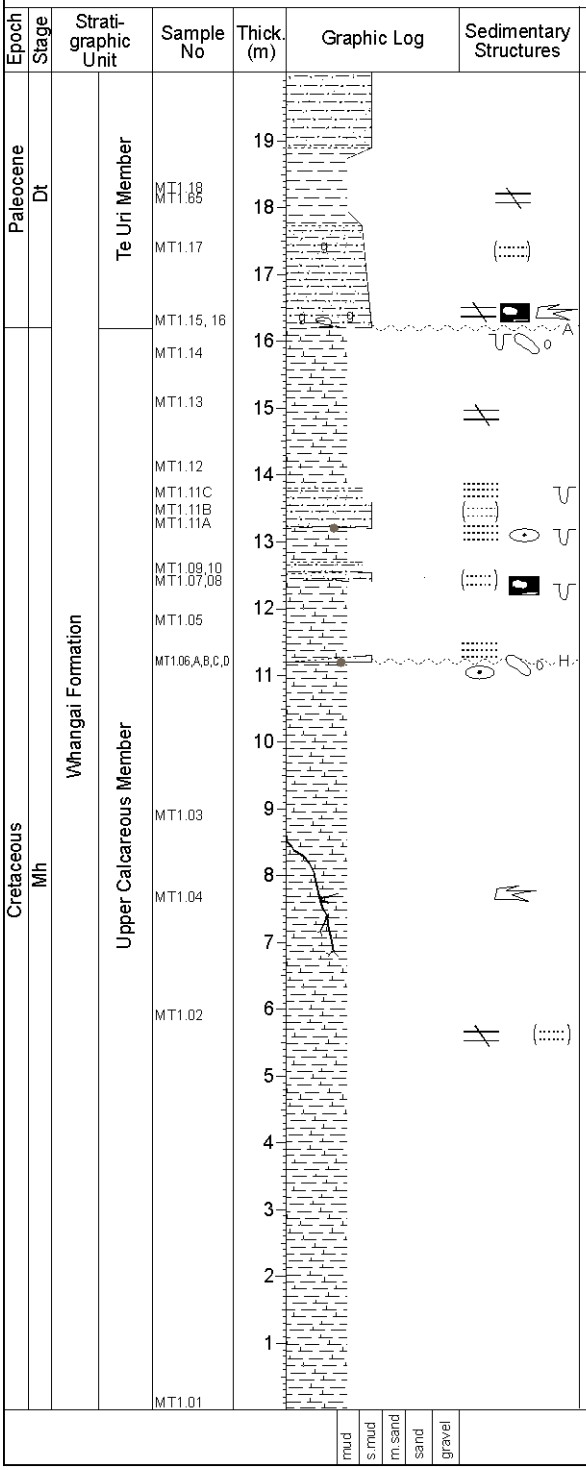

Age	Description
	- 16.2 to 18.9 m Non-calcareous moderately sandy mudstone grading upwards into non-calcareous mudstone: Immediately above the K-T boundary there is a light grey, well indurated, blocky, massive in outcrop slightly glauconitic, non-calcareous moderately sandy mudstone. The sandy mudstone grades upwards into a light grey, moderately well indurated, highly jointed/fractured, massive, non-calcareous mudstone. The abundance of glaucony decreases rapidly upwards. Slabbed samples show that the lower most portion of the bed is massive, the mid regions faintly laminated, and the upper mudstone massive. The rock weathers to an orange brown colour and becomes more frittery upwards. **- 16.2 m K-T boundary:** The contact is sharp and appears to undulate slightly. There are some ovoidal and tubular burrows (a few mm to 2 cm across) penetrating about 10 cm into the underlying mudstone. The contact has mud clasts and calcite veins within a massive slightly glauconitic, calcareous slightly sandy mudstone. **- 13.2 to 13.8 m Calcareous moderately sandy mudstone:** Grey, well indurated, prominantly laminated through the upper & lower portions, slightly glauconitic, calcareous slightly sandy mudstone. The bed appears amalgamated as two seperate turbidites, the lower 40 cm thick and the upper 20 cm thick. Bed thickness pinchs and swells and varies from 40-60 cm. The bed has a sharp basal contact with glaucony infilled burrowing into the underlying mudstone (≤ fingure size) and scattered pyrite nodules. The upper contact seems to rapidly grade into mudstone and possible burrows can be seen. There is limonite staining around the pyrite nodules. 130/26°SE. - **12.4 to 12.5 m Calcareous moderately sandy mudstone:** Grey, well indurated, faint parallel laminations on the lower part of the bed (Bouma B?), moderately glauconitic, calcareous moderately sandy mudstone. Some pyrite filled burrows are evident in cut slabs. The bed thickness varies from 8 - 13 cm & appears to pinch and swell. The lower contact is sharp and undulates, with interweaving of sand and mud, and burrowing at the interface. The upper contact grades into a very slightly glauconitic slightly sandy mudstone. Joint surfaces develop a faun to rusty colour. **- 11.2 to 11.3 m Calcareous moderately sandy mudstone:** Grey, well indurated, prominantly laminated, moderately glauconitic, calcareous, moderately sandy mudstone. The bed thickness varies from being a thin smear of 0 - 2 cm to being 10 cm thick. There are prominant and unusually large glauconitic and pyrite filled mudstone burrows up to depths of 15 cm below the smeared sandy mudstone bed. They consisted of 3 - 8 cm diameter tubes which are sub-circular in cross section. Smaller burrows 0.5 - 1 cm in diameter are also present. There are burrows up to 7 cm in diameter up to 30 cm below the thicker portion of the sandy mudstone. Scattered pyrite nodules are present along the horizon, with locally intensive limonite staining in the vicinity of the nodules. **- 6.8 to 8.5 m Glauconitic calcareous mudstone dike:** Light grey-green, moderately well indurated, glauconitic,calcareous mudstone. The dike is difficult to distinguish from afar, but more obvious close up. The main vein runs across the bedding of the mudstone and splits up into long slender fingers that run away from the main vein at low to high angles. The thickness varies from 2 cm, to very thin near its termination. The source of the dike is not visible. **- 0 to 16.2 m Calcareous mudstone:** Light grey, moderately well indurated, highly jointed/fractured, massive in outcrop but with very vague wispy laminations evident when slabbed, calcareous mudstone succession. The upper contact is sharp and unconformable. The outcrop weathers to a frittery surface with pale yellow joint surfaces. 150/36° SW.

Stratigraphic Column: Tawanui Section - Detailed Log

Column No: 2:6

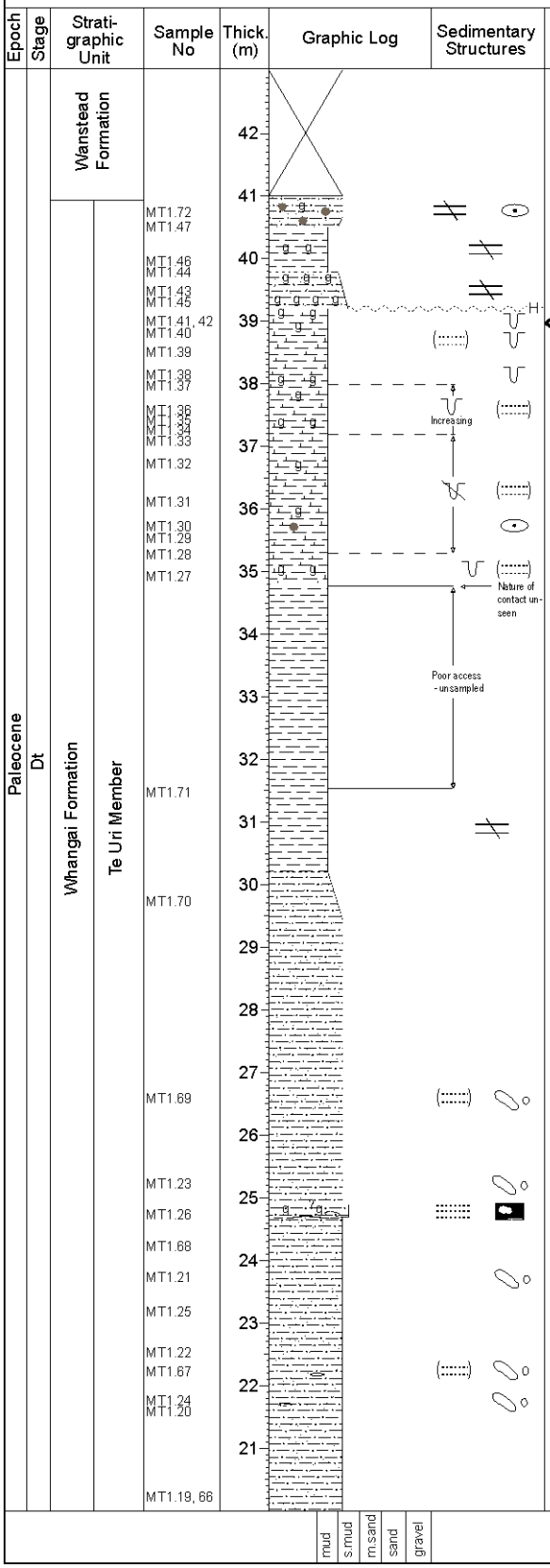

- 40.5 to 41 m Non-calcareous, moderately glauconitic, slightly sandy mudstone: Dark grey and black, moderately to well indurated, massive, glauconitic, non-calcareous, slightly sandy mudstone. Contains hard ovoidal pyrite cemented nodules with in a moderate-poorly indurated matrix. Lower contact is poorly exposed but is possibly sharp. There may be a 10 cm thickness of softer muddier green mudstone between this unit and the hard dark underlying unit. This could be due to weathering however. Upper contact is not exposed.

- 39.8 to 40.5 m Non-calcareous, highly glauconitic mudstone: Very dark green (fresh), well indurated, massive in outcrop with some burrows evident in slabs, calcareous in burrowed areas, non-calcareous in glauconitic areas, highly glauconitic mudstone. The lower contact is sharp to rapidly gradational and the upper contact poorly exposed but possibly sharp. When weathered the rock is a very dark grey and looks like a grey mudstone with abundant glauconite grains. Iron staining was evident around in-situ blocks.

- 39.2 to 39.8 m Non-calcareous, very highly glauconitic, moderately sandy mudstone [greensand]: Green, poorly indurated, massive in outcrop with burrows evident in slabs, very highly to extreemly glauconitic, non-calcareous moderately sandy mudstone [greensand]. The lower contact is sharp with abundant prominant very highly glauconitic burrows penetrating into the underlying mudstone. The burrows are 3-7 cm long and 2 cm wide. The upper contact is sharp to rapidly gradational.

- 38.2 to 39.2 m Calcareous mudstone with burrowed horizon: Grey to brown grey, moderately indurated, massive with a burrowed horizon, slightly glauconitic, calcareous mudstone. A horizon of prominant glaucony infilled burrows occurrs between 38.6 and 39 m. The burrows are fingure like and 6-20cm long, 2-3 cm wide and fill the majority of the horizon. There are smaller (5 cm long and 1 cm wide) less prominant burrows in the top 7 cm of the horizon. These are seperated from the larger burrows by a very thin bed of wispy glauconite interbedded with mudstone, capped with a thinner layer of massive mudstone (c. 5 cm total thickness). The rock weathers to an orange-brown frittery surface.

- 34.8 to 38.2 m Calcareous mudstone: Light grey to dark grey, moderately to moderately well indurated, massive in outcrop with occassional glaucony infilled burrows, slightly glauconitic, calcareous mudstone. Slabbed samples show faint wispy laminations and scattered glaucony grains through out the rock. Glaucony infilled burrows occur between 34.8 and 35.3 m. Between 35.3 and 37.2 m there are rare pyrite nodules and no evidence of burrowing in outcrop. Slabs show possible faint burrows however. At 37 m the mudstone begins becoming more glauconitic and the intensity of burrowing increases up to 38 m. There appears to be a decrease in the intensity of burrowing between 38 m and 38.2 m. The lower contact with the underlying non-calcareous mudstone was not accessable. The rock weathers to a light grey surface.

- 24.7 to ? m Non-calcareous slightly sandy mudstone: Grey, very well indurated, moderately glauconitic, non-calcareous slightly sandy mudstone with wispy laminations. The bed is visually difficult to distinguish from the surrounding rock in outcrop, with only a slightly rustier colour differentiating it from the rock below. It has a higher induration however. A slab of the rock shows the bed has a sharp, wavy lower contact with rip up clasts. The upper contact was not observed.

- 21.2 and 22.3 m Glauconitic non-calcareous slightly sandy mudstone lenses: Two glauconitic, non-calcareous slightly sandy mudstone lenses are present at c. 21.2 m and 22.2 m. The lower lense is about 2 cm thick at its thickest, and discontinuous, with the bed unable to be traced for any great distance. Its length is c. 30 cm. The higher lense is c. 1.5 cm thick and 14 cm long, and a slab of the sample shows that the surrounding rock is dark grey with a yellow tint.

- 18.9 - 34.8 m Non-calcareous slightly sandy mudstone grading into non-calcareous mudstone: Light grey, moderately well to well indurated, blocky to highly jointed/fractured, massive, very slightly to slightly glauconitic, non-calcareous slightly sandy mudstone and mudstone. The rock is blocky/frittery and massive in outcrop, but when slabbed there are faint wispy laminations, and some have evidence of burrowing. At 30 m the slightly sandy mudstone grades upwards into a mudstone. In outcrop this is seen as frittery rock grading upwards into a more coherent rock. The mudstone protrudes out and overhangs the underlying slightly sandy mudstone. It is only possible to reach the base of the mudstone and the upper contact between the non-calcareous mudstone and the overlying calcareous mudstone is not accessable. 043/50°SE.

Stratigraphic Column: Tawanui Section - Detailed Log

Column No: 3:6

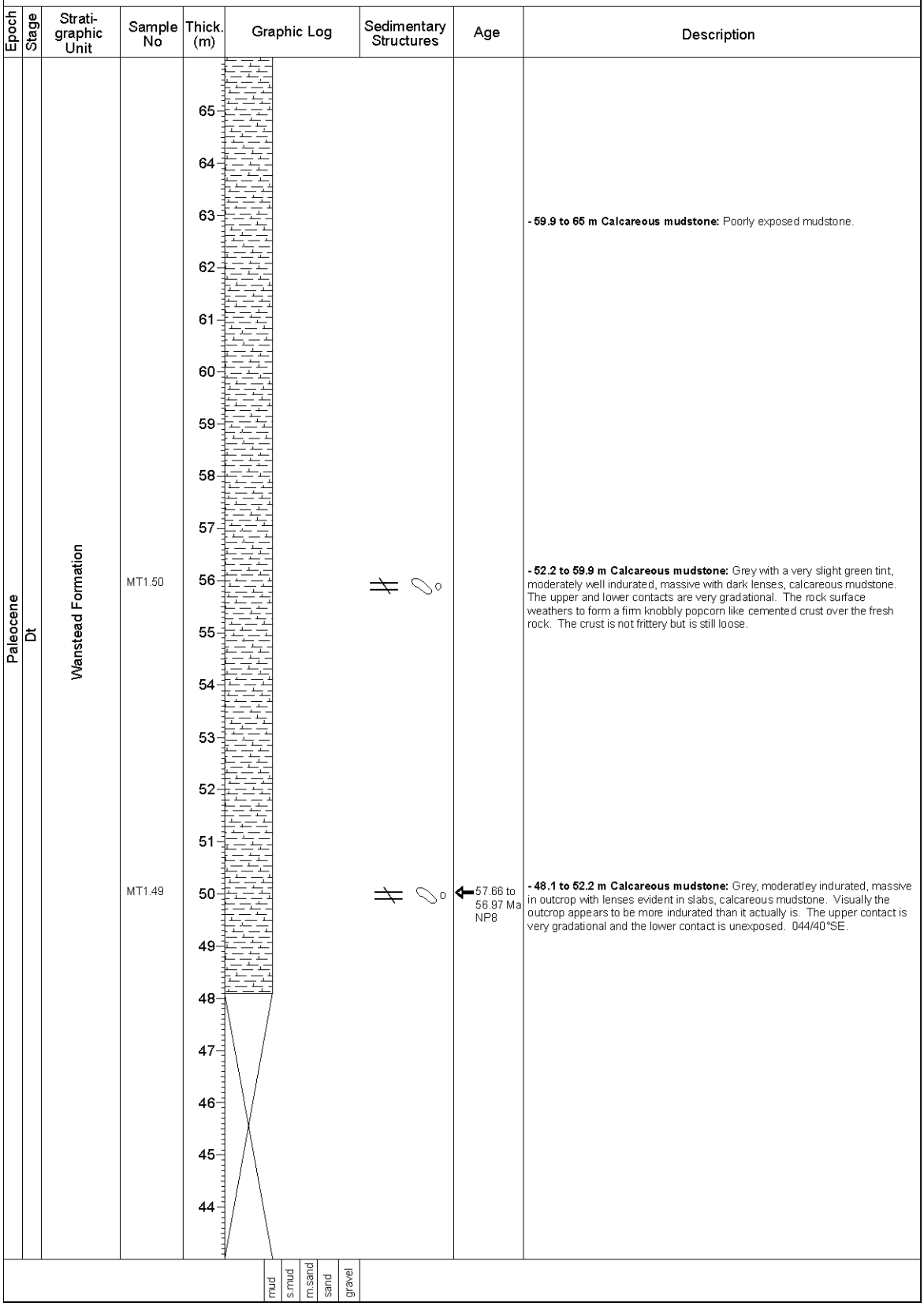

Stratigraphic Column: Tawanui Section - Detailed Log

Column No: 4:6

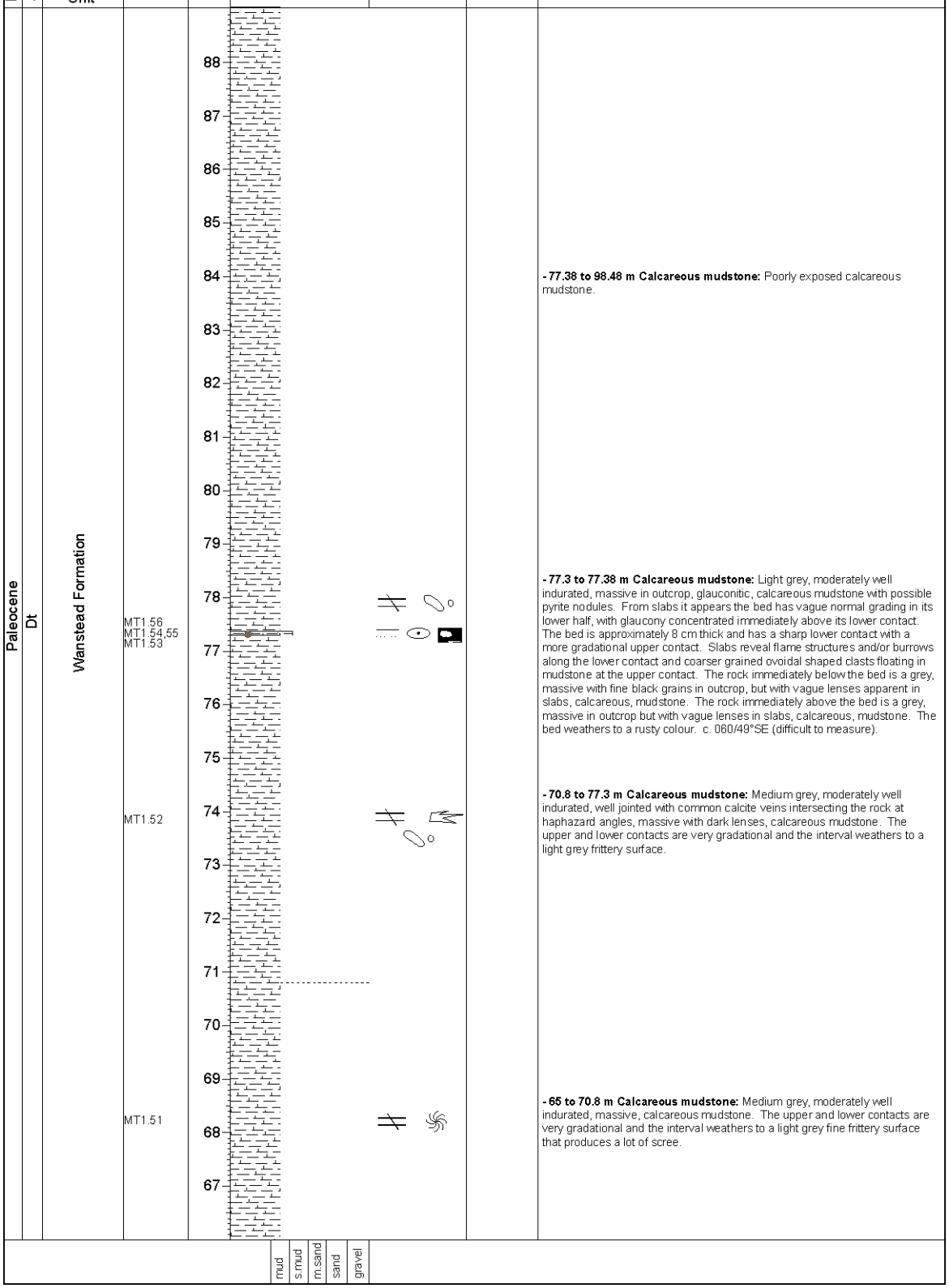

- 77.38 to 98.48 m Calcareous mudstone: Poorly exposed calcareous mudstone.

- 77.3 to 77.38 m Calcareous mudstone: Light grey, moderately well indurated, massive in outcrop, glauconitic, calcareous mudstone with possible pyrite nodules. From slabs it appears the bed has vague normal grading in its lower half, with glaucony concentrated immediately above its lower contact. The bed is approximately 8 cm thick and has a sharp lower contact with a more gradational upper contact. Slabs reveal flame structures and/or burrows along the lower contact and coarser grained ovoidal shaped clasts floating in mudstone at the upper contact. The rock immediately below the bed is a grey, massive with fine black grains in outcrop, but with vague lenses apparent in slabs, calcareous, mudstone. The rock immediately above the bed is a grey, massive in outcrop but with vague lenses in slabs, calcareous, mudstone. The bed weathers to a rusty colour. c. 060/49°SE (difficult to measure).

- 70.8 to 77.3 m Calcareous mudstone: Medium grey, moderately well indurated, well jointed with common calcite veins intersecting the rock at haphazard angles, massive with dark lenses, calcareous mudstone. The upper and lower contacts are very gradational and the interval weathers to a light grey frittery surface.

- 65 to 70.8 m Calcareous mudstone: Medium grey, moderately well indurated, massive, calcareous mudstone. The upper and lower contacts are very gradational and the interval weathers to a light grey fine frittery surface that produces a lot of scree.

Stratigraphic Column: Tawanui Section - Detailed Log

Column No: 5:6

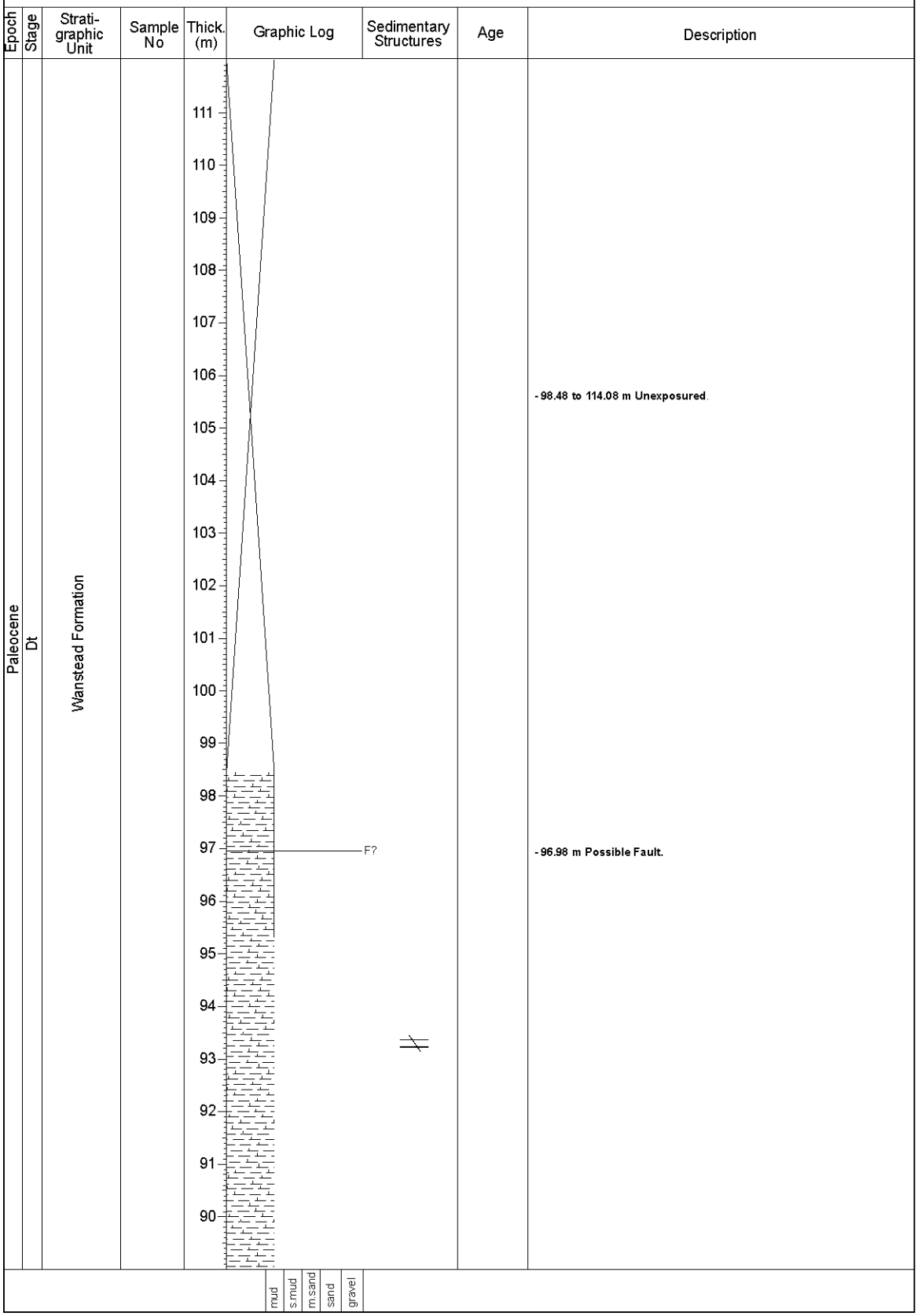

Stratigraphic Column: Tawanui Section - Detailed Log

Column No: 6:6

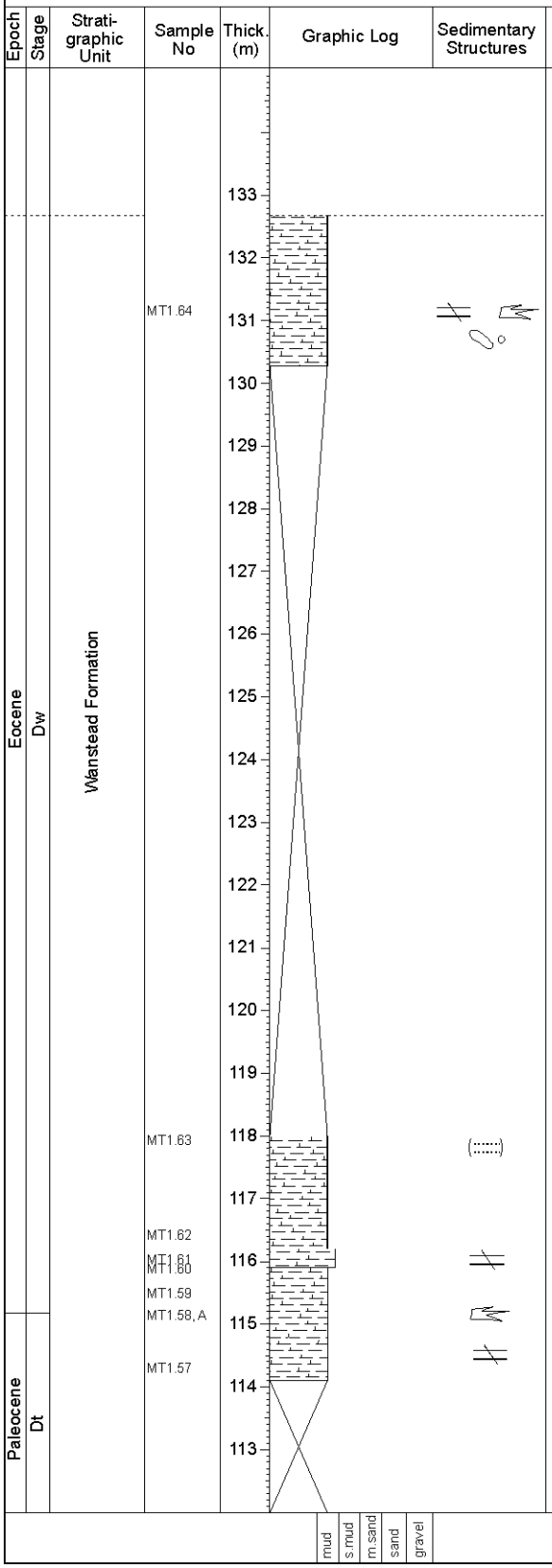

- End of log.

- 131.2 m Calcareous mudstone: Very light grey, well indurated, massive in outcrop but with common vague lenses and some calcite veins evident in slabs, calcareous mudstone. The upper and lower contacts of the outcrop are not visible. The rock has a blocky appearance with individual blocks measuring up to 0.5 m wide. There is little colour change between fresh and weathered rock.

- 118 m Calcareous mudstone: Light grey, well indurated, massive in outcrop but with vague wispy laminations evident in slabs, calcareous mudstone. The rock weathers to relatively large frittery blocks.

- 116.4 m Calcareous mudstone: Grey, moderately indurated, massive with some scattered sand sized glauconite grains, calcareous mudstone. The interval has gradational lower and upper contacts and weathers to a light grey frittery surface.

- 116 m Calcareous mudstone: Light grey, moderately well indurated, massive with common scattered sand sized glaucony grains, calcareous coarse mudstone/siltstone. The bed is approximately 30 cm thick and has a sharp lower contact and a rapidly gradational upper contact. It weathers to a rusty colour.

- 115.9 m Calcareous mudstone: Medium grey with a very vague green tint (not represented in all the samples), moderately well indurated, massive with vague black lenses, calcareous mudstone. Slabbing reveiled a possible very vague burrow. The interval has a gradational lower contact and sharp upper contact with a coarser grained bed. Weathers to a brown colour.

- 115.5 m Calcareous mudstone: Medium grey, poorly indurated, massive, calcareous mudstone. The upper and lower contacts are gradational. The rock is highly weathered, more so than any of the other rocks in the vicinity of the P-E boundary, and it weathers to a brown colour.

- 115.2 m P-E boundary: The contact appears gradational and is much less distinct compared with the K-T boundary. On the right hand side of the outcrop the boundary is marked by a thin calcite vein and a change in the weathering characteristics of the mudstone above and below the boundary. Coarse sub-rounded green grains lie immediately above the contact in this area. These large grains float in a matrix consisting of a mixture of massive mud and glauconitic sand. On the left hand side of the outcrop the rock seems to be more weathered and the P-E boundary is difficult to see. It has been taken as where there is a change in the weathering characteristics of the mudstone.

- 115.2 m Calcareous mudstone: Grey with a green tint, moderately indurated, massive with predominant black lenses (in some samples), calcareous mudstone. The upper and lower contacts are gradational. The rock weathers to a light grey, frittery mudstone and the size of the individual disintergrating rock clasts are larger than those of the underlying mudstone.

- 114.3 m Calcareous mudstone: Medium grey, moderately indurated, massive with very faint black lenses, calcareous mudstone. Gradational upper and lower contacts. Weatheres to a frittery grey surface.

Appendix F

LOWER MANGAHOUANGA STREAM DETAILED STRATIGRAPHIC COLUMN

Stratigraphic Column: Lower Mangahouanga Stream

Column No: 1:1

Region: Northern Hawke Bay, New Zealand

Location: LOWER MANGAHOUANGA STREAM. Measured section located in stream exposure near the "Rock Hounds" hut, Te Hoe Road, Maungataniwha Forest.

Logged by: Michael Tayler, Poul Schiøler, Chris Hollis

Date: 09 02 2010 (day month year)

GPS base: E2841654 N6247258

GPS top:

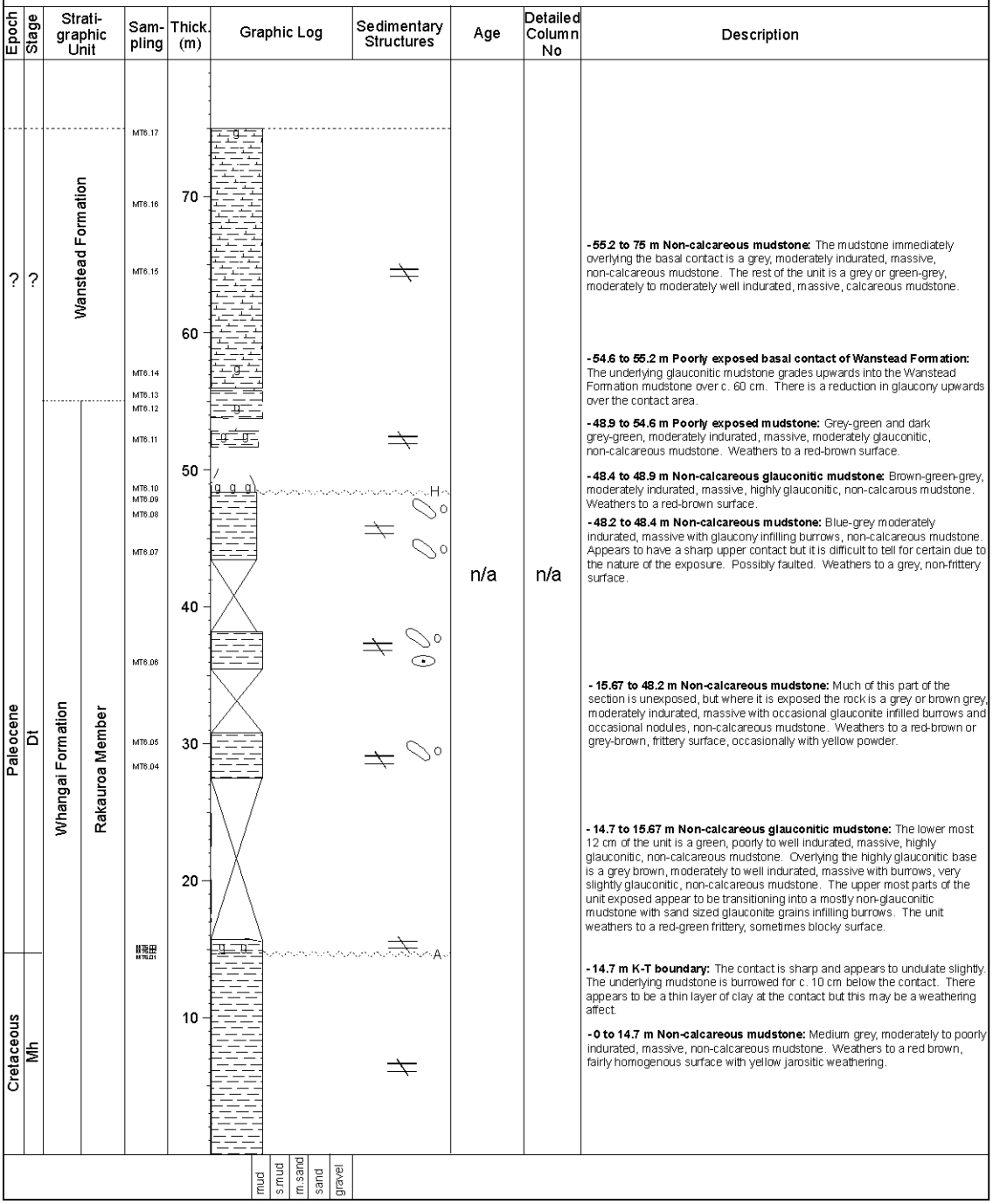

-55.2 to 75 m Non-calcareous mudstone: The mudstone immediately overlying the basal contact is a grey, moderately indurated, massive, non-calcareous mudstone. The rest of the unit is a grey or green-grey, moderately to moderately well indurated, massive, calcareous mudstone.

-54.6 to 55.2 m Poorly exposed basal contact of Wanstead Formation: The underlying glauconitic mudstone grades upwards into the Wanstead Formation mudstone over c. 60 cm. There is a reduction in glaucony upwards over the contact area.

-48.9 to 54.6 m Poorly exposed mudstone: Grey-green and dark grey-green, moderately indurated, massive, moderately glauconitic, non-calcareous mudstone. Weathers to a red-brown surface.

-48.4 to 48.9 m Non-calcareous glauconitic mudstone: Brown-green-grey, moderately indurated, massive, highly glauconitic, non-calcarous mudstone. Weathers to a red-brown surface.

-48.2 to 48.4 m Non-calcareous mudstone: Blue-grey moderately indurated, massive with glaucony infilling burrows, non-calcareous mudstone. Appears to have a sharp upper contact but it is difficult to tell for certain due to the nature of the exposure. Possibly faulted. Weathers to a grey, non-frittery surface.

- 15.67 to 48.2 m Non-calcareous mudstone: Much of this part of the section is unexposed, but where it is exposed the rock is a grey or brown grey, moderately indurated, massive with occasional glauconite infilled burrows and occasional nodules, non-calcareous mudstone. Weathers to a red-brown or grey-brown, frittery surface, occasionally with yellow powder.

- 14.7 to 15.67 m Non-calcareous glauconitic mudstone: The lower most 12 cm of the unit is a green, poorly to well indurated, massive, highly glauconitic, non-calcareous mudstone. Overlying the highly glauconitic base is a grey brown, moderately to well indurated, massive with burrows, very slightly glauconitic, non-calcareous mudstone. The upper most parts of the unit exposed appear to be transitioning into a mostly non-glauconitic mudstone with sand sized glauconite grains infilling burrows. The unit weathers to a red-green frittery, sometimes blocky surface.

-14.7 m K-T boundary: The contact is sharp and appears to undulate slightly. The underlying mudstone is burrowed for c. 10 cm below the contact. There appears to be a thin layer of clay at the contact but this may be a weathering affect.

-0 to 14.7 m Non-calcareous mudstone: Medium grey, moderately to poorly indurated, massive, non-calcareous mudstone. Weathers to a red brown, fairly homogenous surface with yellow jarositic weathering.

Appendix G

AKITIO RIVER DETAILED STRATIGRAPHIC COLUMN

Stratigraphic Column: Akitio River - Overview

Column No: 1:1

Region: Southern Hawkes Bay, New Zealand

Location: AKITIO RIVER. Measured section located in the middle reaches of the Akitio River, mid-way between Waipatiki and Weber.

Logged by: Michael Tayler, Deborah Davey

Date: 08 (day) 12 (month) 2009 (year)

and:

GPS base: E2790305 N6086584

GPS top: E2790287 N6086621

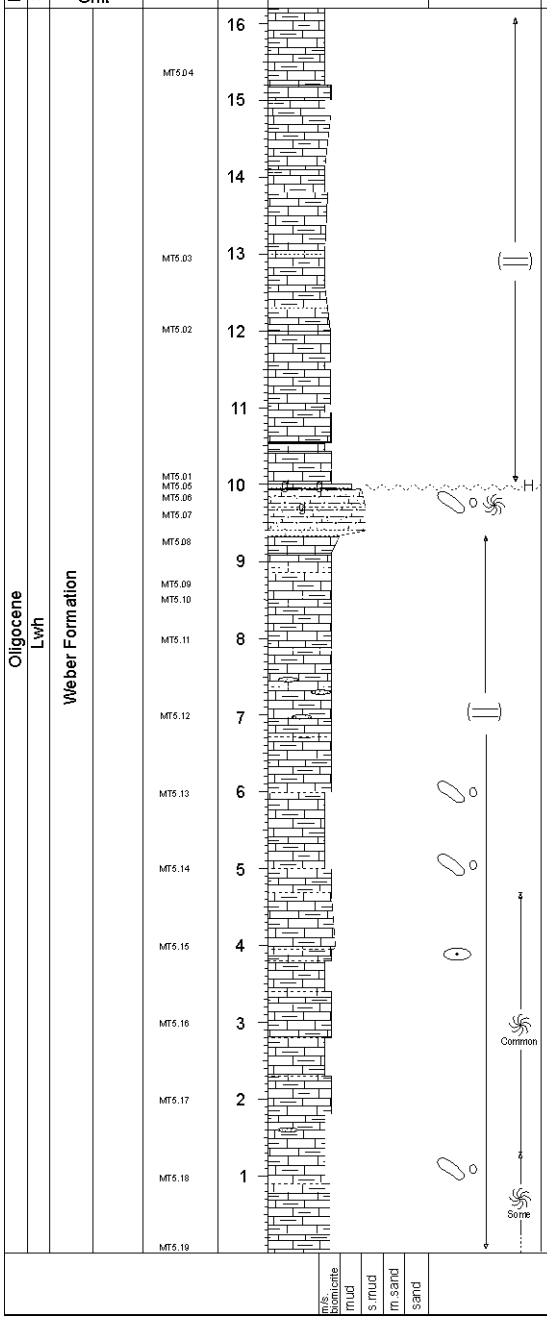

- 10 to 16.1 m Muddy limestone: Medium grey and blue-green-grey, moderately to moderately well indurated, massive in hand specimen, poorly bedded in outcrop, very slightly glauconitic, calcareous muddy limestone. Between 10 and 12 m beds are faint and difficult to define. The contacts may be more gradational and/or there is only a small difference in grain size between beds. Between 12 and 15 m the beds become more defined, with sharper bottom contacts in some beds exposed on the stream bed. Some of these contacts may be undulating but it is difficult to tell for certain due to the small difference in grainsize.

- 9.3 to 10 m Slightly sandy mudstone (Marshall Unconformity?): Very poorly to moderately indurated, massive with some burrowing, calcareous, slightly glauconitic sandy mudstone. Through the lower portion of the sequence the grain size appears to coarsen upwards. The middle portion of the succession seems to remain relatively coarse grained for 40 cm, and then fines upwards. This is capped with a thin bed of more glauconitic mudstone. The more glauconitic beds lower contact appears to be sharp to rapidly gradational and has faint burrowing. The other contacts appear gradational.

- 6.0 to 9.3 m Muddy limestone: Consists of grey, moderately to well indurated, massive in hand specimen, massive to moderately bedded in outcrop, calcareous muddy limestone. Dark lenses occur between 6.9 and 7.6 m. Succession begins to become muddier towards its upper contact.

- 0 to 6.0 m Muddy limestone: Light to medium grey, moderately to well indurated, massive in hand specimen, poorly bedded in outcrop, sometimes burrowed, calcareous muddy limestone. Zoophycos trace fossils occur up to c. 4.7 m, with an increase in abundance between about 1.2 and 4.7 m. It is not known if they are present in the rock record below the logged area. Note that the area corresponding with the high abundance of Zoophycos also corresponds with where the river has eroded the rock in a way that exposed a larger area of the rocks bedding plane which could account for the greater number of Zoophycos that are seen in the area. Both the upper and lower contacts appear gradational to rapidly gradational.

- Note: (1) In outcrop the limestone looks like a mudstone/siltstone; (2) The profile of the muddy limestone in the graphic log is inverted from the outcrop profile because limestones with a lower proportion of clastics seem to be less prone to erosion than muddier limestones, and consequently protrude further out of the outcrop; (3) The profile presented in the graphic log of the sandy mudstone lithologies is similar to the outcrop profile; (4) Between 10 and 16.1 m the descriptions came from examination of rock exposed along the river bed. This was poorly exposed so the measurements for the column were taken from the better exposed cliff face.

Appendix H

UDDEN-WENTWORTH GRAIN-SIZE SCALE

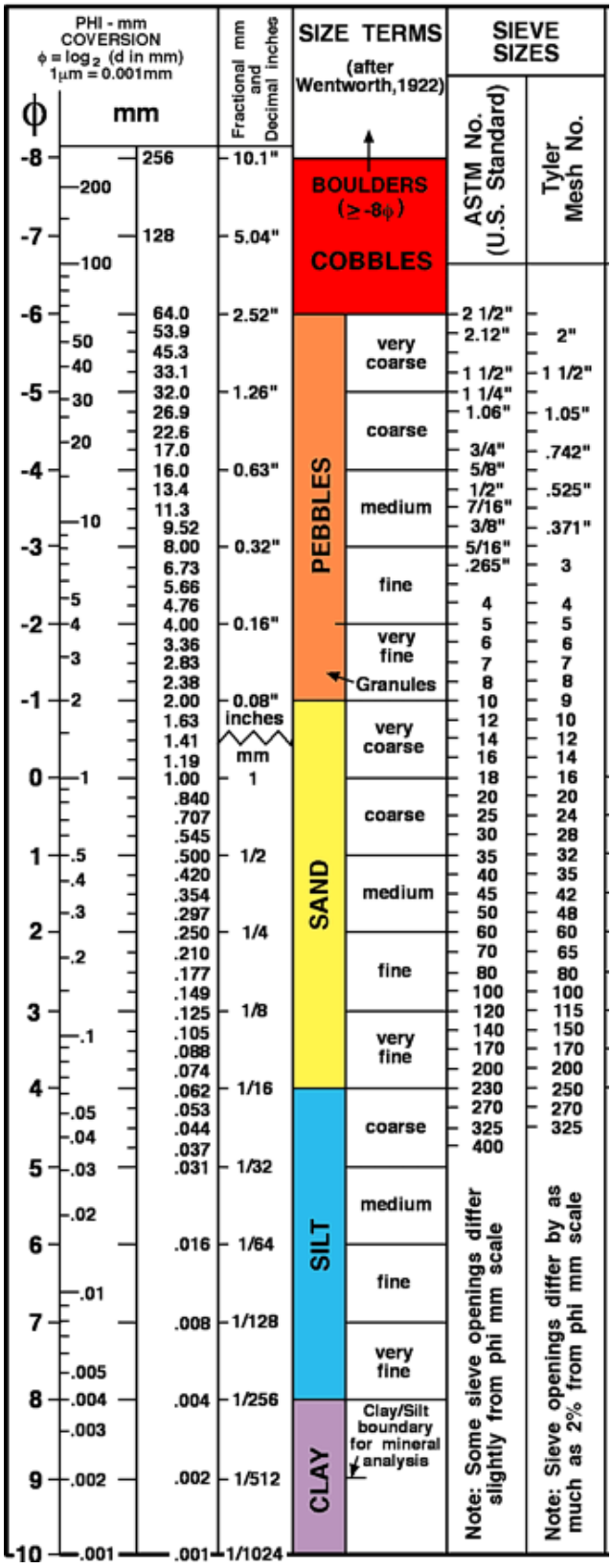

Appendix I

XRD INTENSITY-CONCENTRATION PLOTS

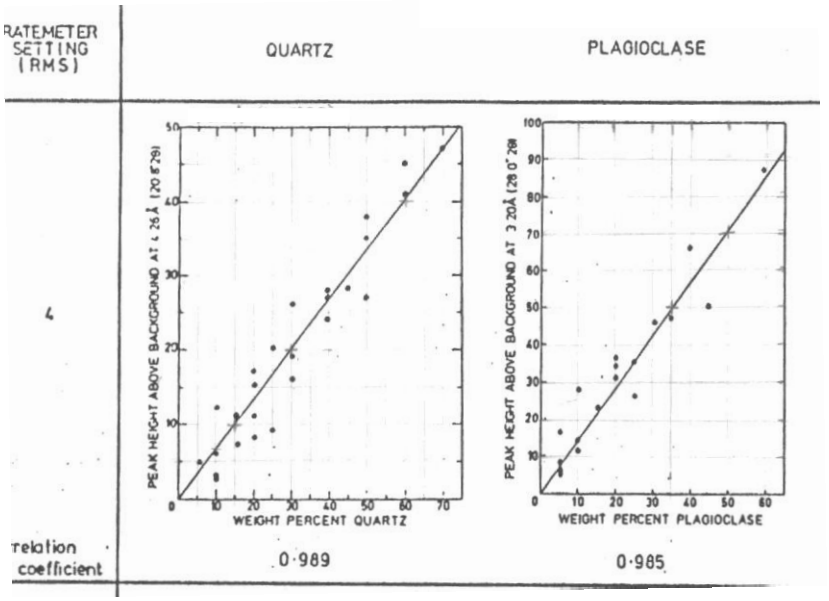

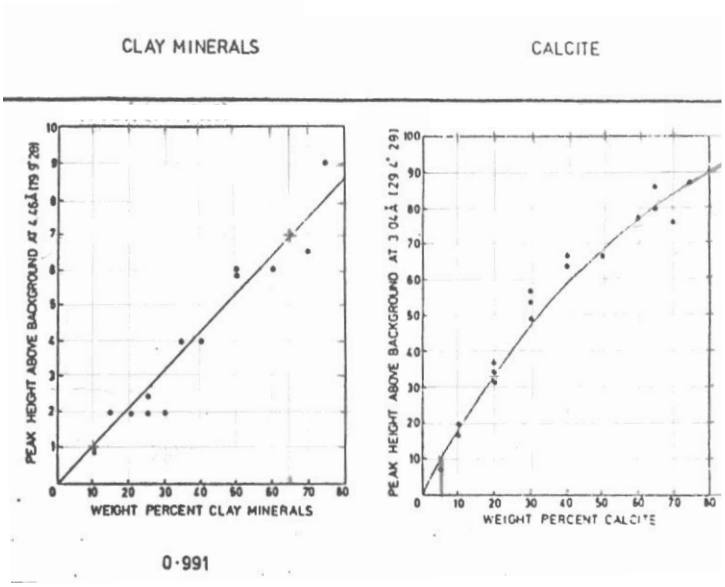

Figure I1: XRD intensity plots for an earlier XRD machine at the University of Waikato, for quartz, plagioclase, calcite, and clay minerals.